Defective Mitochondria Contribute to Impaired Translation in Spinal Muscular Atrophy

Inaugural Dissertation
zur
Erlangung des Doktorgrades
der Mathematisch-Naturwissenschaftlichen Fakultät
der Universität zu Köln

vorgelegt von
Maximilian Paul Thelen
aus Euskirchen

Köln
2021

The Doctoral Thesis "Defective Mitochondria Contribute to Impaired Translation in Spinal Muscular Atrophy" was performed at the Institute of Human Genetics and the Center for Molecular Medicine Cologne (CMMC) of the University of Cologne from April 2017 to April 2021.

Berichterstatter:	Prof. Dr. Brunhilde Wirth
	Prof. Dr. Elena I. Rugarli
Datum der mündlichen Prüfung:	26.04.2021

Für meine Eltern, Georg & Gabriele
Für meine Geschwister, Martin & Christine

CONTENTS

CONTENTS I

LIST OF FIGURES V

LIST OF TABLES VII

ABBREVIATIONS VIII

ABSTRACT XI

ZUSAMMENFASSUNG XIII

1 INTRODUCTION 1

1.1 Spinal muscular atrophy (SMA) . . . 1
1.1.1 Pathology and classification . . . 1
1.1.2 SMA as a multisystem disorder . . . 2
1.1.3 Genetics . . . 3
1.1.4 Molecular background (SMN protein) . . . 5
1.1.5 Function of SMN . . . 6
1.1.6 Mouse models . . . 8
1.1.7 Treatment . . . 10
1.2 Energy homeostasis . . . 12
1.2.1 Glycolysis . . . 14
1.2.2 Mitochondria . . . 15
1.2.3 Reactive oxygen species (ROS) . . . 16
1.2.4 Mitochondria in neurodegenerative disease . . . 16
1.3 Translation . . . 19
1.3.1 Cap dependent translation . . . 20
1.3.2 Local translation . . . 22
1.3.3 mTOR . . . 23
1.3.4 mRNA translation in neurodegenerative disease . . . 25

2 AIMS AND OBJECTIVES OF THE STUDY 27

3 RESULTS 29

3.1 Quantitative screening of primary MN proteins . . . 29
3.1.1 Mitochondrial proteins are dysregulated in SMA MNs . . . 29
3.1.2 Pathway analysis in WT vs SMA . . . 31
3.2 Characterization of mitochondria in MNs . . . 33
3.2.1 Axonal mitochondria are reduced . . . 33
3.2.2 Total amount of mitochondria is increased . . . 35
3.3 Defective complex I causes higher ROS levels and hypercarbonylation of proteins in SMA MNs . . . 37

3.3.1 Complex I activity is reduced . . . 37
3.3.2 ROS levels are increased in SMA MNs . . . 41
3.3.3 Proteins are hypercarbonylated in SMA MNs . . . 42
3.4 Energy homeostasis in MNs . . . 44
3.4.1 Glucose uptake is reduced in SMA MNs . . . 44
3.4.2 ATP levels are lower in SMA MNs . . . 44
3.5 Oxidative stress impairs global translation in SMA MNs . . . 46
3.5.1 Global translation is impaired in SMA MNs . . . 46
3.6 Pyruvate restores ATP levels and reduces ROS levels in SMA MNs . . . 49
3.6.1 Lactate does not increase intracellular ATP . . . 49
3.6.2 Pyruvate increases intracellular ATP . . . 49
3.6.3 Pyruvate reduces ROS . . . 52
3.7 Effect of ROS on global protein synthesis in neurons . . . 54
3.7.1 Regulating ROS has no effect on global translation in NSC-34 cells or WT MNs . . . 54
3.7.2 Regulating ROS modulates global protein synthesis in SMA MNs . . . 56
3.8 Effect of ROS on local protein synthesis in neurons . . . 58
3.8.1 Local protein synthesis is reduced in SMA MNs . . . 58
3.8.2 Regulating ROS does not improve local protein synthesis in WT MNs 59
3.8.3 Regulating ROS modulates axonal protein synthesis in SMA MNs . 62
3.9 Whole proteome analysis of MNs with ROS manipulation . . . 64
3.9.1 Pyruvate . . . 64
3.9.2 N-acetylcysteine (NAC) . . . 71
3.9.3 Menadione . . . 76
3.10 ROS regulates mRNA translation . . . 81
3.10.1 Translation elongation in primary MNs . . . 81
3.10.2 Translation initiation is reduced in SMA MNs . . . 84
3.11 SMN protein levels are regulated by pyruvate and ROS via mTOR . . . 87
3.11.1 Pyruvate increases SMN in NSC-34 cells, WT MNs and SMA MNs 87
3.11.2 Increase of SMN is post-transcriptionally regulated . . . 88
3.11.3 Modulation of ROS regulates SMN . . . 89
3.11.4 Increase of SMN is mTOR-dependent . . . 89

4 DISCUSSION 93
4.1 The mitochondrial proteome is significantly altered in SMA MNs . . . 94
4.2 The number of mitochondria is reduced in SMA MN axons . . . 94
4.3 Complex I activity is impaired in SMA MNs . . . 95
4.4 Oxidative stress is increased in SMA MNs . . . 96
4.5 Glycolysis does not compensate for mitochondrial defects . . . 98
4.6 Rescuing energy homeostasis fails to rescue SMA pathology fully . . . 98
4.6.1 The astrocyte-neuron lactate shuttle hypothesis and why lactate fails to increase ATP in neurons . . . 99
4.6.2 Pyruvate improves energy homeostasis and reduces ROS . . . 100

4.7 Reducing ROS, not increasing ATP improves global translation 101
4.8 Local translation in SMA MNs 101
4.9 Whole proteome analysis after pyruvate treatment 102
4.10 Whole proteome analysis after NAC treatment 102
4.11 Whole proteome analysis after menadione treatment 103
4.12 Cap-dependent translation initiation is inhibited in SMA MNs 103
4.13 The mTOR pathways regulates translation in SMA MNs 104
4.14 Increase of SMN by pyruvate and NAC supplementation is mTOR-dependent 105

5 CONCLUDING REMARKS AND FUTURE OUTLOOK 106

6 MATERIAL AND METHODS 108
6.1 Material 108
6.1.1 Equipment 108
6.1.2 Chemicals 109
6.1.3 Reagents 110
6.1.4 Enzymes 111
6.1.5 Drugs 112
6.1.6 Primary antibodies and staining reagents 112
6.1.7 Secondary antibodies 113
6.1.8 Primers 113
6.1.9 Mouse & cell lines 114
6.1.10 Solutions and media 114
6.1.11 Kits 116
6.1.12 Software packages 117
6.1.13 Internet databases 117
6.2 Methods 117
6.2.1 Working with laboratory mice 117
6.2.2 SMA mouse model 118
6.2.3 Cell culture work 118
6.2.4 Counting cells 118
6.2.5 Cultivation of NSC-34 cells 119
6.2.6 Culture of primary motor neurons 119
6.2.7 Surface SEnsing of Translation assay (SUnSET) 120
6.2.8 SUnSET-based Ribosome Speed of Elongation assay (SunRiSE) . . 120
6.2.9 Drug treatment 120
6.2.10 Nucleic acid methods 120
6.2.11 Proteinbiochemistry methods 124
6.2.12 Proteomics 127
6.2.13 Immunofluorescence methods 129
6.2.14 Complex I activity assay 130
6.2.15 ATP assay 130
6.2.16 Glucose uptake assay 130

6.2.17 Pyruvate uptake assay 130
6.2.18 Detection of oxidative stress 131
6.2.19 Protein carbonylation assay 131
6.2.20 AHA-click iT assay 131
6.2.21 Statistical analyses 132

7 REFERENCES **133**

8 PUBLICATIONS AND PRESENTATIONS **177**

APPENDIX **XV**

A Thelen *et al.*, (2020) *Acta Neuropathologica Communications* **XV**

B Supplementary material **XLVI**

ACKNOWLEDGEMENTS **LXXXVII**

EIDESSTATTLICHE ERKLÄRUNG **LXXXVIII**

LIST OF FIGURES

1 Illustration of *SMN* splicing and expression . . . 5
2 Functions of SMN in MNs . . . 8
3 Energy consumption and neurotransmitter release in neurons . . . 13
4 Eukaryotic cap-dependent translation initiation and its regulation by mTOR 20
5 The mTOR signaling pathways . . . 25
6 Quantitative proteomics of WT and SMA MNs . . . 30
7 Significantly changed proteins in SMA MNs . . . 30
8 Quantitative proteomics of mitochondrial proteins of SMA and WT MNs . 31
9 Pathway analysis of SMA MNs . . . 32
10 Immunofluorescence of mitochondria . . . 34
11 Immunofluorescence of mitochondrial appearance . . . 35
12 TOM20 protein levels are increased in SMA MNs . . . 36
13 KEGG OXPHOS . . . 39
14 Optimization of complex I assay in primary WT MNs . . . 40
15 Complex I activity is reduced in SMA MNs . . . 40
16 Complex I activity is not changed in heart or spinal cord . . . 41
17 ROS levels are increased in SMA MNs . . . 42
18 Proteins are hypercarbonylated in SMA MNs . . . 43
19 Glucose uptake is reduced in primary SMA MNs . . . 44
20 ATP levels are reduced in primary SMA MNs . . . 45
21 Translation is reduced in SMA MNs (SUnSET) . . . 47
22 Translation is reduced in SMA MNs (AHA) . . . 48
23 Lactate does not increase ATP in NSC-34 cells . . . 49
24 Pyruvate 50 mM increases ATP in NSC-34 cells . . . 50
25 Pyruvate uptake in MNs . . . 50
26 Pyruvate increases ATP in MNs . . . 51
27 Pyruvate increases ATP in SMA MNs . . . 51
28 Pyruvate reduces ROS after pharmacologically induced oxidative stress . . . 52
29 Pyruvate reduces ROS in SMA MNs . . . 53
30 Experimental set up of SUnSET assay in NSC-34 cells, WT & SMA MNs . 54
31 Regulating ROS has no effect on NSC-34 cells . . . 55
32 Regulating ROS has no effect on protein synthesis in WT MNs . . . 56
33 Regulating ROS with NAC increases protein synthesis in SMA MNs . . . 57
34 Axonal local translation is reduced in SMA MNs . . . 59
35 Modification of ROS does not increase protein synthesis in WT MN soma . 60
36 Modification of ROS does not alter protein synthesis in WT MN axons . . 61
37 Reducing ROS increases protein synthesis in SMA MN soma . . . 62
38 Reducing ROS increases local protein synthesis in SMA MN axons . . . 63
39 Pyruvate modifies the proteome of MNs . . . 64
40 Pyruvate regulates a similar number of proteins in WT and SMA MNs . . . 66
41 Pyruvate changes more proteins in SMA than in WT MNs . . . 68

42 NAC modifies the proteome of MNs 71
43 NAC regulates the same number of proteins in WT and SMA MNs 73
44 NAC changes proteins in SMA more than in WT MNs 74
45 Menadione modifies the proteome of MNs 77
46 Menadione changes proteins in WT MNs, that are also altered in SMA MNs 77
47 Menadione reduces protein levels in WT MNs 78
48 Quantitative proteomics of translation related proteins of SMA and WT MNs 81
49 Scheme of SunRiSE assay 82
50 SunRiSE assay of WT and SMA MNs 83
51 SunRiSE assay in WT MNs 83
52 SunRiSE assay in SMA MNs 84
53 Cap-dependent translation initiation 84
54 Phosphorylation status of 4E-BP in WT and SMA MNs 85
55 Translation initiation in WT MNs 85
56 4E-BP mediated translation initiation in SMA MNs 86
57 Pyruvate increases SMN protein levels 87
58 Pyruvate does not change *Smn* mRNA expression 88
59 Increase of SMN by pyruvate is abolished by anisomycin 88
60 SMN levels after 1 h NAC and menadione treatment 89
61 Increase of SMN by pyruvate is blocked by mTOR inhibition 90
62 Pyruvate increases mTOR in WT and SMA MNs 91
63 Reducing ROS increases mTOR in SMA MNs 92
64 Representation of impairments, targeted by NAC and pyruvate in SMA. . . 107

LIST OF TABLES

1 Differentially expressed proteins in the OXPHOS of SMA MNs 37
2 GO analysis: Pathways regulated by pyruvate in SMA MNs 65
3 Differentially expressed proteins in SMA compared to WT MNs and in WT MNs after pyruvate treatment 69
4 Differentially expressed proteins in SMA compared to WT MNs and in SMA MNs after pyruvate treatment 70
5 GO analysis: Pathways regulated by NAC in SMA MNs 71
6 Differentially expressed proteins in SMA compared to WT MNs and in WT MNs after NAC treatment 74
7 Differentially expressed proteins in SMA compared to WT MNs and in SMA MNs after NAC treatment 75
8 Differentially expressed proteins in SMA compared to WT MNs and in WT MNs after menadione treatment 78
9 Components and volumes for genotyping PCR reactions. 122
10 Thermocycler *Smn* PCR program. 122
11 Components for cDNA synthesis 123
12 Conditions for cDNA synthesis PCR 123
13 Components for qRT-PCR 124
14 Conditions for qRT-PCR 124
S1 Differentially expressed proteins in SMA compared to WT MNs XLVI
S2 Differentially expressed proteins in WT MNs after pyruvate treatment . . . LX
S3 Differentially expressed proteins in SMA MNs after pyruvate treatment . . . LXIV
S4 Differentially expressed proteins in WT MNs after NAC treatment LXVIII
S5 Differentially expressed proteins in SMA MNs after NAC treatment LXXI
S6 Differentially expressed proteins in WT MNs after menadione treatment . . LXXVI

ABBREVIATIONS

4E-BP1	eukaryotic initiation factor 4E (eIF4E)-binding protein
ACTB	actin beta
AD	Alzheimer's disease
AHA	azidohomoalanine
ALS	amyotrophic lateral sclerosis
ANLS	astrocyte- neuron lactate shuttle model
ANOVA	analysis of variance
APS	ammonium persulfate
AraC	cytosine arabinoside
ASD	Autism spectrum disorder
ASO	antisense oligonucleotide
ATP	adenosine triphosphate
a.u.	arbitrary unit
bp	base pairs
BSA	bovine serum albumin
C	celsius
Ca	calcium
cDNA	coding DNA
CNS	central nervous system
Complex I	NADH:ubiquinone oxidoreductase
Cu	copper
DAVID	Database for Annotation, Visualization and Integrated Discovery
DIV	days *in vitro*
DLGAP1	DLG-associated protein 1
DMEM	Dulbecco's modified eagle medium
DMSO	dimethyl sulfoxide
DNA	deoxyribonucleic acid
DTT	dithiothreitol
E	embryonic day
EDTA	ethylene diamine tetraacetic acid
eIF	eukaryotic translation initiation factor
EMA	European Medicine Agency
ESE	exonic splicing enhancer
ESS	exonic splicing silencer
et al.	*et alii*
FC	fold change
FCS	fetal calf serum
FDA	Food & Drug Administration
FDR	false discovery rate
FL	full length
fw	forward

g	gravitational force
GLUT	Glucose transporter
GO	gene ontology
h	hour(s)
HD	Huntington's disease
hnRNP	heterogeneous nuclear ribonuclear protein
ICA1	islet cell autoantigen
IF	immunofluorescent
IgG	immunoglobulin G
iPSC	induced pluripotent stem cell
ISS	intronic splicing silencer
IT	intrathecal
IV	intravenous
kb	kilobases
kDa	kilodalton
ko	knockout
L	liter
log	logarithm
m	mili
µ	micro
m^7G	7-methylguanosine
M	molar
MGI	Mouse Genome Informatics
min	minutes
miRNA	micro RNA
MN	motor neuron
mRBP	mRNA- binding protein
mRNA	messenger RNA
MS	mass spectrometry
mtDNA	mitochondrial DNA
mTOR	mammalian target of rapamycin
n	number of technical replicates
N	number of biological replicates
NAC	N-acetylcysteine
NMJ	neuromuscular junction
ns	not significant
Non	untreated
OMIM	Online Mendelian Inheritance in Man
ON	over night
OXPHOS	oxidative phosphorylation
P	postnatal day
p	probability

PAGE	polyacrylamide gel electrophoresis
PBS	phosphate buffered saline
PCR	polymerase chain reaction
PD	Parkinson's disease
PDL	poly-D-lysine
PFA	paraformaldehyde
pH	power of hydrogen
PIC	preinitiation complex
pmol	picomol
Pen/Strep	penicillin/streptomycin
RBP	RNA-binding protein
rev	reverse
RNA	ribonucleic acid
RNP	ribonucleoprotein
ROS	reactive oxygen species
rpm	rotations per minute
rRNA	ribosomal RNA
RT	room temperature
qRT-PCR	quantitative real time-PCR
S6	ribosomal protein S6
S6K	S6 kinase
SC	spinal cord
scAAV9	self-complementary adeno-associated virus 9
SD	standard deviation
SDB-RPS	styrenedivinylbenzene-reverse phase sulfonate
SDS	sodium dodecyl sulfate
sec	seconds
SMA	spinal muscular atrophy
SMN	survival motor neuron
snRNP	small nuclear ribonucleoprotein
SOD	superoxide dismutase
SunRiSE	SUnSET-based Ribosome Speed of Elongation
SUnSET	surface sensing of translation
TCA	tricarboxylic acid
TEMED	N,N,N',N'-tetramethylethylenediamine
tg	transgene
tRNA	transfer RNA
TOMM20	Mitochondrial import receptor subunit TOM20 homolog
UTR	untranslated region
WB	western blot
WT	wildtype

ABSTRACT

Spinal muscular atrophy (SMA) is a devastating, autosomal-recessive neurodegenerative disease. It is characterized by the loss of alpha motor neurons (MNs) located in the ventral horn of the spinal cord. Degeneration of lower MNs leads to proximal muscle weakness and can ultimately result in respiratory failure. Accordingly, SMA is among the most common genetic causes of infant death. Causative for SMA is a reduced survival motor neuron (SMN) protein level. The reduction of ubiquitously expressed SMN results mainly from biallelic deletions or partially from point mutations in the *SMN1* gene. Solely an almost identical copy of *SMN1* - *SMN2* - prevents embryonic lethality in SMA patients. A plethora of molecular defects, including RNA processing, protein synthesis, metabolic defects, and mitochondrial function, contribute to SMA pathology. Furthermore, reduced SMN levels delay maturation of acetylcholine receptor subunits and morphological and functional abnormalities at the neuromuscular junction.

Neurons highly depend on energy production via oxidative phosphorylation (OXPHOS) by mitochondria. Dysfunctional mitochondria in SMA produce fewer ATP molecules and generate massive amounts of reactive oxygen species (ROS), resulting in oxidative stress. Oxidative stress challenges the cells with DNA damage, protein carbonylation, and impaired protein synthesis. Based on these findings, we hypothesized that defective mitochondria contribute to impaired protein synthesis in SMA. Another central question is whether increasing ATP and reducing oxidative stress ameliorates SMA pathology.

We performed a whole proteome analysis of cultured primary MNs, derived from SMA and WT embryos. Using mass spectrometry (MS), we confirmed previously known molecular mechanisms altered by SMN deficiency and contributing to SMA pathology. Particularly, a tendency of altered proteins localized to mitochondria was determined. In detail, complex I of the respiratory chain was identified as the major disturbed complex in SMA mitochondria. Besides alterations in mitochondrial protein abundance, immunostainings showed a decreased number and altered mitochondrial shape in the axon of SMA MNs. However, results from the whole proteome analysis and immunochemical results reveal an increase of mitochondrial proteins in whole-cell lysates, suggesting an accumulation of dysfunctional mitochondria in the soma.

Biochemical assays revealed functional impairments such as reduced ATP, impaired respiratory complex I activity, and increased ROS production. Additionally, a reduced glucose uptake suggested no compensation of energy deprivation by glycolysis. Previous studies implicated a reduced protein synthesis in SMA. We confirmed those findings with this study and further linked reduced protein synthesis to protein carbonylation resulting from increased oxidative stress. Moreover, we provide evidence that protein synthesis is also reduced in the axonal compartment of SMA MNs. Protein carbonylation and protein synthesis were quantified using immunochemical approaches. These findings prompted us to evaluate the mechanism of impaired protein synthesis. To decipher the contribution of translation initiation and elongation during impaired protein synthesis, we performed the SUnSET and SunRiSE assay, respectively. Based on our results, impaired protein synthesis in SMA results from impaired translation initiation and not elongation. While the SunRiSE assay shows a similar elongation speed in

WT and SMA MNs, the phosphorylation status of the eIF4E-binding protein (4E-BP) reveals an impaired translation initiation in SMA MNs.

To increase ATP and decrease ROS, the cell culture medium of MNs and MN-like NSC-34 cells was supplied with lactate, pyruvate, and N-acetylcysteine (NAC). Effects of substrate supplementation on the whole proteome of MNs were determined by MS. Supplementation of pyruvate was able to increase ATP levels in SMA MNs, measured biochemically. Furthermore, pyruvate and NAC supplementation reduced excessive ROS and improved impaired protein synthesis, including local translation in SMA MNs.

While the antioxidant NAC can enhance global mRNA translation, pyruvate could only increase a subset of proteins. However, both pyruvate and NAC increased SMN in SMA MNs. Downstream targets of the mTOR pathway were measured immunochemically after NAC and pyruvate supplementation. Up-regulation of protein synthesis upon NAC and pyruvate supplementation is due to increased translation initiation mediated by the mTOR pathway. The mTOR-mediated increase of SMN after pyruvate supplementation was confirmed by pharmacological inhibition of the mTOR pathway.

In summary, we found that excessive ROS generated by defective complex I inhibits the initiation of mRNA translation in SMA MNs. Our findings suggest a new molecular networking system among dysfunctional mitochondria, excessive ROS production, and impaired protein synthesis via the mTOR pathway. This study opens up new treatment possibilities concerning SMA pathology by improving mitochondria, reducing ROS, and influencing impaired protein synthesis. As many neuropathies display molecular defects in mitochondria, including excessive ROS production, additional research fields despite SMA will benefit from our study.

ZUSAMMENFASSUNG

Die Spinale Muskelatrophie (SMA) ist eine verheerende, autosomal-rezessive neurodegenerative Erkrankung. Sie ist gekennzeichnet durch den Verlust von Alpha-Motorneuronen (MN), die sich im ventralen Horn des Rückenmarks befinden. Die Degeneration der unteren MN führt zu einer proximalen Muskelschwäche und kann schließlich zu einem Atemstillstand führen. Dementsprechend gehört die SMA zu den häufigsten genetischen Ursachen des Kindstodes. Ursächlich für die SMA ist ein verminderter Survival Motor Neuron (SMN) Proteinspiegel. Die Reduktion des ubiquitär vorkommenden SMN resultiert hauptsächlich aus biallelischen Deletionen oder teilweise aus Punktmutationen im *SMN1*-Gen. Lediglich eine fast identische Kopie von *SMN1* - *SMN2* - verhindert die embryonale Letalität bei SMA-Patienten. Eine Fülle von molekularen Defekten, einschließlich RNA-Verarbeitung, Proteinsynthese, Stoffwechseldefekten und mitochondrialen Funktionen, tragen zur SMA-Pathologie bei. Darüber hinaus verzögern reduzierte SMN-Spiegel die Reifung von Acetylcholinrezeptor-Untereinheiten und führen zu morphologischen und funktionellen Anomalien an der neuromuskulären Endplatte.

Neuronen sind in hohem Maße von der Energieproduktion über oxidative Phosphorylierung (OXPHOS) durch Mitochondrien abhängig. Dysfunktionale Mitochondrien in SMA produzieren weniger ATP-Moleküle und erzeugen massive Mengen an reaktiven Sauerstoffspezies (ROS), was zu oxidativem Stress führt. Oxidativer Stress belastet die Zellen mit DNA-Schäden, Protein-Carbonylierung und beeinträchtigter Proteinsynthese. Basierend auf diesen Erkenntnissen stellten wir die Hypothese auf, dass defekte Mitochondrien zu einer gestörten Proteinsynthese bei SMA beitragen. Eine weitere zentrale Frage ist, ob die Erhöhung von ATP und die Reduzierung von oxidativem Stress die SMA-Pathologie verbessert.

Wir führten eine Analyse des gesamten Proteoms von kultivierten primären MN, die von SMA- und WT-Embryonen stamen, durch. Mittels Massenspektrometrie (MS) konnten wir bereits bekannte molekulare Mechanismen bestätigen, die durch SMN-Mangel verändert werden und zur SMA-Pathologie beitragen. Insbesondere zeichnete sich eine Tendenz ab von veränderten Proteinen, die in Mitochondrien lokalisiert sind. Der Komplex I der Atmungskette wurde als der am meisten gestörte Komplex in SMA-Mitochondrien identifiziert. Neben Veränderungen in der mitochondrialen Proteinhäufigkeit zeigten Immunfärbungen eine verminderte Anzahl und veränderte Form der Mitochondrien im Axon von SMA-MN. Die Ergebnisse der Gesamtproteomanalyse sowie immunochemische Versuche zeigen jedoch einen Anstieg der mitochondrialen Proteine in Lysaten ganzer Zellen, was auf eine Anhäufung von dysfunktionalen Mitochondrien im Soma hindeutet.

Biochemische Versuche zeigten funktionelle Beeinträchtigungen wie reduziertes ATP, beeinträchtigte Aktivität des Atmungskomplexes I und erhöhte ROS-Produktion. Zusätzlich deutete eine reduzierte Glukoseaufnahme auf eine fehlende Kompensation des Energiemangels durch die Glykolyse hin. Frühere Studien deuteten auf eine reduzierte Proteinsynthese bei SMA hin. Wir bestätigten diese Ergebnisse mit dieser Studie und brachten die reduzierte Proteinsynthese mit der Proteincarbonylierung in Verbindung, die durch erhöhten oxidativen Stress entsteht. Außerdem konnten wir nachweisen, dass die Proteinsynthese auch im axonalen Kompartiment von SMA-MN reduziert ist. Die Protein-Carbonylierung und die Proteinsynthese

wurden mit immunochemischen Ansätzen quantifiziert. Diese Ergebnisse veranlassten uns, den Mechanismus der gestörten Proteinsynthese zu untersuchen. Um den Beitrag der Translationsinitiation und -elongation während der gestörten Proteinsynthese zu entschlüsseln, führten wir den SUnSET- bzw. SunRiSE-Assay durch. Basierend auf unseren Ergebnissen resultiert die gestörte Proteinsynthese bei SMA aus einer gestörten Translationsinitiation und nicht aus der Elongation. Während der SunRiSE-Assay eine ähnliche Elongationsgeschwindigkeit in WT- und SMA-MN zeigt, offenbart der Phosphorylierungsstatus des eIF4E-bindenden Proteins (4E-BP) eine gestörte Translationsinitiation in SMA-MN.

Um ATP zu erhöhen und ROS zu verringern, wurde das Zellkulturmedium von MN und MN-ähnlichen NSC-34-Zellen mit Laktat, Pyruvat und N-Acetylcystein (NAC) zugesetzt. Die Auswirkungen der Substratsupplementierung auf das gesamte Proteom der MN wurden mittels MS bestimmt. Die Supplementierung von Pyruvat war in der Lage, den ATP-Gehalt in SMA-MN zu erhöhen, was biochemisch gemessen wurde. Außerdem reduzierte die Pyruvat- und NAC-Supplementierung exzessive ROS und verbesserte die beeinträchtigte Proteinsynthese, einschließlich der lokalen Translation in SMA-MN.

Während das Antioxidant NAC die globale mRNA-Translation verbessern kann, konnte Pyruvat nur eine Untergruppe von Proteinen erhöhen. Allerdings erhöhten sowohl Pyruvat als auch NAC SMN in SMA-MN. Nachgeschaltete Ziele des mTOR-Wegs wurden nach NAC- und Pyruvat-Supplementierung immunochemisch gemessen. Die Hochregulierung der Proteinsynthese nach NAC- und Pyruvat-Supplementierung ist auf eine erhöhte Translationsinitiation zurückzuführen, die durch den mTOR-Signalweg vermittelt wird. Der mTOR-vermittelte Anstieg von SMN nach Pyruvat-Supplementierung wurde durch pharmakologische Hemmung des mTOR-Weges bestätigt.

Zusammenfassend fanden wir, dass exzessive ROS, die durch einen defekten Komplex I erzeugt werden, die Initiation der mRNA-Translation in SMA MN hemmen. Unsere Ergebnisse deuten auf eine neue molekulare Verbindung zwischen dysfunktionalen Mitochondrien, exzessiver ROS-Produktion und gestörter Proteinsynthese über den mTOR-Weg hin. Diese Studie eröffnet neue Behandlungsmöglichkeiten bezüglich der SMA-Pathologie, indem sie die Mitochondrien verbessert, ROS reduziert und die gestörte Proteinsynthese beeinflusst. Da viele Neuropathien molekulare Defekte in Mitochondrien aufweisen, einschließlich einer übermäßigen ROS-Produktion, werden weitere Forschungsfelder zusätzlich zur SMA von unserer Studie profitieren.

1 INTRODUCTION

1.1 Spinal muscular atrophy (SMA)

Spinal muscular atrophy (SMA) is an inherited neuromuscular disease characterized by selective loss of lower alpha motor neurons (MNs), which leads to proximal muscle weakness and atrophy. SMA is caused by reduced levels of ubiquitously expressed survival of motor neuron protein (SMN) due to biallelic deletions or mutations in the *SMN1* gene at chromosome 5 and primarily non-functional *SMN2* gene copies, which each patient carries in the genome (Melki et al., 1990). Besides the classical SMA linked to inheritance at chromosome 5 (5q-SMA), other forms of SMA with a similar spectrum of symptoms can be classified. The classification is based on their mode of inheritance (autosomal recessive, dominant, or X-linked) and affected muscle weaknesses (i.e., proximal or distal) (Lefebvre et al., 1995; Kugelberg & Welander, 1956; Farrar & Kiernan, 2015; Kennedy et al., 1968). However, the majority ($\approx$ 90%) of SMA cases are autosomal recessive linked to chromosome 5 with a rate of 2% *de novo* mutations (Lefebvre et al., 1995; Alías et al., 2009; Zerres, 1997; Wirth et al., 1997). The incidence varies between 1 in 6.000- 10.000 live births, with a worldwide carrier frequency of 1:51 (Pearn, 1978; Feldkötter et al., 2002; Melki et al., 1994; Verhaart et al., 2017; Wirth et al., 2020). However, the carrier frequency varies in different ethnic groups, with the lowest occurrence of 1:145 in the sub-Saharan African population and a frequency of 1:41 in the European population (Sangaré et al., 2014; Wirth et al., 2020). With an increasing number of countries performing SMN newborn screenings, the incidence can be determined more precisely (Vidal-Folch et al., 2017; Vill et al., 2019).

When SMN levels fall under a certain threshold, a plethora of cellular pathways are disturbed. SMA is one of the most common genetic causes of infant mortality caused by respiratory failure (Lewelt et al., 2012). Overall, SMA is presented with progressive degeneration and subsequent loss of α-MNs in the ventral (anterior) horn of the spinal cord (Mercuri, Finkel, et al., 2018; Finkel et al., 2018).

1.1.1 Pathology and classification

Even though SMA is a monogenic disease caused by the loss of SMN protein, it leads to a heterogeneous manifestation of neuromuscular features. The pathological spectrum ranges from severe generalized weakness with respiratory failure in the early period of life to mild proximal limb weakness in adulthood. The characteristic symptoms are hypotonia, muscular atrophy, and weakness of proximal muscles, predominantly affecting the lower extremities. Besides the neuropathology in SMA, maturation of acetylcholine receptor subunits is delayed, and morphological and functional abnormalities at the neuromuscular junction (NMJ) are observed (Harding et al., 2015). The muscle atrophy affects type I and type II muscle fibers with hypertrophy of the surviving type I fibers (Baloh et al., 2007; Soubrouillard et al., 1995).

In the early days of SMA research, the disease was classified based on the severity, age of onset, and achieved motor milestones (Munsat & Davies, 1992). In the beginning, only three types of SMA (Typ I-III) were distinguished (Robak & Marcinkiewicz, 1995). Later, the classification was extended with an extremely severe type, called Type 0 (Dubowitz, 1999;

Macleod et al., 1999). Type 0, leading to death within weeks, initiates during prenatal development, and patients harbor only one copy of *SMN2* (Dubowitz, 1999; Macleod et al., 1999). Furthermore, the classification was extended by a very mild form (Type IV, OMIM # 271150), leading to proximal leg weakness in adulthood but with a normal lifespan (Zerres et al., 1995). However, only less than 1% of SMA patients are classified as Type IV SMA (Wirth et al., 2020).

Type I SMA (OMIM #253300), which is also called the Werdnig- Hoffman disease, is diagnosed in about 35% of SMA cases (Calucho et al., 2018). However, although its equal distribution at diagnosis compared to other SMA types, Type I has a relatively small prevalence in the number of all SMA patients living in the population due to the short survival of $\approx$ 7.4 months (range 3-56 months) (Pearn, 1980; Farrar et al., 2013; Lally et al., 2017). However, due to current therapies, the prevalence of Type I patients among all SMA patients will change. Diagnosis usually occurs in the first six months of birth when symptoms start. Those symptoms involve poor control of head movement, muscle weakness, coughing, and trouble breathing. This type of SMA is very characteristic for the lack of resistance to passive movement (hypotonia), resulting in a "floppy infant" appearance.

Type II SMA (OMIM #253550) patients gain the ability to sit unaided but never achieve the ability to walk (Mercuri, Finkel, et al., 2018). First symptoms appear after 6 months of age, and the life expectancy is between 5 and 25 years. Natural history of SMA Type II patients reveals a survival rate of 68.5% at 25 years (Zerres et al., 1997). Similar to Type I SMA, patients with Type II show hypotonia, but they also develop intercostal weakness, respiratory complications, and scoliosis (Zerres, 1995).

Type III SMA (OMIM #253400) is a mild form of SMA. The age of onset for Type III SMA is after 18 months with the ability to walk, but in some cases, wheelchair support is needed later in life (Zerres et al., 1997). Type III can be divided based on the age of onset into the subclasses Type IIIa ($>$1.5 years) and Type IIIb ($>$3 years). Type III is also called Kugelberg- Welander disease (Kugelberg & Welander, 1956).

However, the development of therapies and the increasing supportive measures, including respiratory and physical therapy, change the course of the natural history of SMA. Due to the increasing overlap between SMA types, this old classification is revised (Mercuri, Finkel, et al., 2018; Finkel et al., 2018; Wirth et al., 2020). Furthermore, the population's prevalence will change due to increased survival, especially of type I patients. The new SMA classification is less based on the age of onset but more on the motor milestones achieved. The recommended classification divides SMA patients into non-sitters, sitters, and walkers (Mercuri, Finkel, et al., 2018; Finkel et al., 2018).

1.1.2 SMA as a multisystem disorder

Besides the MN pathology, morphological and functional impairments are observed in other tissues. Impairments in non-neuronal tissues are mainly observed in SMA mouse models and severe SMA type I patients with extremely low levels of SMN (Hamilton & Gillingwater, 2013; Yeo & Darras, 2021). However, the prevalence of non-motor symptoms is low in adult SMA

patients (Günther et al., 2019). Mostly congenital heart disease is characterized as a feature of severe SMA type I patients due to SMN deficiency (Rudnik-Schoneborn et al., 2008). Other impairments are found in blood vessels, liver, bone, intestine, and pancreas (Hamilton & Gillingwater, 2013; Yeo & Darras, 2021). Defects in other organs correlate with differential cell-type-specific SMN amounts. In contrast, MNs show high susceptibility to low levels of SMN (Sleigh et al., 2011). However, muscle requires less SMN, and SMN levels produced from two copies of *SMN2* are sufficient for normal muscle function in mice (Iyer et al., 2015). Also, severe defects in the liver have been shown in SMA mouse models with murine *Smn* exon 7 deletion (Vitte et al., 2004). Also, impairments of sensory-motor connectivity have been reported in SMA mice and patients (Shorrock et al., 2019; Mentis et al., 2011; Rudnik-Schoneborn et al., 2003). It remains unclear whether low SMN levels cause impairments of proprioceptive sensory neurons (Mentis et al., 2011) or as a consequence of MN dysfunction (Gogliotti et al., 2012). Results showing that loss of sensory neurons was prevented upon MN-specific restoration of SMN supports the hypothesis that sensory-motor defects are a consequence and not a cause of MN dysfunction (Gogliotti et al., 2012). Further research in a human stem cell model supports the idea that sensory neurons do not induce MN loss (Schwab & Ebert, 2014). However, sensory neuron loss was also observed to occur prior to MN loss, suggesting a primary cause of motor dysfunction (Mentis et al., 2011).

This multisystemic nature of SMA suggests that restoring SMN levels in non-neuronal tissues is crucial to compensate for internal organ defects other than MN failure. Especially with newly developed therapies aiming to increase tissue-specific SMN levels in MNs, extremely low levels of SMN in other tissues can lead to defects in those tissues also in older patients.

1.1.3 Genetics

Thirty years ago, the phenotypically classified SMA types I-II were mapped to the same chromosomal region 5q11.2-q14 by linkage analysis (Melki et al., 1990; Brzustowicz et al., 1990; Gilliam et al., 1990). After all, this 500 Kb region is duplicated and highly polymorphic, resulting in two copies of the *SMN* gene. Up to four copies per chromosome have been identified (Schmutz et al., 2004; Mérette et al., 1994; M. Y. Dennis et al., 2017). The disease-determining gene was conclusively located to chromosome 5q13 and identified as *SMN1* in 1995 (Lefebvre et al., 1995). The centromeric *SMN2* is a 99% homologous gene of the disease causing telomeric *SMN1* gene (Lefebvre et al., 1995). Unfortunately, only *SMN1* encodes for the full length SMN protein and *SMN2* is resulting in most of the cases in a highly unstable form, that is rapidly degraded by the proteasome (**Figure 1**) (Lorson et al., 1998; Chang et al., 2004; Burnett et al., 2009).

Despite the high heterogeneity of SMA characteristics, homozygous *SMN1* deletions or mutations are found in all 5q SMA patients (Lefebvre et al., 1995; Wirth, 2000). In fact, 96% of SMA patients show biallelic deletions in *SMN1* or gene conversions of *SMN1* into *SMN2* and 4% have point mutations (Wirth, 2000).

Albeit it has been stated initially that the 29 kb gene *SMN1* contains 8 exons (Lefebvre et al., 1995), exon 2 is composed of two exons, 2a, and 2b, with a stop codon in exon 7, leaving exon 8 untranslated (Bürglen et al., 1996). Furthermore, an additional exon generated

by exonization of an intronic Alu-like sequence, called exon 6b was identified to appear in *SMN1* and *SMN2* (Seo et al., 2016). Transcripts containing exon 6b appear to be more stable than transcripts lacking exon 7 transcribed from *SMN2* (Seo et al., 2016). However, *SMN1* and *SMN2* show high similarity with only five base pair substitutions (Seo et al., 2016). Nevertheless, three substitutions 27092 G>A (intron 6), 27289 A>G and 27404 A>G (both intron 7), are intronic, and only the c.840C>T (exon 7) transition and 27869 G>A (exon 8) are within exons (**Figure 1**) (Bürglen et al., 1996). However, since exon 8 is not translated, only the c.840C>T (exon 7) transition is within the coding region (Seo et al., 2016; Burlet et al., 1996). While *SMN1* produces mainly the full-length SMN protein, *SMN2* encodes for alternatively spliced transcripts (Wirth, 2000). Alternatively spliced *SMN2* transcripts lack exon 7 (*SMNΔ7*) (Lorson et al., 1999). Nevertheless, the C-to-T transition at codon 280 in exon 7 is a silent variant, which does not lead to an amino acid exchange (Lefebvre et al., 1995; Bürglen et al., 1996). However, the c.840C>T transition affects correct splicing of exon 7 by forming an exon splicing silencer (ESS) site from a previous exon splicing enhancer (ESE) site (Lorson et al., 1999; Kashima & Manley, 2003; Cartegni & Krainer, 2002).

The major modifier of SMA severity is *SMN2*. Disease severity inversely correlates with the copy number of *SMN2* leading to milder phenotypes with more copies and more severe phenotypes with fewer *SMN2* copies (Feldkötter et al., 2002). Most SMA type I patients carry only two copies of *SMN2*, most type II patients have three copies, whereas the majority of type III patients carries three to four copies, and more than four copies are found in patients with type IV (Feldkötter et al., 2002; Calucho et al., 2018; Wirth et al., 2006). Complete loss of SMN protein results in embryonic lethality (Schrank et al., 1997). Due to gene conversion, up to eight copies on *SMN2* are found (Schmutz et al., 2004; Mérette et al., 1994; M. Y. Dennis et al., 2017). Nevertheless, disease severity and progression can not be fully predicted by *SMN2* alone. Besides the copy number of *SMN2*, the severity can be influenced by missense mutations in the *SMN1* gene. The point mutations p.Tyr272Cys and p.Thr274Ile are the two most frequent missense mutations (Lefebvre et al., 1995; Jędrzejowska et al., 2014; Wirth, 2000; Hahnen et al., 1997). A more severe phenotype is observed in patients with the point mutation p.Tyr272Cys, and the mutation p.Thr274Ile was associated with a mild phenotype (Jędrzejowska et al., 2014).

Furthermore, SMN-independent modifiers of SMA phenotype have been identified in SMA patients (Wirth et al., 2013). Those modifier genes are differentially expressed in asymptomatic *SMN1*-deleted individuals. SMN-independent modifiers include F-actin binding and bundling protein plastin 3 (PLS3), coronin 1C (CORO1C), neurocalcin delta (NCALD) as well as calcineurin-like EF-hand protein 1 (CHP1) (Oprea et al., 2008; Hosseinibarkooie et al., 2016; Riessland et al., 2017; Janzen et al., 2018). While overexpression of PLS3 and CORO1C was found to ameliorate the SMA phenotype (Oprea et al., 2008; Hosseinibarkooie et al., 2016), reduction of NCALD or CHIP1 was found to be beneficial to SMA pathology (Riessland et al., 2017; Janzen et al., 2018). While the mechanism of PLS3 up-regulation and NCALD down-regulation is still under investigation, the protective effect is attributed to an increase of endocytosis, which is impaired in SMA (Riessland et al., 2017; Janzen et al., 2018; Hosseinibarkooie et al., 2016).

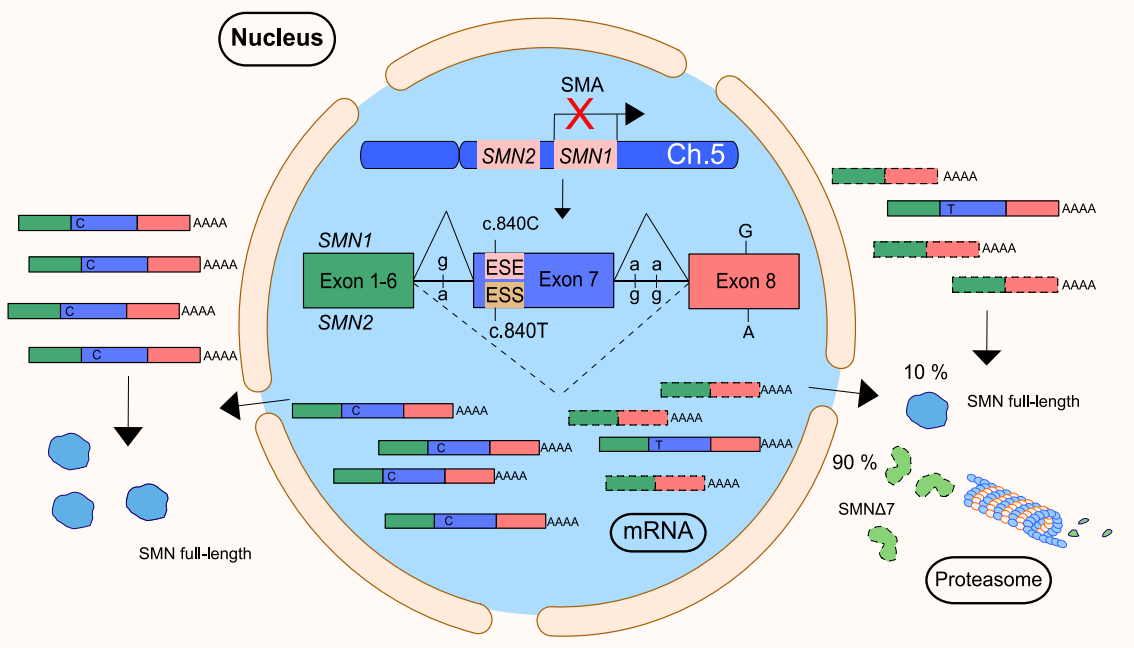

Figure 1: Illustration of *SMN* splicing and expression.
The telomeric *SMN1* and the centromeric *SMN2* are both located on chromosome 5. SMA patients rely sole on SMN produced from *SMN2* as they lack SMN protein from *SMN1* due to mutations or deletions in *SMN1*. *SMN1* and *SMN2* differ only in 5 nucleotide substitutions. Substitutions in the introns (lines) and exons (bars) are displayed. The only critical substitution is the C-to-T transition in exon 7 of *SMN2*. This transition creates an exon splicing silencer, resulting in the exclusion of exon 7 in $\approx$ 90% of the transcripts. Only $\approx$ 10% show exon 7 inclusion leading to full-length SMN protein expression. Transcripts lacking exon 7 result in SMNΔ7 protein which is rapidly degraded by the proteasome.

Besides those forms of SMA caused by mutations/ deletions in *SMN1*, there are also other types of SMA mediated by mutations in other genes. These include spinal muscular atrophy respiratory distress (SMARD, OMIM #604320), affecting primarily distal limb muscles, leading to severe respiratory distress caused by homozygous or compound heterozygous mutation in the IGHMBP2 gene (Mellins et al., 1974). Furthermore, Kennedy's disease is a rare form of SMA. The X-linked genetic disorder appears between the third and fifth decade of life and causes muscle weakness and wasting. Different from the 5q-SMA, it primarily affects the face and throat.

1.1.4 Molecular background (SMN protein)

SMN is a 294 amino acid, 38 kDa protein, which is ubiquitously abundant and performs multiple essential cellular functions, especially in RNA processing. The abundance of SMN protein is regulated during development, showing decreasing levels after the embryonic stage (Jablonka & Sendtner, 2017). Mouse models of SMA reveal that SMN abundancy is high in early neonates and significantly reduced in early postnatal days (Groen et al., 2018). Therefore, it is not surprising that severe SMA mice are born with a typical number of MNs but lose 35-40% of the spinal cord and lower brainstem MNs by day 5 (Monani et al., 2000). Consequently, conditional depletion of SMN in adults shows little effect compared to depletion of SMN in neonatal mice (Kariya et al., 2014). This effect was attributed to the temporal requirement for SMN at the NMJ maturation (Kariya et al., 2014). Consistent with the decreasing levels of SMN after

embryonic development, the small nuclear ribonucleoprotein (snRNP) assembly activity, being mediated by SMN, declines in mouse spinal cord in the first postnatal weeks (Sleigh et al., 2011).

Together with a highly conserved sequence of RNA and other proteins, SMN forms a ribonucleoprotein (RNP) complex, forming so-called 'gemini of coiled bodies' or 'gems'. This SMN RNP complex consists of small- nuclear RNAs (snRNA) and 7 proteins, Gemin2-8 (**Figure 2**) (Q. Liu & Dreyfuss, 1996; Pellizzoni, 2007; Gubitz, 2004). Furthermore, snRNA levels resemble the amount of snRNP as snRNAs that are not associated with Sm cores are unstable (Sauterer et al., 1988).

The SMN complex is localized in the cytoplasm, nucleus, and nuclear gems (Gemini of Cajal bodies), called Cajal bodies or coiled bodies (**Figure 2**) (Carvalho et al., 1999). In neurons, SMN localizes to axons and dendrites (Pagliardini, 2000). Since the cytoplasmic localization is exon 7 dependent, this might have a pathological effect in SMA (H. L. Zhang et al., 2003). SMNΔ7, encoded by the *SMN2* gene, is highly unstable and rapidly degraded by the proteasome (Chang et al., 2004). Moreover, full-length SMN itself is also relatively unstable without its binding partners (Lorson et al., 1998; Otter et al., 2007). Especially reactive oxygen species (ROS) can inhibit the complex formation by inducing intramolecular disulfide bridging, even at a subtoxic ROS level (Wan et al., 2008). SMN complex activity and formation are mainly regulated by phosphorylation, and mostly higher phosphorylation of cytoplasmic SMN indicates the regulation of snRNP biogenesis via phosphorylation status (Grimmler et al., 2005; Renvoisé et al., 2012).

1.1.5 Function of SMN

Despite the predominant MN related symptoms of SMA, complete loss of SMN protein is embryonic lethal, suggesting an essential function for fundamental cellular processes in all cells (Schrank et al., 1997). It is known that the SMN complex mainly functions as an assemblysome, regulating snRNP structure, biogenesis, and function (Q. Liu et al., 1997). The assembly of snRNPs is the best-characterized function of SMN. While the assembly of snRNPs can occur spontaneously *in vitro*, it is a highly conserved and tightly regulated process in cells (Pellizzoni, 2002). In the biogenesis of those snRNPs, SMN binds specifically to Sm proteins and snRNAs and facilitates the assembly of the Sm proteins onto the Sm site of the RNA (Buhler et al., 1999). The majority of snRNP biogenesis occurs in the cytoplasm after U small nuclear RNAs are transcribed in the nucleus and exported to the cytoplasm. SMN is only necessary for the assembly of snRNPs, as it has been shown that injection of snRNPs is sufficient to rescue the pathologic phenotype in zebrafish (Winkler, 2005). Accordingly, the SMN complex acts as a molecular chaperone, assembling the snRNP complex without being part of the final structure (D. K. Li et al., 2014). Correct splicing of pre-messenger RNA (mRNA) is essential for eukaryotic gene expression, and an incorrect assembly of the spliceosome leads to severe defects such as seen in SMA. The spliceosome is composed of five uridine-rich snRNPs, namely U1, U2, U5, and U4/U6 (Will & Lührmann, 2001).

Based on the role of SMN in spliceosome formation and the loss of SMN in SMA, missplicing of MN-specific pre-mRNAs has been hypothesized. Those pre-mRNA sets might be crucial for

MN development and survival. Indeed, *Agrin* is misspliced in MNs of SMA mice and functions in organizing acetylcholine receptors at the NMJ (J.-K. Kim et al., 2017). Additionally, several other splicing changes were found after SMN depletion, and those contribute to late pathology in SMA mice (Custer et al., 2016; Bäumer et al., 2009).

Besides the assembly of snRNPs, which ensures correct pre-messenger RNA splicing, SMN functions in the metabolism, transport, and assembly of other RNP classes, including telomerase RNPs or microRNPs (Mourelatos, 2001, 2002; Buhler et al., 1999). Furthermore, after being assembled into mRNA- binding proteins (mRBPs), SMN fulfills additional steps in mRNA processing (**Figure 2**). Those additional functions include but are not limited to intracellular trafficking, nuclear export of mRNA, and translation. SMN interacts with mRBPs to assemble mRNA transport granules directing to axons (Akten et al., 2011; Rossoll et al., 2003). Such mRBPs include hnRNP, HuD (ELAVL4, ELAV like RNA binding protein 4), KSRP (KH-type splicing regulatory protein), hnRNPs (heterogeneous nuclear ribonucleoproteins), and IMP1 (also known as IGF2BP1, Insulin like growth factor 2 mRNA binding protein 1) (Akten et al., 2011; Tadesse et al., 2007; Fallini et al., 2011; Dombert et al., 2014; Fallini et al., 2014). Those mRNP transport granules are formed by the association of mRBPs with the 3' untranslated region (3' UTR) of the mRNAs (Andreassi & Riccio, 2009). In this context, axonal bidirectional transport has been shown in axons of primary MNs, and forebrain (H. L. Zhang et al., 2003; Fallini et al., 2011; Rossoll et al., 2003). After being transported to specific subcellular compartments, mRNAs and mRPBs form micro-environments for local translation that can create stimulus-driven responses (Wu et al., 2005; K.-M. Leung et al., 2006). In SMA, reduced local translation of several mRNAs including β-*actin*, *growth-associated protein 43 (GAP43)* and *neuritin/cpg15* have been described upon defective trafficking (Akten et al., 2011; Rossoll et al., 2003; Hubers et al., 2011).

As SMN is highly abundant, especially during nervous system development in the axons of MNs, the MN-specific phenotype in SMA might be related to the function as a molecular chaperone for β-actin mRNA localization (Giavazzi et al., 2006). Furthermore, mislocalization and a general reduction of axonal mRNAs have been shown in *Smn* KD mouse MNs (Fallini et al., 2011, 2016).

Moreover, SMN can directly bind to ribosomes in a tissue-dependent manner. This direct association of SMN with ribosomes regulates the translation of SMA-related transcripts, including mRNAs associated with translation, neurogenesis, ubiquitination, and lipid metabolism. Furthermore, reduced SMN levels induce ribosome depletion (Lauria et al., 2020).

Reduced and/or mislocalized SMN protein levels lead to several pathomechanisms affected in SMA. Those include defects in endocytosis, RNA processing, protein synthesis and homeostasis, metabolic dysfunction, defects in the actin cytoskeleton, and Ca^{2+} homeostasis have been identified using those mouse models (Bernabò et al., 2017; Hosseinibarkooie et al., 2016; Custer et al., 2016; Kye et al., 2014; Rossoll et al., 2003; Jablonka et al., 2007). Additionally, defects in micro RNA (miRNA) metabolism have been associated with reduced SMN levels (Kye et al., 2014). Especially miR-183 was found to be increased and associated with translation through mTOR via direct binding to its 3' UTR (Kye et al., 2014). Other miRNAs are also associated with SMN deficiency due to altered DROSHA levels in SMA MNs (Kye et al., 2014; Gonçalves

et al., 2018). Furthermore, the reduction of MN-specific miR-218 has been associated with systemic neuromuscular failure due to NMJ impairments, hyperexcitability, and MN cell death (Amin et al., 2015). Additionally, multiple miRNAs have been linked to neurodegenerative diseases such as Alzheimer's (AD), Parkinson's (PD), amyotrophic lateral sclerosis (ALS), or Huntington's (HD) (Kye et al., 2014; John et al., 2020). Moreover, mitochondria specific miRNAs have been shown to play an essential role in aging and neurodegeneration (John et al., 2020; Catanesi et al., 2020).

Unlike other neurodegenerative diseases, where accumulations of RNA-binding proteins form pathological aggregates, SMA is characterized as an RNP hypo-assembly disease, deficient in RNP formation (Shukla & Parker, 2016).

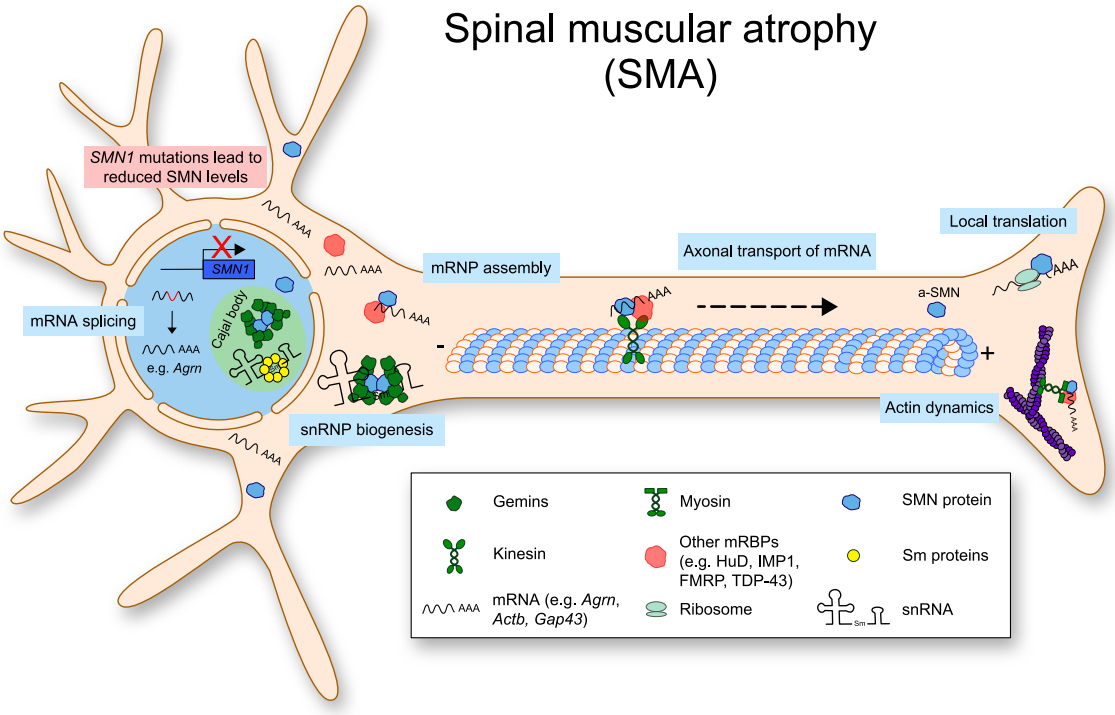

Figure 2: Functions of SMN in MNs.
SMN is localized to the nucleus, the soma, dendrites, and axon. Here, SMN forms the SMN complex by binding to snRNAs and other proteins. SMN performs multiple functions in MNs. Besides its main function in snRNP biogenesis and splicing, SMN is important for mRNP assembly, axonal transport of mRNA, actin dynamics, and local translation. SMN binds to mRNAs and mRBPs. Anterograde, axonal transport is accomplished by motor proteins such as kinesin. (Thelen & Kye, 2020).

1.1.6 Mouse models

When patient material is inaccessible, it is quite useful to work with an animal model to study basic pathological mechanisms. In SMA, MNs, the primary affected cell type, are only available for postmortem analyses. Alternatively, MNs can be differentiated from induced pluripotent stem cells (iPSCs) or by direct conversion of fibroblasts (Son et al., 2011). This limits the use of MNs to validate therapeutic approaches or to identify basic cellular mechanisms causing SMA. For this reason, many animal models in various organisms have been generated.

Those organisms include invertebrates such as *Caenorhabditis elegans* and *Drosophila*, but also vertebrates such as zebrafish, mice, and pigs (Edens et al., 2015; Duque et al., 2015). However, the duplication of the *SMN1* gene is unique to the human genome, and therefore none of the species develop SMA naturally. Over the last years, many different techniques have been developed to mimic genetic diseases in other organisms.

Here, we want to focus on SMA mouse models. As SMN is crucial for cell survival, homozygous knockout of *Smn* is embryonically lethal due to massive cell death during early blastocyst formation (Schrank et al., 1997). Some techniques used to mimic SMA are conditional knockout, the introduction of mutations, or the introduction of the human *SMN2* gene (Monani et al., 2000; Hsieh-Li et al., 2000; Le et al., 2005). When human *SMN2* or *SMN* lacking exon 7 (*SMN*Δ*7*) are introduced, the disease severity varies upon the copy number, similar to what is observed in humans (Monani et al., 2000; Hsieh-Li et al., 2000). This fact has been used to create various mouse models differing in their severity.

The first SMA mouse models, called the "Taiwanese" mouse model and "Line89", were created in 2000 (Hsieh-Li et al., 2000; Monani et al., 2000). However, being genetically and phenotypically similar, the Taiwanese mouse model was generated by introduction of the human *SMN2* transgene and knocking out of the murine *Smn* exon 7 (Hsieh-Li et al., 2000), for the Line89 model an *Smn* exon 2 knockout was used (Monani et al., 2000). With an average lifespan of 5.2 days the Line89 mice, harbouring two human *SMN2* copies on a murine *Smn* null background, resemble a severe SMA phenotype (Monani et al., 2000). Further addition of an *SMN*Δ*7* transgene extends the lifespan from 5.2 to 13.3 days and results in a milder phenotype (Le et al., 2005). Besides adding human *SMN*Δ*7* copies on an *Smn* null background with two *SMN2* copies, the introduction of an *SMN1* A2G missense mutation ($Smn^{-/-}$; $SMN2^{tg/-}$; *SMN1*A2G, stock #005026) results in a mild type III SMA phenotype. Furthermore, the introduction of eight *SMN2* copies is enough to fully rescue the phenotype, resulting in an expanded lifespan (Monani et al., 2000).

In this study, the Taiwanese mouse model was used. A phenotypically normal, heterozygous $Smn^{+/-}$ animal was crossbreed with a homozygous mouse harbouring 4 copies of human *SMN2* on a murine *Smn* null background, $Smn^{-/-}$; $SMN2^{tg/tg}$ (Riessland et al., 2010). The homozygous animal with 4 human *SMN2* transcripts does not show a MN phenotype but shows necrosis in the tail, toes, and ears. The resulting mouse model has no murine *Smn*, but 2 copies of human *SMN2*, $Smn^{-/-}$; $SMN2^{tg/-}$. Finally, these mice show a severe phenotype that closely resembles the human Type I SMA phenotype, including impaired motor function, loss of spinal MNs, defects in the NMJ, and survival of 10-15 days (Ackermann et al., 2013; Riessland et al., 2010). However, the mean survival varies between C57BL/6 background and FVB/N background with a shorter lifespan of SMA mice on an FVB/N background (Ackermann et al., 2013; Riessland et al., 2010; Hosseinibarkooie et al., 2016).

Conditional knockout can be used to evaluate tissue-specific disease mechanisms. Whereas neuronal deletion of *Smn* exon 7 leads to MN loss and an average lifespan of 25 days (Frugier et al., 2000), knockout in muscles lead to muscle necrosis, paralysis, and death (Cifuentes-Diaz et al., 2001). The conditional knockout of *Smn* in muscle and the resulting phenotype allows for studies of muscle-specific defects in SMA. Similar to the phenotype observed in humans,

transgenic mice show loss of spinal MNs, defective NMJs, impaired muscle function, and reduced survival.

In addition to the genetic variability in those mouse models, the phenotype can be modulated by up-regulation of SMN levels using antisense oligonucleotides (ASOs). The use of ASOs results in a milder phenotype that can be used to study the effects of reduced SMN in internal organs later in disease progression. Many SMA pathomechanisms, including defects in endocytosis, RNA processing, protein synthesis, protein homeostasis, metabolic defects, and defects in the actin cytoskeleton, and Ca^{2+} homeostasis have been identified using those mouse models (Bernabò et al., 2017; Hosseinibarkooie et al., 2016; Custer et al., 2016; Kye et al., 2014; Rossoll et al., 2003; Jablonka et al., 2007). Severe mouse models of SMA revealed that impairments of internal organs drive lethality.

1.1.7 Treatment

As a reduction of SMN causes SMA, several therapies have been developed to increase SMN levels. Further, attempts aim to improve SMA pathology targeting SMN-independent pathways. The different approaches can be classified as SMN dependent or SMN independent therapies based on their mode of action. Fortunately, the duplication of the genetic region of *SMN1*, creating *SMN2* gives a unique opportunity for treatments. As lack of SMN is embryonically lethal (Schrank et al., 1997), patients with the most severe form of SMA have at least one copy of *SMN2* (Macleod et al., 1999). Therapies aiming to increase SMN levels can therefore enhance correct splicing of *SMN2* to form more of the full-length protein or repair the mutated *SMN1* gene directly (Farrar et al., 2017; Sumner & Crawford, 2018; Wirth, 2021). The first approved drug is Nusinersen.

Currently, all approved drugs are based on SMN-enhancing approaches. However, multiple therapies not focusing on SMN enhancement are in the pipeline of clinical trials.

Spinraza (Nusinersen), developed by Ionis Pharmaceuticals and Biogen, was approved in 2016 by the Food and drug administration (FDA) and in 2017 by the European medicines agency (EMA) to treat all patients with SMA. Multiple intrathecal (IT) injections of Spinraza maintaining doses are needed with 4 months intervals for a lifetime after loading doses are completed (Neil & Bisaccia, 2019; Wirth, 2021).

The drug is designed to enhance correct splicing and inclusion of exon 7 from *SMN2* by ASOs. The small single-stranded, synthetic oligonucleotides bind to the *SMN2* pre-mRNA intron downstream of exon 7. By blocking an intron splicing silencer (ISS), it enhances the inclusion of exon 7, leading to an increase of full-length SMN production (Hua et al., 2008). The intronic target is identified to be the ISS-N1 gene sequence (Singh et al., 2006). Blocking the ISS-N1 site with an ASO increases the stability of the U1 snRNP machinery that recognizes exon 7 (Hua et al., 2008).

Even though the treatment of very severe SMA type 0 patients with Spinraza is reported, it showed only minimal improvement on mobility, but it was insufficient to mitigate the multisystemic involvement and overall severity (Tiberi et al., 2020; Kitaoka et al., 2020). Even though treatment with Nusinersen prolonged survival and lead to motoric improvements in all

types of SMA patients, effectiveness depends on several factors, including *SMN2* copy number, disease stage, and age (Finkel et al., 2017; Mercuri, Darras, et al., 2018; Wirth, 2021). Here, the occurrence of non-responders highlights the need for SMN-independent strategies (Hensel et al., 2020).

Zolgensma (Onasemnogene Abeparvovec), developed by Avexis and Novartis, was approved by the FDA in 2019 to treat patients younger than 2 years with infantile-onset SMA. The administration later in life is not possible due to the impenetrable blood-brain barrier for self-complementary adeno-associated virus 9 (scAAV9). Approval by the EMA was given in 2020 for patients diagnosed with SMA Type I or SMA patients with less than 3 *SMN2* copies. According to the EMA's approved dosing guidance, approval covers children with SMA up to 21 kg. The administration of Zolgensma is a one-time intravenous (IV) infusion.

The gene replacement therapy with Zolgensma uses a scAAV9 targeting MNs and expressing *SMN1* cDNA under a strong chicken β- actin promotor. It replaces the missing or mutated *SMN1* gene to produce full-length SMN resulting in improved muscle movement and function and extended lifetime (Mendell et al., 2017).

Evrysdi (Risdiplam), developed by PTC Therapeutics and Roche, was approved by the FDA in 2020 and Marketing Authorization Application (MAA) for orphan designation by the EMA in 2020. It is a daily, orally administered small molecule for patients at two months of age and older.

Like Spinraza, Evrysdi is designed to act as an *SMN2*-directed RNA splicing modifier (Naryshkin et al., 2014). However, as it is intended to be a small molecule, oral administration is possible (Poirier et al., 2018). Furthermore, while Spinraza is designed to target the central nervous system (CNS), Evrysdi distributes evenly through the whole body.

In addition, combinatorial therapies are possible. However, treating a Type 0 infant with Spinraza and Zolgensma lead to the need for tracheostomy with only some motor improvement with significant medical morbidity (Matesanz et al., 2020). Regardless of the therapy, additional measures such as pulmonary, gastrointestinal, nutritional, and spinal management are required. Therefore, specific standard of care considerations have been developed based on the motor ability of the SMA patients: non-sitter, sitter, and walker (Mercuri, Finkel, et al., 2018; Finkel et al., 2018). Untreated, most SMA patients develop scoliosis, an abnormally curved spine that requires surgery (Granata et al., 1989).

In the end, the starting point of treatment is crucial and is dependent on the maturation status of the NMJ (Kariya et al., 2014). Therefore, it is crucial to start therapy as soon as the diagnosis is available or even better before symptoms arise. This requires newborn screening as symptoms in the severe form of SMA can already occur quickly after birth. In fact, up to 90% of MNs can be lost already six months after birth in severe SMA type I patients (Courtney et al., 2019). Accordingly, neuronal death can not be reverted. Despite the number of life-prolonging treatments available for SMA, there is still no cure.

1.2 Energy homeostasis

Energy homeostasis is the crucial step in keeping the balance between energy consumption and energy production, mainly in the form of adenosine triphosphate (ATP). Besides using glucose to generate ATP, cells can also handle amino acids or fatty acids. However, glucose is the obligatory energy substrate for the brain (Kety & Schmidt, 1948). Neurons are the most energy-consuming cell type, and as a result, the brain is the most energy-consuming organ (Vergara et al., 2019; Howarth et al., 2012). Even though the brain makes up only 2% of the body weight, it consumes 20% of the total energy produced by the body (Mink et al., 1981; Rolfe & Brown, 1997).

Neuronal energy consumption used for signaling can be divided in 47% to generate action potentials, 34% for postsynaptic currents, 13% to sustain the resting potential and 3% for glutamate recycling (**Figure 3**) (Attwell & Laughlin, 2001). First, ATP-driven Na^+/K^+-ATPases along the axon claim energy to generate the action potential and restore the membrane potential (Harris et al., 2012). Therefore, oxygen consumption, necessary for ATP production, is mainly controlled by the axonal length, branching complexity, ion channel density, and the action potential rate (Attwell & Laughlin, 2001). Second, axonal transport of mitochondria, ribosomes, or RNPs require energy, and their dysfunction is a common pathological mechanism in peripheral neuropathies (**Figure 3**) (Prior et al., 2017).

Due to the high energy demand during synaptic transmission, it is not surprising that the white matter consumes less than 0.5% of the energy compared to the grey matter, as the white matter contains 80- fold fewer synapses (Harris & Attwell, 2012). Furthermore, inhibitory neurons require less energy than excitatory, as the reversal potential is closer to the resting potential (Howarth et al., 2010).

In general, translation is a highly energy-demanding process that consumes up to 20% - 30% of total ATP in mammals (Buttgereit & Brand, 1995). Neurons use most of their so-called housekeeping energy, which is not used for signaling, for lipid synthesis, and mitochondrial proton leak (Rolfe & Brown, 1997). Protein synthesis is used for only 1.3% of total energy consumption in the brain (Attwell & Laughlin, 2001; Rolfe & Brown, 1997). Protein synthesis requires 4 ATP molecules per peptide bond (Waterlow, 1984). Energy is needed for the activation of acyl-tRNA, initiation, and termination. The amount of ATP required for initiation depends on the mRNA species (Jackson, 1991). It is assumed that cap-dependent processes consume the highest amount of ATP during initiation (Jackson, 1991).

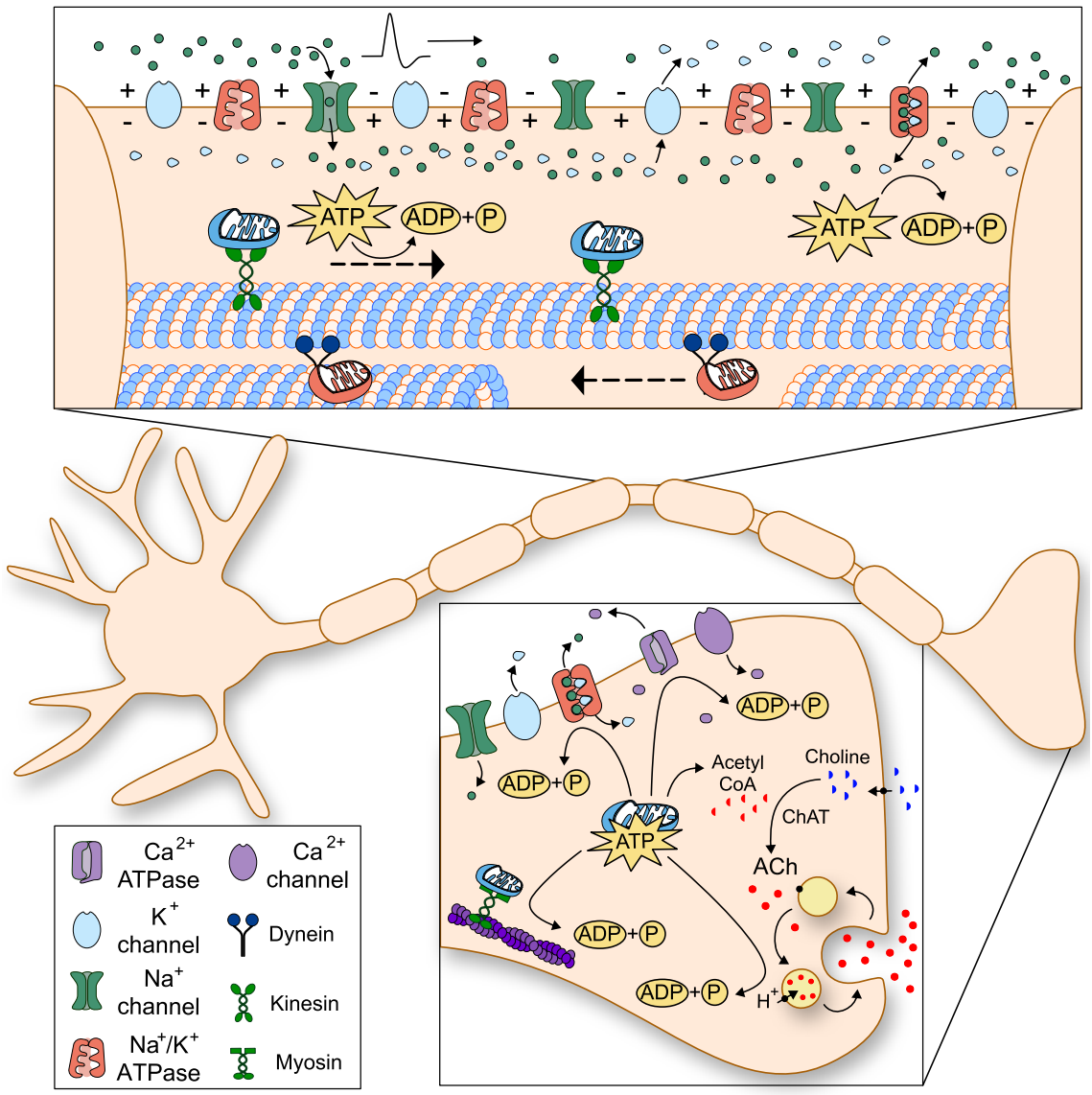

Figure 3: Energy consumption and neurotransmitter release in neurons.
Neurons consume energy in various processes. Especially, active synaptic transmission is highly energy demanding. Energy in the form of ATP is necessary for the transport of mitochondria and several mRBPs by kinesin in the anterograde and dynein in the retrograde direction. Mitochondria are transported anterogradely to provide ATP at distal ends of the neurons and retrogradely to return defective mitochondria to the soma for degradation. During an action potential, Na^+ accesses the axon via voltage-gated Na^+ channels, causing a depolarization. Further, K^+ extrusion via voltage-gated K^+ channels, results in a repolarization of the axon. Further, ATP is required by the Na^+/K^+-ATPase to restore the membrane potential by exchanging Na^+ and K^+. As soon as the action potential reaches the axonal tip, influx of Ca^{2+} promotes the release of neurotransmitter at the active zone. Here, ATP is needed to fuel Ca^{2+}-ATPases for Ca^{2+} export. In addition, vacuolar H^+- ATPases energize vesicle transmitter uptake for neurotransmitter release. Mitochondria are further needed to provide acetyl coenzyme A (CoA), which is necessary for acetylcholine production by the enzyme choline acetyltransferase (ChAT).

1.2.1 Glycolysis

Glucose can be metabolized aerobically in the cytosol into pyruvate that is further used in mitochondria. When oxygen is limited, glucose can be metabolized into pyruvate and further reduced to lactate to regenerate NAD^+ from NADH. However, full oxidation of glucose leads to much higher ATP levels as glycolysis only generates 2 mol ATP per mol glucose.

Glucose transporters (GLUT) facilitate glucose import. Among the GLUT superfamily of 14 isoforms expressed in humans, GLUT1 and GLUT3 are the predominant isoforms in neurons (Vannucci et al., 1997). GLUT3 is found to be 6-10-fold higher expressed than GLUT1 (Maher & Simpson, 1994). GLUT4 is present at nerve terminals and recruited to the plasma membrane upon neuronal stimulation (Ashrafi et al., 2017). GLUT4 seems essential for synaptic transmission, as loss of GLUT4 leads to an arrest of synaptic vesicle endocytosis (Ashrafi et al., 2017). GLUT3 provides a constant glucose source in physiological and pathophysiological conditions (Gerhart et al., 1992).

Besides glucose, neurons can use lactate derived from glia. The controversial astrocyte-neuron lactate shuttle model (ANLS) demonstrates the lactate production in astrocytes upon glutamate transients and the subsequent shuttle of lactate from astrocytes into neurons (Brooks, 2002; Mächler et al., 2016; Pellerin & Magistretti, 1994). Moreover, lactate has been demonstrated to sustain neuronal activity upon glucose deprivation *in vitro* and *in vivo* (Schurr, 2002; Wyss et al., 2011). More recent studies identified that glycolysis is increased upon neuronal activation, but lactate uptake is unaltered (Díaz-García et al., 2017; Yellen, 2018). *In vivo* studies even further suggested that neurons rather export than import lactate upon stimulation (Díaz-García et al., 2017).

Glycolysis is facilitated to produce energy and generate reducing equivalents for subsequent oxidative phosphorylation (OXPHOS) in neurons. Especially, neuronal activation leads to a transient increase of cytosolic NADH:NAD^+ (Díaz-García et al., 2017). However, lactate import is not required to generate the transient NADH as glycolysis up-regulation is sufficient to cover the need for reducing equivalents (Díaz-García et al., 2017).

Even though OXPHOS bears the advantage of producing higher ATP yields, glycolysis can be facilitated at a much higher rate (Pfeiffer et al., 2001). The higher energy production rate can be beneficial to adapt to recent events and external stimuli (Rangaraju et al., 2014). Therefore, glycolytic enzymes can be redistributed or locally translated under energy stress to form clusters termed "glycolytic metabolon" (Jang et al., 2016). The spatial compartmentalization is mainly required to facilitate the synaptic vesicle cycle and localizes to nerve endings (Jang et al., 2016; Rangaraju et al., 2014; Knull et al., 1980).

The metabolic compartment harboring glycolytic enzymes was also observed *in vivo* in *Caenorhabditis elegans* (Jang et al., 2016). The glycolytic metabolon formation was suppressed after phosphofructokinase 1 (PFK-1.1) depletion, a rate-limiting enzyme in glycolysis (Jang et al., 2016). Impaired glycolysis has been associated with neurodegenerative diseases. Glucose metabolism is impaired in neurons of an ALS mouse model carrying a mutation in the SOD1 gene (Tefera & Borges, 2019). However, up-regulation of glycolysis by overexpression of human GLUT3 in *Drosophila* MNs has been shown to be beneficial (Manzo et al., 2019). Furthermore, glycolytic impairments with a reduced glycolytic flux were observed in AD patients (An et al.,

2018).

1.2.2 Mitochondria

Mitochondria are membrane-bound organelles composed of two membranes. The outer membrane enclosing the whole organelle, and the inner membrane is forming the folded structure of the cristae surrounding the matrix. Proteins of the electron transport chain are localized to the cristae, the folded inner mitochondrial membrane. The electron transport chain consists of five complexes, transferring electrons from electron donors to electron acceptors, performing a series of oxidation-reduction reactions. Therefore, reducing agents generated by the glycolysis or the tricarboxylic acid (TCA) cycle are oxidized, and protons are exported into the intermembrane space. The NADH: ubiquinone oxidoreductase (complex I) of the electron transport chains is the largest complex, the rate-limiting step in respiration, and the primary entry point for electrons (L. Sharma et al., 2009; Hirst, 2011). The ATPase performs the actual generation of energy at the end of the electron transport chain. Here, protons generate an electrical potential, the mitochondrial membrane potential that drives the ATPase upon extrusion.

Mitochondrial proteins are encoded in the nucleus and within their own mitochondrial DNA (mtDNA). Only 13 protein-coding genes are found in the mitochondrial genome, and most protein-coding genes are encoded in the nucleus. The largest complex, namely complex I, consists of 44 proteins, contains 7 proteins encoded in the mtDNA and 38 proteins encoded in the nucleus (Chinnery & Hudson, 2013; Hirst, 2011). The tasks of mitochondria range from ATP generation, Ca^{2+} buffering, ROS generation, cell signaling activities, to antioxidant activity (Adam-Vizi & Starkov, 2010; McBride et al., 2006).

After glycolysis, respiration continues within the mitochondria in the TCA cycle and OXPHOS. The TCA cycle uses acetyl-CoA derived from proteins, fats, or carbohydrates. The TCA cycle produces energy in the form of 2 mol ATP per mol glucose and precursors for amino acids and reducing equivalents for subsequent OXPHOS. The highest amount of energy is generated by the OXPHOS; in the form of 34 mol ATP per mol glucose.

Mitochondria are not only localized in the soma but also the distal ends of neuronal cells. The number of mitochondria varies as certain cells such as muscle or liver contain many mitochondria, but red blood cells have none. The importance of local mitochondria at the synapse becomes clear considering that ATP synthesized in the soma needs 2 min to diffuse along a 200 µm neurite (Harris et al., 2012). Mitochondria are transported by kinesin and dynein motor proteins along the microtubule at $\approx$ 0.3-1 µm/s to overcome the slow diffusion rate (MacAskill et al., 2010). The major kinesin motor protein transporting mitochondria away from the soma is the Kinesin-related protein 5 (KIF5) (Tanaka et al., 1998). Nevertheless, KIF1B has been identified as a microtubule plus end-directed motor protein transporting mitochondria (Nangaku et al., 1994). Once mitochondria reach dendritic spines or the synapses, myosins transport them along actin filaments (Ligon & Steward, 2000). Nevertheless, the majority of mitochondria ($\approx$ 80%) are stationary to provide energy. Mitochondrial stalling primarily occurs at axonal branching points or presynaptic terminals or the axon tip (Sakata & Jones, 2003; Spillane et al., 2013). Mitochondria cluster in spatially defined compartments to meet local energy demands and localization to the clusters is regulated by neuronal activity (X. Wang &

Schwarz, 2009).

Besides the transport of mitochondria along the axon, biogenesis of mitochondrial protein can occur locally upon stimulation (Kuzniewska et al., 2020). Accordingly, local mitochondria produce energy to fuel local translation for mitochondrial proteins to assemble the electron transport chain to provide more energy (Kuzniewska et al., 2020).

1.2.3 Reactive oxygen species (ROS)

ROS are highly reactive molecules generated upon reduction of molecular oxygen. ROS can emerge as unstable free radicals, carrying an unpaired electron or as more stable non-radical in the cell (Kohen & Nyska, 2002; Phaniendra et al., 2015). Superoxide ($O_2^{\bullet -}$) is the main free radical produced in the mitochondrial matrix (Munro & Treberg, 2017; Jensen, 1966). Besides ($O_2^{\bullet -}$), hydroxyl radicals ($^{\bullet}OH$) can be found with an even shorter half-life than $O_2^{\bullet -}$ (Phaniendra et al., 2015). However, the copper/zinc superoxide dismutase 1 (SOD1) in the cytoplasm and the manganese superoxide dismutase 2 (SOD2) in the mitochondrial intermembrane space convert $O_2^{\bullet -}$ rapidly into the non-radical, membrane-permeable hydrogen peroxide (H_2O_2) (Chance et al., 1979; Loschen et al., 1974; Forman & Kennedy, 1974; Weisiger & Fridovich, 1973).

Besides being the primary energy producer, mitochondria also generate the highest amounts of reactive oxygen species (ROS) in the electron transport chain. The leakage of electrons leads to a partial reduction of oxygen, resulting in the formation of $O_2^{\bullet -}$. The generation of free radicals increases exponentially with an increased membrane potential (Korshunov et al., 1997; S.-s. Liu, 1999). Being the primary entry point for electrons, complex I is also the major producer of ROS (Y. Liu et al., 2002). ROS levels are exceptionally high when the proton motive force (mitochondrial membrane potential) and the $NADH/NAD^+$ ratio are high in the absence of ATP production (Murphy, 2009). ROS needs to be well balanced in a cell to execute various functions. At non-toxic concentrations, ROS activates different pathways, including the MAPK, PI3K, Akt, p38 MAPK, mTOR, and Ca*2+* signaling (J. Zhang et al., 2016). For example, low ROS levels can stimulate mTOR activity, but in high doses, it decreases mTOR activity via the oxidative stress pathway (M. Li et al., 2010).

When ROS levels exceed the antioxidative capacity of a cell, they can lead to oxidative stress and damage proteins or DNA. Accordingly, ROS can lead to irreversible and unrepairable carbonylations of proteins (Nyström, 2005; Stadtman, 1990). Furthermore, carbonylations can lead to conformational changes, proteolysis, or the formation of high-molecular-weight aggregates that accumulate within the cell (Nyström, 2005). When proteins involved in the translational machinery are affected by carbonylation, global protein synthesis can be attenuated (Topf et al., 2018).

1.2.4 Mitochondria in neurodegenerative disease

Based on the multiple functions of mitochondria, it is not surprising that defects lead to pathological features. Accordingly, defective respiration and impairments in the biosynthesis of amino acids, Ca^{2+} buffering, β-oxidation, and regulation of ROS results in neurodegeneration (Davis & Williams, 2012). Additionally, mitochondria play a role in regulating apoptosis

(C. Wang & Youle, 2009). Further, it has been suggested that mitochondrial defects are a cause rather than a consequence of neurodegeneration (Johri & Beal, 2012).

Sustained imbalance of a cell's redox state leads to oxidative stress that has been associated with aging and various diseases, including neurodegenerative diseases (Ashok & Ali, 1999). The imbalance is a result of increased ROS generation or an impaired antioxidative capacity. Persistent oxidative stress can alter lipids, proteins, and DNA. Accordingly, an increase of carbonylated proteins resulting from sustained oxidative stress has been associated with PD, AD, and HD (Levine, 2002; Dalle-Donne et al., 2003; Schulz & Beal, 1994; Browne et al., 1997). In PD, oxidative stress further results in DNA damage, leading to 8-hydroxy-2'-deoxyguanosine formation (Alam et al., 2002). Furthermore, damage on nuclear and mitochondrial DNA upon increased oxidative stress has been shown in AD (J. Wang et al., 2005; Mecocci et al., 1994).

Moreover, oxidative stress leads to damage of proteins, lipids, and DNA in the neuromuscular diseases ALS, where SOD1 is mutated (Ferrante et al., 2002; Rosen et al., 1993). Here, the loss of antioxidative capacity is detrimental to the cell and the formation of toxic aggregates within the mitochondria, resulting in impaired respiration and mitochondrial function (Boillée et al., 2006; Vijayvergiya, 2005; Ferri et al., 2006).

Over the last years, various impairments in energy homeostasis, including defective mitochondria and increased oxidative stress, have been found in SMA (Acsadi et al., 2009; Hayashi et al., 2002; C. C. Xu et al., 2016; Miller et al., 2016). Moreover, the hypothesis that mitochondrial defects are instead a cause than a secondary effect is strengthened by the fact that mitochondrial defects occurred before the onset of disease symptoms in SMA (Miller et al., 2016). Transcriptome analyses showed a reduction in vacuolar H^+-ATPase at a pre-symptomatic stage in a *Caenorhabditis elegans* SMA model (X. Gao et al., 2019). Early studies on SMA energy homeostasis revealed reduced ATP levels upon SMN reduction in NSC-34 cells (Acsadi et al., 2009). Moreover, a decrease of SMN leads to increased oxidative stress in those cells (Acsadi et al., 2009). Later, spinal MNs generated from SMA type 1 patient-specific iPSCs display a reduced mitochondrial number, area, transport, and membrane potential (C. C. Xu et al., 2016). This circumstance was further shown to be MN-specific, as the impairments observed in iPSCs were not observed in SMA forebrain neurons (C. C. Xu et al., 2016). Moreover, the impairments in mobility, shape, and membrane potential could be rescued upon the addition of N-acetylcysteine (NAC) (C. C. Xu et al., 2016). Additionally, a transcriptome analysis of spinal MNs in an SMA mouse model revealed changes in mitochondrial genes (Miller et al., 2016). Further functional analyses in this study confirmed the impairments of reduced respiration, mitochondrial mobility, and increased oxidative stress seen in iPSCs (Miller et al., 2016). Recent studies confirmed the ATP reduction in an *in vivo* SMA zebrafish model (Boyd et al., 2017).

However, contradictory findings about the increase of oxidative stress in SMA iPSC- derived astrocytes and MNs has emerged (Patitucci & Ebert, 2016). This finding implicated that oxidative stress caused by SMN deficiency is cell-type specific.

Furthermore, impaired mitochondrial biogenesis and depletion of mtDNA have been found to be impaired in quadriceps muscles of SMA type I-III patients (Ripolone et al., 2015). Moreover, it has been shown that the bioenergetic status of MNs innervating different muscles contributes

to their vulnerability in mice (Boyd et al., 2017). On a molecular basis, oxidative stress can impair SMN function by inactivating the SMN complex formation (Wan et al., 2008).

Additionally, miRNA biogenesis defects have been suggested to contribute to neurodegenerative and neuromuscular diseases, including AD, HD, ALS, and SMA (Gonçalves et al., 2018; Kye & Gonçalves, 2014). Further, many miRNAs are associated with mitochondria (Duarte et al., 2014).

1.3 Translation

The translation is part of the gene expression and is performed by ribosomes in the cytoplasm or on the endoplasmic reticulum (ER). Briefly, long chains of amino acids are formed by the binding of amino groups and carboxyl groups of amino acids. In general, translation is a process, which is performed through the decoding of mRNA by ribosomes, supported by other proteins, called translation factors (Nürenberg-Goloub & Tampé, 2019; Nakamoto, 2011).

The traditional translation of ribosomes is divided into three phases: Initiation, elongation, and termination. The starting point of the translation is the attachment of the mRNA to the small 40S ribosomal subunit of the ribosome. With this, the mRNA is attached to the ribosome and a transfer RNA (tRNA) conjugated with a methionine (Met) residue that can bind to the peptidyl (P) site of the small ribosomal subunit, specifically at the start codon AUG. Binding of the 40S subunit with GTP- bound eukaryotic initiation factor (eIF)2 and the Met-tRNA forms a ternary complex required for translation initiation (**Figure 4**). Together with other proteins including eIF1, eIF1A, eIF5, and eIF3 the 43S preinitiation complex (PIC) is formed (**Figure 4**). Attachment of the 43S PIC to the 5' 7-methylguanosine (m^7G) cap of the mRNA is facilitated by the heterotrimeric eIF4F complex (**Figure 4**). The eIF4F complex contains the DEAD-box RNA helicase eIF4A, the cap-binding protein eIF4E, and the large "scaffold" protein eIF4G and forms the 48S PIC together with the 43S PIC. Upon phosphorylation, eIF4B associates with eIF4A and enhances its helicase activity (Andreou et al., 2017). Interaction of eIF4G with eIF4E increases the affinity of eIF4E to the 5' cap structure (Gross et al., 2003). The cap-binding protein eIF4E is phosphorylated via the protein kinases MAP kinase-interacting serine/threonine-protein kinase 1 (MKNK1) and MKNK2, downstream of the activated extracellular signal-regulated kinase (ERK) and p38. Circularization of the mRNA is enabled after binding of the poly(A) binding protein (PABP) to the poly-A tail, and eIF4G (Kahvejian et al., 2005). Using ATP, eIF4A unwinds the 5' UTR, and the 48S PIC can scan the mRNA for the start codon, AUG. After scanning was successful, several initiation factors are released, and the large 60S ribosomal subunit attaches to the complex, forming the 80S ribosome (Jackson et al., 2010; Sonenberg & Hinnebusch, 2009; Hinnebusch, 2014).

The eIF4F complex can regulate not only global protein synthesis but also favor specific mRNAs. Some mRNAs with highly structured 5' UTRs can be more dependent on eIF4F interaction than others (Sonenberg & Hinnebusch, 2009). Here, the helicase eIF4A unwinds secondary structures that would interfere with the recruitment of the 43S PIC. Proteins with this eIF4E-sensitivity are important for cellular growth, angiogenesis, and survival, such as cyclin D1, c-myc, vascular endothelial growth factor (De Benedetti & Graff, 2004).

After the PIC is assembled on the mRNA, elongation occurs at the ribosome's acceptor (A) side. The correct sequence is mediated through the binding of tRNAs specific to the next mRNA codons (**Figure 4**). Elongation is terminated when a peptidyl tRNA binds to a stop codon on the mRNA. Non-AUG translation, called Internal Ribosome Entry Site (IRES)-mediated translation can happen independently of the start codon (Lacerda et al., 2017). Even though the mechanism of pathogenesis is unclear, it has been shown that Tau protein, which contributes to AD pathology, is synthesized via IRES-mediated translation (Veo & Krushel, 2009).

As protein synthesis is a high energy-consuming process, protein synthesis is tightly regulated by the process of translational control (Buttgereit & Brand, 1995; Gebauer & Hentze, 2004). This regulation can affect global translation or specific mRNAs. Translation of specific mRNAs can be regulated by miRNAs in a sequence-specific manner (Sonenberg & Hinnebusch, 2009). In neurons, protein synthesis and its regulation is particularly important as it supplies proteins in the cell body and also distal parts of axons or dendrites (Holt et al., 2019). Therefore, it is not surprising that mutations in genes involved in RNA metabolism can cause various diseases, especially neurodegenerative, neurodevelopmental, and neuromuscular diseases (Thelen & Kye, 2020). Various dysregulations in translation, including tRNA synthesis, ribosome biogenesis, sequestration of mRNA, or mislocalization of mRNA, can lead to multiple pathologies with a heterogeneity of disease phenotypes (Nussbacher et al., 2019). Furthermore, proper control of protein synthesis is crucial for learning, and memory formation and defects are associated with multiple cognitive diseases (Buffington et al., 2014; Richter & Coller, 2015).

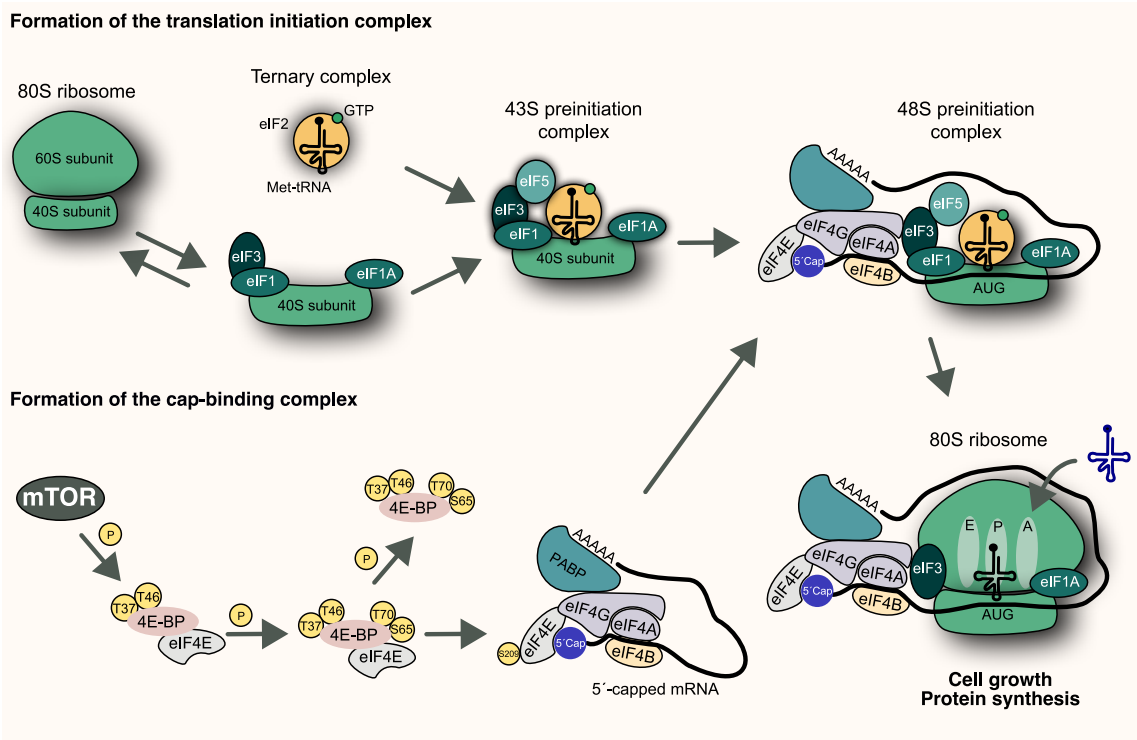

Figure 4: Eukaryotic cap-dependent translation initiation and its regulation by mTOR. Binding of eIF1, eIF1A and eIF3 to the 40S subunit promotes dissociation of the 40S subunit from the 80S ribosome. Further, the 43S preinitiation complex (PIC) is formed after binding of the ternary complex (eIF2-GTP-Met-tRNA) to the free 40S subunit and eIF5. Formation of the cap-binding complex is promoted via mTOR by the release of 4E-BP from eIF4E. Afterwards, the eIF4F complex (eIF4A-eIF4E-eIF4G) binds to the 5' capped mRNA. Binding of the poly-A tail to PABP results in circularization of the mRNA. The 48S PIC complex is formed upon binding of the 43S PIC to the 5' capped mRNA. After successful scanning for the start codon on the mRNA, the large 60S ribosomal subunit attaches, forming the 80S ribosome (adapted from (Kapur et al., 2017)).

1.3.1 Cap dependent translation

Initially, genes are transcribed as precursor mRNAs (pre-mRNAs) that undergo maturation. Maturation of pre-mRNA is achieved by adding a 5' cap to the 5' end of the primary transcript,

a poly-adenosine tail to the 3' end, and splicing out introns. The term 5' cap refers to a specifically modified nucleotide at the 5' end of pre-mRNAs. In contrast, mitochondrial mRNAs do not possess the 5' cap structure (Temperley et al., 2010). The 5' cap structure facilitates multiple functions. Besides regulating nuclear export (Visa et al., 1996; Lewis & Izaurflde, 1997) or protection against degradation by 5' exonucleases (Burkard & Butler, 2000; M. Gao et al., 2000), it regulates splicing (M. Gao et al., 2000) and also promotes translation (Shatkin, 1976; Banerjee, 1980; Sonenberg & Gingras, 1998). The 5' cap contains a 7-methylguanosine (m^7G) connected by a triphosphate bridge to the first nucleotide of the mRNA (Banerjee, 1980). This form of a 5' cap is sufficient to increase resistance to exonuclease mediated degradation and promotes recruiting translation initiation factors. Additional methylations at the first nucleosides can occur and regulate gene expression *in vivo* (Elliott et al., 2019). Furthermore, the methylation of the 2' hydroxy-groups of the first two ribose sugars of the 5' end controls recognition of the mRNA by the innate immune system and promotes innate immune tolerance (Schuberth-Wagner et al., 2015; D. W. Leung & Amarasinghe, 2016; Daffis et al., 2010).

In addition to mRNAs, non-coding RNAs, such as snRNAs and snoRNAs, contain 5' cap structures (Ro-Choi, 1999). However, different from the m^7G cap on most mRNAs, ncRNAs, and several selenoprotein mRNAs contain 5'-trimethylguanosine (TMG) caps (Matera et al., 2007; Wurth et al., 2014). Catalysis of the m^7G cap into a TMG cap is facilitated in two serial methylation steps by the trimethylguanosine synthase (TGS1) (Mouaikel et al., 2002; Girard et al., 2008). The cytoplasmic modification of the TMG cap on snRNAs and the cytoplasmic assembly of the Sm-core complex is required for nuclear re-entry of snRNAs (Hamm et al., 1990). Interestingly, TGS1 directly interacts with SMN, providing an additional function to the Sm-core complex assembly by SMN in recruiting TGS1 (Mouaikel et al., 2003; Maccallini et al., 2020).

Most often, the regulation of global translation takes place at the initiation step. Therefore, phosphorylation or availability of initiation factors affects the efficiency of global translation. Accordingly, the availability of the eIF4E is crucial for the initiation of cap-dependent translation. The interaction of the cap-binding protein eIF4E and the ribosomal-subunit-associated eIF4G plays an essential role at this step, as eIF4G links the small ribosomal subunit to the 5' cap. Several eIF4E inhibitory proteins modulate this interaction. However, phosphorylation of eIF4G does increase cap-dependent translation and IRES-dependent translation (León et al., 2014). The availability of eIF4E is regulated by the phosphorylation of 4E-binding proteins (4E-BPs). Translation initiation is repressed by binding of 4E-BP1 to eIF4E (Haghighat et al., 1995). mTOR can regulate the release of 4E-BP1 by phosphorylation (K. Hara et al., 1997). Protein synthesis should be well regulated as it is vital for cell growth, development, and synaptic plasticity (Buffington et al., 2014; Costa-Mattioli et al., 2009; Shanbhogue et al., 1992).

In addition to translational control by 4E-BP, other proteins can regulate cap-dependent translation initiation (Sonenberg & Hinnebusch, 2009). Those eIF4E inhibitory proteins modify the interaction of eIF4E with eIF4G (Sonenberg & Hinnebusch, 2009). Moreover, those eIF4E inhibitory proteins can interact with eIF4E on specific mRNAs via RBPs or interaction with certain RNA elements (Richter & Sonenberg, 2005). In *Xenopus*, Maskin and the cytoplasmic polyadenylation element-binding protein CPEB bind to RNAs that contain a CPE and in

Drosophila Cup has been identified to interact together with Bruno on Bruno response element (BRE) containing RNAs (Richter & Sonenberg, 2005). Mammalian eIF4E inhibitors include the homeodomain transcription factor EMX2 and the proline-rich homeodomain protein PRH (Nedelec et al., 2004; Topisirovic et al., 2003). However, regulation of cap-dependent translation initiation in the nervous system heavily relies on the control of 4E-BP (Richter & Sonenberg, 2005).

1.3.2 Local translation

Especially in neurons, it is necessary to respond to extracellular stimuli distal from the cell body. However, establishing a local proteome in dendritic spines, along axons, and at the growth cone can be challenging due to the high polarization and extreme length of the axons. Local protein synthesis in dendrites supports neurons during development, in synapse formation and function, axonal branching, and growth and steering at the growth cones (J.-M. M. Cioni et al., 2018). It is believed that activity-dependent synaptic plasticity occurs, especially during learning and memory formation processes (Buffington et al., 2014).

The ability to establish a specific axonal proteome is based on the trafficking of proteins and mRNAs or local protein synthesis. It has been suggested that mRNA localization is the major contributor to maintain this local proteome (Zappulo et al., 2017). In fact, mRNA localization contributes to half of the proteome localized to neurites (Zappulo et al., 2017). Localization of mRNAs is facilitated by transport via RBPs to the axons and dendrites. After maturation, nuclear-exported mRNAs bind to proteins that remain attached to the mRNA in the cytoplasm (Moore, 2005; Cole & Scarcelli, 2006). Those mRNA bound RBPs, also called ribonucleotide particles (RNPs), are further transported to their subcellular destination (Andreassi & Riccio, 2009). Furthermore, RNPs can be associated with motile late endosomes that act as a site for translation (J.-M. Cioni et al., 2019).

While the 5' UTR of mRNAs is predominantly involved in the regulation of translation (Pickering & Willis, 2005), several steps of mRNA metabolism are regulated by the 3' UTR (Moore, 2005). Those functions of RNA metabolism include translation efficiency and mRNA stability and nuclear export and localization to the cytoplasm (Moore, 2005). Furthermore, the localization sequence to neuronal projections is often located in the 3'-UTR of the mRNA (Andreassi & Riccio, 2009). Explicitly, subcellular localization is determined by cis-acting sequences, called "localizer" or "zip-codes" (Kislauskis & Singer, 1992). Interestingly, in some cases, the localization sequence can appear in multiple copies or can be formed by different elements and therefore range from a few nucleotides to over 1 kb (Jambhekar & DeRisi, 2007).

Many factors are present at the synaptic site that enable or regulate local translation. These factors include mRNAs, tRNAs, ribosomes, translation initiation, elongation factors, RNA-induced silencing complex (RISC), and miRNAs. Alterations in the supply of those molecules can lead to disturbed cellular function and neurodegenerative diseases (Kapur et al., 2017; S. Sharma & Lu, 2018; Fernandopulle et al., 2021).

Additionally, local translation in neurons can be mediated by the formation of RNA granules. Those macromolecular structures repress translation of mRNA until the final destination is reached (Kiebler & Bassell, 2006). Upon depolarization, RNA granules can be disassembled

and shift to polysomes in an activity-dependent manner (Krichevsky & Kosik, 2001). Prion-like domains mediate the assembly and the disassembly of such mRNP granules with low amino acid complexity (LC domain) on RNA-binding proteins (Malinovska et al., 2013). Mutations in the domains that mediate assembly and disassembly of mRNP granules can lead to neurodegenerative diseases, such as ALS through the biophysical properties of stress granule formation (H. J. Kim et al., 2013).

In general, axonal local translation appears to happen predominantly during development (Fallini et al., 2016; Jung & Holt, 2011). With the spatial and temporal abundance of SMN, an important neuron-specific role in axonogenesis and axonal sprouting has been suggested (Giavazzi et al., 2006). Components of the mTOR cascade have been found at the synapse, and given its role as an essential regulator of mRNA translation, it influences synaptic plasticity locally (Huber et al., 2015).

1.3.3 mTOR

Precise regulation of cell growth is essential during all phases of a eukaryotic cell. One important regulator is the serine/ threonine kinase, the mammalian target of rapamycin (mTOR). mTOR responds to nutrients and growth factors balancing anabolic and catabolic pathways (**Figure 5**) (Laplante & Sabatini, 2012). The mTOR pathway is activated by the phosphoinositide 3-kinase (PI3K) and ERK pathways (Costa-Mattioli et al., 2009). mTOR was first discovered after isolation of rapamycin, a cytostatic compound produced by *Streptomyces hygroscopicus*. It was identified to target the TOR kinases in yeast (Brown et al., 1994; Cafferkey et al., 1993; Kunz et al., 1993). In mammals, mTOR can form two signaling complexes based on its binding partners: mTOR complex 1 (mTORC1) and mTOR complex 2 (mTORC2) (**Figure 5**). Since mTORC1 binds to the regulatory-associated protein of TOR (Raptor), mTORC2 binds to the rapamycin-insensitive companion of TOR (Rictor). As the name of the mTORC2 binding partner Rictor already suggests, mTORC2 is less sensitive to rapamycin. Nevertheless, chronic treatment of rapamycin has been shown to impair also mTORC2 (Sarbassov et al., 2006). Furthermore, mTOR binds in both complexes to the GTPase β-subunit like protein (GβL or mLST8) (Jacinto et al., 2004; D.-H. Kim et al., 2003), the DEP domain-containing mTOR-interacting protein (DEPTOR) (Peterson et al., 2009), and the Tti1/Tel2 complex (Kaizuka et al., 2010). Even though mTORC2 has been shown to interact with ribosomes, translation regulation is mainly mediated by mTORC1 (Oh et al., 2010; Zinzalla et al., 2011). Furthermore, in contrast to mTOR1, mTORC2 is insensitive to nutrient signaling but is regulated by growth factors (Laplante & Sabatini, 2012). In addition to regulating apoptosis or the cell cycle, mTORC2 regulates cytoskeletal organization via the protein kinase C alpha (PKCα) **Figure 5**) (Angliker & Rüegg, 2013; X. Li & Gao, 2014).

mTOR complex 1 (mTORC1) is a positive regulator of cell growth and proliferation and acts as an integral node between cellular energy production and consumption. It promotes anabolic processes such as protein synthesis, lipogenesis and restricts catabolic processes such as autophagy (T. Hara & Mizushima, 2009; Noda & Ohsumi, 1998; Scott et al., 2004). mTORC1 can be activated through the PI3K pathway and several other stimuli, including nutrients, energy levels, oxygen, amino acids, and stress signals. One of the anabolic processes promoted

by mTORC1 is the transcription of mitochondrial biogenesis and metabolism by controlling the transcriptional activity of PPARα-coactivator-1 (PGC1α) (**Figure 5**) (Cunningham et al., 2007). Furthermore, mTORC1 leads to an up-regulation of transcription factor hypoxia-inducible factor 1 (HIF1α), resulting in increased glucose uptake and glycolysis (Yecies & Manning, 2011; Dodd et al., 2015). Another anabolic process controlled by mTOR is the translation of mRNA into proteins. mTOR positively regulates translation initiation by phosphorylation of the initiation factors eIF4B and eIF4G. Furthermore, it promotes the release of eIF4A from the programmed cell death 4 (PDCD4) protein after phosphorylation of PDCD4 (Dorrello et al., 2006; M. D. Dennis et al., 2012). Additionally, cap-dependent translation initiation is promoted by mTORC1. The rate-limiting step in translation initiation is the association of the cap-binding protein, eukaryotic translation initiation factor 4E (eIF4E) into the eIF4F complex, that recruits the small ribosomal unit to mRNAs (Yanagiya et al., 2012; K. Hara et al., 1997) (**Figure 4**). mTORC1 phosphorylates 4E-BP and promotes the dissociation of 4E-BP from eIF4E to increase cap-dependent translation (Gingras et al., 1999). Furthermore, translation initiation is promoted by phosphorylation of S6 kinase (S6K), phosphorylating eIF4B. Besides translational initiation, mTOR promotes ribosomal biogenesis through phosphorylation of the ribosomal protein S6, downstream of the S6K, and further control of the ribosome biogenesis transcriptional program (Kapahi et al., 2010; Laplante & Sabatini, 2012; Chauvin et al., 2014).

Besides mediating global translation, mTOR has been shown to increase the translation of 5' terminal oligopyrimidine (5' TOP) mRNAs, which encode proteins mainly involved in translation (Thoreen, 2017). It is assumed that around 100 mRNAs display this motif (Meyuhas & Kahan, 2015). However, based on bioinformatic analyses, it is speculated that up to 10% of the transcriptome shows this motif (Yamashita et al., 2008). Nevertheless, all ribosomal proteins, elongation factors, and PABPs are shown to bear the 5' TOP motif (Yamashita et al., 2008). The expression of TOP mRNAs can be repressed by different stresses such as ribosomal stress, mechanical stress, deprivation of oxygen, and amino acids (Meyuhas & Kahan, 2015).

Previous research has indicated that phosphorylation of 4E-BP1, 4E-BP2, and the ribosomal protein S6 is abolished by mTOR inhibition (Morita et al., 2013). It is also known that mTOR regulates the translation of a subset of mitochondria-related mRNAs (Morita et al., 2013). It has been demonstrated that mTOR controls mitochondrial function and ATP production through 4EBP inhibition *in vivo* (Morita et al., 2013).

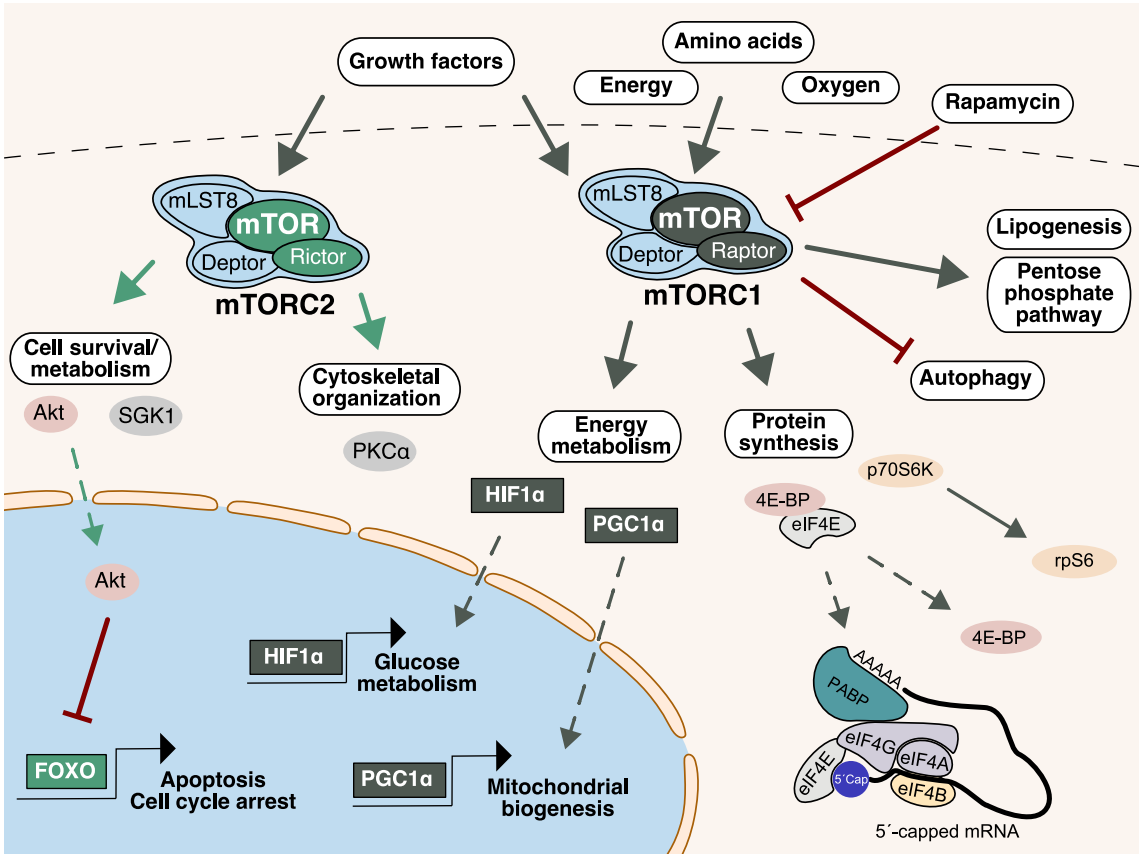

Figure 5: The mTOR signaling pathways.
mTOR forms the two distinct complexes, mTORC1 and mTORC2, based on its binding partners. Growth factors activate both complexes. Additionally, mTORC1 is activated by amino acids, the energy status of the cell, or oxygen. Rapamycin primarily inhibits the activity of mTORC1. mTORC2 promotes cytoskeletal organization, cell survival, and metabolism. Active mTORC1 inhibits autophagy and promotes lipogenesis and the pentose phosphate pathway. In addition, mTORC1 regulates energy metabolism via the transcriptional activity of PGC1α and HIF1α. Protein synthesis is regulated at the translation initiation step.

1.3.4 mRNA translation in neurodegenerative disease

The impaired or altered mRNA translation is a typical phenotype in neurodegenerative disorders. Such neurodegenerative diseases include ALS/FTD, Fragile X syndrome (FXS), AD, and SMA (Thelen & Kye, 2020). mRNA translation can be dysregulated by sequestration of mRNAs or initiation factors, failed localization of mRNAs, an altered tRNA synthesis, altered miRNA processing, or defects in ribosome biogenesis (Lehmkuhl & Zarnescu, 2018).

In ALS/FTD, defects in the mRNA translation are linked to impaired RNA processing due to mutations in the TAR DNA-binding protein 43 (*TARDBP*) gene, encoding TDP-43. Physiologically TDP-43 is predominantly nuclear and functions in various mechanisms of RNA regulation, including RNA stability, mRNA transport, splicing, and miRNA processing (Ratti & Buratti, 2016). However, mutations in *TARDBP* can result in cytoplasmic aggregations linked to ALS/ FTD neuropathology (Lee et al., 2011). Furthermore, FXS and autism spectrum disorder (ASD) are examples of defective protein synthesis in dendrites based on defective RBPs (Belmonte et al., 2004).

In SMA, a reduction of global translation has been associated with reduced mTOR activity

(Kye et al., 2014). This can be attributed to the interaction of SMN with many proteins along the axon, including ribosomes (Lauria et al., 2020). Further, reduced SMN levels are associated with reduced local translation as SMN is involved in trafficking of mRNAs along the axon (Béchade et al., 1999; Pagliardini, 2000). In fact, SMN can localize to the nucleus and the cytoplasm. However, for cytoplasmic localization and bidirectional transport along the axon, exon 7 is required (H. L. Zhang et al., 2003). Consequently, correct localization of mRNA, which is essential for local translation as seen by the localization defects of β-actin mRNA in SMA, is caused by SMN (Giavazzi et al., 2006). Besides, the zipcode binding protein 1 (ZBP1) binds the 3'UTR of β-actin and prevents translation initiation unless β-actin mRNA is not localized to its destination (Hüttelmaier et al., 2005). Previous studies have shown that reduced SMN levels impair mRNA localization and result in a reduced local translation (Fallini et al., 2016).

2 AIMS AND OBJECTIVES OF THE STUDY

Loss of *SMN1* results in insufficient SMN levels, causing degeneration of alpha MNs and muscle wasting. Multiple studies aimed to increase SMN production in MNs. Recently developed therapies focused on MNs lead to significant improvement in clinical phenotypes of SMA patients. However, there is still no ideal cure, and especially multisystemic effects in SMA patients are barely investigated. Especially, the increased life expectancy might reveal unexpected pathological defects in other tissues than MNs.

Previous studies implicated energy deprivation and contribution of oxidative stress to SMA pathology (Acsadi et al., 2009; Miller et al., 2016; C. C. Xu et al., 2016). However, the role of both impairments in SMA pathology remains mostly unknown. Furthermore, while reduced protein synthesis is documented in SMA, the possible molecular connections among energy homeostasis, oxidative stress, and protein synthesis are not well understood.

Based on previous findings, we hypothesize that energy deprivation is a major driver of SMA pathology. As energy homeostasis is crucial for cell survival and growth, it might contribute to impaired protein synthesis in SMA. Therefore, it can be beneficial to restore impaired energy homeostasis in SMA MNs. Furthermore, systemically improving energy homeostasis might have global effects also on other tissues.

This study aimed to clarify several aspects of energy homeostasis and protein synthesis, contributing to SMA pathology. In detail, this study aimed to address the following topics:

(1) Identify the major contributors of impaired energy homeostasis in SMA MNs by whole proteome analysis.

(a) Restore energy homeostasis via improving glycolysis and mitochondrial function by supplementation of energy substrates.

(b) Reduce oxidative stress in SMA MNs with anti-oxidative supplements.

(2) Identify the mechanism of impaired translation in SMA MNs.

(a) Rescue defective protein synthesis by supplementation of substrates. Protein synthesis efficiency can be improved by an enhanced energy production due to pyruvate or lactate supplementation or oxidative stress reduction by anti-oxidative agents such as N-acetylcysteine (NAC).

The following experimental objectives are set to resolve those aims.

(1) This research examines the emerging role of energy homeostasis in the context of SMA pathology. Comparing primary WT and SMA MNs by whole proteome analysis will highlight key pathways contributing to SMA pathology. Focusing the proteomics approach on energy-producing pathways will guide further research to molecular defects involved in energy homeostasis. Possible defects involve respiration by mitochondria or glycolysis. Whole proteome analysis will reveal alterations in mitochondrial respiratory complexes. Biochemical quantification of the ATP levels and glucose uptake ability will

verify and further characterize energy homeostasis in SMA.

(a) Since previous studies suggested defects in energy homeostasis in SMA, improving ATP production is supposed to mitigate SMA pathology. The external supply of lactate or pyruvate will be used as energy substrates.

(b) As the implications of oxidative stress in SMA are not fully resolved, this study aims to elaborate the influence of oxidative stress on SMA pathology. Therefore, biochemical detection of ROS might verify oxidative stress in primary SMA MNs. Additionally, reducing ROS by the antioxidant NAC or pyruvate supplementation might reduce oxidative stress in SMA MNs.

(2) Oxidative stress can alter protein synthesis. This mechanism needs further investigation. Protein carbonylation will be quantified to understand the molecular link between oxidative stress and impaired protein synthesis. Additionally, SUnSET and SunRiSE assays will be used to distinguish the effect of translation initiation and elongation, respectively.

(a) Impaired protein synthesis can be ameliorated by ROS reduction and improving energy homeostasis. Therefore, pyruvate and NAC supplementation can counteract oxidative stress, and pyruvate or lactate supplementation can be used to increase ATP levels in MNs.

3 RESULTS

3.1 Quantitative screening of primary MN proteins

Previous studies have shown that translation in SMA is impaired, and therefore a differential expression of proteins might contribute to SMA pathology in MNs (Sanchez et al., 2013; Kye et al., 2014). Recent evidence suggests that SMN binds to ribosomes and regulates a subset of proteins translationally (Lauria et al., 2020). As the clinical manifestation of SMA is first observed in MNs, investigating the proteome of primary MNs might reveal dysfunctional pathways, leading to the progression of SMA. Changes in the proteome of primary MNs isolated from an SMA mouse model (Hsieh-Li et al., 2000) and wild-type (WT) mice were compared using quantitative mass spectrometry analysis in a 2 h data-independent acquisition. Four independent biological samples of WT MNs were used to compare the proteome with three independent biological samples of SMA MNs. Raw data of the whole proteome analysis has been deposited at the ProteomeXchange Consortium via the PRIDE (Perez-Riverol et al., 2019) partner repository with the dataset identifier PXD020403. The mass spectrometry dataset results, supporting the conclusions of this thesis, are included within the research article (Thelen et al., 2020) as "Additional file 2: Mass Spectrometry source data". Furthermore, significantly changed proteins are listed within the results section and the Appendix of this thesis.

3.1.1 Mitochondrial proteins are dysregulated in SMA MNs

Whole proteome analysis was performed on primary MNs isolated from E13.5 WT and SMA mice after 10 days *in vitro* (DIV). Based on the literature, around 8101 proteins are expressed in MNs from E12.5 mouse embryos (Hornburg et al., 2014). In total, 5165 proteins were identified in our whole proteome analysis in WT and SMA primary MNs (**Figure 6A**). The data shows that the majority of significantly changed proteins are down-regulated in SMA MNs compared to WT ones (**Figure 6B and Table S1**). The dataset was annotated with the MitoCarta2.0 database, which includes 1158 proteins with strong support for mitochondrial localization, to compare the proteins detected in this whole proteome analysis with mitochondrial proteins. Compared to the MitoCarta2.0 database (Calvo et al., 2016), 681 (~13 %) proteins are associated with mitochondrial function and localization (**Figure 6A and Figure 8**).

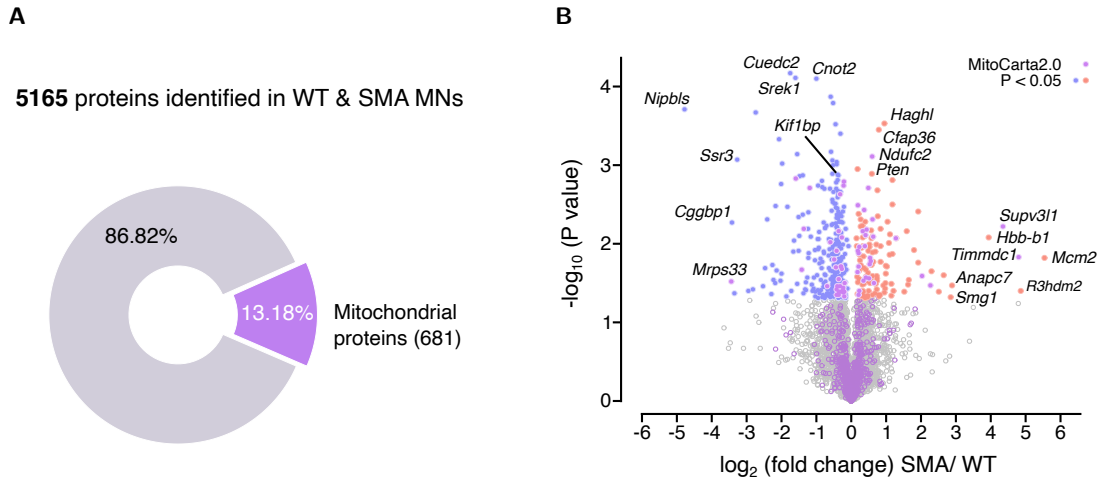

Figure 6: Quantitative proteomics of WT and SMA MNs.
A) Pie chart of proteins identified by whole proteome analysis between WT and SMA MNs (10DIV). Mitochondria associated proteins (681) are highlighted in purple. **B)** Volcano plot of whole proteome analysis comparing WT and SMA MNs; plotted p-values ($-\log_{10}$) against fold changes ($\log_2$, SMA/ WT). Four independent samples of WT MNs and three independent samples of SMA MNs were used for analysis. P- values were determined using unpaired two-sided t-test. Proteins with $p < 0.05$ are highlighted in blue (313 down-regulated) and red (120 up-regulated), and proteins with localization in mitochondria are marked in purple (32 down-regulated and 29 up-regulated). Annotations show corresponding gene names.

Among 5165 identified proteins, 494 proteins were significantly changed in SMA compared to WT, and 61 (~12 %) are localized to mitochondria based on the MitoCarta2.0 database (Calvo et al., 2016) (**Figure 7 and Table S1**). Significantly changed mitochondrial proteins divide into equal parts of up-and down-regulated proteins. In contrast, the majority of all significantly changed proteins was lower expressed in SMA MNs compared to WT MNs. Overall 345 (~70 %) proteins were down-regulated and 149 proteins (~30 %) were increased in their expression levels (**Figure 7 and Table S1**).

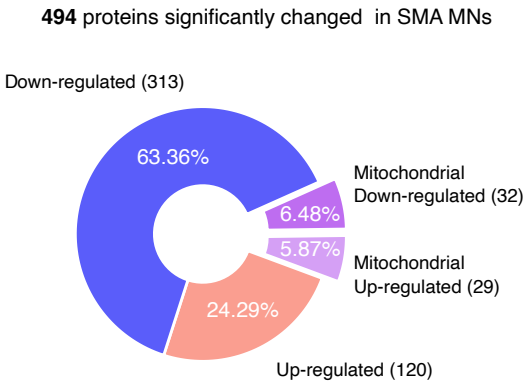

Figure 7: Significantly changed proteins in SMA MNs.
Pie chart of whole proteome analysis comparing WT and SMA MNs. Four independent samples of WT MNs and three independent samples of SMA MNs were used for analysis. Proteins with $p < 0.05$ are highlighted in blue (313 down-regulated) and red (120 up-regulated), and proteins with localization to mitochondria are marked in purple (32 down-regulated and 29 up-regulated).

A focused view on the mitochondrial proteins found in our whole proteome analysis identified 35 proteins of the respiratory complex I. Thereby, we detected about 92% of nuclear-encoded proteins of this complex (**Figure 8**). In total, one quarter (9 proteins) of the detected complex I proteins were significantly changed in SMA MNs (**see Box Figure 8**). In addition to complex I proteins, mitochondrial motor proteins KIF1B and KIF1BP are down-regulated in SMA MNs (**Figure 6B, Figure 8, and Table S1**). In summary, these results strengthen the hypothesis of defective mitochondria in SMA MNs.

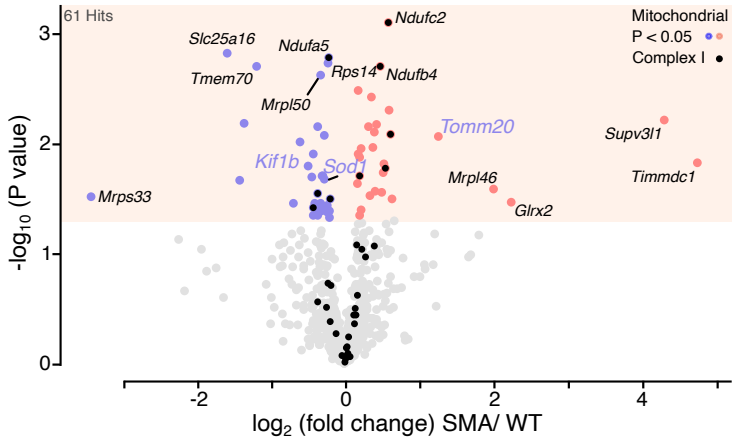

• Complex I Hits	P value	Fold change
Ndufb8	0,038	0,75
Ndufv2	0,028	0,78
Ndufa5	0,002	0,86
Ndufb5	0,032	0,88
Ndufa6	0,008	1,55
Ndufc2	0,001	1,52
Ndufab1	0,017	1,47
Ndufb4	0,002	1,40
Ndufa10	0,019	1,16

Figure 8: Quantitative proteomics of mitochondrial proteins of SMA and WT MNs.
Volcano plot of proteins identified in whole proteome analysis that overlap with the MitoCarta 2.0 database; plotted p-values ($-\log_{10}$) against fold changes ($\log_2$, SMA/ WT). Four independent samples of WT MNs and three independent samples of SMA MNs were used for analysis. P-values were determined using unpaired two-sided t-test. Proteins with $p < 0.05$ are highlighted in blue (32 down-regulated) or red (29 up-regulated). Annotations show corresponding gene names.

3.1.2 Pathway analysis in WT vs SMA

To understand the biological meaning of dysregulated proteins in SMA MNs, we analyzed gene ontology (GO) terms using the online database DAVID 6.7. 345 significantly down-regulated and 149 significantly up-regulated proteins were analyzed separately (**Figure 9**). Enriched GO terms were clustered in biological process, cellular compartment, and molecular function. Among the down-regulated proteins in SMA MNs, we identified previously documented pathways in SMA pathology such as RNA binding, protein transport, ribonucleoprotein complexes, and protein synthesis, confirming the reliability of the data set (**Figure 9A**) (Akten et al., 2011; Fallini et al., 2011; Kye et al., 2014; Pellizzoni, 2002; Rossoll et al., 2003). Especially ribosomes and their function in translation were affected in all three categories. Among the 149 up-regulated proteins, especially mitochondrial dysfunction and ATP production was annotated (**Figure 9B**). Also, the cellular compartment annotation of up-regulated proteins showed strong support for mitochondrial dysfunction in SMA MNs.

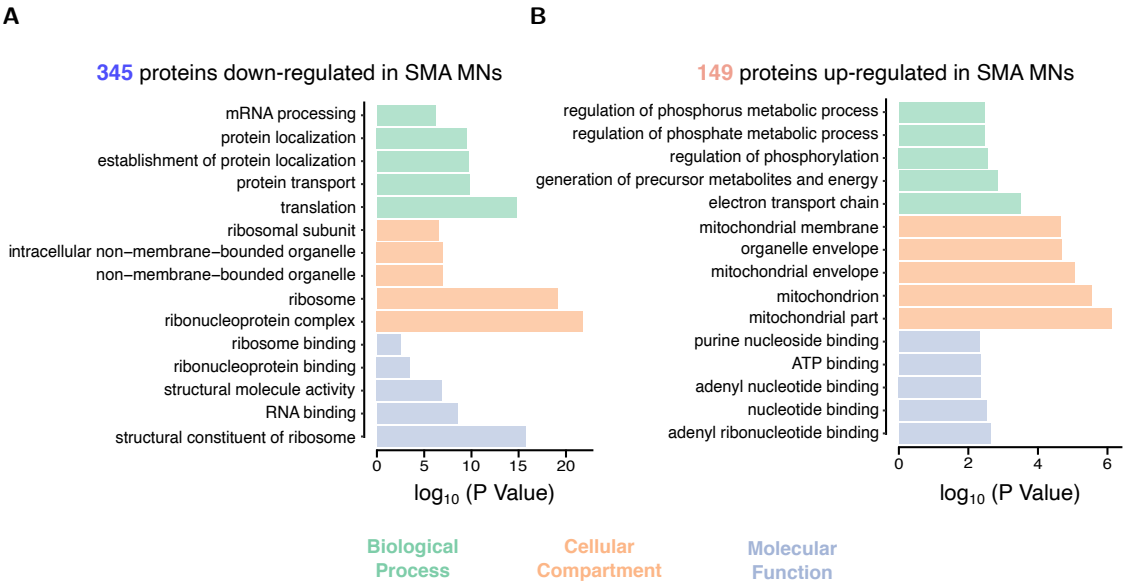

Figure 9: Pathway analysis of SMA MNs.
Gene ontology (GO) analysis of 345 down-regulated (**A**) and 149 up-regulated proteins (**B**) in SMA MNs. Enriched annotations are divided into biological process, cellular compartment and molecular function. The 5 most significant terms in each category are shown.

3.2 Characterization of mitochondria in MNs

A variety of defective cellular pathways are described in SMA. Malfunctional mitochondria and impaired OXPHOS have been associated with a wide range of neurological disorders and are shown to play an important role in neurodegenerative diseases such as PD, AD, HD, and ALS (Hauser & Hastings, 2013; Fukui & Moraes, 2008; Carmo et al., 2018). Also, in SMA, metabolic defects and defective mitochondrial biogenesis have been shown (Bowerman et al., 2014; Ripolone et al., 2015). Furthermore, functional mitochondrial defects are associated with SMA pathology (Acsadi et al., 2009; Miller et al., 2016; C. C. Xu et al., 2016). A reduced oxygen consumption rate and increased oxidative stress, and a dysregulated mitochondrial membrane potential were found (Miller et al., 2016; C. C. Xu et al., 2016).

Due to our findings, a significant number of mitochondrial proteins are dysregulated in SMA MNs (**Figure 8**). Therefore, the impact of those dysregulated proteins on mitochondrial function and the associated pathological outcome in SMA needs to be investigated.

Furthermore, dysfunctional mitochondria can be characterized by a fragmented shape. Consequently, the shape of mitochondria might indicate mitochondrial defects in SMA MNs. Due to the compartmentalization of MNs and the high energy demand in the cell body and the distal parts of the axons, mitochondria need to be available throughout the whole cell. Therefore, we focused not only on the cell body but also investigated the availability of mitochondria along the axons.

3.2.1 Axonal mitochondria are reduced

To investigate the localization and function of mitochondria in motor axons, labeling of mitochondria using the fluorescent dye MitoTracker and specific antibody staining against TOM20 was performed (**Figure 10A**). Two different methods were applied to distinguish between the total number of mitochondria and the number of functional mitochondria. By labeling the mitochondrial protein TOM20, the entirety of neuronal mitochondria is tagged, and by use of the membrane intercalating dye MitoTracker, only mitochondria with a functional membrane potential are stained. At least 100 µm of the axon from 10DIV MNs was measured, and mitochondrial signals were quantified automatically using a modified version of the ImageJ Mitophagy Macro (Dagda et al., 2008). In brief, axons were followed by the segmented line tool based on the channel representing the Tau-antibody staining. Subsequently, the outside of the selection was cleared to remove signals from other cells. Individual mitochondria were labeled with a threshold on the channel representing either the MitoTracker staining or immunostaining with TOM20 specific antibodies. Mitochondrial number and shape were quantified automatically by ImageJ based on the given threshold. Both numbers of total and functional mitochondria are reduced in SMA axons (**Figure 10B**). On average, the number of mitochondria labeled with TOM20 antibody (~8.7 mitochondria/ 100 µm neurite) was decreased by half (reduction by ~51 %) in SMA axons compared to WT ones (~17.8 mitochondria/ 100 µm neurite) (**Figure 10B**). The number of functional mitochondria based on MitoTracker staining was even more reduced (reduction by ~64 %) in SMA axons (~4.7 mitochondria/ 100 µm neurite) compared to WT ones (~12.9 mitochondria/ 100 µm neurite). Interestingly, not only SMA axons showed reduced numbers of mitochondria compared to WT ones but also the number of functional

mitochondria within each group was lower than the number of total mitochondria labeled with TOM20 antibody staining (**Figure 10B**). The finding of mitochondrial mislocalization is further strengthened by down-regulated mitochondrial motor proteins KIF1B and KIF1BP in SMA MNs in our whole proteome analysis (**Figure 6B, Figure 8, and Table S1**). However, KIF1BP is not shown in (**Figure 8**), as it is not annotated in the MitoCarta2.0 database.

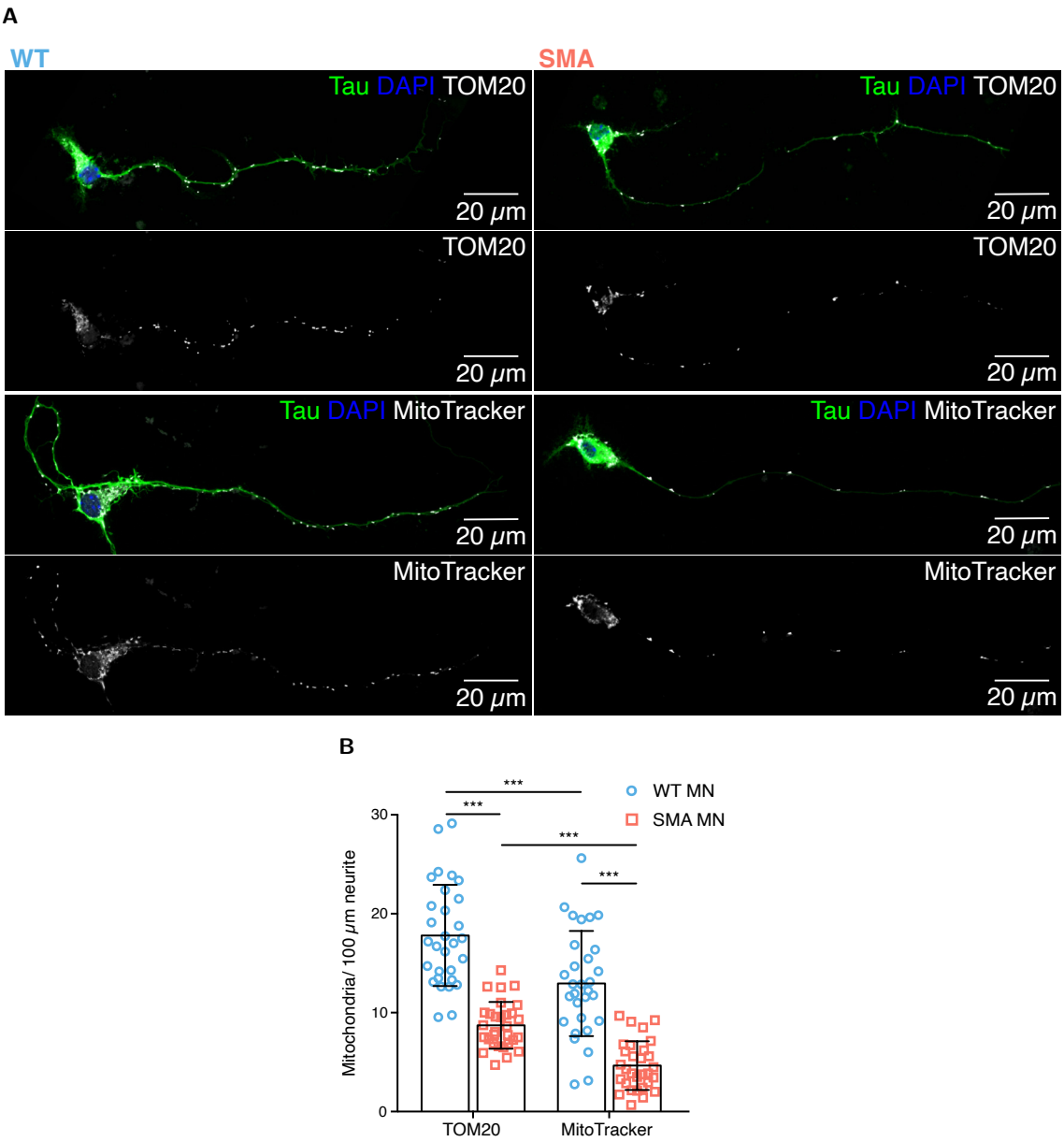

Figure 10: Immunofluorescence of mitochondria.
A) Representative images of mitochondria in 100 µm long primary axons of WT and SMA MNs (10DIV) labelled with anti-Tau antibody (green), DAPI (blue) and anti-TOM20 antibody or MitoTracker® (white). Scale bars: 20 µm. **B)** Quantification of mitochondria in neurites. Each dot represents the average number of mitochondria in each neuron (n=30; biological replicates N=3). Two-way ANOVA with Tukey HSD post hoc analysis was used on independent biological replicates to determine statistical significance. Bar graphs depict the mean ± SD. ***p <0.001.

In addition to the mitochondrial number, the appearance was investigated. For this analysis, the ImageJ Mitophagy Macro, which was used to quantify mitochondria, was used. As a result, mitochondria are smaller and more fragmented in SMA MNs compared to WT ones

(**Figure 11**). Mitochondria were labeled by antibody staining or MitoTracker. No differences between the two groups were observed when comparing the two staining methods. However, mitochondria of SMA MNs showed a reduction in their average size (~0.67 µm^2) compared with ones (~1.03 µm^2) in WT MNs using TOM20 staining. Furthermore, also MitoTracker staining revealed a reduction of mitochondrial size in SMA MNs (~0.72 µm^2) compared with mitochondria of WT MNs (~0.97 µm^2) (**Figure 11B**). Interestingly, there were also differences in the ratio of mitochondrial circularity. Based on TOM20 staining, WT MNs have more elongated mitochondria in their axons, and SMA MNs display more round mitochondria than WT ones. The analysis shows that the average circularity of all mitochondria in WT axons (~0.65 a.u.) is significantly higher compared to mitochondria in SMA MNs (~0.75 a.u.). In addition, functional mitochondria are also fragmented in SMA MNs (~ 0.7 a.u.) compared to mitochondria of WT MNs (~0.63 a.u.) (**Figure 11B**).

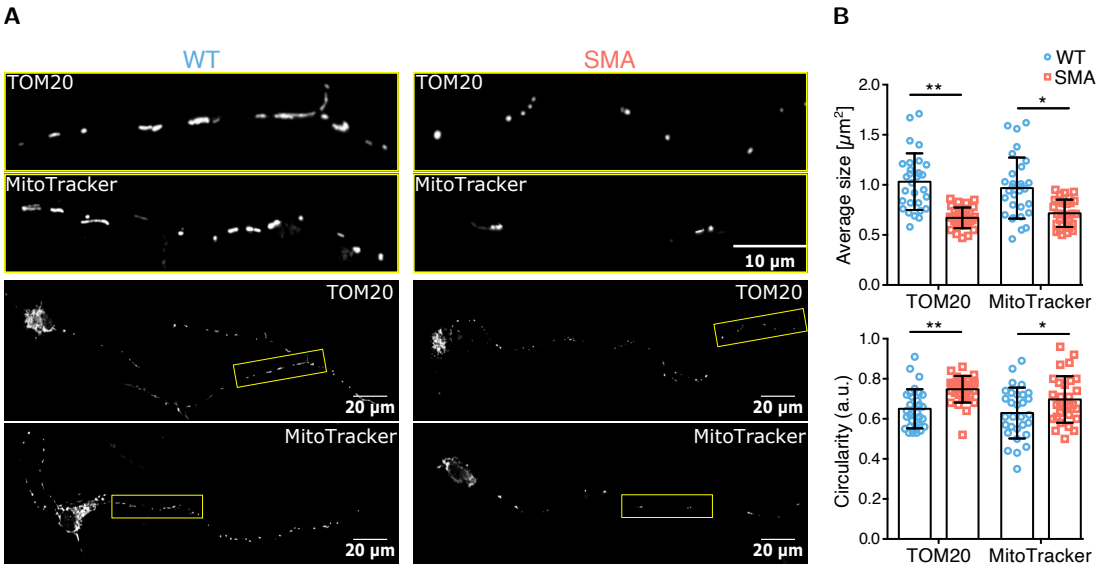

Figure 11: Immunofluorescence of mitochondrial appearance.
A) Representative images of mitochondrial size and circularity of WT and SMA MNs (10DIV) labelled with anti-TOM20 antibody or MitoTracker®. Enlarged areas are highlighted with yellow boxes in the corresponding image of the whole neuron. Scale bar in enlarged images: 10 µm; Scale bar in whole neuron images: 20 µm. **B)** Quantification of mitochondrial size and circularity of WT and SMA MNs (10DIV). Each dot represents the quantification of individual neurons (n=30). To compare WT (blue circles) and SMA (red squares), two-way ANOVA with Tukey HSD post hoc analysis was used on independent biological replicates (N=3) to determine statistical significance. Bar graphs depict the mean ± SD. *p <0.05, **p <0.01.

3.2.2 Total amount of mitochondria is increased

Most surprisingly, even though the number of axonal mitochondria is reduced, elevated TOM20 protein levels were observed in the quantitative proteomics (**Figure 8**), as well as after western blot analysis of 10DIV primary MNs (**Figure 12**). These results suggest an accumulation of mitochondria in the soma.

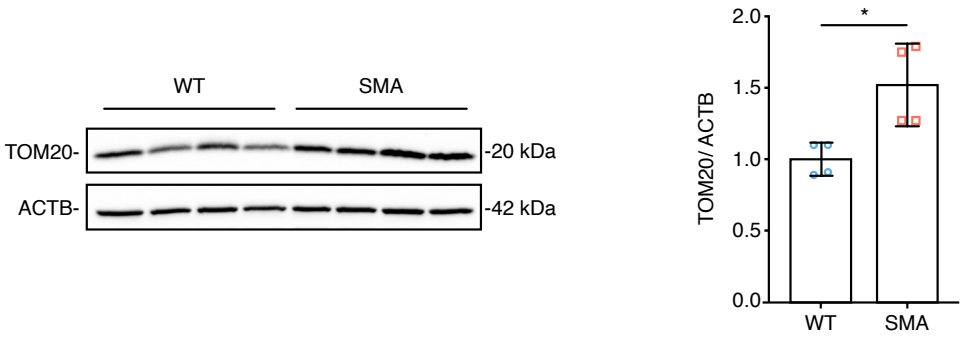

Figure 12: TOM20 protein levels are increased in SMA MNs.
Western blot analysis and quantification of TOM20 protein in 10DIV MNs. Each dot represents data from biological replicates (N=4). Two-tailed unpaired t-test was used to determine statistical significance. Bar graph depict the mean ± SD. *p <0.05. Blue circles represent WT MNs and red squares represent SMA MNs.

3.3 Defective complex I causes higher ROS levels and hypercarbonylation of proteins in SMA MNs

Based on our whole proteome analysis, a great amount of mitochondrial proteins is dysregulated in SMA. Moreover, fewer mitochondria with a different shape were observed in axons of SMA MNs compared to WT axons. However, recent evidence suggests that also the functionality of mitochondria is impaired in SMA MNs. This includes the energy metabolism, Ca^{2+} buffering, and reactive oxygen species (ROS) regulation (Acsadi et al., 2009; Boyd et al., 2017; Miller et al., 2016; McGivern et al., 2013). In particular, complex I, the rate-limiting enzyme in respiration and the primary producer of ROS (L. Sharma et al., 2009; Y. Liu et al., 2002) seems to be affected in SMA due to our data. Consequently, mitochondrial energy production might be impaired, and ROS production might be increased in SMA MNs. Increased ROS levels could lead to excessive protein carbonylation resulting in impaired protein synthesis (Stadtman, 1990; Topf et al., 2018).

3.3.1 Complex I activity is reduced

Among the 61 proteins dysregulated in SMA and located to mitochondria, 11 proteins are localized to the OXPHOS machinery (**Figure 13**, **Table 1**). Complex I of the OXPHOS is a large multi-subunit protein complex comprised of 45 subunits. The vast majority of (38) proteins are encoded in the nucleus, whether only 7 proteins are encoded by mtDNA. Interestingly, 35 of the 38 nuclear-encoded proteins of complex I were detected in our whole proteome analysis, and 9 of them were significantly altered in SMA MNs (**Figure 13**).

Table 1: Differentially expressed proteins in the OXPHOS of SMA MNs.
List of significantly changed proteins in the respiratory chain complexes of SMA compared to WT MNs ($p < 0.05$). For all proteins, gene names, protein description, p-value and fold change (FC) are listed. Proteins associated with complex I of the respiratory chain are marked with bold letters. Proteins above the red line are down-regulated and below the red line are up-regulated.

Gene name	Protein description	p-value	Fold change SMA/ WT
Cox7c	Cytochrome c oxidase subunit 7C, mitochondrial	0.006	0.39
Ndufb8	NADH dehydrogenase [ubiquinone] 1 beta subcomplex subunit 8, mitochondrial	0.038	0.75
Ndufv2	NADH dehydrogenase [ubiquinone] flavoprotein 2, mitochondrial	0.028	0.78
Ppa2	Inorganic pyrophosphatase 2, mitochondrial	0.008	0.83
Ndufa5	NADH dehydrogenase [ubiquinone] 1 alpha subcomplex subunit 5	0.002	0.86
Ndufb5	NADH dehydrogenase [ubiquinone] 1 beta subcomplex subunit 5, mitochondrial	0.032	0.88
Ndufa6	NADH dehydrogenase [ubiquinone] 1 alpha subcomplex subunit 6	0.008	1.55
Ndufc2	NADH dehydrogenase [ubiquinone] 1 subunit C2	0.001	1.52

Table 1: (continued)

Gene name	Protein description	p-value	Fold change SMA/ WT
Ndufab1	Acyl carrier protein. mitochondrial	0.017	1.47
Ndufb4	NADH dehydrogenase [ubiquinone] 1 beta subcomplex subunit 4	0.002	1.40
Ndufa10	NADH dehydrogenase [ubiquinone] 1 alpha subcomplex subunit 10, mitochondrial	0.019	1,16

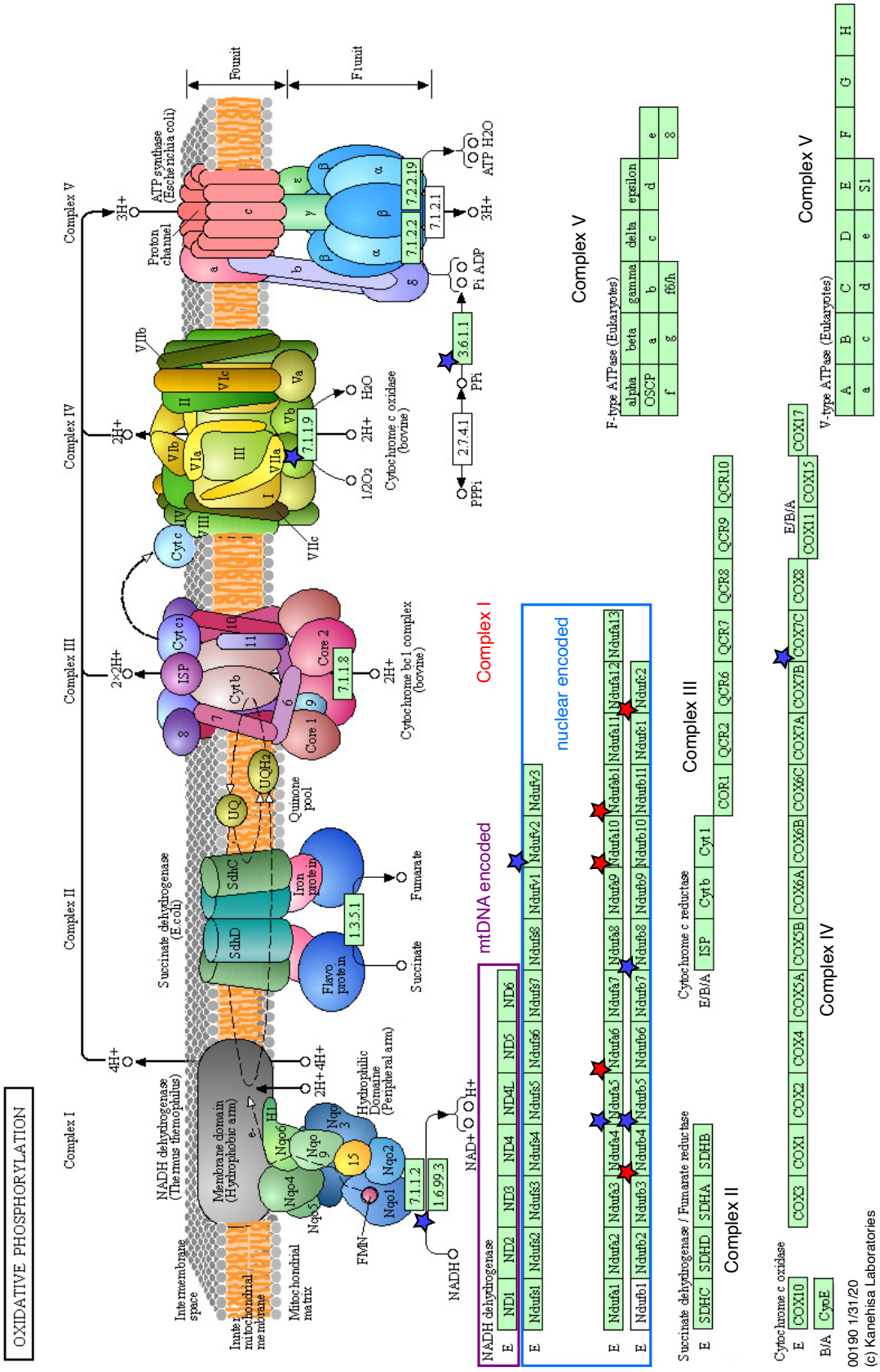

Figure 13: Representation of oxidative phosphorylation KEGG Pathway (mmu00190). Green boxes highlight organism-specific complexes (*Mus musculus*). Stars mark significantly up- regulated (red) and down-regulated (blue) proteins in SMA MNs (10DIV). Copyright permission obtained from KEGG (Kanehisa, 2000).

Based on our MS results indicating defects in complex I of the electron transport chain, we measured the activity of complex I in WT and SMA MNs biochemically. In brief, mitochondria were isolated from 10DIV MNs and subsequently lysed. After isolation of individual respiratory complexes, complex I was bound to a 96-well plate with specific antibodies attached to the plate. After unbound proteins were removed, the oxidation of NADH to NAD^+ is visualized by simultaneous reduction of a dye, resulting in an increased absorbance at OD = 450 nm.

Different amounts of mitochondrial extracts from WT MNs were tested to evaluate the sensitivity of the assay (**Figure 14**). The assay showed high sensitivity in a range between 1.88 µg to 15 µg of mitochondria. The increased absorbance at OD = 450 nm was measured for 1 h.

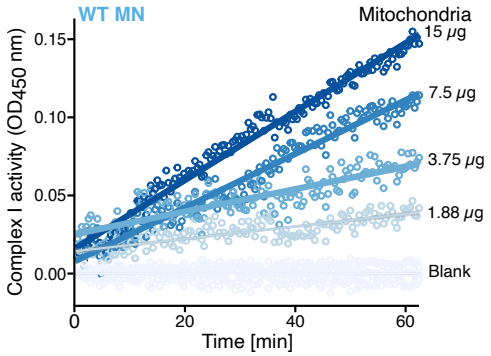

Figure 14: Optimization of complex I assay in primary WT MNs.
Optimization of Complex I activity for 1 h using different amounts of mitochondria extract isolated from WT MNs (10DIV).

As the complex I assay showed high sensitivity with 15 µg of isolated mitochondria, but we hypothesized a lower enzyme activity in SMA, 20 µg extract was used when comparing WT and SMA MNs. Indeed, complex I activity is significantly reduced in SMA MNs compared to WT MNs by comparing the two slopes (**Figure 15A**). By comparing the ratio of mean OD_{450} per h, complex I activity is reduced by half in SMA MNs (**Figure 15B**).

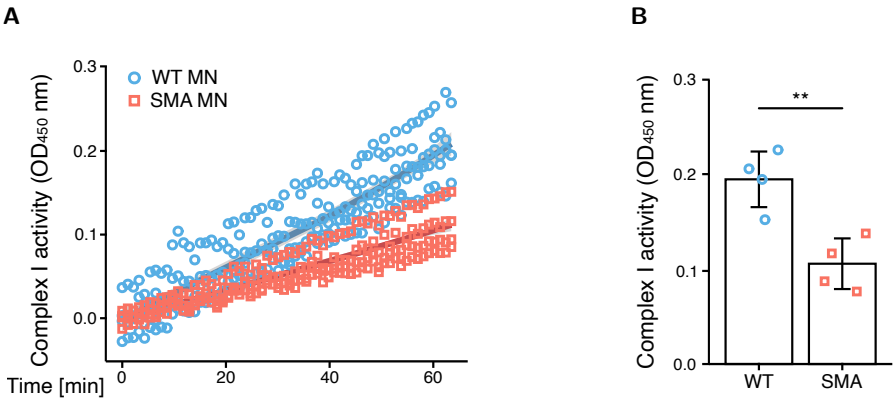

Figure 15: Complex I activity is reduced in SMA MNs.
A) Complex I activity using 20 µg mitochondria extract isolated from WT and SMA MNs (10DIV). Quantification represents the increase of OD_{450} nm during 1 h. **B)** Complex I activity rate using 20 µg mitochondria extract isolated from WT and SMA MNs (10DIV) (N=4). Quantification represents the increase of mean OD_{450} nm/ h. Bar graph depict the mean ± SD. Two-tailed unpaired t-test was used on independent biological replicates to determine statistical significance **p <0.01.

Furthermore, we measured the complex I activity in two other tissues. One was the metabolically active heart tissue, and the other one was the spinal cord (**Figure 16**). Neither heart nor spinal cord showed reduced activity of complex I (**Figure 16**).

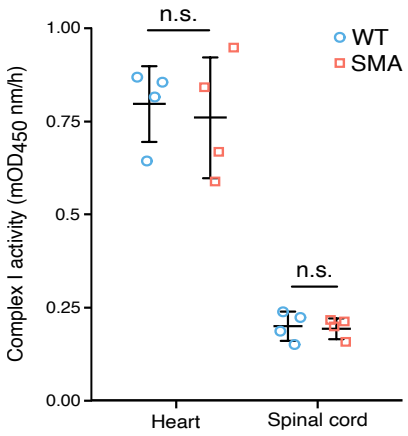

Figure 16: Complex I activity is not changed in heart or spinal cord.
Complex I activity using 300 µg protein extracts of heart and spinal cord from P7 WT and SMA mice (N=4). Quantification represents the increase of mean OD_{450} nm/ h ± SD. To compare WT (blue circles) and SMA (red squares), two-way ANOVA with Tukey HSD post hoc analysis was used on independent biological replicates (N=4) to determine statistical significance. ns $p > 0.05$.

3.3.2 ROS levels are increased in SMA MNs

As our MS results indicated defects in complex I and activity measurements confirmed the dysfunction biochemically, we measured intracellular ROS levels using CellROX® (**Figure 17A and Figure 17B**). In brief, CellROX™ Green is a cell-permeant nonfluorescent probe, which exhibits fluorescence upon oxidation by the sample. The oxidized probe remains localized within the cell due to binding to DNA.

As mitochondria are accumulated in the soma, differences in ROS between WT and SMA MNs can be measured most precisely in the soma. Indeed, our data showed that ROS levels were higher in SMA compared to WT (**Figure 17A and Figure 17B**). Two independent detection methods confirmed this finding. First, fluorescence signals of individual neurons were observed and quantified by imaging. This technique showed an ~25% increase of ROS in SMA somata compared to WT ones (**Figure 17A**). In addition to individual quantification of cell bodies, ROS levels in whole cells were quantified. Measurements using a microplate reader, resulted in an ~40% increase of ROS in SMA MNs compared to WT ones (**Figure 17B**). In healthy condition, ROS can be eliminated by oxidative stress defense proteins such as superoxide dismutase (SOD1), which clears ROS from the mitochondrial intermembrane space (Klöppel et al., 2010). Interestingly, SOD1 protein levels are down-regulated in SMA MNs due to our proteomics analysis, indicating defective oxidative stress defense mechanism in SMA (**Figure 8**).

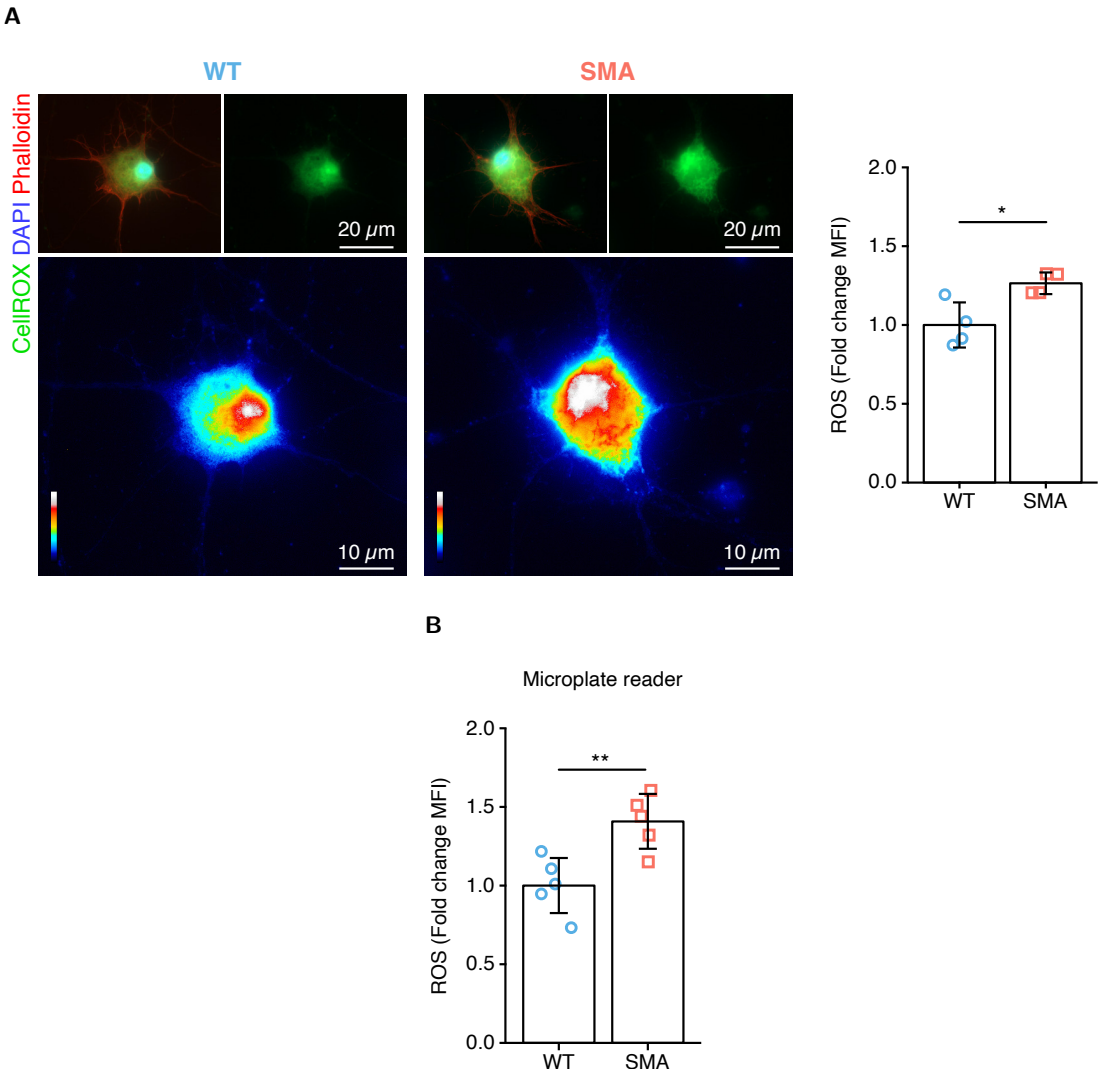

Figure 17: ROS levels are increased in SMA MNs.
A) Representative images of WT and SMA MNs labelled with CellROX® (green and rainbow color) for reactive oxygen species (ROS) detection, DAPI (blue) and Phalloidin (red). Rainbow color indicates the intensity of CellROX® signal. Scale bar of enlarged CellROX® images: 10 µm; Scale bar of neuron: 20 µm. Quantification of mean fluorescence intensity of the CellROX® signal in WT and SMA MN (red squares) (n=40, N=4). **B)** Quantification of CellROX® signal of WT and SMA MNs measured with microplate reader (N=5). Bar graphs depict the mean ± SD. Two-tailed unpaired t-test was used on independent biological replicates to determine statistical significance *p <0.05, **p <0.01.

3.3.3 Proteins are hypercarbonylated in SMA MNs

One direct effect of oxidative stress on proteins is carbonylation (Suzuki et al., 2010). Thus, carbonylation is a well-used indicator for oxidative stress. The oxidation of proteins occurs when excessive ROS form reactive ketones or aldehydes at the amino acid side chains. We made use of the hydrazone formation by reaction of the ketone or aldehyde side chains with 2,4-dinitrophenylhydrazine (DNPH). Subsequently, DNP moieties were detected using an anti-DNP antibody and quantified the signals by western blotting. As higher levels of ROS were detected in SMA MNs, we measured levels of carbonylated proteins in SMA MNs (**Figure 18**). Indeed, nearly double the amount (~89%) of protein carbonylation was detected in SMA MNs

compared to WT ones (**Figure 18**). This data confirmed our finding that SMA MNs are under oxidative stress by increased levels of ROS.

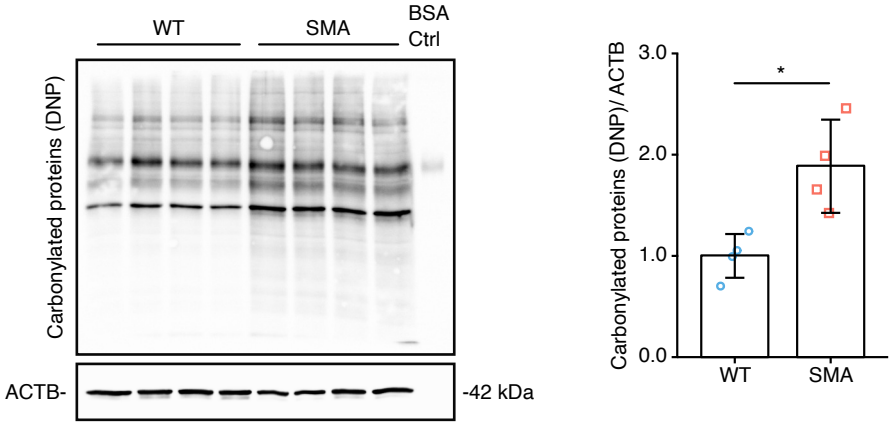

Figure 18: Proteins are hypercarbonylated in SMA MNs.
Western blot analysis and quantification of carbonylated proteins (DNP = 2,4-dinitrophenyl) in 10DIV WT and SMA MNs (N=4). Quantification of DNP signal was normalized to ACTB. Bar graphs depict the mean ± SD. Two-tailed unpaired t-test was used on independent biological replicates to determine statistical significance *p <0.05.

3.4 Energy homeostasis in MNs

During development, neurons switch their way of producing energy from aerobic glycolysis towards oxidative phosphorylation (Zheng et al., 2016). In this study, primary MNs were used after 10DIV as it is assumed that, after 7 to 14 days in culture, embryonic and postnatal neurons show similar properties in their energy homeostasis and response to oxidative stress (Surin et al., 2013).

3.4.1 Glucose uptake is reduced in SMA MNs

Mature neurons are considered to produce their energy mainly through OXPHOS (Zheng et al., 2016), but neurons can produce energy from glycolysis to compensate for their high energy demand (Díaz-García et al., 2017). Especially, neurons are shown to up-regulate glycolysis at nerve terminals upon high energy demand in firing neurons (Ashrafi et al., 2017). Therefore, glucose uptake was monitored. In brief, 10DIV MNs were lysed, and intracellular glucose is detected by a coupled enzyme reaction of glucose oxidation, leading to NADH production with a bioluminescent NADH detection system. Interestingly, glucose uptake is impaired in SMA MNs by half (**Figure 19**).

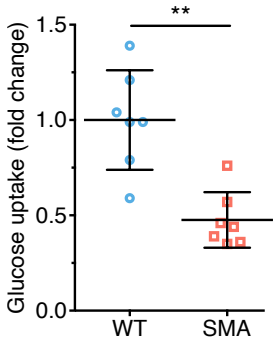

Figure 19: Glucose uptake is reduced in primary SMA MNs.
Each dot represents data from biological replicates (N=7). Two-tailed unpaired t-test was used to determine statistical significance. Graphs depict the mean ± SD. **p <0.01. Blue circles represent WT MNs and red squares represent SMA MNs. 10DIV MNs were used.

3.4.2 ATP levels are lower in SMA MNs

As both energy-producing pathways, glycolysis, and OXPHOS are impaired in SMA MNs, we next measured the intracellular ATP concentrations. Intracellular ATP concentrations can be measured in different ways. Here, we used a fluorimetric but also a luminescence approach. The fluorimetric detection is achieved by phosphorylation of glycerol, consuming the intracellular ATP, subsequently resulting in a proportional fluorimetric signal (λ ex = 535/λem = 587 nm). The luminescence approach uses a recombinant firefly luciferase, generating a light signal by consuming intracellular ATP together with the substrate D-luciferin (emission maximum ~560 nm at pH 7.8). Indeed, ATP concentration is between 3-fold and 4-fold lower in SMA compared to WT MNs (**Figure 20**). Together, these results suggest that energy homeostasis is impaired in SMA MNs due to defective mitochondria, and glycolysis cannot compensate for this defect.

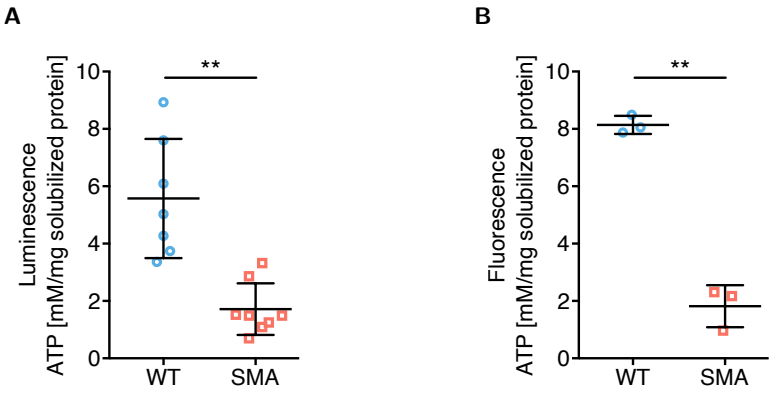

Figure 20: ATP levels are reduced in primary SMA MNs.
Intracellular ATP levels of primary MNs normalized to solubilized protein detected by luminescence (**A**) and fluorescence (**B**). Each dot represents data from biological replicates of WT MNs (N=7) and SMA MNs (N=8) (**A**) and (N=3) (**B**). Two-tailed unpaired t-test was used to determine statistical significance. Graphs depict the mean ± SD. **p <0.01. Blue circles represent WT MNs and red squares represent SMA MNs. 10DIV MNs were used.

3.5 Oxidative stress impairs global translation in SMA MNs

Mitochondria are considered the major producer of intracellular ROS. An imbalance of ROS can occur due to increased electron leakage of dysfunctional respiratory chain complexes. Mostly, complex I of the electron transport chain is known to be the major source of ROS in mitochondria (Y. Liu et al., 2002). Increased levels of ROS can lead to intracellular oxidative stress and amplify mitochondrial defects by damaging mitochondrial DNA. However, mitochondrial DNA damage is not the only impairment resulting from increased ROS levels. Also, increased ROS can result in reversible and irreversible changes in the translation machinery (Topf et al., 2018).

3.5.1 Global translation is impaired in SMA MNs

Furthermore, irreversible carbonylation of proteins can alter their conformation and lead to protein degradation by the proteasome (Nyström, 2005). In case ribosomal proteins are affected by carbonylation, this can alter subsequent protein synthesis (Nyström, 2005; Scott et al., 2004). Due to our quantitative proteomics approach, proteins associated with ribosomes and translation-related proteins are dysregulated in SMA. Therefore, we measured protein synthesis efficiency with Surface sensing of translation (SUnSET) (Schmidt et al., 2009) and AHA-Click-iT assay in WT and SMA MNs (**Figure 21A and Figure 22A**). Both methods are used to label newly synthesized proteins by either low concentrations (1 µM) of the tyrosyl-aminoacyl-tRNA analog puromycin (**Figure 21A**) or the methionine analog L-azidohomoalanine (L-AHA). Due to the lack of a hydrolyzable amide bond, the incorporation of puromycin leads to translation elongation termination. However, even though puromycin can be used as a protein synthesis inhibitor, at low dosage, it does not interfere with the overall rate of protein synthesis (Schmidt et al., 2009).
10DIV primary WT and SMA MNs were incubated with 1 µM puromycin for 30 min. Subsequently, puromycin labeled proteins were detected by western blotting and normalized to ACTB levels. Indeed, we show that SMA MNs have a reduced protein synthesis efficiency (~42%) compared to WT MNs by SUnSET assay (**Figure 21B**).

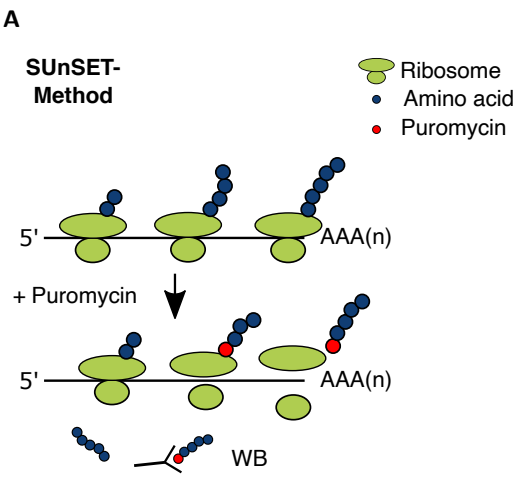

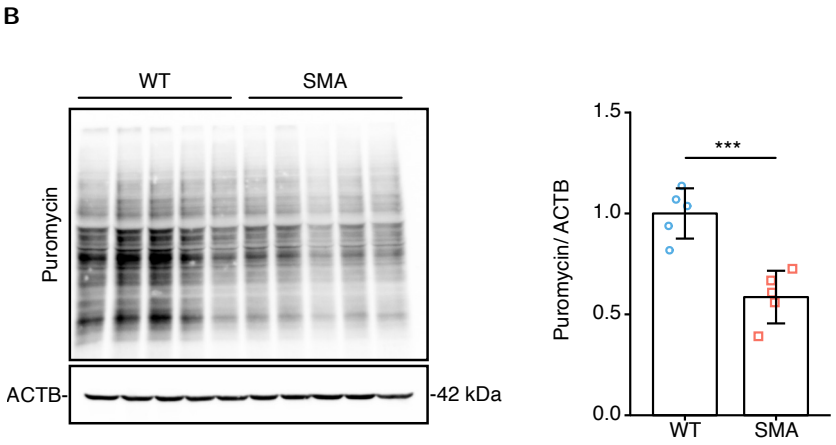

Figure 21: Translation is reduced in SMA MNs (SUnSET).
A) Schematic drawing of SUnSET method. Puromycin labels newly synthesized proteins. Puromycin is detected by an anti-puromycin antibody. **B)** SUnSET assay in WT and SMA MNs (N=5). ACTB was used as loading control. Blue circles represent data from WT, and red squares represent SMA MNs. Bar graph depict the mean ± SD. Two-tailed unpaired t-test was used on independent biological replicates to determine statistical significance ***p <0.001.

To rule out any inhibitory effects of the increased ROS levels on the SUnSET assay, the results were confirmed by an alternative method, the AHA-Click-iT assay. In brief, 500 µM of the methionine analog L-azidohomoalanine (L-AHA) were added to 10DIV MNs for 1 h after endogenous methionine reserves were depleted by incubation for 30 min in HBSS. After incorporation of AHA during protein synthesis, the azide residue is covalently bound with biotin alkyne by click chemistry. Further, biotin is detected with specific antibodies during western blot analysis. As a result, a reduction of one third was observed in SMA MNs compared to WT ones (**Figure 22B**). Taken together, these results suggest a negative relationship between ROS levels and protein synthesis in SMA MNs.

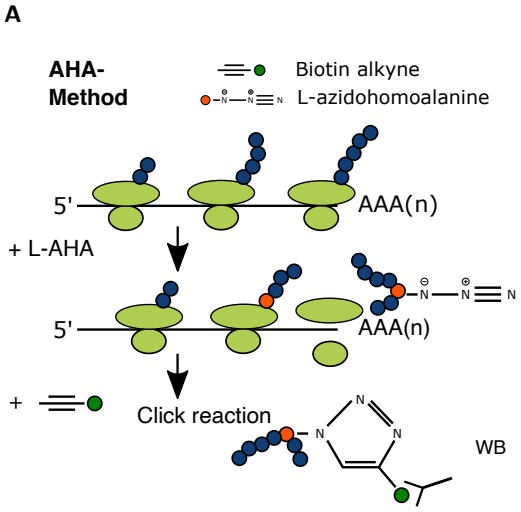

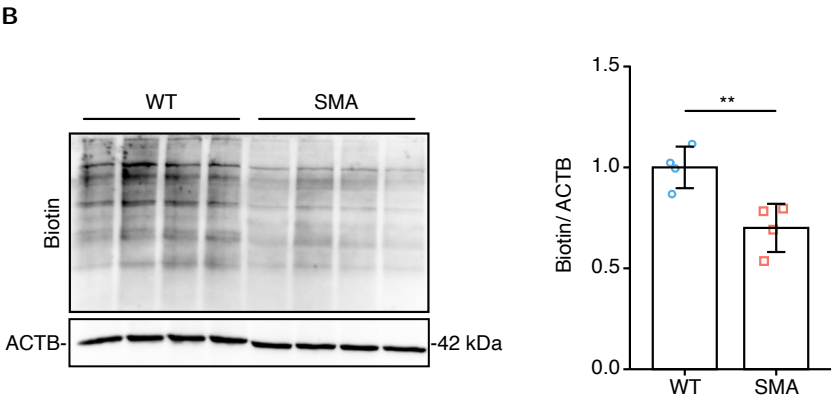

Figure 22: Translation is reduced in SMA MNs (AHA).
A) Schematic drawing of the AHA method. L-azidohomoalanine (L-AHA) is incorporated into newly synthesized proteins, followed by click chemistry reaction with biotin alkyne. Biotin labelled proteins can be detected by western blot analysis. **B)** AHA assay in WT and SMA MNs (N=4). ACTB was used as loading control. Blue circles represent data from WT, and red squares represent SMA MNs. Bar graph depicts the mean ± SD. Two-tailed unpaired t-test was used on independent biological replicates to determine statistical significance **p <0.01.

3.6 Pyruvate restores ATP levels and reduces ROS levels in SMA MNs

Based on the imbalanced energy homeostasis in SMA MNs, we aimed to restore intracellular ATP levels by supplementing appropriate substrates used for energy production. By now, lactate is not only seen as a by-product of glycolysis but rather an important energy substrate for neurons. Prior studies that have noted the importance of lactate in neurons revealed a shuttle of astrocyte-derived lactate towards neurons *in vivo* (Mächler et al., 2016). In addition, pyruvate can be used by neurons directly for energy production via OXPHOS in mitochondria. Also, we pursued to counteract oxidative stress, the consequence of defective mitochondria in SMA. As pyruvate is known to reduce ROS in a non-enzymatic way and is a known substrate of the TCA cycle (Desagher et al., 1997), we supplemented NSC-34 cells as well as WT and SMA MNs with 10 mM or 50 mM sodium lactate or sodium pyruvate.

3.6.1 Lactate does not increase intracellular ATP

To optimize lactate concentrations as a substrate for energy production, NSC-34 cells were used. Those cells have well-working mitochondria, and therefore supplementing lactate is supposed to be beneficial. Over a time period of 1 h, two concentrations, 10 mM and 50 mM lactate were added into the culture medium (**Figure 23A and Figure 23B**). None of the concentrations increased the intracellular ATP levels significantly over 1 h supplementation (**Figure 23**).

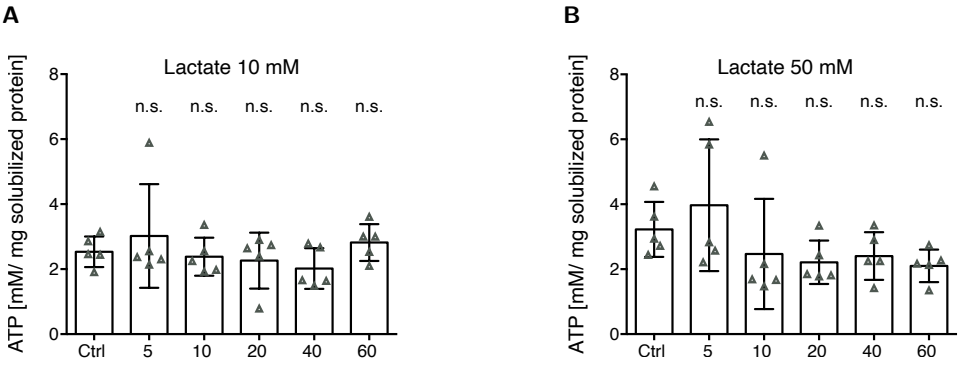

Figure 23: Lactate does not increase ATP in NSC-34 cells.
Optimization of treatment with 10 mM lactate (**A**) and 50 mM lactate (**B**) for 1 h. 10 mM lactate and 50 mM lactate supplement do not increase ATP levels in NSC-34 cells (N=5). Bar graph depicts the mean ± SD. One-way ANOVA with Dunnett post hoc analysis was used to compare each timepoint with the control.

3.6.2 Pyruvate increases intracellular ATP

Since lactate was unable to increase intracellular ATP levels, pyruvate was used as a supplement. Pyruvate is proposed to increase ATP levels in postnatal neurons upon glucose deprivation (Surin et al., 2013). Again, NSC-34 cells were used to optimize the concentration over 1 h. No significant increase of intracellular ATP was observed after 1 h supplementation of 10 mM pyruvate (**Figure 24A**). However, supplementation of 50 mM pyruvate increased ATP levels significantly in NSC-34 cells within 1 h (**Figure 24B**). Already 10 min of supplementation with 50 mM pyruvate were sufficient to double the concentration of intracellular ATP (**Figure 24B**).

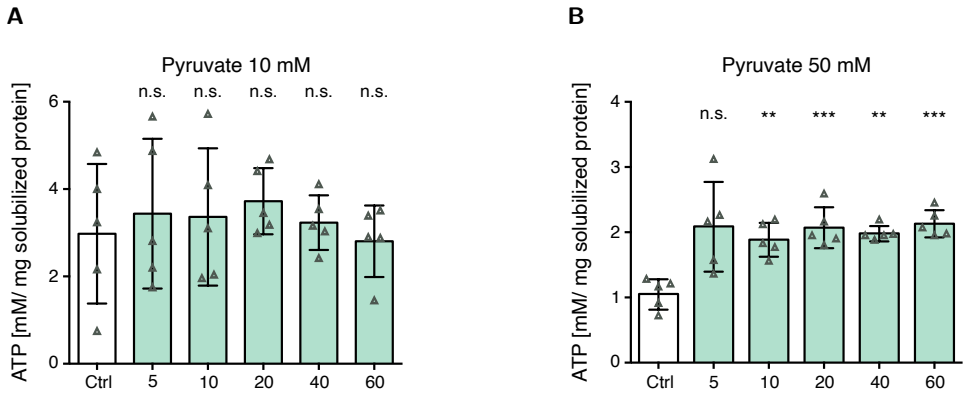

Figure 24: Pyruvate 50 mM increases ATP in NSC-34 cells.
Optimization of treatment with 10 mM pyruvate (**A**) and 50 mM pyruvate (**B**) for 1 h. 10 mM pyruvate supplement does not increase ATP levels in NSC-34 cells (N=5). 50 mM pyruvate increases ATP levels after 10 min in NSC-34 cells (N=5). Bar graph depicts the mean ± SD. One-way ANOVA with Dunnett post hoc analysis was used on independent biological replicates to compare each timepoint with the control. **p <0.01, ***p <0.001.

Pyruvate needs to be taken up by the cell to reach the mitochondria for energy production. Therefore 50 mM pyruvate was added into the culture medium for 10 min, 20 min, and 60 min. Afterward, cells were lysed and intracellular pyruvate concentration was measured by a coupled enzyme assay, which results in a fluorometric (λ_{ex} = 535/ λ_{em} = 587 nm) product, proportional to the pyruvate in the sample. Interestingly, the intracellular pyruvate concentration was significantly increased already after 10 min (**Figure 25**). The intracellular pyruvate concentration was stable over 1 h, meaning the amount of pyruvate supplied to MNs is sufficient for this period of time.

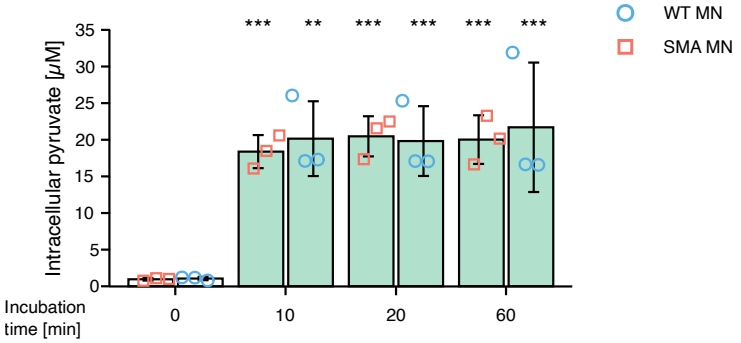

Figure 25: Pyruvate uptake in MNs.
Supplementation of WT MNs (blue circles) and SMA MNs (red squares) with 50 mM pyruvate shows a significant increase of intracellular pyruvate uptake (N=3). Bar graph depicts the mean ± SD. One-way ANOVA with Dunnett post hoc analysis was used to compare each timepoint with the control. **p <0.01, ***p <0.001.

Surprisingly, lactate did not only fail to increase ATP levels in NSC-34 cells but also showed no effect in WT MNs or SMA MNs (**Figure 26**).

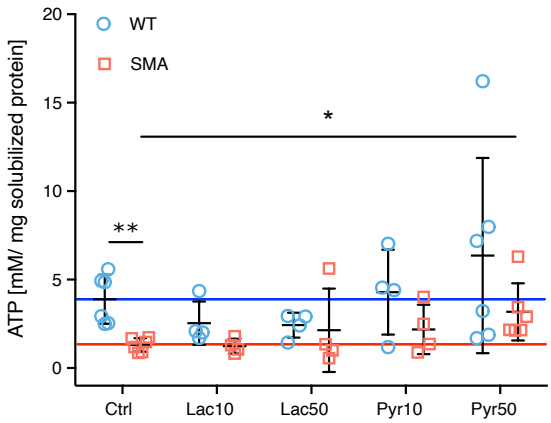

Figure 26: Pyruvate increases ATP in MNs.
Supplementation of WT MNs (blue circles) and SMA MNs (red squares) with 10 mM/ 50 mM lactate or 10 mM/ 50 mM pyruvate for 1 h. 50 mM pyruvate treatment shows a significant increase of ATP levels in SMA MNs (N=6). Graph depicts the mean ± SD. Two-tailed unpaired t-test was used on independent biological replicates to determine statistical significance. Means of two groups were compared, *p <0.05, **p <0.01.

The single most striking observation to emerge from supplementing lactate and pyruvate as substrates was the increase of ATP in SMA MNs after 50 mM pyurvate supplementation for 1 h (**Figure 26 & Figure 27**). However pyruvate did not significantly increase ATP levels in WT MNs (**Figure 26 & Figure 27**).

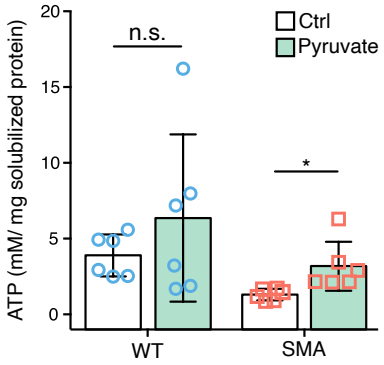

Figure 27: Pyruvate increases ATP in SMA MNs.
ATP levels in WT and SMA MNs normalized to solubilized protein after 50 mM pyruvate supplementation for 1 h. 50 mM pyruvate increased ATP in SMA MNs with no effect in WT MNs. Two-tailed unpaired t-test was used on independent biological replicates to determine statistical significance *p <0.05. Blue circles represent data from WT and red squares represent SMA MNs. Each dot represents the quantification of individual biological replicates (N=6). Bar graphs depict the mean ± SD.

Overall, lactate, which can be converted to pyruvate by lactate dehydrogenase in the cytoplasm (Adams et al., 1973), neither improved ATP levels in NSC-34 cell (**Figure 23**) nor in primary MNs (**Figure 26**). However, direct supplementation of pyruvate was sufficient to increase ATP levels in SMA MNs (**Figure 27**).

3.6.3 Pyruvate reduces ROS

In addition, as pyruvate has been suggested to act as a ROS scavenger (Kładna et al., 2015), we treated SMA MNs with 50 mM pyruvate for 1 h and measured ROS levels via fluorescence CellROX® dye. Detection of the fluorescence signal was achieved by a microplate reader. As a positive control, 10 µM of the antioxidant NAC was supplied for 1 h to NSC-34 cells. Since NSC-34 cells do not have elevated ROS levels, supplementation of pyruvate or NAC showed no effect (**Figure 28**). Nevertheless, menadione, which increases intracellular ROS levels via futile redox cycling (Loor et al., 2010), increased ROS levels in NSC-34 cells drastically up to four times (**Figure 28**). Instead, 50 mM pyruvate or 10 µM NAC simultaneously applied with 100 µM menadione for 1 h could reduce menadione-induced ROS levels by ~25% (**Figure 28**). Overall, these results indicate a possible benefit of antioxidants for cells with elevated ROS levels such as SMA MNs.

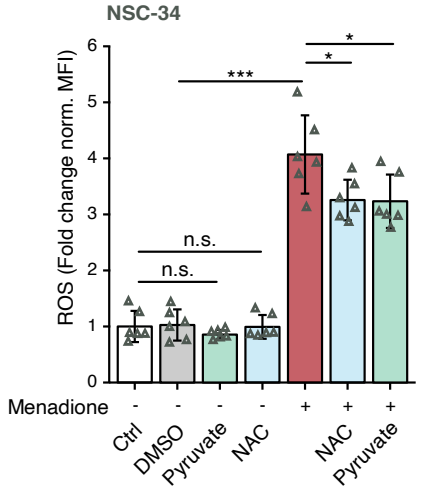

Figure 28: Pyruvate reduces ROS after pharmacologically induced oxidative stress.
Quantification of mean fluorescence intensity of CellROX® signal in NSC-34 cells. Menadione increases ROS levels, whereas 10 µM NAC or 50 mM pyruvate reduces ROS induced by 100 µM menadione for 1 h (N=6). One-way ANOVA with Tukey HSD post hoc analysis was used on independent biological replicates (N=3) to determine statistical significance. *p <0.05, ***p <0.001. Each dot represents the quantification of individual biological replicates. Bar graphs depict the mean ± SD.

Since pyruvate and NAC were able to reduce pharmacologically induced ROS, the effect of pyruvate or NAC on ROS levels in SMA MNs needs to be investigated. Indeed, pyruvate successfully reduces ROS levels in SMA MNs. However, menadione further increased ROS levels in SMA MNs as it was observed in NSC-34 cells (**Figure 29**). These results suggest that pyruvate is a valuable supplement to restore ATP levels and simultaneously balance intracellular ROS levels in SMA MNs. Our results are in line with previous experiments, stating the ant-oxidative effect of pyruvate (Kładna et al., 2015).

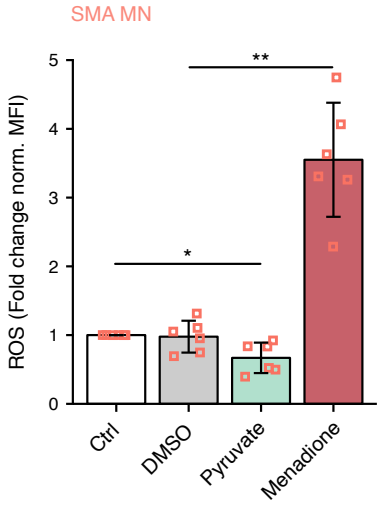

Figure 29: Pyruvate reduces ROS in SMA MNs.
ROS levels of SMA MNs after 50 mM pyruvate and 100 µM menadione supplementation for 1 h. While pyruvate reduces ROS, menadione increases ROS in SMA MNs. Two-tailed unpaired t-tests with Holm-Bonferroni correction for multiple comparisons were used to determine statistical significance. *p $<$0.05, **p $<$0.01. Each dot represents the quantification of individual biological replicates (N=6). Bar graphs depict the mean $\pm$ SD.

3.7 Effect of ROS on global protein synthesis in neurons

Based on our data, we hypothesized that the elevated ROS levels and the associated hypercarbonylation hinder protein synthesis. Thus, the reduction of ROS might restore impaired protein synthesis in SMA MNs. To further understand the effect of ROS on protein synthesis, we modified cellular ROS levels in MNs and measured protein synthesis efficiency. To measure the protein synthesis rate, again, the nonradioactive SUnSET assay was used. The relationship between ROS and protein synthesis was examined in NSC-34 cells, WT MNs, and SMA MNs. NSC-34 cells were differentiated for three days using retinoic acid. Primary MNs were harvested 10 days after isolation from E13.5 embryonic spinal cords. All cells were supplied with 10 µM NAC or 50 mM pyruvate for 1 h. To evaluate the effect of induced ROS, 100 µM menadione was used. As a negative control, 50 µM of the protein synthesis inhibitor anisomycin was added for 1 h. Labeling with 1 µM puromycin was carried out 30 min before cells were harvested. Our experimental set up is outlined in **Figure 30**.

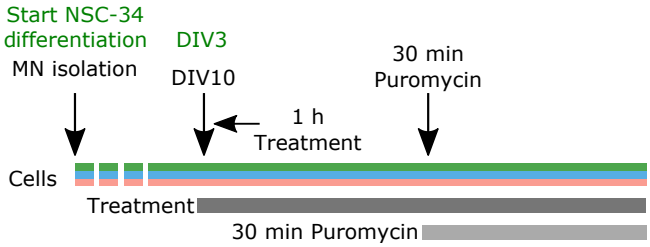

Figure 30: Experimental set up of SUnSET assay in NSC-34 cells, WT & SMA MNs.
NSC-34 cells are differentiated for 3 days before treatment with 50 mM pyruvate, 10 µM NAC or 100 µM menadione for 1 h. WT & SMA MNs were additionally treated with 50 µM anisomycin for 1 h. 1 µM puromycin was added after 30 min of treatment for an additional 30 min.

3.7.1 Regulating ROS has no effect on global translation in NSC-34 cells or WT MNs

As we already found out, pyruvate or NAC had no anti-oxidative effect on NSC-34 cells, whose ROS levels are in a normal range. Therefore, it is not surprising that protein synthesis efficiency is also unaltered by pyruvate or NAC in NSC-34 cells (**Figure 31**). However, 100 µM menadione induced ROS clearly and, therefore, also reduced protein synthesis drastically (**Figure 31**).

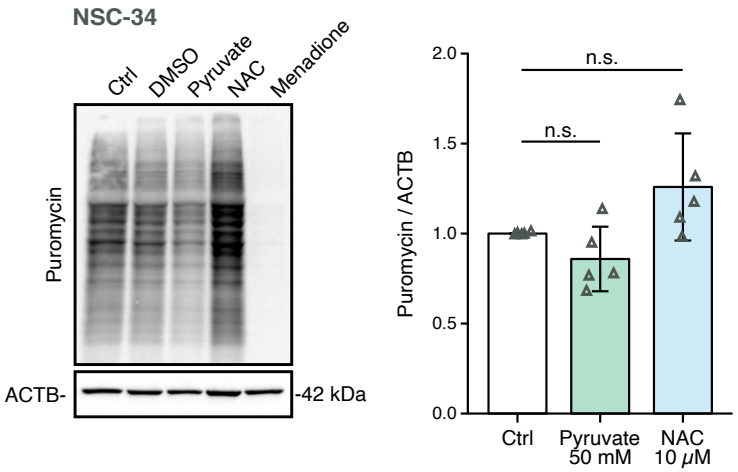

Figure 31: Regulating ROS has no effect on NSC-34 cells.
Representative western blot and quantification of SUnSET assay in NSC-34 cells. Neither 50 mM pyruvate nor 10 µM NAC changed protein synthesis significantly. Each dot represents the quantification of individual biological replicates (N=5). Bar graphs depict the mean ± SD. Two- tailed unpaired t-test with Holm-Bonferroni correction for multiple comparisons was used to determine statistical significance. ns p >0.05.

Similar to NSC-34 cells, WT MNs are capable of regulating intracellular ROS levels. Therefore, it is not particularly surprising that 50 mM pyruvate and 10 µM NAC does not increase protein synthesis efficiency in WT MNs (**Figure 32**). Nevertheless, inducing ROS by 100 µM menadione results in a reduction of protein synthesis efficiency (**Figure 32**), which means that inducing ROS, in general, does reduce global protein synthesis. As a negative control, 50 µM anisomycin was used.

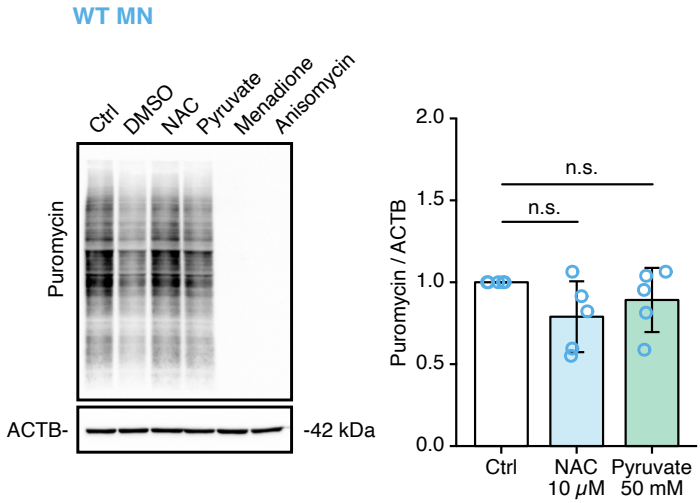

Figure 32: Regulating ROS has no effect on protein synthesis in WT MNs.
Representative western blot and quantification of SUnSET assay after ROS modification in WT MNs (N=5). Neither 10 µM NAC nor 50 mM pyruvate supplementation for 1 h changed protein synthesis significantly in WT MNs. Bar graphs depict the mean ± SD. Two-tailed unpaired t-tests with Holm-Bonferroni correction for multiple comparisons were used to determine statistical significance. ns p >0.05.

3.7.2 Regulating ROS modulates global protein synthesis in SMA MNs

Interestingly, for SMA MNs, where cellular ROS levels are higher, a reduction of ROS by adding 10 µM NAC could increase protein synthesis (**Figure 33**). However, no consistent increase in protein synthesis was observed in pyruvate supplemented SMA MNs. The use of 100 µM menadione further increased ROS in SMA MNs (**Figure 29**) and therefore reduced protein synthesis even further (**Figure 33**).
Taken together, our data strongly suggests that intracellular ROS influences protein synthesis in MNs. Modulating ROS can inversely regulate global protein synthesis.

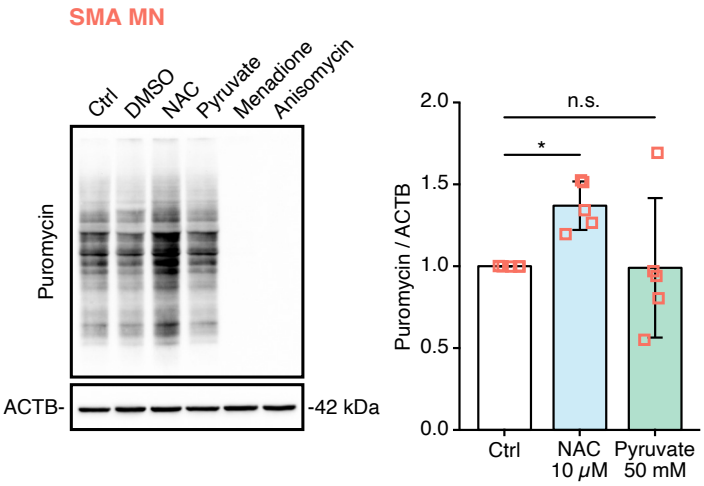

Figure 33: Regulating ROS with NAC increases protein synthesis in SMA MNs.
Representative western blot and quantification of SUnSET assay after ROS modification in SMA MNs (N=5). Supplementation of 10 µM NAC increased protein synthesis in SMA MNs. However, 50 mM pyruvate supplementation for 1 h did not change protein synthesis in SMA MNs. Bar graphs depict the mean ± SD. Two-tailed unpaired t-tests with Holm-Bonferroni correction for multiple comparisons were used to determine statistical significance. ns $p > 0.05$, *$p < 0.05$.

3.8 Effect of ROS on local protein synthesis in neurons

One important aspect of investigating neurons is the subcellular compartmentalization. More frequently, defective local translation is observed in neurodegenerative disorders (Thelen & Kye, 2020). In order to investigate local protein synthesis in primary MNs, we performed the SUnSET experiment. However, instead of evaluating global translation by western blotting, we analyzed the neuronal compartments individually by imaging analysis. Furthermore, we investigated whether ROS regulates axonal local protein synthesis in MNs. Same with previous experiments, 10DIV MNs were used and supplied with 1 µM puromycin to mark newly synthesized proteins. However, puromycin labeled proteins were detected with a fluorescently conjugated secondary antibody. To track the axon, MNs were simultaneously labeled with anti-Tau specific antibodies. For the quantification of the protein synthesis along the axon, 100 µm fractions were analyzed separately. To compare WT and SMA MNs with and without ROS modification, five biological replicates were analyzed.

3.8.1 Local protein synthesis is reduced in SMA MNs

As we used 10DIV MNs, protein synthesis is expected to be lower compared to actively growing neurons. Therefore, we analyzed newly synthesized proteins in different axonal compartments. First, we measured the mean fluorescence signals of newly synthesized proteins labeled with puromycin in the soma of WT and SMA MNs. Our data reveals a reduction of ~50% in SMA MNs compared to WT ones (**Figure 34B**). The axonal compartment was divided into 20 µm bins, and the mean values of each 100 µm fraction were compared between WT and SMA MNs. As expected, proximal fractions have higher anti-puromycin signals compared to distal parts. However, a significant reduction of protein synthesis in SMA MNs compared to WT MNs was observed in the first three, most proximal fractions (**Figure 34C**).
Overall, protein synthesis is globally impaired in SMA MNs, but also individual compartments such as soma and axon show reduced protein synthesis in SMA MNs.

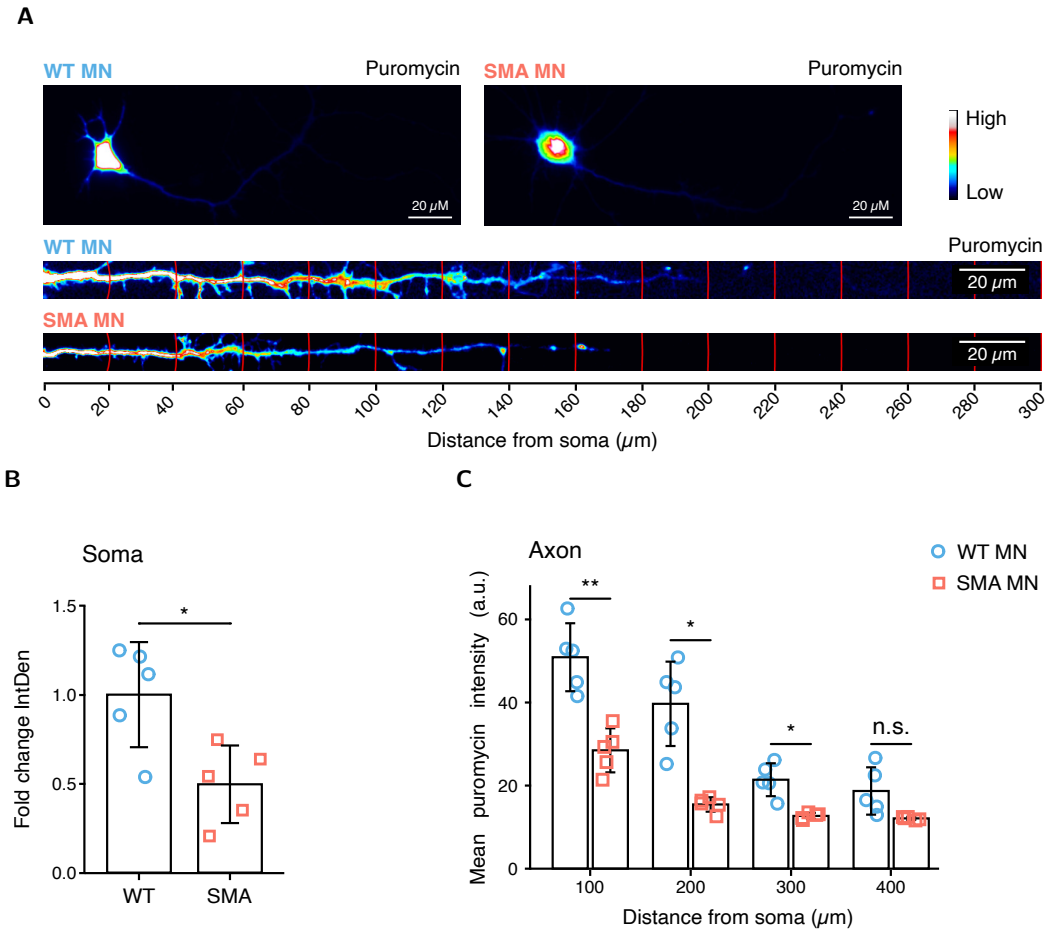

Figure 34: Axonal local translation is reduced in SMA MNs.
Quantification of mean puromycin intensity profiles confirms that protein synthesis is reduced in soma and axonal compartment of SMA MNs. **A)** Representative images of 10DIV WT and SMA MNs labelled with anti-puromycin antibody (rainbow color). Neurites were selected with a segmented line, straightened and divided into 20 µm bins using the concentric circles plugin. **B)** Quantification of mean puromycin intensity of soma. **C)** Quantification of mean puromycin intensity profiles in axonal compartment. Scale bar: 20 µm. Each dot represents the average quantification of 10 neurons of 5 individual biological replicates (N=5). Bar graphs depict the mean ± SD. Two-tailed unpaired t-test with Holm-Bonferroni correction for multiple comparisons was used to determine statistical significance. ns p >0.05, *p <0.05, **p <0.01.

3.8.2 Regulating ROS does not improve local protein synthesis in WT MNs

We were able to modulate ROS levels in primary MNs by supplementation of NAC or pyruvate. Furthermore, global protein synthesis was modulated by ROS regulation presented in **section 3.7**. However, NAC and pyruvate did not change global translation in NSC-34 cells or WT MNs, whose ROS levels are in an optimal range. Nevertheless, a closer look comparing the soma of WT MNs treated with 10 µM NAC, 50 mM pyruvate, 100 µM menadione, or 50 µM anisomycin for 1 h confirmed our previous results of global protein synthesis. Neither NAC, nor pyruvate changed protein synthesis in the soma of WT MNs (**Figure 35**). However, induction of ROS by menadione or inhibition of translation by anisomycin showed a clear reduction of protein synthesis in the soma of WT MNs (**Figure 35B**).

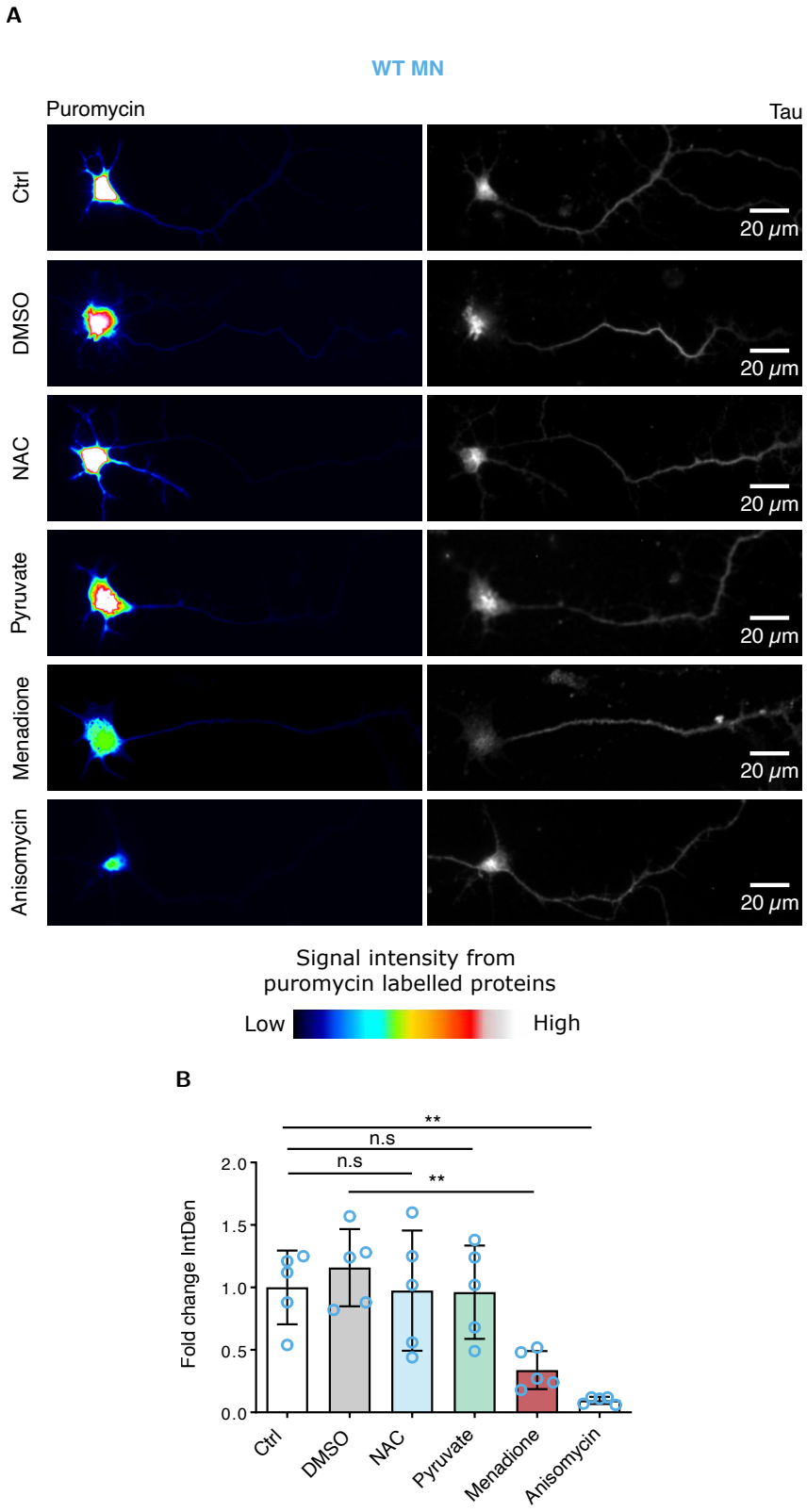

Figure 35: Modification of ROS does not increase protein synthesis in WT MN soma. **A)** Representative images of WT MNs labelled with anti-puromycin antibody (rainbow color) and anti-Tau antibody (white). MNs were treated with 10 µM NAC or 50 mM pyruvate or 100 µM menadione or 50 µM anisomycin for 1 h. Images confirm that protein synthesis is blocked by anisomycin or menadione in WT MNs. Scale bar: 20 µm. **B)** Quantification of mean puromycin intensity in soma of WT MNs, corresponding to protein levels. Each dot represents the average quantification of 10 neurons of 5 individual biological replicates (N=5). Bar graph depict the mean ± SD. Two-tailed unpaired t-test with Holm-Bonferroni correction for multiple comparisons was used to determine statistical significance. ns $p > 0.05$, **$p < 0.01$.

Additionally, we analyzed the axonal compartment after ROS modulation. Consistent with previous results of global protein synthesis and protein synthesis in the soma of WT MN, no effect was observed in the axonal compartment after ROS reduction by NAC or pyruvate (**Figure 36**). Again anisomycin and menadione reduced protein synthesis in WT MNs drastically even in the axonal compartment (**Figure 36B**).

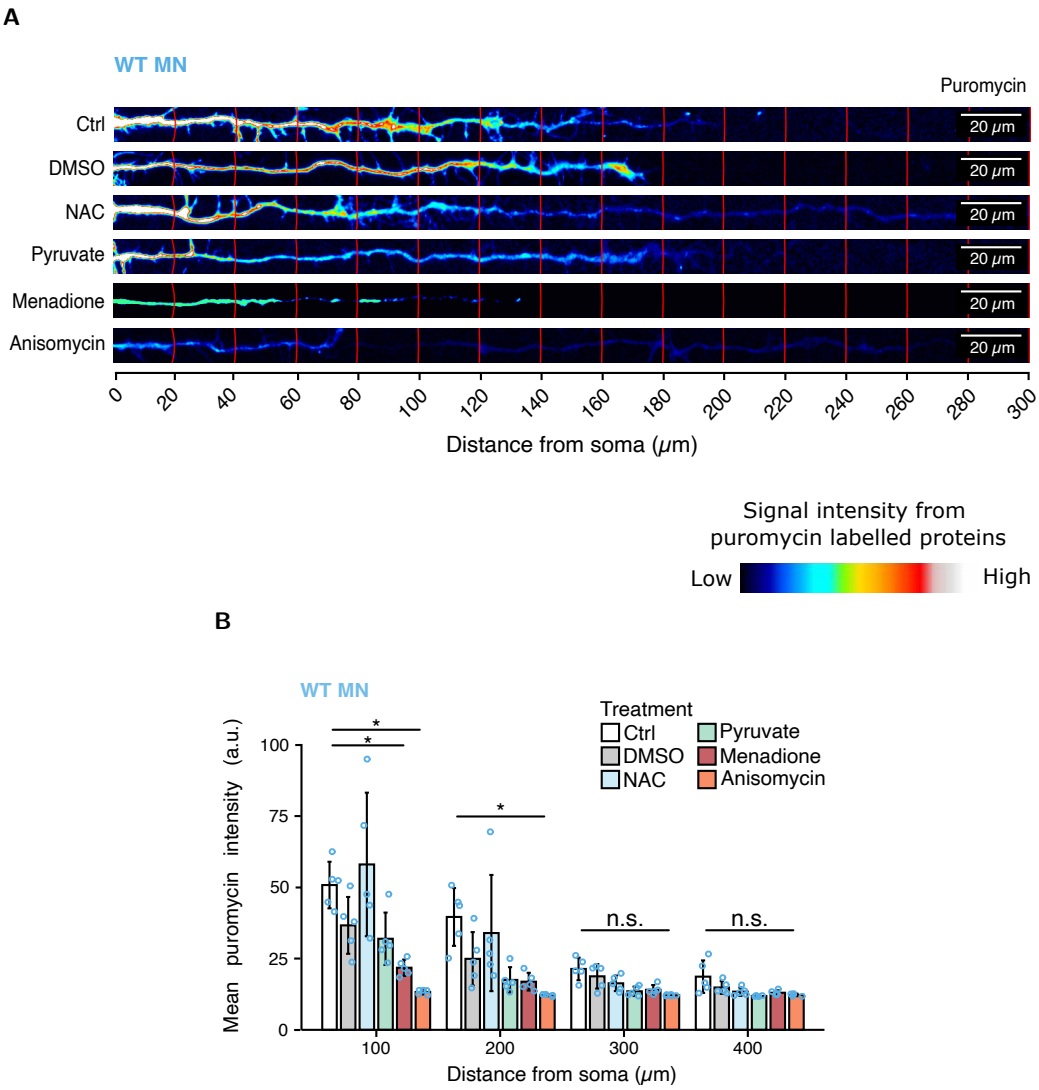

Figure 36: Modification of ROS does not alter protein synthesis in WT MN axons.
A) Representative images of WT MNs labelled with anti-puromycin antibody (rainbow color). Neurites were selected with a segmented line, straightened and divided into 20 qµm bins using the concentric circles plugin. MNs were treated with 10 µM NAC or 50 mM pyruvate or 100 µM menadione or 50 µM anisomycin for 1 h. Images confirm that protein synthesis is blocked by anisomycin or menadione. Scale bar: 20 µm. **B)** Quantification of mean puromycin intensity profiles, corresponding to protein levels, against distance in discrete categories. Each dot represents the average quantification of 10 neurons of 5 individual biological replicates (N=5). Bar graph depict the mean ± SD. Two-tailed unpaired t-test with Holm-Bonferroni correction for multiple comparisons was used to determine statistical significance. ns p >0.05, **p <0.01.

3.8.3 Regulating ROS modulates axonal protein synthesis in SMA MNs

More importantly, we wanted to see the effect on local protein synthesis after reducing ROS in SMA MNs. Supplementation of 10 µM NAC for 1 h was already sufficient to reduce ROS and increased global translation. Of note, supplementation of 50 mM pyruvate did not increase global protein synthesis consistently (**Figure 33**). In agreement with the change in global translation, protein synthesis was also increased in the somatic compartment after NAC supplementation and not changed after the addition of pyruvate (**Figure 37**). However, 100 µM menadione and 50 µM anisomycin blocked protein synthesis (**Figure 37B**).

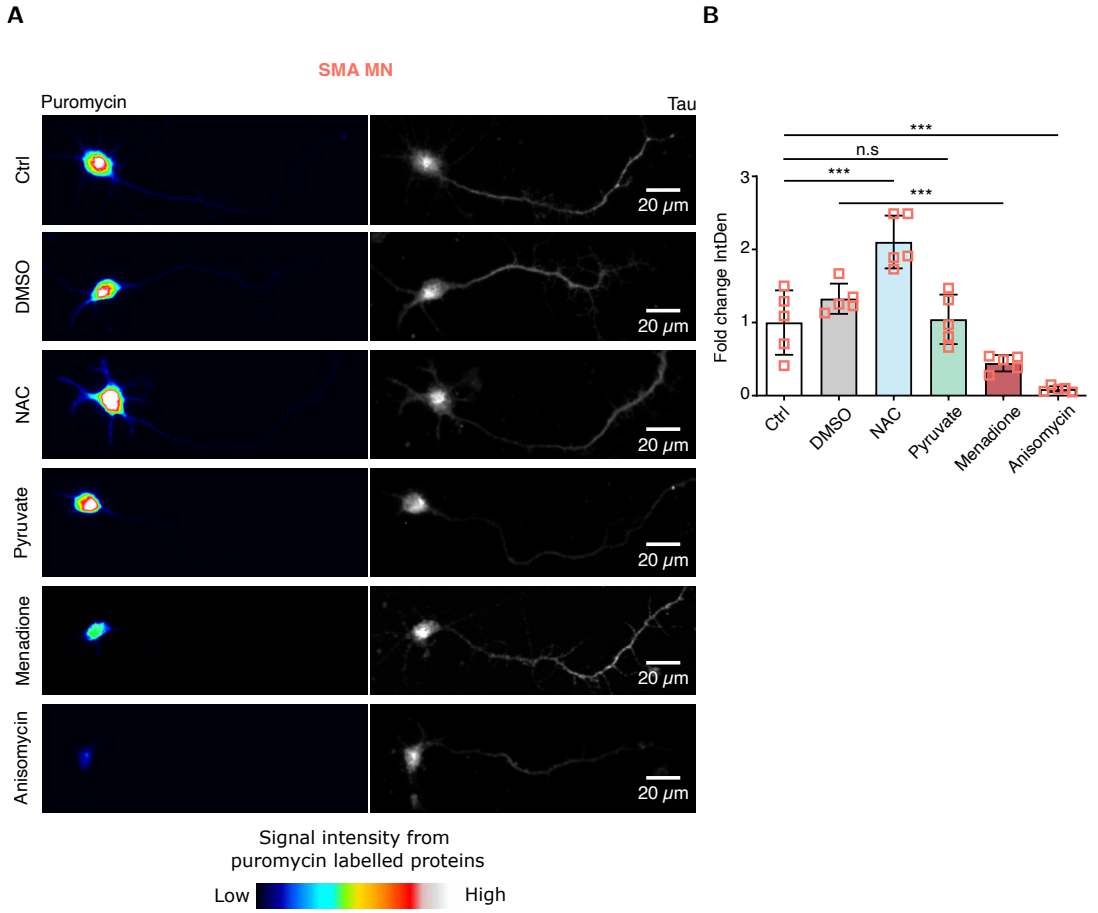

Figure 37: Reducing ROS increases protein synthesis in SMA MN soma.
A) Representative images of neurons after SUnSET assay after ROS modification in SMA MNs. Tau staining (white) shows whole neuronal morphology and puromycin signal represents newly synthesized proteins in given time. Rainbow color scale shows the intensity of puromycin signal. Scale bar: 20 µm. **B)** Quantification of mean puromycin intensity profiles, corresponding to protein levels in SMA soma. 10 µM NAC enhanced and 100 µM menadione or 50 µM anisomycin inhibited protein synthesis in SMA MNs. Supplementation of 50 mM pyruvate for 1 h showed no effect on protein synthesis in SMA MN soma. Each dot represents the average intensity of 15 neurons (N=5). One-way ANOVA with Tukey HSD post hoc analysis was used to determine statistical significance for multiple comparisons. Bar graphs depict the mean ± SD. ns $p > 0.05$, ***$p < 0.001$.

In SMA MNs, the antioxidant NAC increased protein synthesis in the first three most proximal fractions of the axon (**Figure 38**). These results confirmed that NAC could restore impaired protein synthesis efficiently in SMA MNs. Overall, reducing ROS in SMA MNs shows benefit in all compartments of the neurons. However, supplementation of 50 mM pyruvate for

1 h did not change protein synthesis in any fraction of the axon.

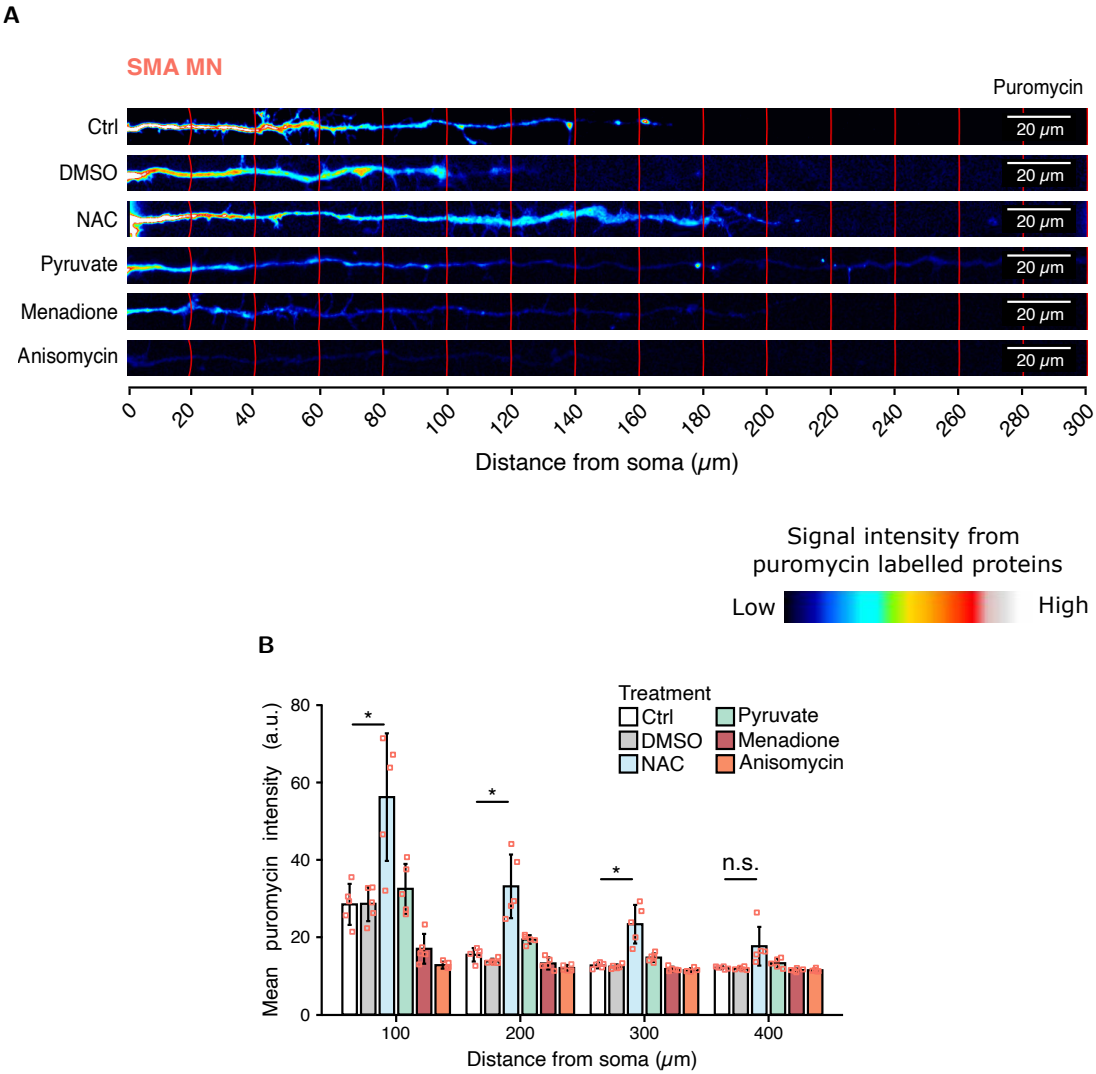

Figure 38: Reducing ROS increases local protein synthesis in SMA MN axons.
A) Representative images of SMA MN axons labelled with anti-puromycin antibody (rainbow color) and anti-Tau antibody (white). Neurites were selected with a segmented line, straightened and divided into 20 µm bins using the concentric circles plugin. MNs were treated with 10 µM NAC or 50 mM pyruvate or 100 µM menadione or 50 µM anisomycin for 1 h. Images confirm that protein synthesis is blocked by anisomycin or menadione and increased by 10 µM NAC in SMA MNs. Scale bar: 20 µm. **B)** Quantification of mean puromycin intensity profiles, corresponding to protein levels, against distance in discrete categories. Each dot represents the average quantification of 10 neurons of 5 individual biological replicates (N=5). Bar graph depicts the mean ± SD. Two-tailed unpaired t-test with Holm-Bonferroni correction for multiple comparisons was used to determine statistical significance. ns $p > 0.05$, *$p < 0.05$.

3.9 Whole proteome analysis of MNs with ROS manipulation

As our results suggested a relationship between ATP increase, ROS reduction, and increased protein synthesis by pyruvate and NAC, we aimed to identify systemic changes in the proteome of WT and SMA MNs after ATP and/or ROS modifications. Quantitative MS analysis in a 2 h data-independent acquisition was performed after primary WT and SMA MNs were treated with 50 mM pyruvate, 10 µM NAC, or 100 µM menadione 1 h. Whole proteome analysis was performed on four independent biological replicates of 10DIV WT MNs from E13.5 mice and three biological replicates of SMA MNs after 10DIV.

3.9.1 Pyruvate

First, cells were incubated with 50 mM pyruvate for 1 h, and the whole proteome was analyzed by MS. We found that the levels of 144 proteins were altered in WT MNs (**Figure 39A and Table S2**) and 122 proteins were altered in SMA MNs (**Figure 39B and Table S3**). Among those 144 proteins, 115 proteins were significantly up-regulated after pyruvate treatment in WT MNs. However, the amount of up-or down-regulated proteins after pyruvate treatment in SMA MNs was rather balanced: 59 proteins were up-regulated, and 63 proteins were down-regulated. Comparing WT and SMA MNs treated with pyruvate, only two proteins, namely DLG-associated protein 1 (DLGAP1) and Islet cell autoantigen 1 (ICA1), were commonly changed. However, DLGAP1 was down-regulated in WT MNs and up-regulated in SMA MNs upon pyruvate treatment (**Figure 39**). The opposite was observed for ICA1. In pyruvate-treated WT MNs, ICA1 was up-regulated, and in pyruvate-treated SMA MNs, ICA1 was down-regulated (**Figure 39**).

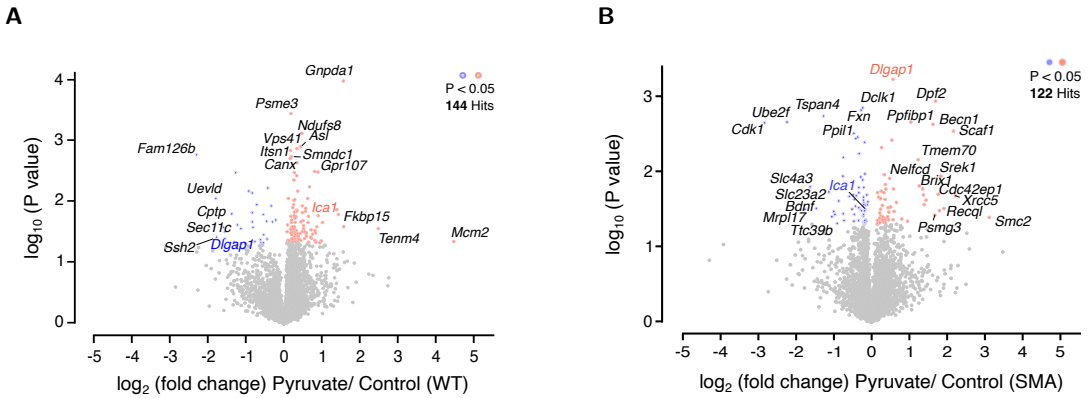

Figure 39: Pyruvate modifies the proteome of MNs.
Volcano plot of whole proteome analysis in WT (**A**) and SMA MNs (**B**) after 50 mM pyruvate treatment for 1 h; plotted p-value (-$\log_{10}$) against fold change ($\log_2$) (N=3). P-values were determined by unpaired two-sided t-test. Significantly changed proteins with $p < 0.05$ are highlighted in blue (down-regulated) or in red (up-regulated). Annotations show corresponding gene names.

To understand the biological meaning of pyruvate treatment on the proteome of SMA MNs, we performed pathway analyses on the significantly changed proteins. Gene ontology (GO) analyses are grouped in biological process, cellular compartment, and molecular function. The 5 most significantly changed pathways in each category are listed. All of those categories suggest a strong involvement of mitochondria (**Table 2**). The biological process of oxidative

phosphorylation was enriched, and the cellular compartment of mitochondria was affected by pyruvate supplementation (**Table 2**). Also, ribonucleotide binding, spliceosome, RNA splicing, and mRNA processing were affected by pyruvate. Interestingly, these terms have been reported as altered pathways in SMA (Pellizzoni, 2002; Fallini et al., 2011; Custer et al., 2016).

Table 2: GO analysis: Pathways regulated by pyruvate in SMA MNs.
Biological processes, cellular compartments and molecular functions affected by significantly changed proteins after 50 mM pyruvate treatment for 1h in SMA MNs.

Term	P-Value	Gene name
Biological Process		
Mitochondrion organization	2,79E-04	*Fxn*, *Mrpl17*, *Spg7*, *Timm13*, *Tmem70*
RNA splicing	1,26E-03	*Ddx39a*, *Pabpc1*, *Ppil1*, *Scaf1*, *Snrpb*, *Srek1*, *Syncrip*
Oxidative phosphorylation	4,51E-03	*Atp6v0a1*, *Atp6v1h*, *Fxn*, *Ndufb8*
mRNA processing	4,71E-03	*Ddx39a*, *Pabpc1*, *Ppil1*, *Scaf1*, *Snrpb*, *Srek1*, *Syncrip*
mRNA metabolic process	9,24E-03	*Ddx39a*, *Pabpc1*, *Ppil1*, *Scaf1*, *Snrpb*, *Srek1*, *Syncrip*
Cellular compartment		
Extrinsic to membrane	1,76E-06	*Becn1*, *Cdc42ep1*, *Dlgap1*, *Dnm1l*, *Gng4*, *Gphn*, *Ica1*, *Jup*, *Map3k12*, *Pitpnm2*, *Plcd4*, *Plekha2*, *Sh2d3c*, *Stambp*, *Strn3*
Internal side of plasma membrane	5,27E-04	*Adi1*, *Fnbp1*, *Gng4*, *Gphn*, *Gpsm1*, *Jup*, *Rab39b, Rhog*, *Snap91*
Mitochondrion	4,22E-03	*Akap1*, *Amacr*, *Clpp*, *Comt*, *Fxn*, *Lypla1*, *Micu1*, *Mmaa*, *Mrpl17*, *Mrpl50*, *Ndufb8*, *Rpl35a*, *Spg7*, *Timm13*, *Tmem11*, *Tmem70*, *Tst*
Spliceosome	8,52E-03	*Pabpc1*, *Ppil1*, *Snrpb*, *Srek1*, *Syncrip*
Ribonucleoprotein complex	9,94E-03	*Commd1*, *Mrpl17*, *Mrpl50*, *Pabpc1*, *Ppil1*, *Rpl35a*, *Snrpb*, *Srek1*, *Syncrip*
Molecular function		
Nucleotide binding	1,77E-05	*Cdk1*, *Clpp*, *Cpeb3*, *Dclk1*, *Ddx39a*, *Dhfr*, *Dnm1l*, *Dock7*, *Gnl1*, *Gphn*, *Grk2*, *Hcn3*, *Kif5c*, *Map3k12*, *Map4k3*, *Mmaa*, *Myo5b*, *Pabpc1*, *Rab39b*, *Rbm26*, *Recql*, *Rhog*, *Rimklb*, *Septin7*, *Smc2*, *Spg7*, *Srek1*, *Stk24*, *Stk38*, *Syncrip*, *Ube2f*, *Xrcc5*

Table 2: (continued)

Term	P-Value	Gene name
Ribonucleotide binding	5,59E-04	*Cdk1*, *Clpp*, *Dclk1*, *Ddx39a*, *Dnm1l*, *Dock7*, *Gnl1*, *Grk2*, *Hcn3*, *Kif5c*, *Map3k12*, *Map4k3*, *Mmaa*, *Myo5b*, *Rab39b*, *Recql*, *Rhog*, *Rimklb*, *Septin7*, *Smc2*, *Spg7*, *Stk24*, *Stk38*, *Ube2f*, *Xrcc5*
Purine ribonucleotide binding	5,59E-04	*Cdk1*, *Clpp*, *Dclk1*, *Ddx39a*, *Dnm1l*, *Dock7*, *Gnl1*, *Grk2*, *Hcn3*, *Kif5c*, *Map3k12*, *Map4k3*, *Mmaa*, *Myo5b*, *Rab39b*, *Recql*, *Rhog*, *Rimklb*, *Septin7*, *Smc2*, *Spg7*, *Stk24*, *Stk38*, *Ube2f*, *Xrcc5*
Purine nucleotide binding	1,01E-03	*Cdk1*, *Clpp*, *Dclk1*, *Ddx39a*, *Dnm1l*, *Dock7*, *Gnl1*, *Grk2*, *Hcn3*, *Kif5c*, *Map3k12*, *Map4k3*, *Mmaa*, *Myo5b*, *Rab39b*, *Recql*, *Rhog*, *Rimklb*, *Septin7*, *Smc2*, *Spg7*, *Stk24*, *Stk38*, *Ube2f*, *Xrcc5*
Adenyl ribonucleotide binding	7,42E-03	*Cdk1*, *Clpp*, *Dclk1*, *Ddx39a*, *Grk2*, *Hcn3*, *Kif5c*, *Map3k12*, *Map4k3*, *Mmaa*, *Myo5b*, *Recql*, *Rimklb*, *Smc2*, *Spg7*, *Stk24*, *Stk38*, *Ube2f*, *Xrcc5*

Next, we pursued identifying common proteins whose levels are altered by SMA and changed by pyruvate treatment in MNs. Among the 494 proteins changed in SMA MNs compared to WT MNs, 22 were also altered by pyruvate in WT MNs, and 28 were altered by pyruvate in SMA MNs (**Figure 40, Table 3, and Table 4**).

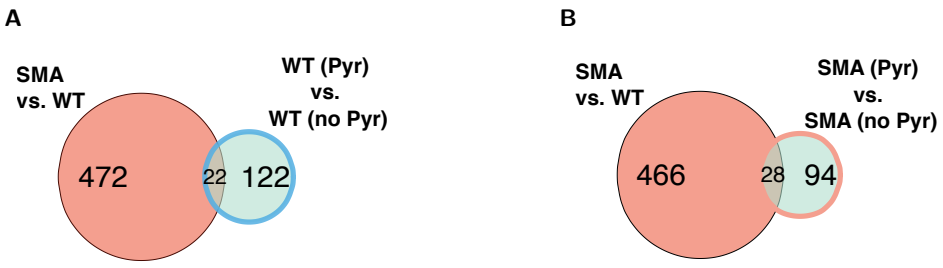

Figure 40: Pyruvate regulates a similar number of proteins in WT and SMA MNs.
Venn diagram showing overlap of 'altered proteins in SMA compared to WT' and 'changed proteins by pyruvate' in WT (**A**) or in SMA MNs (**B**).

Focusing on the fold change of those 22 proteins changed in WT MNs (**Table 3**), and 28 proteins changed in SMA MNs (**Table 4**), which overlap with proteins changed in SMA MNs without treatment, we found that the effect of pyruvate was more apparent in SMA MNs (**Figure 41**). Proteins that were down-regulated in SMA MNs were still down-regulated after pyruvate treatment and also up-regulated proteins were not affected by pyruvate treatment

(**Figure 41A**). However, among the 28 proteins changed in SMA MNs and after pyruvate treatment in SMA MNs, 21 proteins were down-regulated in SMA compared to WT and up-regulated by pyruvate in SMA (**Figure 41B**).

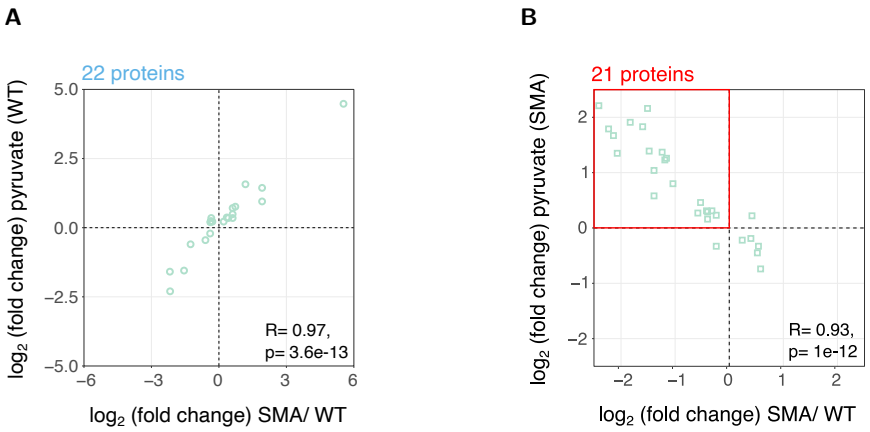

Figure 41: Pyruvate changes proteins in SMA more than in WT MNs.
Scatterplot showing the fold change (log_2) of SMA MNs compared to WT MNs against significantly changed proteins in pyruvate treated WT (**A**) or SMA MNs (**B**).

Table 3: Differentially expressed proteins in SMA compared to WT MNs and in WT MNs after pyruvate treatment.
List of 22 changed proteins in SMA compared to WT MNs ($p < 0.05$), which are also changed in WT MNs after pyruvate treatment. Gene names, protein names, and fold changes (FC) are listed.

Gene name	Protein name	log_2 FC SMA/ WT	log_2 FC Pyruvate/ WT
Cptp	Ceramide-1-phosphate transfer protein	-2.18	-1.59
Fam126b	Protein FAM126B	-2.17	-2.30
Sec11c	Signal peptidase complex catalytic subunit SEC11C	-1.55	-1.55
Toe1	Target of EGR1 protein 1	-1.26	-0.60
Mrpl37	39S ribosomal protein L37, mitochondrial	-0.60	-0.45
Kif1bp	KIF1-binding protein	-0.39	-0.21
Rpl9	60S ribosomal protein L9	-0.38	0.20
Srp68	Signal recognition particle subunit SRP68	-0.37	0.21
Cstf1	Cleavage stimulation factor subunit 1	-0.36	0.24
Rwdd1	RWD domain-containing protein 1	-0.34	0.35
Ppia	Peptidyl-prolyl cis-trans isomerase A	-0.29	0.22
Mrps17	28S ribosomal protein S17, mitochondrial	0.21	0.22
Arxes1	Adipocyte-related X-chromosome expressed sequence 1	0.35	0.37
Gpr107	Protein GPR107	0.42	0.35
Afg3l1	AFG3-like protein 1	0.61	0.49
GOLGA7B	Golgin subfamily A member 7B	0.61	0.35

Gene name	Protein name	log_2 FC SMA/ WT	log_2 FC Pyruvate/ WT
Prpf38b	Pre-mRNA-splicing factor 38B	0.61	0.71
Rad23a	UV excision repair protein RAD23 homolog A	0.73	0.76
Gnpda1	Glucosamine-6-phosphate isomerase 1	1.18	1.57
Cdkn1a	Cyclin-dependent kinase inhibitor 1	1.92	0.95
Jakmip1	Janus kinase and microtubule-interacting protein 1	1.92	1.44
Mcm2	DNA replication licensing factor MCM2	5.54	4.48

Table 4: Differentially expressed proteins in SMA compared to WT MNs and in SMA MNs after pyruvate treatment.
List of 28 changed proteins in SMA compared to WT MNs ($p < 0.05$), which are also changed in SMA MNs after pyruvate treatment. Gene names, protein names, and fold changes (FC) are listed. Gene names in red mark 21 proteins which were down-regulated in SMA compared to WT and up-regulated by pyruvate in SMA MNs.

Gene name	Protein name	log_2 FC SMA/ WT	log_2 FC Pyruvate/ SMA
Xrcc5	X-ray repair cross-complementing protein 5	-2.41	2.21
Commd1	COMM domain-containing protein 1	-2.23	1.79
Psmg3	Proteasome assembly chaperone 3	-2.14	1.67
Brix1	Ribosome biogenesis protein BRX1 homolog	-2.07	1.35
Recql	ATP-dependent DNA helicase Q1	-1.83	1.91
Srek1	Splicing regulatory glutamine/lysine-rich protein 1	-1.60	1.83
Scaf1	Splicing factor, arginine/serine-rich 19	-1.51	2.16
Lbr	Delta(14)-sterol reductase LBR	-1.48	1.39
Mmaa	Methylmalonic aciduria type A homolog, mitochondrial	-1.39	0.58
Ppfibp1	Liprin-beta-1	-1.39	1.04
Tmem175	Endosomal/lysosomal potassium channel TMEM175	-1.24	1.37
Tmem70	Transmembrane protein 70, mitochondrial	-1.19	1.23
Nelfcd	Negative elongation factor D	-1.16	1.26
Map3k12	Mitogen-activated protein kinase kinase kinase 12	-1.04	0.80
Slc8a2	Sodium/calcium exchanger 2	-0.58	0.27
Otud6b	Deubiquitinase OTUD6B	-0.53	0.46
Ndufb8	NADH dehydrogenase [ubiquinone] 1 beta subcomplex subunit 8, mitochondrial	-0.42	0.31

Gene name	Protein name	log_2 FC SMA/ WT	log_2 FC Pyruvate/ SMA
Cul1	Cullin-1	-0.40	0.16
Fam20b	Glycosaminoglycan xylosylkinase	-0.40	0.29
Mrpl50	39S ribosomal protein L50, mitochondrial	-0.32	0.31
Dtd1	D-aminoacyl-tRNA deacylase 1	-0.24	-0.33
Clpp	ATP-dependent Clp protease proteolytic subunit, mitochondrial	-0.24	0.23
Ddx39a	ATP-dependent RNA helicase DDX39A	0.24	-0.22
Syncrip	Heterogeneous nuclear ribonucleoprotein Q	0.40	-0.19
Jup	Junction plakoglobin	0.42	0.22
Grk2	Beta-adrenergic receptor kinase 1	0.52	-0.45
Akap1	A-kinase anchor protein 1, mitochondrial	0.54	-0.33
Arid1a	AT-rich interactive domain-containing protein 1A	0.58	-0.74

3.9.2 N-acetylcysteine (NAC)

Next, to obtain an overview of the antioxidant effect on the MN proteome, WT and SMA MNs were treated with 10 µM NAC for 1 h. Whole proteome analysis identified that 105 proteins were changed by NAC treatment in WT MNs (**Figure 42A and Table S4**) and 143 proteins were changed in SMA MNs (**Figure 42B and Table S5**). Here, no clear difference in the number of up- (54) or down-regulated (51) proteins was observed in WT MNs after NAC treatment. However, the majority (91 proteins) of proteins was down-regulated after NAC treatment in SMA MNs. Interestingly, NAC changed only one protein commonly in WT and SMA MNs. The deubiquitinase OTUD6B was down-regulated after NAC treatment in WT and up-regulated in SMA MNs, respectively (**Figure 42**).

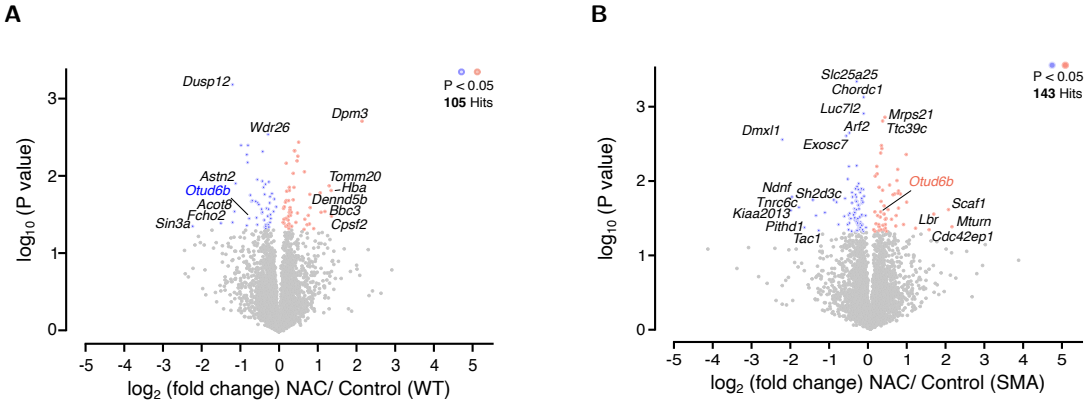

Figure 42: NAC modifies the proteome of MNs.
Volcano plot of whole proteome analysis in WT (**A**) and SMA MNs (**B**) after 10 µM NAC treatment for 1 h; plotted p-value ($-log_{10}$) against fold change (log_2) (N=3). P-values were determined by unpaired two-sided t-test. Significantly changed proteins with $p < 0.05$ are highlighted in blue (down-regulated) or in red (up-regulated). Annotations show corresponding gene names.

Next, GO analysis was performed on the significantly changed proteins. The data suggested a variety of functions including nucleotide-binding and RNA processing (**Table 5**). The biological processes category suggested strong involvement of RNA metabolism, including RNA splicing, RNA processing, or mRNA processing.

Table 5: GO analysis: Pathways regulated by NAC in SMA MNs.
Biological processes, cellular compartments and molecular functions affected by significantly changed proteins after 10 µM NAC treatment for 1 h in SMA MNs.

Term	P-Value	Gene name
Biological Process		
RNA splicing	2,81E-07	*Ddx39a*, *Ddx5*, *Lsm6*, *Nono*, *Pabpc1*, *Prpf3*, *Sart1*, *Scaf1*, *Snrpb*, *Snrpg*, *Usp39*, *Ybx1*
RNA processing	7,57E-07	*Ddx39a*, *Ddx5*, *Exosc7*, *Gar1*, *Lsm6*, *Nono*, *Nop2*, *Pabpc1*, *Prpf3*, *Sart1*, *Scaf1*, *Snrpb*, *Snrpg*, *Trmt10c*, *Usp39*, *Ybx1*
mRNA processing	3,81E-06	*Ddx39a*, *Ddx5*, *Lsm6*, *Nono*, *Pabpc1*, *Prpf3*, *Sart1*, *Scaf1*, *Snrpb*, *Snrpg*, *Usp39*, *Ybx1*
mRNA metabolic process	1,46E-05	*Ddx39a*, *Ddx5*, *Lsm6*, *Nono*, *Pabpc1*, *Prpf3*, *Sart1*, *Scaf1*, *Snrpb*, *Snrpg*, *Usp39*, *Ybx1*
Protein modification by small protein conjugation or removal	1,22E-04	*Gspt1*, *Nedd4*, *Rnf2*, *Sumo3*, *Trim32*, *Ube3a*, *Uchl1*
Cellular compartment		
Ribonucleoprotein complex	2,09E-04	*Ddx5*, *Gar1*, *Hnrnpul1*, *Lsm6*, *Mrpl14*, *Mrps21*, *Mrps5*, *Pabpc1*, *Prpf3*, *Rpl32*, *Sart1*, *Snrpb*, *Snrpg*
Mitochondrion	2,21E-03	*Adck1*, *Armc10*, *Bcs1l*, *Gatd3a*, *Idh3a*, *Mmaa*, *Mrpl14*, *Mrps21*, *Mrps5*, *Mtg1*, *Ndufa5*, *Ndufaf4*, *Pacs2*, *Pde12*, *Rab1b*, *Rexo2*, *Slc25a25*, *Timm8b*, *Tmem65*, *Trmt10c*, *Tst*
Spliceosome	2,63E-03	*Ddx5*, *Pabpc1*, *Prpf3*, *Sart1*, *Snrpb*, *Snrpg*
Axon	9,22E-03	*Dock7*, *L1cam*, *Scn2a*, *Tac1*, *Uchl1*
Organelle inner membrane	1,01E-02	*Bcs1l*, *Lbr*, *Lemd3*, *Mrps21*, *Ndufa5*, *Slc25a25*, *Timm8b*, *Tst*
Molecular function		
Nucleotide binding	2,72E-05	*Adck1*, *Arf2*, *Arl5a*, *Atl1*, *Atrx*, *Bcs1l*, *Clcn6*, *Cpne1*, *Csnk1a1*, *Dclk1*, *Ddx39a*, *Ddx5*, *Dhfr*, *Dock7*, *Fyn*, *G3bp2*, *Gphn*, *Grk2*, *Gspt1*, *Hcn3*, *Idh3a*, *Lemd3*, *Mink1*, *Mmaa*, *Mtg1*, *Nono*, *Pabpc1*, *Ppip5k2*, *Rab10*, *Rab1b*, *Rab39b*, *Rab6a*, *Tnrc6c*, *Ube2r2*

Table 5: (continued)

Term	P-Value	Gene name
RNA binding	3,42E-05	*Cpne1*, *Ddx5*, *Exosc7*, *G3bp2*, *Gar1*, *Hnrnpul1*, *Lsm6*, *Mrps5*, *Nono*, *Nop2*, *Pabpc1*, *Scaf1*, *Snrpb*, *Snrpg*, *Thumpd3*, *Tnrc6c*, *Ybx1*
GTP binding	1,28E-03	*Arf2*, *Arl5a*, *Atl1*, *Dock7*, *Gspt1*, *Mtg1*, *Rab10*, *Rab1b*, *Rab39b*, *Rab6a*
Guanyl ribonucleotide binding	1,53E-03	*Arf2*, *Arl5a*, *Atl1*, *Dock7*, *Gspt1*, *Mtg1*, *Rab10*, *Rab1b*, *Rab39b*, *Rab6a*
Guanyl nucleotide binding	1,53E-03	*Arf2*, *Arl5a*, *Atl1*, *Dock7*, *Gspt1*, *Mtg1*, *Rab10*, *Rab1b*, *Rab39b*, *Rab6a*

Compared with differentially expressed proteins between WT and SMA MNs, 40 proteins were common with NAC treatment in WT MNs (**Figure 43A and Table 6**) and 31 proteins were common with NAC treatment in SMA MNs (**Figure 43B and Table 7**).

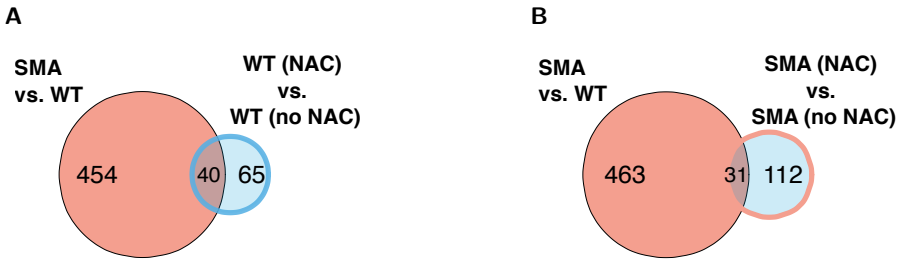

Figure 43: NAC regulates the same number of proteins in WT and SMA MNs.
Venn diagram showing overlap of 'altered proteins in SMA compared to WT' and 'changed proteins by NAC' in WT (**A**) or SMA MNs (**B**).

Again, NAC treatment showed only little effect on WT MNs (**Figure 44A and Table 6**), whereas 17 proteins were down-regulated in SMA compared to WT, and up-regulated by NAC treatment in SMA (**Figure 44B and Table 7**).

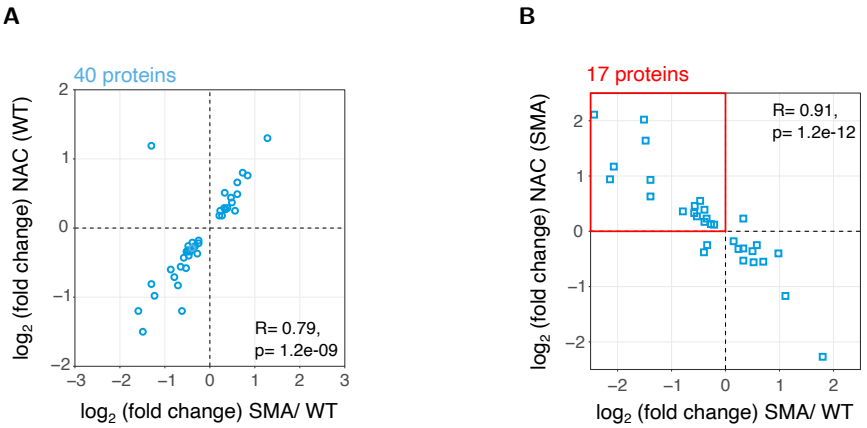

Figure 44: NAC changes proteins in SMA more than in WT MNs.
Scatterplot showing the fold change (log_2) of SMA MNs compared to WT MNs against significantly changed proteins in NAC treated WT (**A**) or SMA MNs (**B**).

Table 6: Differentially expressed proteins in SMA compared to WT MNs and in WT MNs after NAC treatment.
List of 40 changed proteins in SMA compared to WT MNs ($p < 0.05$), which are also changed in WT MNs after NAC treatment. Gene names, protein names, and fold changes (FC) are listed.

Gene name	Protein name	log_2 FC SMA/ WT	log_2 FC NAC/ WT
Slc25a16	Graves disease carrier protein homolog	-1.59	-1.20
Fcho2	F-BAR domain only protein 2	-1.49	-1.50
Bbc3	Bcl-2-binding component 3	-1.30	1.19
Stat3	Signal transducer and activator of transcription 3	-1.30	-0.81
Cyp46a1	Cholesterol 24-hydroxylase	-1.23	-0.98
Kctd16	BTB/POZ domain-containing protein KCTD16	-0.87	-0.60
Smyd3	Histone-lysine N-methyltransferase SMYD3	-0.79	-0.71
Washc4	WASH complex subunit 4	-0.71	-0.83
Ap1s1	AP-1 complex subunit sigma-1A	-0.65	-0.56
Dusp12	Dual specificity protein phosphatase 12	-0.62	-1.20
Cyp51a1	Lanosterol 14-alpha demethylase	-0.58	-0.43
Otud6b	Deubiquitinase OTUD6B	-0.53	-0.58
Sar1b	GTP-binding protein SAR1b	-0.52	-0.34
Kif1b	Kinesin-like protein KIF1B	-0.49	-0.34
Rpl27a	60S ribosomal protein L27a	-0.48	-0.26
Sec24a	Protein transport protein Sec24A	-0.48	-0.32
Pid1	PTB-containing, cubilin and LRP1-interacting protein	-0.47	-0.40
Epb41l3	Band 4.1-like protein 3	-0.44	-0.34
Kif1bp	KIF1-binding protein	-0.39	-0.29
Rpl7a	60S ribosomal protein L7a	-0.39	-0.21

Gene name	Protein name	log_2 FC SMA/ WT	log_2 FC NAC/ WT
Mrpl45	39S ribosomal protein L45, mitochondrial	-0.36	-0.29
Elp2	Elongator complex protein 2	-0.33	-0.26
Rab9a	Ras-related protein Rab-9A	-0.28	-0.37
Rack1	Receptor of activated protein C kinase 1	-0.25	-0.18
Lrrc47	Leucine-rich repeat-containing protein 47	-0.25	-0.22
Ndufa10	NADH dehydrogenase [ubiquinone] 1 alpha subcomplex subunit 10, mitochondrial	0.21	0.18
Ppm1l	Protein phosphatase 1L	0.23	0.25
Ergic3	Endoplasmic reticulum-Golgi intermediate compartment protein 3	0.27	0.18
Gnai2	Guanine nucleotide-binding protein G(i) subunit alpha-2	0.32	0.29
Cuedc1	CUE domain-containing protein 1	0.33	0.51
Arxes1	Adipocyte-related X-chromosome expressed sequence 1	0.35	0.27
Ano10	Anoctamin-10	0.39	0.29
Mrto4	mRNA turnover protein 4 homolog	0.47	0.44
Bcap29	B-cell receptor-associated protein 29	0.49	0.37
Ndufab1	Acyl carrier protein, mitochondrial	0.56	0.25
Afg3l1	AFG3-like protein 1	0.61	0.49
Hdac4	Histone deacetylase 4	0.61	0.66
Rad23a	UV excision repair protein RAD23 homolog A	0.73	0.80
Asic1	Acid-sensing ion channel 1	0.84	0.76
Tomm20	Mitochondrial import receptor subunit TOM20 homolog	1.28	1.30

Table 7: Differentially expressed proteins in SMA compared to WT MNs and in SMA MNs after NAC treatment.
List of 31 changed proteins in SMA compared to WT MNs ($p < 0.05$), which are also changed in SMA MNs after NAC treatment. Gene names, protein names, and fold changes (FC) are listed. Gene names in red mark 17 proteins which were down-regulated in SMA compared to WT and up-regulated by NAC in SMA MNs.

Gene name	Protein name	log_2 FC SMA/ WT	log_2 FC NAC/ SMA
Mturn	Maturin	-2.47	2.11
Psmg3	Proteasome assembly chaperone 3	-2.14	0.94
Brix1	Ribosome biogenesis protein BRX1 homolog	-2.07	1.17
Scaf1	Splicing factor, arginine/serine-rich 19	-1.51	2.02
Lbr	Delta(14)-sterol reductase LBR	-1.48	1.64
Ppfibp1	Liprin-beta-1	-1.39	0.93

Gene name	Protein name	log_2 FC SMA/ WT	log_2 FC NAC/ SMA
Mmaa	Methylmalonic aciduria type A homolog, mitochondrial	-1.39	0.63
Prpf3	U4/U6 small nuclear ribonucleoprotein Prp3	-0.79	0.36
Slc8a2	Sodium/calcium exchanger 2	-0.58	0.33
Atrx	Transcriptional regulator ATRX	-0.57	0.46
Otud6b	Deubiquitinase OTUD6B	-0.53	0.27
Scrib	Protein scribble homolog	-0.47	0.55
Timm8b	Mitochondrial import inner membrane translocase subunit Tim8 B	-0.40	-0.38
Ube3a	Ubiquitin-protein ligase E3A	-0.39	0.17
Ciapin1	Anamorsin	-0.39	0.39
Hnrnpul1	Heterogeneous nuclear ribonucleoprotein U-like protein 1	-0.35	0.23
Ybx1	Nuclease-sensitive element-binding protein 1	-0.34	-0.25
Rpl32	60S ribosomal protein L32	-0.27	0.13
Ndufa5	NADH dehydrogenase [ubiquinone] 1 alpha subcomplex subunit 5	-0.21	0.12
Ttc9c	Tetratricopeptide repeat protein 9C	0.15	-0.18
Ddx39a	ATP-dependent RNA helicase DDX39A	0.24	-0.32
Bcs1l	Mitochondrial chaperone BCS1	0.33	0.23
Nptx1	Neuronal pentraxin-1	0.33	-0.31
Snrpg	Small nuclear ribonucleoprotein G	0.33	-0.53
Ppip5k2	Inositol hexakisphosphate and diphosphoinositol-pentakisphosphate kinase 2	0.50	-0.36
Grk2	Beta-adrenergic receptor kinase 1	0.52	-0.56
Arid1a	AT-rich interactive domain-containing protein 1A	0.58	-0.25
Thumpd3	THUMP domain-containing protein 3	0.70	-0.55
Ints14	Integrator complex subunit 14	0.98	-0.40
Foxk2	Forkhead box protein K2	1.11	-1.17
Dmxl1	DmX-like protein 1	1.80	-2.27

3.9.3 Menadione

ROS induction in WT MNs had the most prominent effects on the proteome. Supplementation of 100 µM menadione for 1 h altered expression of 344 proteins (**Figure 45 and Table S6**). However, the majority of proteins were down-regulated. Only 119 proteins were up-regulated, but 225 proteins were down-regulated after menadione treatment in WT MNs.

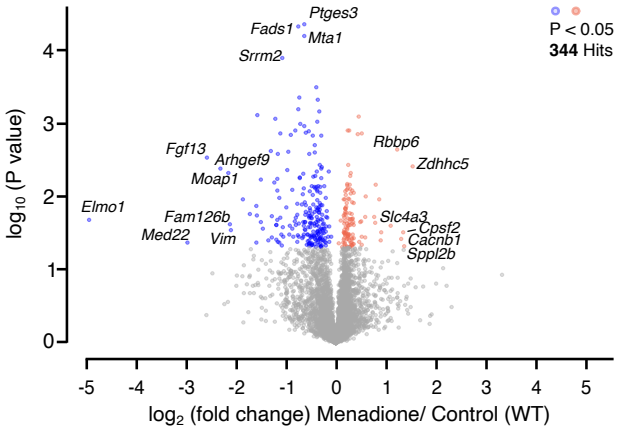

Figure 45: Menadione modifies the proteome of MNs.
Volcano plot of whole proteome analysis in WT MNs after 100 µM menadione treatment for 1 h; plotted p-value (-$\log_{10}$) against fold change ($\log_2$) (N=3). P-values were determined by unpaired two-sided t-test. Significantly changed proteins with $p < 0.05$ are highlighted in blue (down-regulated) or in red (up-regulated). Annotations show corresponding gene names.

In addition, menadione also showed the biggest overlap of altered proteins with SMA affected proteins; 56 proteins (**Figure 46 and Table 8**).

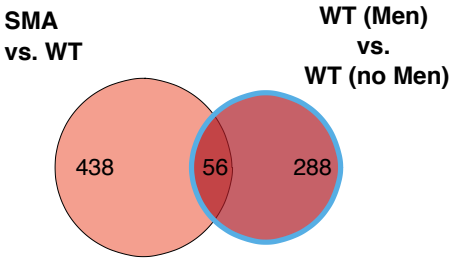

Figure 46: Menadione changes proteins in WT MNs, that are also altered in SMA MNs.
Venn diagram showing overlap of 'altered proteins in SMA compared to WT' and 'changed proteins by menadione' in WT MNs.

Menadione treated WT MNs showed great overlap with altered proteins in SMA. As visualized by the scatter plot in **Figure 47**, proteins with a negative fold change (down-regulated) in SMA compared to WT MNs also show a lower expression in WT MNs after menadione treatment. Similar, proteins with a positive fold change in SMA MNs compared to WT MNs were also up-regulated in WT MNs after ROS induction by menadione. Those results show that increasing ROS in WT MNs affects similar proteins that are affected by SMA.

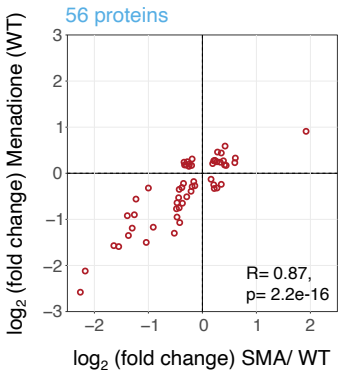

Figure 47: Menadione reduces protein levels in WT MNs.
Scatterplot showing the fold change (log_2) of protein levels in SMA MNs compared to WT MNs against significantly changed proteins in menadione treated WT MNs.

Table 8: Differentially expressed proteins in SMA compared to WT MNs and in WT MNs after menadione treatment.
List of 56 changed proteins in SMA compared to WT MNs ($p < 0.05$), which are also changed in WT MNs after menadione treatment. Gene names, protein names, and fold changes (FC) are listed.

Gene name	Protein name	log_2 FC SMA/ WT	log_2 FC Men/ WT
Fgf13	Fibroblast growth factor 13	-2.26	-2.58
Fam126b	Protein FAM126B	-2.17	-2.12
Ehmt1	Histone-lysine N-methyltransferase EHMT1	-1.64	-1.57
Ntrk3	NT-3 growth factor receptor	-1.55	-1.59
Mmaa	Methylmalonic aciduria type A homolog, mitochondrial	-1.39	-0.92
Ddx20	Probable ATP-dependent RNA helicase DDX20	-1.37	-1.35
Stat3	Signal transducer and activator of transcription 3	-1.30	-1.19
Toe1	Target of EGR1 protein 1	-1.26	-0.90
Cyp46a1	Cholesterol 24-hydroxylase	-1.23	-0.56
Map3k12	Mitogen-activated protein kinase kinase kinase 12	-1.04	-1.50
Cnot2	CCR4-NOT transcription complex subunit 2	-1.00	-0.32
Usp22	Ubiquitin carboxyl-terminal hydrolase 22	-0.91	-1.17
Son	Protein SON	-0.52	-1.30
Eml1	Echinoderm microtubule-associated protein-like 1	-0.48	-0.77
Scrib	Protein scribble homolog	-0.47	-0.95
Mlf2	Myeloid leukemia factor 2	-0.47	-0.64
Dtx3	Probable E3 ubiquitin-protein ligase DTX3	-0.44	-0.53
Nup43	Nucleoporin Nup43	-0.43	-0.35
Fads1	Acyl-CoA (8-3)-desaturase	-0.43	-0.75

Gene name	Protein name	log_2 FC SMA/ WT	log_2 FC Men/ WT
Srrm2	Serine/arginine repetitive matrix protein 2	-0.42	-1.07
Fndc3a	Fibronectin type-III domain-containing protein 3A	-0.38	-0.31
Cep170b	Centrosomal protein of 170 kDa protein B	-0.37	-0.65
Srpk1	SRSF protein kinase 1	-0.35	-0.22
Rwdd1	RWD domain-containing protein 1	-0.34	0.24
Ddah2	N(G),N(G)-dimethylarginine dimethylaminohydrolase 2	-0.33	0.18
Rpl12	60S ribosomal protein L12	-0.30	0.18
Hnrnpa0	Heterogeneous nuclear ribonucleoprotein A0	-0.29	-0.51
Bclaf1	Bcl-2-associated transcription factor 1	-0.28	0.25
Rack1	Receptor of activated protein C kinase 1	-0.25	0.15
Impa1	Inositol monophosphatase 1	-0.24	0.20
Poldip3	Polymerase delta-interacting protein 3	-0.21	-0.39
Eif2s1	Eukaryotic translation initiation factor 2 subunit 1	-0.20	0.17
Fip1l1	Pre-mRNA 3'-end-processing factor FIP1	-0.19	-0.29
Ndufb5	NADH dehydrogenase [ubiquinone] 1 beta subcomplex subunit 5, mitochondrial	-0.19	0.31
Zdhhc17	Palmitoyltransferase ZDHHC17	-0.16	-0.18
Ppp6c	Serine/threonine-protein phosphatase 6 catalytic subunit	-0.14	-0.27
Prkaa2	5'-AMP-activated protein kinase catalytic subunit alpha-2	0.16	-0.13
Dhodh	Dihydroorotate dehydrogenase (quinone), mitochondrial	0.19	0.21
Dmac2l	ATP synthase subunit s, mitochondrial	0.21	-0.25
Mrpl15	39S ribosomal protein L15, mitochondrial	0.21	0.27
Raf1	RAF proto-oncogene serine/threonine-protein kinase	0.22	-0.33
Ppm1l	Protein phosphatase 1L	0.23	0.27
Dnajc11	DnaJ homolog subfamily C member 11	0.23	0.28
Ergic3	Endoplasmic reticulum-Golgi intermediate compartment protein 3	0.27	0.25
Pelp1	Proline-, glutamic acid- and leucine-rich protein 1	0.27	-0.32
Actr1b	Beta-centractin	0.28	0.46
Cuedc1	CUE domain-containing protein 1	0.33	0.24
Prkar1a	cAMP-dependent protein kinase type I-alpha regulatory subunit	0.35	-0.24

Gene name	Protein name	log_2 FC SMA/ WT	log_2 FC Men/ WT
Arxes1	Adipocyte-related X-chromosome expressed sequence 1	0.35	0.44
Ano10	Anoctamin-10	0.39	0.27
Vdac1	Voltage-dependent anion-selective channel protein 1	0.41	0.18
Gpr107	Protein GPR107	0.42	0.59
Pgs1	CDP-diacylglycerol–glycerol-3-phosphate 3-phosphatidyltransferase, mitochondrial	0.44	0.17
Ndufc2	NADH dehydrogenase [ubiquinone] 1 subunit C2	0.60	0.23
Afg3l1	AFG3-like protein 1	0.61	0.33
Cdkn1a	Cyclin-dependent kinase inhibitor 1	1.92	0.91

3.10 ROS regulates mRNA translation

Protein synthesis is tightly regulated in eukaryotic cells by two major processes; initiation and elongation. Due to our data and previous studies, protein synthesis is impaired in SMA MNs (Akten et al., 2011; Kye et al., 2014). However, it is still unclear at which step of protein synthesis is impaired. It has not yet been established whether translation initiation or elongation is affected by the loss of SMN. Therefore, we measured both processes in WT and SMA MNs. As our pathway analysis of the whole proteomics approach suggested, that mRNA translation might be dysregulated in SMA MNs (**Figure 9A**). Based on these findings, we filtered the whole proteomics data by proteins related to mRNA translation. For this, we used the MGI database with 616 annotated proteins. From the database, we detected 360 proteins in our whole proteome data (**Figure 48**). Among them, 47 proteins were significantly changed between WT and SMA MNs. Interestingly, 40 out of those 47 significantly changed proteins were down-regulated in SMA MNs compared to WT ones, and only 7 proteins were up-regulated (**Figure 48 and Table S1**). These results indicate an impairment in translation-related proteins.

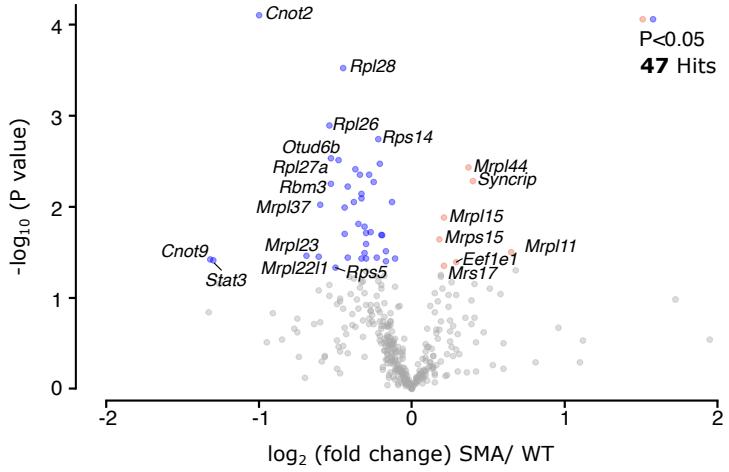

Figure 48: Quantitative proteomics of translation related proteins of SMA and WT MNs. Volcano plot of translation related proteins comparing WT and SMA MNs; plotted p-value (-$\log_{10}$) against fold change ($\log_2$, SMA/ WT). Four independent samples of WT MNs and three independent samples for SMA MNs were used for analysis. P-values were determined using an unpaired two-sided t-test. Proteins with $p < 0.05$ are highlighted in blue (down-regulated) and red (up-regulated). Annotations show corresponding gene names.

3.10.1 Translation elongation in primary MNs

In order to assess the rate of protein elongation, we used the SunRiSE assay. This assay is a modified version of the SUnSET assay (Argüello et al., 2018). In brief, translation initiation was blocked by 2 µg/ml harringtonine at different time intervals. Subsequently, newly synthesized peptides were labeled with 10 µg/ml puromycin for 10 min and detected by western blot analysis using an anti-puromycin specific antibody (**Figure 49**). All signals were normalized to ACTB after puromycin signals were eradicated.

Blocking translation initiation at the same time and adding puromycin at different timepoints

after ribosomes run off the mRNA or blocking translation at different time points before labeling with puromycin at the same time gives similar results (Argüello et al., 2018). To ensure that the concentration of puromycin was homogenous, we choose to block translation first at different time points and added puromycin to all cells simultaneously. Again, WT and SMA MNs were used after 10DIV. Furthermore, we aimed to measure translation elongation speed by supplementation of 10 µM NAC or 50 mM pyruvate for 1 h.
We separated the analysis into three categories to see if only specific proteins with different molecular weights are affected - first, proteins with high molecular weight over 100 kDa. Second, proteins in the range of 35 kDa and 100 kDa, and lastly, small proteins with a molecular weight under 35 kDa.

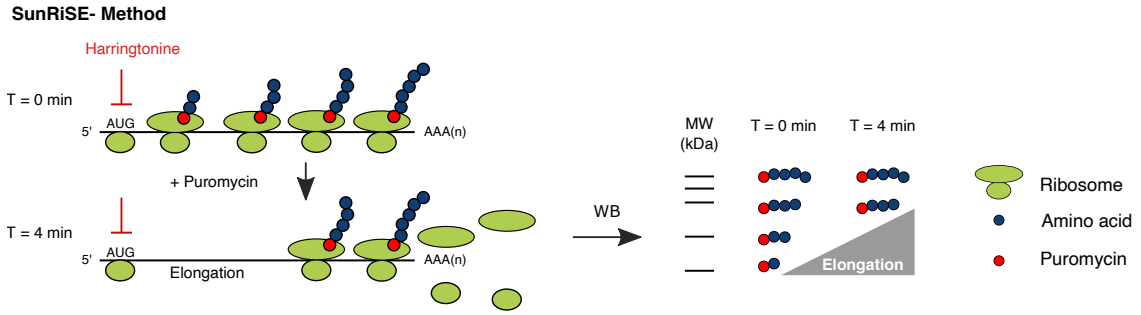

Figure 49: Scheme of SunRiSE assay.
Translation initiation of 10DIV WT or SMA MNs was blocked with 2 µg/ml harringtonine at different timepoints before adding 10 µg/ml puromycin for 10 min and subsequent western blot analysis.

3.10.1.1 Translation elongation is not changed in SMA MNs

To identify the mechanism that contributes to the impaired protein synthesis in SMA, we compared elongation speeds between WT and SMA MNs. As mentioned above, we detected newly synthesized proteins by western blot analysis after translation initiation was blocked. For this, we analyzed four individual biological replicates and compared the puromycin signal slopes between different conditions and genotypes. However, no differences in the elongation speed of WT and SMA MNs was observed comparing the least squared means of the regression analysis (**Figure 50**).

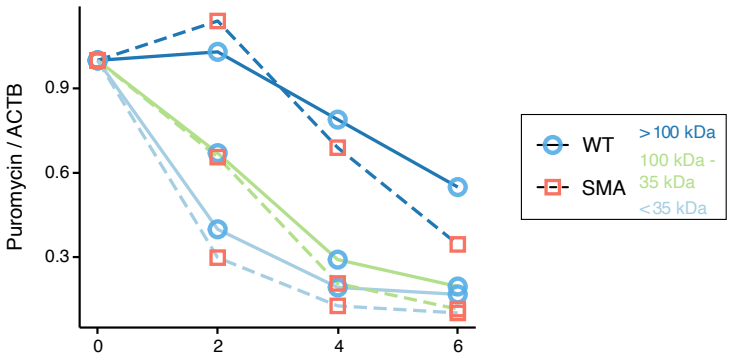

Figure 50: SunRiSE assay of WT and SMA MNs.
Elongation speed is not altered in SMA MN compared to WT MNs. Each dot and line represent the average of four independent biological replicates (N=4). Regression analysis comparing the least square means does not show any significant difference between WT MNs (blue circles) and SMA MNs (red squares).

3.10.1.2 ROS modulation does not change translation elongation in WT MNs

To test whether NAC or pyruvate can improve the elongation speed and exclude any adverse effects on elongation, we first used WT MNs. Before performing the SunRiSE assay, MNs were treated with 10 µM NAC or 50 mM pyruvate for 1 h. Not surprisingly, elongation speed was not altered by either NAC or pyruvate treatment in WT MNs. This was expected as global and local translation were not changed after adding NAC or pyruvate to WT MNs.

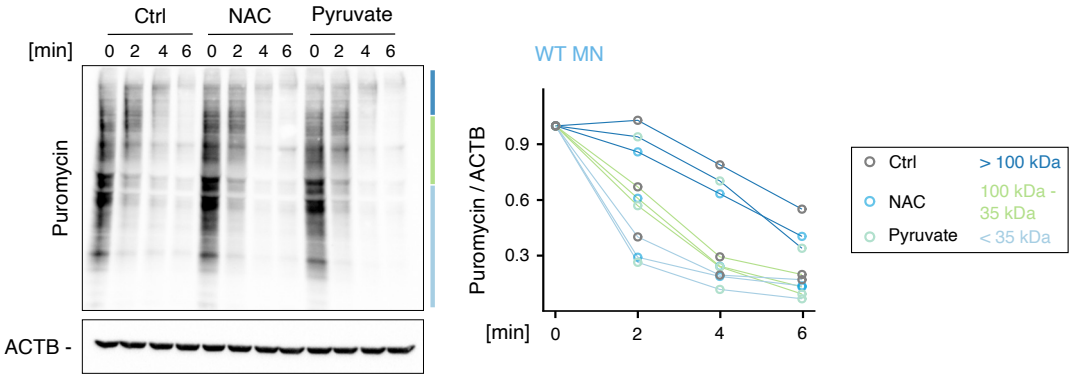

Figure 51: SunRiSE assay in WT MNs.
NAC or pyruvate does not change elongation speed in WT MNs. Each dot and line represent the average of four independent biological replicates (N=4). Regression analysis comparing the least square means does not show any significant difference between different treatments.

3.10.1.3 ROS modulation does not change translation elongation in SMA MNs

As we already showed the positive effect of NAC on reducing ROS, improving global and local translation, it is essential to evaluate if translation elongation is affected by this. Same as with WT MNs, we treated 10 µM NAC and 50 mM pyruvate 1 h before performing the SunRiSE assay. However, using four independent biological replicates, regression analysis did not reveal any significant difference after treatment in any of the three MW categories.

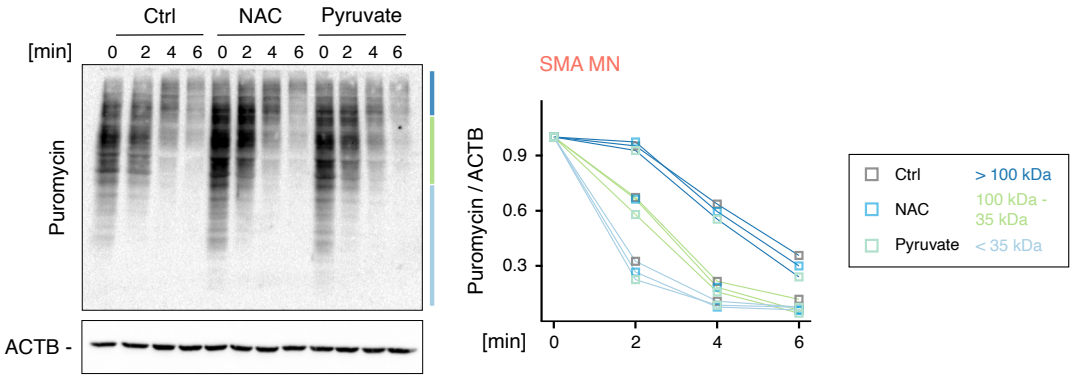

Figure 52: SunRiSE assay in SMA MNs.
NAC or pyruvate does not change elongation speed in SMA MNs. Each dot and line represent the average of four independent biological replicates (N=4). Regression analysis comparing the least square means does not show any significant difference between different treatments.

3.10.2 Translation initiation is reduced in SMA MNs

As translational elongation is unaltered in SMA or by ROS modification, next, we tested translational initiation. One of the well-described translational initiation mechanisms is cap-dependent translation initiation by 4E-BP1 (eukaryotic translation initiation factor 4E-binding protein 1). The rate-limiting step in translation initiation is the association of the cap-binding protein, eukaryotic translation initiation factor 4E (eIF4E) into the eIF4F complex that recruits the small ribosomal unit to mRNAs (Yanagiya et al., 2012). Translation initiation is repressed by 4E-BP1 (Pause et al., 1994). In the first phosphorylation step, 4E-BP1 is phosphorylated at Threonine residue 37 and Threonine 46. Subsequent phosphorylation at Threonine residue 70 and Serine 65 enables the release of 4E-BP from eIF4E.

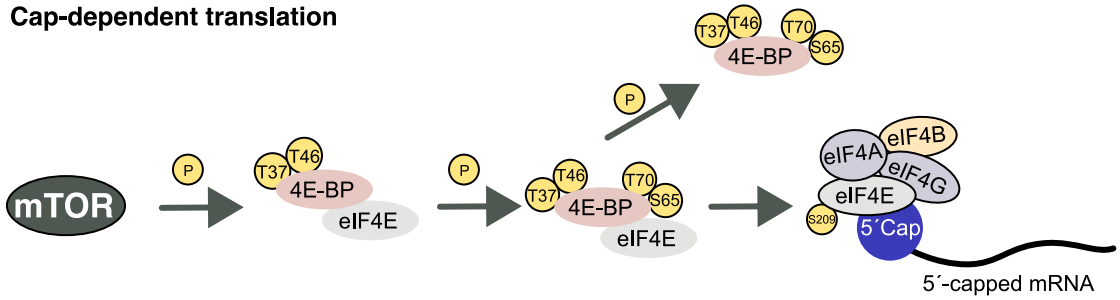

Figure 53: Cap-dependent translation initiation.
mTORC1 increases phosphorylation of the translation-initiation repressor 4E-BP. After additional phosphorylation, 4E-BP dissociates from eIF4E. Unbound eIF4E can bind the 5´ cap of mRNA and assembles the eIF4F pre-initiation complex required for cap-dependent translation.

In order to test translation initiation in SMA, we measured the phosphorylation of 4E-BP1 in WT and SMA MNs at residue Thr37/46. A reduced phosphorylation status of 4E-BP1 indicates that initiation of mRNA translation is impaired in SMA MNs (**Figure 54**).

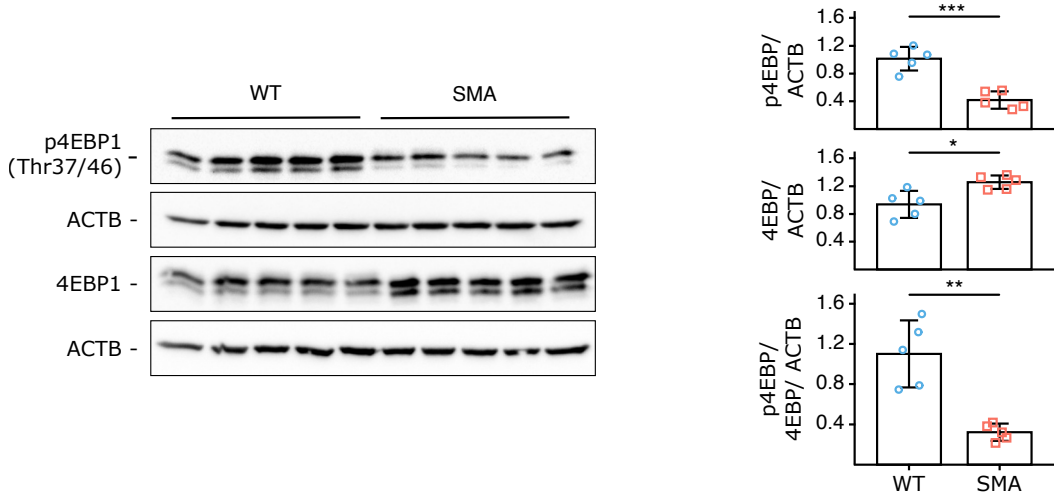

Figure 54: Phosphorylation status of 4E-BP in WT and SMA MNs.
Western blot analysis measuring p4E-BP1 and total 4E-BP1 levels in WT (blue circles) and SMA MNs (red squares) (N=5). ATCB was used as loading control. Each dot represents the data from individual biological replicates. Bar graphs depict the mean ± SD. Two-tailed unpaired t-test was used to determine statistical significance *p <0.05, **p <0.01, ***p <0.001.

3.10.2.1 ROS inhibits translation initiation in WT MNs

Next, we evaluated the effect of ROS modulation on 4E-BP mediated translation initiation. Again, we supplied WT MNs with the ROS modulating supplements NAC, pyruvate, or menadione for 1 h and measured the phosphorylation status of the translation repressor 4E-BP1. No significant difference was observed after pyruvate or NAC supplementation in WT cells (**Figure 55**). While induction of ROS by 100 µM menadione resulted in a reduction of 4E-BP1 phosphorylation. This result suggests that excessive ROS can inhibit mRNA translation at the initiation step. Additionally, overall levels of 4E-BP1 were not changed after ROS modulation.

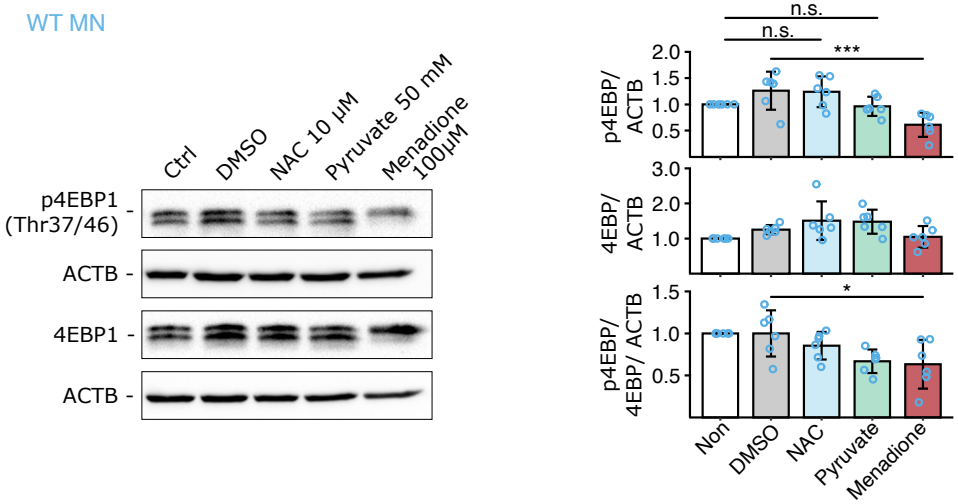

Figure 55: Translation initiation in WT MNs.
Western blot analysis shows that pharmacologically modifying ROS levels changes p4E-BP1 levels in WT MNs (N=6). Each dot represents the data from individual biological replicates. One-way ANOVA with Tukey HSD post hoc analysis was used to determine statistical significance for multiple comparisons. Bar graphs depict the mean ± SD. ns p >0.05, *p <0.05, ***p <0.001.

3.10.2.2 Reducing ROS increases translation initiation in SMA MNs

As we are particularly interested in the effect of reducing ROS on translation initiation in SMA, we performed the same experiments with SMA MNs. Indeed, pyruvate and NAC increased the phosphorylation of 4E- BP1 in SMA MNs (**Figure 55**). Moreover, further increase of ROS by 100 µM menadione did not reduce phosphorylation as observed in WT MNs.
Taken together, this unprecedented data reveals that mRNA translation is impaired at the initiation step in SMA MNs, while elongation is unaltered. Moreover, the initiation of mRNA translation is regulated by ROS via 4E-BP1.

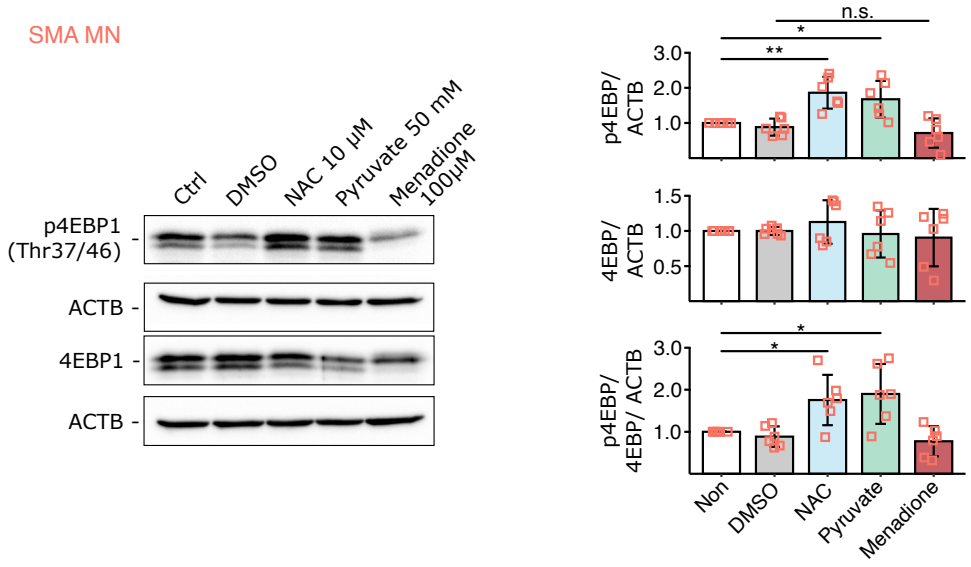

Figure 56: 4E-BP mediated translation initiation in SMA MNs.
Western blot analysis shows that pharmacologically modifying ROS levels changes p4E-BP1 levels in SMA MNs (N=6). Each dot represents the data from individual biological replicates. One-way ANOVA with Tukey HSD post hoc analysis was used to determine statistical significance for multiple comparisons. Bar graphs depict the mean ± SD. ns p >0.05, *p <0.05, **p <0.01.

3.11 SMN protein levels are regulated by pyruvate and ROS via mTOR

Since we aim to ameliorate the phenotypes of SMA, it is crucial to investigate the effect of ROS on the disease-causing protein SMN. As pyruvate increased ATP levels and reduced ROS, we further investigated the effect of pyruvate on SMN protein levels. Additionally, it is interesting to identify by which pathway the translational regulation is mediated. Here, the mTOR pathway is one candidate as it regulates protein synthesis post-transcriptionally.

3.11.1 Pyruvate increases SMN in NSC-34 cells, WT MNs and SMA MNs

As our previous results suggested, pyruvate had no beneficial effect in NSC-34 cells or WT MNs on protein synthesis or ROS regulation when those levels were in a normal range. However, we were able to increase ATP levels in those cells. Therefore, to exclude any negative effects of pyruvate on the SMN levels, we added 50 mM pyruvate over 1 h to those cells. Surprisingly, pyruvate increased SMN protein levels in NSC-34 cells and also in WT MNs (**Figure 57A & Figure 57B**). Even though SMN levels doubled in NSC-34 after 10 min, treatment for 40 min or 60 min did not show any significant benefit (**Figure 57A**). Additionally and most importantly, pyruvate increased SMN protein levels over 1 h in SMA MNs (**Figure 57C**).

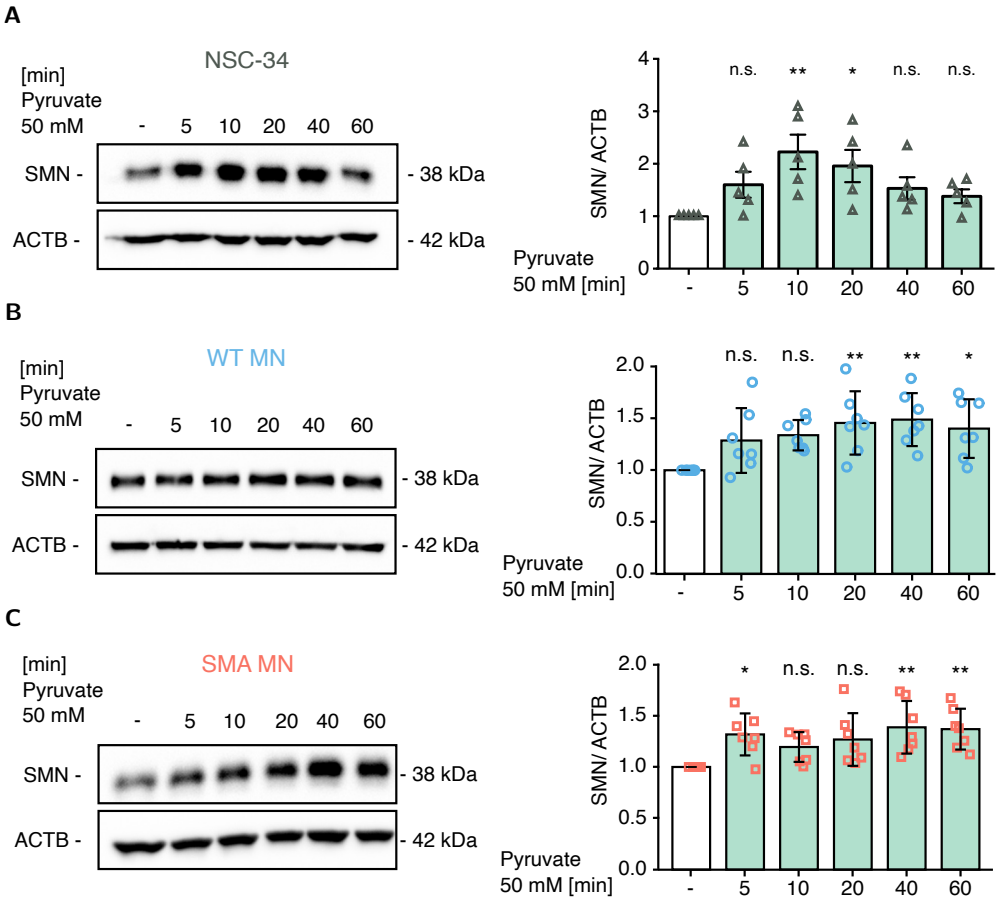

Figure 57: Pyruvate increases SMN protein levels.
Representative western blot and quantification show an increase of SMN protein level after 50 mM pyruvate supplementation for 1 h in NSC-34 cells (N=5) (**A**), WT MNs (N=7) (**B**) and SMA MNs (N=7) (**C**). Bar graphs depict the mean ± SD. One-way ANOVA with Dunnett post hoc analysis was used to compare each timepoint with the control. ns $p>0.05$, *$p<0.05$, **$p<0.01$.

3.11.2 Increase of SMN is post-transcriptionally regulated

As our results showed that pyruvate could increase SMN protein levels, it is important to test whether this increase is mediated transcriptionally or post-transcriptionally. To understand the molecular mechanism underlying increased SMN levels, we performed qRT-PCR with *Smn* specific primers to measure *Smn* mRNA levels in WT MNs and NSC-34 cells after pyruvate treatment. No significant increase of *Smn* mRNA levels was observed after pyruvate supplementation, suggesting post-transcriptional regulation of SMN levels (**Figure 58**).

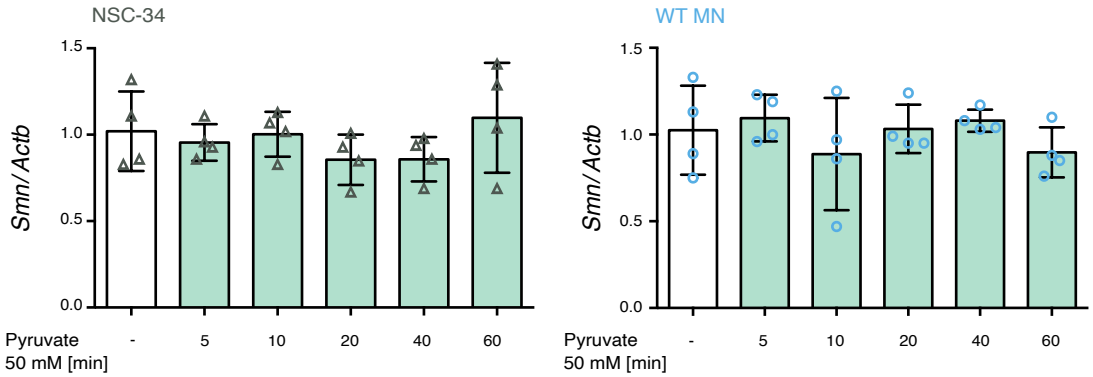

Figure 58: Pyruvate does not change *Smn* mRNA expression.
Quantitative real-time PCR using gene specific *Smn* primers confirms that pyruvate supplementation does not change *Smn* transcript levels in NSC-34 cells and WT MNs (N=4). *Actb* was used as loading control. Bar graphs depict the mean ± SD.

To strengthen our results that pyruvate regulates SMN post-transcriptionally, we blocked translation with 50 µM anisomycin and measured SMN after 50 mM pyruvate supplementation for 10 min and 20 min. In line with our hypothesis, the increase of SMN was abolished entirely when anisomycin was present (**Figure 59**). However, as a control, SMN levels were measured without protein synthesis inhibition, and an increase was detected after 10 min and 20 min of pyruvate (**Figure 59**). This data confirms that protein synthesis of SMN is regulated by pyruvate in a post-transcriptionally manner.

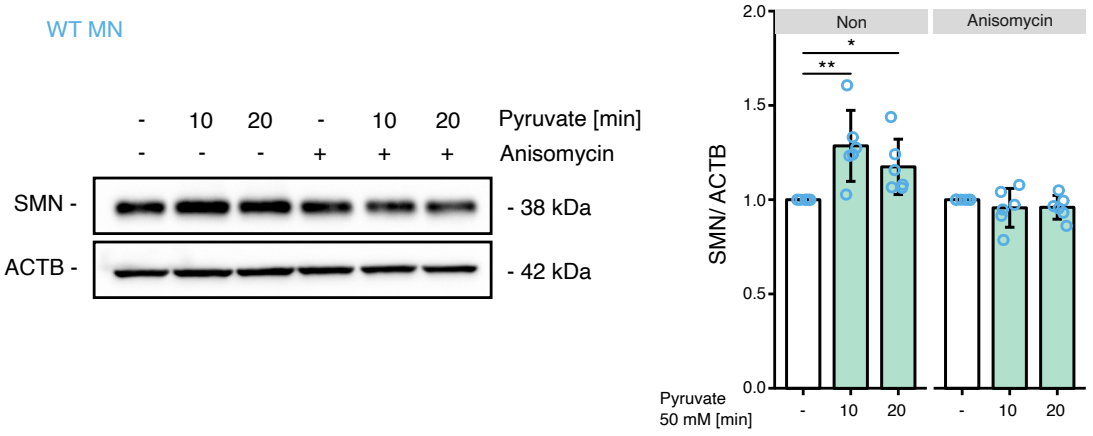

Figure 59: Increase of SMN by pyruvate is abolished by anisomycin.
50 µM anisomycin prevents increase of SMN protein levels induced by pyruvate (N=6). 50 mM pyruvate was treated for 10 min or 20 min. Bar graphs depict the mean ± SD. One-way ANOVA with Tukey HSD post hoc analysis was used to determine statistical significance. *p <0.05, **p <0.01.

3.11.3 Modulation of ROS regulates SMN

Also, we wanted to see the effect of ROS on SMN protein levels. As we already saw the connection between ROS and global or local translation, it is most interesting if SMN is also increased by reducing ROS. Indeed, 10 µM NAC increased SMN levels in WT MNs (**Figure 60A**). Furthermore, SMN was also affected by increasing ROS with menadione in WT MNs. In both WT and SMA MNs, SMN was almost completely depleted after 1 h menadione treatment. Most importantly, treatment with NAC was able to increase SMN levels in SMA MNs by ~50 % (**Figure 60B**).

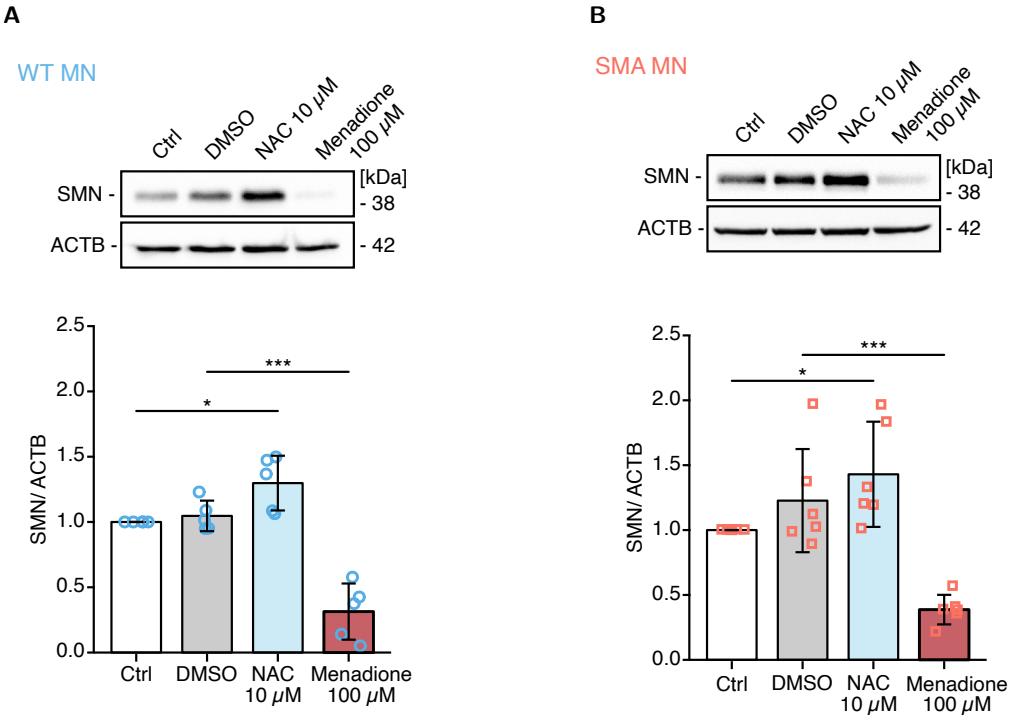

Figure 60: SMN levels after 1h NAC and menadione treatment.
Representative western blot images and quantification of SMN levels treated with 10 µM NAC or 100 µM menadione for 1 h in WT MNs (**A**) and SMA MNs (**B**). One-way ANOVA with Tukey HSD post hoc analysis was used to determine statistical significance for multiple comparisons. Each dot represents the quantification of individual biological replicates. Bar graphs depict the mean ± SD. ns p >0.05, *p <0.05, ***p <0.001.

3.11.4 Increase of SMN is mTOR-dependent

Translation can be regulated by the mTOR pathway. Especially mTORC1 is a central regulator of protein synthesis (Sarbassov & Sabatini, 2005). Therefore, we tested whether the increase in SMN protein levels is mTOR dependent. We treated MNs with 100 nM of the water-soluble mTOR inhibitor, WYE-687 dihydrochloride, and supplied 50 mM pyruvate. As our previous results already showed, pyruvate increased SMN levels in WT MNs after 10 min or 20 min. However, blocking the mTOR pathway by WYE-687 dihydrochloride abolished this effect completely (**Figure 61**).

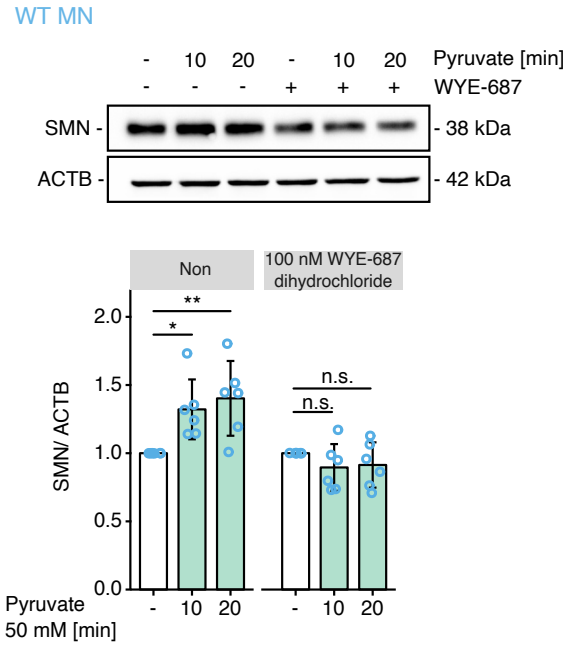

Figure 61: Increase of SMN by pyruvate is blocked by mTOR inhibition.
100 nM WYE-687 dihydrochloride treatment blocks mTOR dependent increase of SMN levels after pyruvate treatment in WT MNs. One-way ANOVA with Tukey HSD post hoc analysis was used to determine statistical significance for multiple comparisons. Each dot represents the quantification of individual biological replicates. Bar graphs depict the mean ± SD. ns p >0.05, *p <0.05, **p <0.01.

To further investigate the effect of pyruvate on the mTOR pathway, we treated WT and SMA MNs with 50 mM pyruvate for 10 min and 20 min and measured phosphorylation of the S6 Kinase as well as phosphorylation of the downstream target ribosomal protein S6 (S6). Supplementation of WT MNs resulted in higher phosphorylation of both, S6K and S6 proteins (**Figure 62A & Figure 62B**). Especially the S6 protein was three-fold higher phosphorylated after 10 min and 20 min pyruvate supplementation in WT MNs. In addition, pyruvate increased the phosphorylation status of S6 in SMA MNs (**Figure 62C**). This data conclusively shows that the activity of the mTOR pathway is increased after pyruvate treatment.

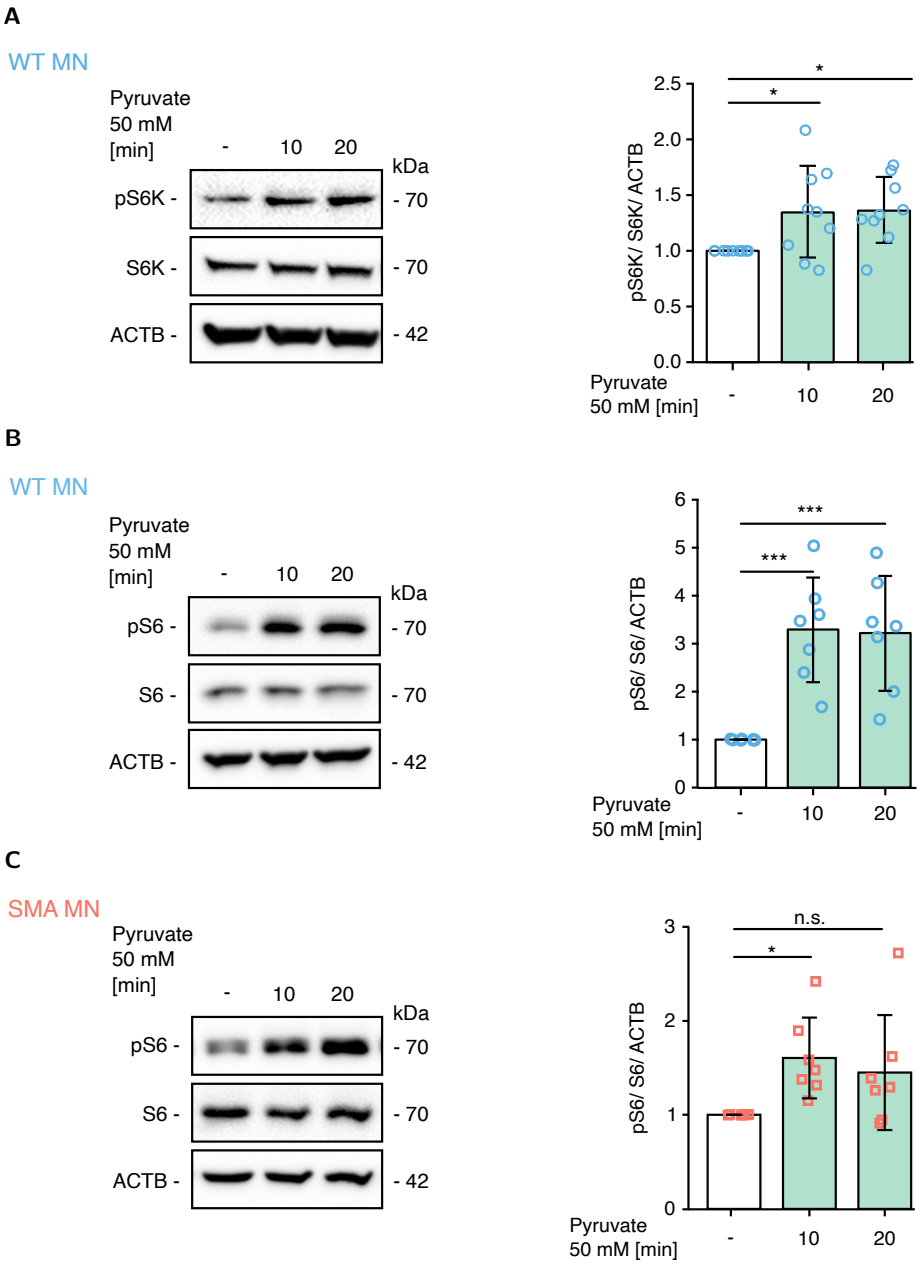

Figure 62: Pyruvate increases mTOR in WT and SMA MNs.
(**A**) Representative western blot and quantification show that pyruvate treatment increases phosphorylation status of p70S6 kinase. (**B**) Representative western blot and quantification of phosphorylated S6 and total S6 protein levels after pyruvate treatment in WT MNs (N=7) and in SMA MNs (N=7) (**C**). One-way ANOVA with Tukey HSD post hoc analysis was used to determine statistical significance for multiple comparisons. Each dot represents the quantification of individual biological replicates. Bar graphs depict the mean ± SD. ns p >0.05, *p <0.05, ***p <0.001.

Further, reduction of ROS by NAC treatment in SMA MNs also increased mTORC1 activity (**Figure 63**).

Taken together, our data showed that cellular ROS and ATP levels regulate SMN protein synthesis via regulating mTORC1. Furthermore, re-balancing ROS levels with an antioxidant in SMA MNs can increase SMN protein synthesis.

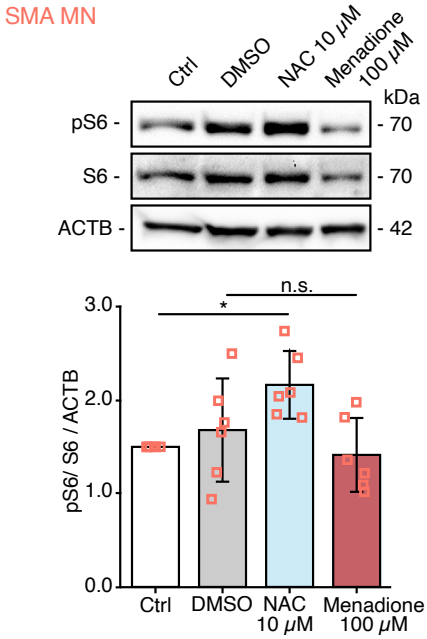

Figure 63: Reducing ROS increases mTOR in SMA MNs.
Representative western blot and quantification of phosphorylated S6 and total S6 protein levels after 10 µM NAC treatment and 100 µM menadione in SMA MNs (N=7). One-way ANOVA with Tukey HSD post hoc analysis was used to determine statistical significance for multiple comparisons. Each dot represents the quantification of individual biological replicates. Bar graphs depict the mean ± SD. ns p >0.05, *p <0.05.

4 DISCUSSION

Previous studies revealed several molecular impairments leading to SMA. Early studies noted indications of disturbed energy homeostasis (Acsadi et al., 2009). Additionally, several studies revealed impairments of mitochondria in SMA (Miller et al., 2016; C. C. Xu et al., 2016; Z.-B. Wang et al., 2013). Moreover, emerging research on ribosome biology revealed a reduced number of ribosomes and impaired translation efficiency in SMA (Bernabò et al., 2017; Lauria et al., 2020). However, the interactions of those impairments remain still elusive. Our study clarified the interplay of energy homeostasis, oxidative stress, and protein synthesis in SMA.

Additionally, we add new insights into tissue-specific impairments of SMA based on our findings of MN specific mitochondrial complex I defects. However, the pathology of SMA exceeds MNs as their primary affected tissue (Hamilton & Gillingwater, 2013). Therefore, determination of tissue-specific impairments is essential, but for future therapies, other tissues affected in SMA must also be taken into consideration.

Some of the molecular impairments, including decreased ATP levels, have been shown to occur at early symptomatic stages (Boyd et al., 2017). However, it was not of aim to answer the question if deprived energy homeostasis or increased oxidative stress is a cause or consequence of SMA. Further studies investigating presymptomatic and symptomatic tissues might answer this question. Regardless of its role in SMA, our study shows that alleviating oxidative stress and improving energy homeostasis is beneficial for SMA MNs. With this study, we attempt to clarify the role of defective energy homeostasis, including the formation of oxidative stress.

By performing a quantitative proteome analysis, we could verify previously known processes that are dysregulated in SMA. Those processes include RNA binding, protein transport, the formation of ribonucleoprotein complexes, and protein synthesis (Akten et al., 2011; Bernabò et al., 2017; Fallini et al., 2011; Kye et al., 2014; Pellizzoni, 2002; Rossoll et al., 2003). The major findings of this study are:

(I) Mitochondrial defects in SMA MNs result in reduced ATP levels that could not be compensated by glycolysis.

(II) We identified a defective complex I in the respiratory chain as causative for increased ROS formation.

(III) Oxidative stress in SMA MNs results in increased protein carbonylation and reduced translation.

Impaired protein synthesis has also been reported earlier in SMA (Kye et al., 2014; Bernabò et al., 2017). However, the molecular link between oxidative stress and impaired protein synthesis was not reported.

(IV) We found out that especially translation initiation is affected by increased oxidative stress.

(V) Counteracting oxidative stress and energy homeostasis results in an improved initiation of mRNA translation. The mTOR pathway mediates this process.

In summary, we revealed a previously unknown relationship between oxidative stress generated by defective mitochondrial complex I and mRNA translation initiation in SMA MNs. Also, this

study conclusively connects oxidative stress to impaired mRNA translation. Furthermore, we showed that targeting mitochondrial defects ameliorates the defective protein synthesis. In addition, ROS reduction results in an increase of SMN, possibly mitigating SMA pathology. The newly found insights will be discussed hereafter in detail under consideration of methodological limitations of this investigation and the perspective of current knowledge.

Primary MNs from SMA mice and control mice were used for *in vitro* experiments to evaluate pathological changes in SMA. Spinal cords of E13.5 embryos were isolated, and primary MNs were cultured for 10 days. Of note, only 3%-5% of all neurons in the spinal cord of E12-E14 embryos are MNs (Arce et al., 1999; Wiese et al., 2010). However, during *in vitro* culture, MNs are enriched. After 2DIV, a 10-fold enrichment of MNs by the culture conditions is already observed, even without enrichment by $p75^{NTR}$-antibody panning (Wiese et al., 2010). Therefore, primary MN cultures are highly enriched after 10DIV. With enrichment by $p75^{NTR}$-antibody panning, MNs can be enriched to about 90% after 7DIV (Wiese et al., 1999, 2010). Furthermore, successful enrichment of MNs, using the same protocol has been shown in previous studies by ChAT stainings (Kye et al., 2014; Gonçalves et al., 2018; Rehorst et al., 2019). Moreover, MNs are morphologically easily distinguishable from other non-neuronal cells.

4.1 The mitochondrial proteome is significantly altered in SMA MNs

The initial objective of this study was to identify altered pathways in SMA MNs. Therefore, quantitative proteome analysis was conducted. As previous studies implicated metabolic defects in SMA and especially an impaired energy homeostasis, we focused on proteins associated with mitochondrial localization or function. Surprisingly no difference in the amount of significantly altered mitochondrial proteins and the overall number of detected mitochondrial proteins was found. Our dataset was compared to the MitoCarta2.0 dataset, including 1158 mitochondrial proteins. Based on literature, it is assumed that $\approx$ 14% - $\approx$ 16% of the neuronal proteome is associated with mitochondria (Hornburg et al., 2014; Calvo et al., 2016; Bogetofte et al., 2019). However, we detected $\approx$ 13% of proteins associated with mitochondria in our proteome analysis. Furthermore, $\approx$ 12% of all significantly changed proteins were also found in the MitoCarta2.0 database. Of note, it is essential to keep the time of differentiation in consideration as neurons shift their metabolism from aerobic glycolysis to OXPHOS during differentiation (Zheng et al., 2016). After 1 or 2 weeks in culture, embryonic and postnatal neurons show similar properties with regard to metabolic properties, energy homeostasis, and stress resistance (Surin et al., 2013). Therefore, neurons in our experiments, which are cultured for 10 days, can be compared to postnatal neurons in terms of energy homeostasis.

4.2 The number of mitochondria is reduced in SMA MN axons

Mitochondria generate ATP and regulate Ca^{2+} homeostasis and apoptosis. Moreover, mitochondria are transported along the axon to support local energy demands or buffer Ca^{2+} necessary for neurotransmitter release and neuronal signaling. Mitochondria are transported anterogradely by kinesin motor proteins of the KIF5 family and retrogradely by dyneins (Sheng & Cai, 2012). In addition, KIF1B and KIF1BP regulate mitochondria localization in the anterograde direction

(Nangaku et al., 1994; Pilling et al., 2006; Wozniak et al., 2005). An axonal Ca^{2+} increase and Na^{+}/K^{+}-ATPase activity upon action potentials, results in mitochondrial immobilization (C. L. Zhang et al., 2010). Even though the mechanism remains unclear, it is hypothesized that mitochondria are stalled upon ATP depletion to generate local energy supplies (C. L. Zhang et al., 2010). Impairments in mitochondrial transport are associated with neurodegeneration caused by an impaired synaptic homeostasis (Sheng & Cai, 2012).

Previous studies in SMA MNs focusing on mitochondrial mobility along the axon showed concordantly a reduced retrograde transport (C. C. Xu et al., 2016; Miller et al., 2016). However, there is little agreement on mitochondrial size and occupancy along the axon. While Xu *et al.* reported a reduced mitochondrial size and number, they noticed no difference in the mitochondrial length (C. C. Xu et al., 2016). In contrast, Miller *et al.* detected a reduced mitochondrial length, but the same density of mitochondria in SMA MNs and control MNs (Miller et al., 2016). Our initial hypothesis suggesting a link between oxidative stress and SMA pathology is further supported by the increased mitochondrial motility upon NAC treatment (C. C. Xu et al., 2016).

In accordance with the results of Xu *et al.*, our investigations demonstrate that the number and size of mitochondria are reduced in the axonal compartment of SMA MNs. In addition, our whole proteome analysis suggested altered levels of mitochondrial proteins in SMA MNs. Increased TOM20 levels found in the MS data were further confirmed by WB analysis. Nonetheless, an increase of TOM20 is contradictory to the quantification of TOM20 within the axon. A reasonable explanation for these results may be that defective mitochondria accumulate in the soma. Therefore, total TOM20 amounts appear to be increased despite the reduction in the axon.

Nevertheless, the diverse results, including ours, might be explained by methodological differences in the studies. While Miller and colleagues visualized mitochondria by aberrantly expressed mitochondrial proteins, Xu *et al.* and we used the mitochondria membrane intercalating dye MitoTracker. In addition, we labeled endogenous TOM20 immunofluorescently to visualize functional and non-functional mitochondria. In SMA and WT MNs, we observed fewer mitochondria by MitoTracker staining than by TOM20 labeling. This finding confirms that MitoTracker labeling visualizes only functional mitochondria, and the actual number, including defective mitochondria, is higher than the ones visualized by MitoTracker staining.

Although our studies did not focus on mitochondrial motility, we found reduced KIF1B and KIF1BP levels in our whole proteome analysis. Reduced motor proteins can explain the reduced motility of mitochondria in the axons and the reduced ATP availability. Further, increased action potentials resulting from hyperexcitability might contribute to the immobilization of mitochondria.

In addition, the increased circularity of mitochondria suggests an impairment and fragmentation of mitochondria in SMA MNs.

4.3 Complex I activity is impaired in SMA MNs

ROS generation arises from proton leakage in the respiratory chain and subsequent partial reduction of oxygen. Although complex I-III can generate ROS, the overall amount generated by

the complexes varies among cell types and their mitochondrial activities (Barja, 1999; Turrens, 2003). However, complex I is the major ROS producer in neurons (Barja & Herrero, 1998).

Most interestingly, proteins of complex I were most prominent among the significantly changed proteins in SMA MNs. Quantitative proteome analysis revealed alterations in one-quarter of the detected proteins in complex I. It is somewhat surprising that no respiratory chain proteins encoded in the mitochondrial DNA were significantly altered in SMA. This finding is unexpected as oxidative stress can damage mtDNA in defective mitochondria, and therefore, an altered expression of those proteins would be not surprising. Furthermore, several translation factors and components of the mitochondrial small and large ribosome subunits encoded in the nucleus were altered in SMA.

Functional analyses of the complex I confirmed an impairment of the respiratory chain activity caused by defective complex I in SMA MNs. Additionally, complex I activity was measured in different tissues of SMA to test a neuron-specific alteration. Interestingly, complex I activity was unchanged in the heart and spinal cord of SMA. While the proper function of complex I implicates a cell type-specific effect, the unaltered activity in SC neurons raises new questions. However, only a small proportion of 3% - 5% of cells in the spinal cord are MNs (Arce et al., 1999; Wiese et al., 2010). Therefore, a MN specific effect of complex I deficiency can not be detected in the whole spinal cord. In addition, tissue samples of heart and SC were taken from P5 mice, while MNs were taken from E13.5 mice and cultured for 10 days. SMA mice of this model show a mean survival of 10 days (Riessland et al., 2010). Moreover, P5 SMA mice are early symptomatic. Therefore it can not be excluded that any effect can be observed when more severe symptoms occur.

4.4 Oxidative stress is increased in SMA MNs

The issue of oxidative stress in SMA has been a controversial and much-disputed subject in the field. Early studies suggested increased oxidative stress with an increased mitochondrial membrane potential upon SMN depletion in NSC-34 cells (Acsadi et al., 2009). In contrast, more recent studies found increased oxidative stress in the soma and axon but a decreased mitochondrial membrane potential (Miller et al., 2016). Additional studies in MNs generated from SMA type 1 patient-specific iPSCs confirmed a reduced membrane potential with an increase of oxidative stress (C. C. Xu et al., 2016; Z.-B. Wang et al., 2013). Nevertheless, the assumption of increased oxidative stress in SMA has recently been challenged by studies in SMA iPSC- derived MNs demonstrating that SMN deficiency does not induce oxidative stress (Patitucci & Ebert, 2016). This controversy highlights the importance of gaining deeper insights into the mechanisms regulating oxidative stress in SMA MNs.

Based on fluorescence labeling, we concluded that SMA MNs suffer from increased ROS levels. We showed elevated ROS by fluorescence labeling in a microplate reader and by microscopy. Here, we did not distinguish between the soma and axonal compartment. As we speculate that ROS affecting SMA MNs is produced in mitochondria, it is not surprising that fluorescence signals appear very faint in the axonal compartment. However, previous studies using transfection of a redox-sensitive green fluorescent protein to visualize ROS distinguished between individual compartments and found increased ROS in both soma and axon (Miller et

al., 2016).

Important enzymatic scavengers of antioxidant defense are superoxide dismutases, catalases, glutathione S-transferases (GSTs), or glutathione peroxidases (GTPx) (Birben et al., 2012). Moreover, the study of Patitucci *et al.* revealed an increase of endogenous catalase expression, suggesting a successful compensatory mechanism of the cellular antioxidant defense (Patitucci & Ebert, 2016). Even though Patitucci and colleagues' study did not observe an increase of oxidative stress in SMA MNs, the upregulation of antioxidative catalases suggests a compensatory mechanism towards oxidative stress. Reducing oxidative stress in SMA MNs with NAC has been proven to mitigate pathology, including defective mitochondrial transport (Z.-B. Wang et al., 2013; C. C. Xu et al., 2016). Nevertheless, those studies did not elaborate further on the mechanism of amelioration.

Several proteins, including SOD1 or GSTP1, were found in our MS data significantly reduced in SMA MNs. It is possible, therefore, that SMA MNs fail to mitigate oxidative stress efficiently. Nonetheless, several other proteins involved in oxidative stress defense, albeit less, were significantly increased in SMA MNs. However, a compensatory mechanism of up-regulated ROS scavengers can not be excluded, based solely on the quantitative proteomics approach. Further functional studies with more focus on oxidative stress defense mechanisms are therefore required. Taken together, it appears that oxidative stress occurs in SMA MNs, but the mechanism of oxidative stress defense is very fragile and might fail to reduce intracellular ROS levels.

Increased ROS levels can result in various pathological changes in a cell. Molecular targets of ROS include DNA, lipids, and proteins (Auten & Davis, 2009). Further, protein oxidation caused by ROS can result in impaired global protein synthesis (Topf et al., 2018). Indeed we detected increased protein carbonylation and reduced protein synthesis in SMA MNs. A reduced protein synthesis in SMA MNs was also observed in previous studies (Kye et al., 2014; Bernabò et al., 2017; Lauria et al., 2020)

As the decrease of protein synthesis in SMA MNs is a substantial impairment, we confirmed the results with two independent methods. The first method uses puromycin labeling; the SUnSET assay. Puromycin labels newly synthesized proteins and causes a termination of protein synthesis. Furthermore, we used a second method to eradicate any possible effect on puromycin due to increased ROS in SMA. The second method uses the stable incorporation of a methionine analog without termination of protein synthesis. Both methods showed conclusively a massive decrease in protein synthesis in SMA MNs.

It has been shown that hypoxia induces ROS production in the brain (Lewén et al., 2000; Maiti et al., 2006). In severe SMA forms of SMA mouse models and patients, vascular defects resulting in hypoxia of MNs have been noticed (Somers et al., 2016). Further, widespread tissue hypoxia, including muscle, was observed in SMA mice, with MNs being especially susceptible to hypoxia (Hernandez-Gerez et al., 2020). As a result of hypoxia, the hypoxia-inducible factor 3 alpha (Hif3α) is increased in symptomatic SMNΔ7 SMA mice. Moreover, hypoxia reduced SMN levels by increased *SMN2* exon 7 skipping (Bebee et al., 2012).

In all our experiments, isolated MNs were cultured under normoxic conditions. Further, our whole proteome analysis did not reveal any increase in hypoxia-inducible factors. However,

considering the vascular defects and the interplay in the organism, the effect of hypoxia and subsequent induction of oxidative stress on other tissues needs to be considered.

4.5 Glycolysis does not compensate for mitochondrial defects

It is widely accepted that mitochondrial OXPHOS is the primary energy-producing process in neurons. However, the preference of energy production in neurons switches during differentiation from glycolysis to OXPHOS (Zheng et al., 2016). Additionally, neurons are capable of adapting to external stimuli and fluctuating energy requests.

In terms of glycolysis, GLUT3 provides a basal supply of glucose to neurons (Gerhart et al., 1992; Ashrafi et al., 2017). Further, it has been shown that energetic demands in neurons can promote the mobilization of GLUT4 to active synapses (Ashrafi et al., 2017). In an ALS *Drosophila* model, glycolysis has been found to be up-regulated as a compensatory mechanism, and supply of glucose was neuroprotective (Manzo et al., 2019). Also, prior studies in SMA suggested metabolic impairments contributing to SMA pathology, including defective glucose metabolism (Bowerman et al., 2014). Moreover, while basal glycolysis has been shown to be unaltered in patient myoblasts, compensatory glycolysis was lower in SMA than healthy control myoblasts (Hellbach et al., 2018). Surprisingly, we found that glucose uptake is reduced in SMA MNs and does not compensate for mitochondrial impairments.

Nevertheless, it remains unclear why SMA MNs fail to adapt to fluctuating energy demands. Direct quantification of glucose transporter at the synapse could reveal if SMA MNs are incapable of glucose transporter exocytosis. Further, the efficiency of glucose utilization remains unclear in SMA.

4.6 Rescuing energy homeostasis fails to rescue SMA pathology fully

As mentioned in the literature review, neuronal signal transmission is metabolically expensive. In fact, action potentials can consume up to 47% of the energy used for synaptic transmission (Attwell & Laughlin, 2001). Furthermore, previous studies revealed that SMA MNs are hyperexcitable due to increased Na^+ channel activity (H. Liu et al., 2015). In addition, focusing on energy used in non-signaling processes, global translation is a very energy-demanding process. Up to 20-30% of the whole energy consumption is attributed to protein synthesis (Buttgereit & Brand, 1995). However, energy consumption is very diverse in different tissues. Even though protein synthesis uses a tremendous amount of the total energy, it is assumed that protein synthesis in neurons only accounts for $\approx 1.3\%$ of energy that is not used for signaling (Rolfe & Brown, 1997; Attwell & Laughlin, 2001; Engl & Attwell, 2015). Still, the impact of protein synthesis can be higher than in other tissues as the overall energy consumption is very high in neurons.

Considering the high energy demands in neurons and the hyperexcitability in SMA MNs, we hypothesized that SMA MNs require significant amounts of ATP. Nevertheless, decreased ATP levels in MNs of different SMA models were observed in previous studies (Acsadi et al., 2009; Boyd et al., 2017). Additionally, Boyd and colleagues' previous study revealed that ATP concentrations were reduced early and late symptomatically in the spinal cord (Boyd et al., 2017). The findings of the current study are consistent with the previous studies and

provide evidence for reduced ATP levels in SMA MNs. Additionally, we provide data from bioluminescence and fluorescence signals showing a consistent decrease of ATP in SMA MNs. Both methods show individual advantages in terms of signal intensity, background signal, and signal stability. However, luminescence has been proven to be more sensitive than fluorescence signals due to a reduced background signal (Fan & Wood, 2007). Still, our results showed a higher reduction of ATP in SMA samples measured by fluorescence. A possible explanation for these outcomes may be the quenching effect of ROS on the fluorescence signal. Therefore, luminescence was used to detect ATP in all further experiments.

4.6.1 The astrocyte-neuron lactate shuttle hypothesis and why lactate fails to increase ATP in neurons

Previous research, including our results, showed an impairment of the energy homeostasis in SMA MNs. Therefore, we hypothesize that rescuing energy homeostasis might ameliorate the SMA phenotype. Therefore, this study set out with the aim to restore energy homeostasis in SMA MNs. However, there are multiple ways to support the energy homeostasis in a cell. One efficient way is to supply the cells with the necessary substrates. As our results suggested that glucose uptake is impaired in SMA MNs, we aimed to bypass glycolysis and supply either lactate or pyruvate.

In 1994, the controversial astrocyte-neuron lactate shuttle hypothesis (ANLS) was established by Pellerin and Magistretti (Pellerin & Magistretti, 1994). Based on the ANLS, it was assumed that neuronal activity could trigger glucose uptake in astrocytes (Pellerin & Magistretti, 1994). The initial ANLS hypothesis focused on the quantitative coupling of synaptically released glutamate with glucose utilization in astrocytes to produce lactate. Also, the shuttle of lactate from astrocytes to neurons has been shown *in vivo* (Mächler et al., 2016).

One major issue in the ANLS hypothesis was raised by more recent research. It was demonstrated that glycolysis and lactate export is instead down-regulated in neurons under neuronal activity (Díaz-García et al., 2017; Díaz-García & Yellen, 2019). These results are in agreement with the increased GLUT4 localization at the plasma membrane under neuronal stimulation (Ashrafi et al., 2017). Therefore, it is more likely that the metabolic response to neuronal activation is determined by the kinetics of neuronal glycolysis rather than increased lactate shuttle. While lactate is undoubtedly a valuable oxidative substrate to neurons. Nevertheless, the importance during neuronal activity is questionable.

As the ANLS still holds true in many aspects, it was reshaped into the concept of astrocyte-neuron communication (ANC) (Roosterman & S. Cottrell, 2020). The ANC concept focuses primarily on the proton-driven transfer of lactate and pyruvate linked to glucose provision. Therefore, a variety of monocarboxylate transporter (MCT) in complexes with proton donors stabilizes the import of lactate to neurons in the presence of glucose, generating an energy flow.

In general, MCT are used to facilitate the transport of molecules containing one carboxylate group such as lactate or pyruvate (Halestrap & Meredith, 2004). Monocarboxylates can be exported unidirectionally from highly glycolytic cells by MCT4 (Dimmer et al., 2000). While MCT4 shows a higher affinity towards lactate, the export of lactate is more likely (Halestrap, 2013; Contreras-Baeza et al., 2019). Additionally, MCT1 unidirectionally imports

monocarboxylates (Debernardi et al., 2003). Here, MCT1 shows a higher affinity towards pyruvate (Halestrap, 2013). However, also lactate shuttle from neurons to astrocytes has been shown *in vivo* (Mangia et al., 2009). Therefore, it is assumed that monocarboxylates can be simultaneously imported and exported in astrocytes (Lynch et al., 2015; Roosterman & S. Cottrell, 2020). In neurons, MCT2 is a major transporter for monocarboxylates and is capable of importing lactate (Pierre et al., 2002). Moreover, the direction of MCT2 transfer can change from import to export based on the MCT2-proton donor complex (Halestrap & Meredith, 2004).

Unquestionably, lactate can be used as an energy substrate regardless of neuronal stimulation. Inside of the neuron, lactate can be converted into pyruvate for subsequent OXPHOS via the lactate dehydrogenase. However, supplementation of lactate failed to increase ATP levels in MNs. The reason for this is not apparent, but it may have something to do with the ability to export lactate from neurons as supposed in the neuron to astrocyte lactate shuttle. Especially, highly active SMA MNs, might tend to export lactate rather than import it as this was also seen *in vivo* in previous studies (Díaz-García et al., 2017). Another possible explanation for this is that we only used two different lactate concentrations, which might not be optimal.

4.6.2 Pyruvate improves energy homeostasis and reduces ROS

Following our aim to restore defective energy homeostasis, we supplied MNs with pyruvate. As described in the previous chapter, pyruvate is imported into neurons via MCT2 and can serve as a substrate during OXPHOS. There are multiple advantages of supplying pyruvate over lactate to neurons.

One disadvantage of lactate is that it can be exported from neurons and shuttle to astrocytes. Further, protonated MCT2 shows a ten-times higher affinity towards pyruvate over lactate (Lin et al., 1998; Halestrap, 2013). Therefore, another advantage of pyruvate is the preferred substrate for import into neurons. Indeed, our results showed stable pyruvate uptake in SMA and control MNs. Even though we did provide evidence for intercellular pyruvate uptake, we did not show pyruvate uptake into mitochondria. Nevertheless, the stable increase of ATP after pyruvate supplementation suggests a successful import into mitochondria.

Additionally, pyruvate can act as a ROS scavenger and reduce oxidative stress (Kładna et al., 2015). The beneficial effect of ROS reduction was not observed in WT MNs or NSC-34 cells. However, these results are not surprising, as oxidative stress does not occur in those cells. Therefore, oxidative stress was induced pharmacologically in those cells by menadione. Those experiments support our hypothesis that ROS reduction is possible by pyruvate supplementation. Additionally, pyruvate supplementation reduced ROS in SMA MNs suffering from oxidative stress.

In contrast, previous studies showed that lactate and pyruvate could also induce ROS (Tauffenberger et al., 2019). Nevertheless, this study suggested a protective effect of lactate and pyruvate. It was suggested that ROS induction results in a transcriptional upregulation of oxidative stress defense genes (Tauffenberger et al., 2019). Accordingly, in this study, neuroprotection is preferably achieved by increased antioxidative proteins than a direct ROS reduction. Nevertheless, the capability of SMA MNs to cope with oxidative stress might be

impaired already, as suggested by our MS data and discussed in section 4.4. Due to defective defense machinery, pyruvate might not result in protective through transcriptional upregulation. Moreover, the effect of ROS reduction and induction might be concentration-dependent.

4.7 Reducing ROS, not increasing ATP improves global translation

The two most striking effects of defective mitochondria we found in SMA MNs are increased ROS and reduced ATP production. One pathological effect linked to excessive ROS is a decreased protein synthesis. Therefore, reducing ROS is hypothesized to restore impaired protein synthesis in SMA MNs.

Indeed, pyruvate increased ATP in NSC-34 cells and SMA MNs but showed no effect on global protein synthesis. Accordingly, it can be assumed that ATP plays only a minor role in regulating global protein synthesis. However, this result is expected as only $\approx 1.3\%$ of the energy consumption that is not used for signaling in neurons accounts for protein synthesis (Rolfe & Brown, 1997; Attwell & Laughlin, 2001; Engl & Attwell, 2015). Moreover, NAC treatment increased protein synthesis in SMA MNs without an effect in WT MNs or NSC-34 cells, as only SMA MNs showed increased ROS levels. One unanticipated finding was that pyruvate did not increase global protein synthesis despite its ROS reducing properties. This somewhat contradictory result may be due to a superior antioxidative effect of NAC compared to pyruvate.

These results collectively outline a critical role for ROS on protein synthesis with only a small impact of ATP availability.

4.8 Local translation in SMA MNs

It is essential for neurons to synthesize proteins at the distal ends of the neurites to adapt to local changes during development and activity. Based on immunofluorescence stainings of the SUnSET assay, we can conclude that protein synthesis is decreased in the soma and the axonal compartment. However, even though we measure the pathological outcome of decreased protein synthesis, we can not conclude the cause of this effect. These data must be interpreted with caution because puromycin labeling is carried out for one hour, and the transport of newly synthesized proteins might be decreased in SMA MNs. Therefore, we can not exclude the possible scenario, based only on this experiment, that the impaired protein synthesis appears mainly in the soma and a reduced transport results in a decreased signal in distal parts of the neurites. A further study with more focus on axonal protein transport is therefore suggested. Blocking protein transport in SMA and WT MNs before facilitating the SUnSET assay might solve this issue. Nevertheless, an impaired local protein synthesis shown in this study corroborates earlier findings showing a reduced number of axonal ribosomes in an SMA *in vivo* model (Bernabò et al., 2017).

Treating MNs with pyruvate and NAC resembled the same results observed in the whole-cell experiments also in the axonal compartment. Here, only NAC increased local translation in SMA MNs. In fact, impaired protein synthesis is regulated by ROS, and newly synthesized proteins are less abundant in the axon.

Moreover, our experimental setup did not allow us to investigate local translation at the growth cone. We used 10DIV MNs in all experiments to keep consistency. However, axons of cultured primary MNs can already exceed 500 µm after 7DIV (Bömmel et al., 2002; Wiese et al., 2010). Additionally, MN axons and dendrites reach their maximum length after 7DIV and do not increase significantly afterward (Wiese et al., 2010). Therefore, it is impossible to trace an entire axon in our cultures.

It has been shown that mitochondria serve as hubs for local translation in dendrites, along the axon, and at the growth cone (Rossoll & Bassell, 2019; Rangaraju et al., 2019; J.-M. Cioni et al., 2019). As our results showed a reduced number of mitochondria along the axon in SMA MNs, this might also affect local translation. Furthermore, RNPs, containing mRNAs important for mitochondrial maintenance, are found to associate with Ras-related protein Rab-7a (Rab7a) endosomes attached to mitochondria (J.-M. Cioni et al., 2019). The interaction of Rab7 and mitochondria, necessary for local translation, opens new avenues for future studies. Co-stainings of those components together with puromycin labeling for newly synthesized proteins can lead to deeper insights into this field.

4.9 Whole proteome analysis after pyruvate treatment

We aimed to determine pathways changed by pyruvate treatment using whole proteome analysis. As we already detected an increase of ATP after pyruvate treatment, alterations in OXPHOS are expected. Moreover, multiple alterations occurred in proteins related to nucleotide and ribonucleotide binding. Biological processes affected by these proteins include RNA splicing and mRNA processing. Furthermore, proteins in the cellular compartments of the spliceosome or RNP complexes are affected by pyruvate treatment. It is essential to keep in mind that those results solely rely on proteome changes observed in MS analysis. Therefore, any conclusions must be interpreted with caution. Furthermore, we observed a translational upregulation of SMN after pyruvate treatment. Therefore, it seems possible that an increase of SMN stabilizes other RNPs, causing increased nucleotide-binding and mRNA processing.

Interestingly, pyruvate did change the proteome of SMA MNs more than WT MNs. The mode of action of pyruvate may explain this result. In WT MNs, ATP and ROS levels are equilibrated, and additional pyruvate does not affect the cells much. Additionally, only two proteins, namely DLGAP1 and ICA1, were changed by pyruvate simultaneously. However, no further conclusions can be drawn from those proteins.

4.10 Whole proteome analysis after NAC treatment

As our results demonstrated, NAC works efficiently as an antioxidant in SMA MNs. Further, whole proteome analysis was facilitated to identify possible pathways altered by NAC treatment. Similar to pyruvate treatment, NAC treatment led to alterations in RNA splicing and mRNA processing. Again, those results need to be evaluated carefully but might be explained by an increase of SMN after NAC treatment.

A more interesting finding was the identification of OTUD6B. While this protein was down-regulated in SMA, it was up-regulated in SMA MNs after NAC treatment. However, it was rather down-regulated in WT MNs after NAC treatment. OTUD6B is a deubiquitinase

involved in ubiquitin-dependent regulation of protein synthesis, downstream of mTORC1 (Sobol et al., 2017). In detail, OTUD6B regulates translation initiation by modifying the 48S PIC (Sobol et al., 2017). Interestingly, there are two splicing isoforms of OTUD6B acting in the opposite direction. While isoform 1 represses protein synthesis (Z. Xu et al., 2011), isoform 2 enhances it (Sobol et al., 2017). Unfortunately, those isoforms can not be distinguished by MS because of the nearly identical sequences. Nevertheless, this is an important protein for future research.

4.11 Whole proteome analysis after menadione treatment

Interestingly, menadione treatment reduced most of the proteins in WT MNs and showed the biggest overlap with proteins altered in SMA. Menadione is used to induce oxidative stress by increasing ROS through futile redox cycling (Loor et al., 2010). Therefore, these findings further support the idea of pathological changes due to increased ROS in SMA MNs. However, the effects of menadione can not solely be restricted to increased proteolysis upon carbonylation due to increased ROS. Additionally, increased ROS by menadione can trigger cell death independent of apoptosis via poly (ADP-ribose) polymerase (PARP) activation (Loor et al., 2010). Nevertheless, increased cell death upon menadione treatment was not observed in our cultures.

4.12 Cap-dependent translation initiation is inhibited in SMA MNs

Recent studies in SMA showed defects in mRNA translation *in vivo* based on impairments of ribosome biogenesis (Bernabò et al., 2017). This study revealed a decreased ribosome number in SMA, and consequently, impairments in the translatome (Bernabò et al., 2017). Moreover, reduced translation efficiency was specifically observed in transcripts, including translation initiation and elongation factors but also ribosome biogenesis.

Focusing on translation-related proteins in our whole proteome approach suggested an impairment of protein synthesis due to several down-regulated proteins in SMA. However, proteins involved in translation elongation were barely changed in our MS data. Further functional experiments in terms of the SunRiSE assay supported the idea of unaltered translation elongation in SMA. eEF1A2 is a translation elongation factor associated with SMA. Our whole proteome approach did not reveal any changes in the expression of eEF1A. However, eEF1A2 is not directly associated with SMA, but by complex formation of eEF1A with SMN (Murray et al., 2008). Loss of eEF1A2 results in disruption of protein synthesis and also to dying-back neuropathies (Murray et al., 2008). However, due to technical limitations, the effect of impaired translation elongation could not be related to the dying back of neurons *in vivo* (Murray et al., 2008). Therefore, no functional evidence in the current literature can be found that shows altered translation elongation in SMA.

Since no difference in translation elongation was detected in SMA MNs, it is not surprising that NAC or pyruvate treatment do not change the elongation speed. Besides translation elongation, translation initiation can limit protein synthesis. Therefore, a major objective of this study was to investigate the role of translation initiation in SMA. Indeed, our data provides sustained evidence of reduced cap-dependent translation initiation. WB analysis revealed

reduced phosphorylation of 4EBP in SMA. Accordingly, 4EBP blocks the formation of the cap-binding complex eIF4F (Pause et al., 1994; Haghighat et al., 1995). Additionally, mTORC1 regulates the phosphorylation of 4EBP and therefore regulating global translation (Gingras et al., 1999).

Previous studies revealed a reduced protein synthesis together with a reduced mTOR activity in SMA (Kye et al., 2014). However, this study did not link the decreased protein synthesis to an impaired translation initiation via 4EBP. Moreover, another study demonstrates the benefits of mTORC1 activation and subsequent phosphorylation of 4EBP by muscle secreted C1q/TNF-related protein 3 (CTRP3) in SMA MNs (Rehorst et al., 2019).

Recently, literature has emerged that offers controversial findings of mTORC1 activity in SMA. In this study, no difference in 4E-BP phosphorylation was observed at P5, and an increase of phosphorylation was noted at P8 in SMA. However, this increase of 4E-BP phosphorylation was observed in SMA brain tissue (Lauria et al., 2020). Moreover, our data suggested a MN specific implication of complex I defects in SMA, resulting in elevated ROS levels in MNs and subsequent inhibition of cap-dependent translation via 4E-BP.

Previous studies also assumed a negative feedback loop of SMN, repressing cap-dependent translation initiation (Sanchez et al., 2013). Indeed, they showed an upregulation of the arginine methyltransferase CARM1 upon SMN depletion *in vitro* (Sanchez et al., 2013). However, based on their own critical discussion, implications of miRNA in this process could not be fully excluded (Sanchez et al., 2013). Since more recent studies demonstrated the influence of reduced mature miRNAs upon DROSHA reduction in SMA, this controversy is not to be neglected (Gonçalves et al., 2018). Moreover, several other studies, including *in vivo* experiments, suggested translational repression upon SMN loss (Fallini et al., 2016; Bernabò et al., 2017; Lauria et al., 2020).

4.13 The mTOR pathways regulates translation in SMA MNs

This study provides sustained evidence of mTOR regulation by pyruvate and NAC. Downstream targets of mTOR, including 4E-BP, S6K, and S6, showed increased phosphorylation upon NAC and pyruvate treatment. Interestingly, the induction of ROS by menadione supplementation did not further reduce mTOR activity in SMA MNs. However, previous studies revealed a reduced mTOR activity in SMA (Kye et al., 2014). Therefore, an additional reduction of mTOR activity by increased ROS might not be detectable as it is already extremely low.

Additionally, mTORC1 controls mitochondrial activity by regulating the synthesis of mitochondrial proteins via 4E-BP (Morita et al., 2013). Furthermore, this study showed that mTOR inhibition impairs energy metabolism and respiration *in vivo* (Morita et al., 2013). This data is in line with our study showing mTORC1 involvement in mitochondrial regulation via 4E-BP. We provide not only data on mitochondrial protein synthesis by whole proteome analysis but also included functional studies on mitochondrial activity.

Besides the regulation of cap-dependent translation, mTORC1 regulates the translation of mRNAs containing a TOP motif. Primarily proteins in the translational machinery, including all ribosomal proteins and all translation elongation factors, contain the TOP motif on their mRNA (Iadevaia et al., 2008; Meyuhas & Kahan, 2015). The whole proteome analysis in

the current study detected several proteins encoded by TOP mRNAs. Furthermore, TOP mRNAs can be translationally repressed upon various stresses, including oxygen or amino acid deprivation independent of 4E-BP activity (Meyuhas & Kahan, 2015; B. B. Li et al., 2018). Based on our experiments, we can not resolve if the regulation of TOP mRNA encoded proteins is based on a cap-dependent or cap-independent manner. Therefore, individual targets need to be tested after mTOR inhibition, similar to the experiments performed in this study on SMN expression. Alternatively, a whole proteome analysis can be performed after inhibition of mTOR or components of the cap-dependent translation machinery.

4.14 Increase of SMN by pyruvate and NAC supplementation is mTOR-dependent

The most striking result for the field of SMA is that NAC and pyruvate increased SMN levels mTOR-dependently. While NAC increased not only SMN but also global translation, pyruvate supplementation led to a specific increase of SMN. The effect was clearly translationally regulated as pyruvate supplementation did not increase *SMN* transcript levels. Furthermore, inhibition of mTOR abolished the effect of pyruvate. Nevertheless, it can not be excluded that NAC increases mTORC1 activity resulting in increased ribosomal biogenesis and accordingly, an increased global translation. However, SMN mRNA does not contain a TOP motif, and therefore direct regulation via mTOR is not possible.

Menadione supplementation of WT and SMA MNs showed even lower SMN levels than untreated cells, implicating that not only translation is inhibited, but SMN protein is additionally degraded. Oxidative stress induction can inhibit SMN complex formation, leading to rapid degradation (Wan et al., 2008).

Recent studies showed the direct association of SMN with ribosomes, which are reduced in SMA (Lauria et al., 2020). Consequently, a subset of SMA specific transcripts have been found differentially translated (Lauria et al., 2020). While our results are in full agreement with this study, we add an additional mechanism contributing to SMA pathology. However, the study of Lauria and colleagues is specific to SMA pathology. Our study describes a more general problem involving oxidative stress and translation initiation in MNs. Therefore, other diseases might also benefit from the regulation of mitochondrial function and oxidative stress.

5 CONCLUDING REMARKS AND FUTURE OUTLOOK

In recent years, there has been an increasing interest in SMN-independent therapies of SMA. With Spinraza and Evrysdi, two very promising drugs have been approved in the last years, focusing on enhancing SMN full-length production from *SMN2*. Additionally, Zolgensma is the first approved gene therapy in SMA that is also SMN dependent. Moreover, Evrysdi is the only drug potentially elevating SMN levels in other tissues than MNs and therefore mitigating multisystemic effects of SMA (Wirth, 2021).

This study set out to determine the effect of deprived energy homeostasis in SMA. Furthermore, the present study was designed to decipher the effect of increased oxidative stress on neuronal protein synthesis in SMA. The four major findings in this study are:

(I) SMA MNs suffer from an impaired energy homeostasis, including defective mitochondria and no compensation by glycolysis.
(II) Oxidative stress in SMA MNs is caused by an impaired mitochondrial respiratory complex I.
(III) Increased oxidative stress leads to reduced translation initiation in SMA MNs.
(IV) Counteracting mitochondrial defects by NAC or pyruvate enhances translation, including mTOR-dependent translation of SMN.

This work contributes to existing knowledge in SMA research by clarifying the role of oxidative stress resulting in impaired translation initiation. Furthermore, this study suggests an additional therapeutic target, enhancing translation by decreasing oxidative stress (**Figure 64**). Still, several questions remain unanswered at present, and further studies on the current topic are therefore recommended:

(1) The present study confirms previous findings of impaired energy homeostasis in SMA and contributes additional evidence that locates mitochondrial defects to complex I. Additionally, it was suggested that glycolysis is not able to compensate for the impaired energy homeostasis. While this study reveals a reduced glucose uptake in SMA MNs, glycolysis efficiency remains largely unknown. However, since upregulation has been shown to be beneficial in ALS (Manzo et al., 2019), it is worth investigating this approach in SMA.
(2) It has conclusively been shown that NAC or pyruvate treatment can be used to increase SMN levels in a short time. It would be interesting to assess the effects of NAC or pyruvate treatment over a longer period *in vitro* and *in vivo*.
(3) Additionally, pyruvate treatment has been shown to increase SMN in WT MNs that are not affected by mitochondrial defects without altering the whole proteome. Considering the multisystemic effects observed in SMA, it would be interesting to evaluate the effect of pyruvate treatment in other cells different from MNs.
(4) This research has shown that pyruvate effectively increases ATP and NAC reduces ROS. As decreased energy and increased ROS are two major events contributing to SMA pathology, a combinatorial treatment is of interest.

(5) Since pyruvate treatment lead to specific upregulation of SMN without altering global protein synthesis, further investigations into the specificity are recommended. Considering new insights by Lauria *et al.*, suggesting SMN primed ribosomes translating SMA specific transcripts might help solve SMN and SMA specificity.
(6) While the whole proteome analysis revealed new insights of SMA affected pathways and NAC or pyruvate treated MNs; it opens new possibilities for further investigation. Here, the role of OTUD6B deserves further examination. Especially due to its involvement in protein synthesis regulation by mTOR.
(7) Several studies, including this one, investigated the role of energy deprivation or impaired protein synthesis in SMA. However, there is still a lack of information on whether those impairments are causative for SMA or result as a consequence of other effects.
(8) Since NAC efficiently reduced ROS in SMA MNs and pyruvate increased ATP levels, it is worth investigating the effects of a combinatorial treatment. Additionally, both supplements lead to an increase of SMN in SMA MNs. Therefore, NAC and pyruvate can be applied simultaneously to primary MN cultures or iPSC derived MNs.
(9) Certainly, the field would highly benefit from confirming the results *in vivo*.

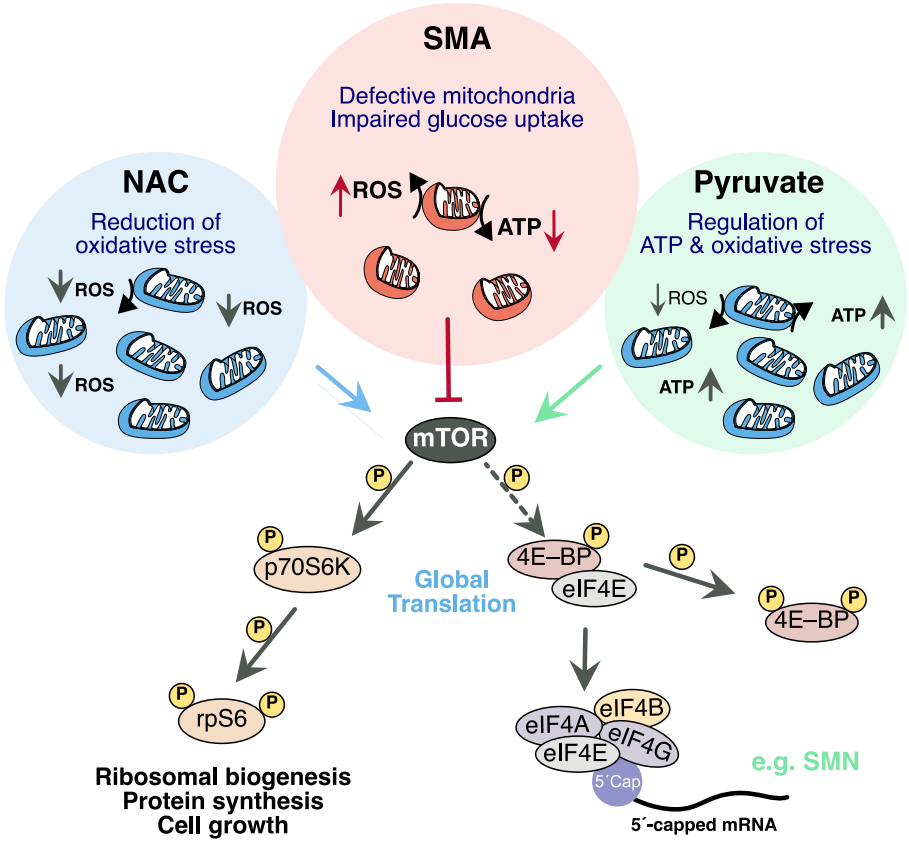

Figure 64: Representation of impairments, targeted by NAC and pyruvate in SMA.
Energy homeostasis is disturbed in SMA MNs due to defective mitochondria and reduced glucose uptake. Additionally, complex I defects result in increased ROS levels. Increased ROS leads to decreased translation initiation. NAC reduces ROS and increases global protein synthesis in SMA MNs via mTOR and translation initiation. Pyruvate reduces ROS and increases ATP. Furthermore, pyruvate increases translation initiation of a subset of proteins in SMA MNs, including SMN via mTOR.

6 MATERIAL AND METHODS

6.1 Material

6.1.1 Equipment

Instrument	Notation	Manufacturer
Cell incubator	Heracell™ 150	Heraeus
	Kelvitron T	Heraeus
Cell culture hood	Herasafe™ KS12	Heraeus
Centrifuges	AllegraX22-R	Beckmann Coulter
	Avanti J-20XPI	Beckmann Coulter
	5415R	Eppendorf
Electrophoresis chambers		
Agarose gels	MGV-620T	C.B.S & Scientific
	SGE-020-02	C.B.S & Scientific
SDS-PAGE gels	Mini-Protean 3 cell	Bio-Rad
	Mini-Trans-Blot cell	Bio-Rad
Filters	FP 30/0.2 CA-S	Whatman
Forceps	BD047R	Aesculap
	FM002R	Aesculap
	Dumont #5, #55	Fine Science Tools
Heating block	HTMR132	HLC Bio Tech
Horizontal shaker	3011, 3015	GFL
Imaging system	ChemiDoc XRS	Biorad
	ChemiDoc MP	Biorad
Luminometer	GloMax 96	Promega
Magnetic stirrer	MR 3001	Heidolph
Microplate Reader	Safire2	Tecan
Microscopes	AxioImager.M2	Zeiss
	Apotome	Zeiss
Neubauer chamber	1100000	LO Laboroptik Ltd
pH meter	inoLab pH Level	WTW
Photometer	NanoDrop 1000	Peqlab
Pipettes	0.1 µl – 5000 µl	Eppendorf
	Research Plus (12/200 µl)	Eppendorf
	Pipetboy acu	Integra Biosciences
	accu-jet pro	Brand
Power Supplies	PowerPac™ Basic/HC	Bio-Rad
Real-time PCR Thermocylcer	7500 RealTimePCR System	Applied Biosciences
Roller mixer	SRT9	Stuart
	RM5	Hartenstein

Instrument	Notation	Manufacturer
Scale	EW 6000-1M	Beckman Coulter
	Analytical balance (fine)	Sartorius
	FD012R	Fine Science Tools
Scissors	BC 321 R	Aesculap
	BC 341 R	Aesculap
SDS-PAGE + Western blot		
Blotting paper	550 g/m^2	Hartenstein
Glasplates	0.75 mm	Bio-Rad
Membranes	PVDF	Millipore
	Nitrocellulose	GE Healthcare
Spectrophotometer	BioPhotometer 6131	Eppendorf
SpeedVac	Concentrator 5301	Eppendorf
Thermocyclers	DNAengine Dyad/Tetrad	MJ Research
	C1000 Touch	Bio-Rad
	S1000	Bio-Rad
Vacuum pump	Vacusip	Integra Biosciences
Vortex mixer	444-1372	VWR
Water bath	1083	GFL

6.1.2 Chemicals

Chemical	Manufacturer
2-Propanol ($\geq$ 99.5%)	Applichem
Agarose	Sigma-Aldrich
β-Mercaptoethanol (99%, p.a.)	AppliChem
Bovine serum albumin (BSA)	Sigma-Aldrich
Bradford - Solution for protein determination	AppliChem
Bromphenol blue	Sigma-Aldrich
Dimethyl sulfoxide (DMSO)	Sigma-Aldrich
Ethanol ($\geq$ 99.5%, p.a.)	Sigma-Aldrich
Ethidium bromide (1% in H_2O)	AppliChem
Ethylenediaminetetratic acid solution 0.5 M (EDTA)	Thermo Fisher Scientific
Formaldehyde (37%)	AppliChem
GelRed® Nucleic Acid Gel Stain	Biotium
Glycerol (86%, p.a.)	AppliChem
Glycine	AppliChem
Hydrochloric acid (37%)	Sigma-Aldrich
Hydroxymethylaminoethane	AppliChem
Methanol ($\geq$ 99.9%, p.a.)	AppliChem
Milk powder (low fat)	AppliChem
Mowiol	AppliChem

Chemical	Manufacturer
Phenol Red	Sigma-Aldrich
Phosphate buffered saline (PBS)	Thermo Fisher Scientific
Ponceau S	Sigma-Aldrich
Silicone elastomer, Sylgard 184	Dowsil
Sodium acetate	AppliChem
Sodium carbonate	AppliChem
Sodium chloride	AppliChem
Sodium dodecyl sulfate (SDS)	AppliChem
Sucrose	AppliChem
TBE buffer	AppliChem
Tetramethylenediamine (TEMED)	AppliChem
Tris (hydroxylmethyl)-aminomethane (TRIS)	AppliChem
Triton X-100	AppliChem
Trizma base	AppliChem
Tween-20	AppliChem
Water (HPLC grade)	AppliChem

6.1.3 Reagents

6.1.3.1 Reagents for molecular biology

Reagent	Manufacturer
Commonly used	
Nuclease-free water	Thermo Fisher Scientific
PBS	Roche
Dithiothreitol (DTT)	Sigma
Nucleic acid work	
6 x DNA loading dye	Thermo Fisher Scientific
DNA ladder (100 bp/ 1 kb)	Thermo Fisher Scientific
Protein work	
Acetonitrile	Biosolve
Acrylamide-bisacrylamide Mix (40%) (39:1)	AppliChem
Ammonium persulfate (APS) (AquaPlus Mix)	AppliChem
Azidohomoalanine (AHA)	Thermo Fisher Scientific
Bradford- solution for protein determination	AppliChem
Complete mini protease inhibitors	Roche
Formic acid	Biosolve
Page Ruler^{TM} Plus Prestained Protein Ladder	Thermo Fisher Scientific
Pierce^{TM} Protease and phosphatase inhibitor mini tablets	Thermo Fisher Scientific
Ponceau S	Sigma-Aldrich

Reagent	Manufacturer
Restore Western Blot Stripping Buffer	Sigma-Aldrich
RIPA buffer	Sigma-Aldrich
Super Signal West Pico ECL Substrate	Thermo Fisher Scientific

6.1.3.2 Cell culture reagents and media

All cell culture media were stored at 4 °C. All cell culture reagents were stored in aliquots at -20 °C until use. Reagents in use were stored at 4 °C.

Reagent	Manufacturer
Amphothericin B	Thermo Fisher Scientific
B-27 Supplement (#17540)	Thermo Fisher Scientific
Brain derived neurotrophic factor (BDNF)	Peprotech
Cilliary neurotrophic factor (CNTF)	Peprotech
Cytosine arabinoside (AraC)	Sigma-Aldrich
DMEM (+ 4.5 g/L D-Glucose, + L-Glutamine, + Pyruvate)	Thermo Fisher Scientific
DMSO (#D12345)	Thermo Fisher Scientific
DNase I (2000 U/ml)	New England Biolabs
DPBS (#14190)	Thermo Fisher Scientic
Fetal calf serum (FCS)	Biochrom AG
Glial cell-line derived neurotrophic factor (GDNF)	Peprotech
Laminin, mouse EHS sarcoma	Sigma-Aldrich
L-Glutamine	Thermo Fisher Scientific
NeuroBasal™ Medium (#21103)	Thermo Fisher Scientific
Penicillin/Streptomycin (Pen/Strep)	Thermo Fisher Scientific
Poly-D-Lysine	Sigma-Aldrich
Puromycin dihydrochloride	Thermo Fisher Scientific
Retinoic acid	Sigma-Aldrich

6.1.4 Enzymes

Enzyme	Manufacturer
LysC Protease	Wako Pure Chemicals Industries
MultiScribe™ Reverse Transcriptase, 50 U/µL	Thermo Fisher Scientific
OneTaq® Quick-Load 2X Master Mix (#M0486)	New England Biolabs
Proteinase K	AppliChem
RNase A	Sigma-Aldrich
Trypsin(TRL3) (for MN Isolation)	Worthington

Enzyme	Manufacturer
Trypsin (for proteomics)	Promega
Trypsin-EDTA	Thermo Fisher Scientific

6.1.5 Drugs

All drugs supplied to motor neuron cultures or NSC-34 cells were diluted in growth medium. Exact concentrations are given in each figure legend.

Drug	Working concentration	Solvent	Manufacturer/ #catalog
Anisomycin	40 µM/ 50 µM	Water	Sigma; A9789
Harringtonine	2 mg/ml	DMSO	Abcam; ab141941
Menadione	0.1 µM-100 µM	DMSO	Sigma; M5625
N-Acetyl-L-cysteine (NAC)	1 µM-1000 µM	Water	Sigma; A9165
Puromycin dihydrochloride	1 µM/ 10 µg/ml	Water	Gibco; A1113803
Sodium pyruvate	1 mM – 50 mM	Water	Sigma; P5280
Sodium lactate	1 mM – 50 mM	Water	Sigma; L7022
WYE-687 dihydrochloride	100 nM	Water	Tocris; #4282

6.1.6 Primary antibodies and staining reagents

All primary and secondary antibodies used for immunofluorescence were incubated in a humidified chamber at 4 °C overnight (ON) or at room temperature (RT) for 3 h.

Primary antibodies	Host species; dilution	Manufacturer; #catalog	RRID
anti-4E-BP1	rabbit; WB 1:1000	Cell Signaling; #9644	AB_2097841
anti-p4E-BP1 (Thr37/46)	rabbit; WB 1:1000	Cell Signaling; #2855	AB_560835
anti-ACTB, HRP-conjugated	mouse; WB 1:10000	Santa Cruz; sc-47778 HRP	AB_2714189
anti-ChAT	rabbit; IF 1:100	Thermo Scientific; PA5-26597	AB_2544097
anti-Puromycin	mouse; WB 1:1500 IF 1:150	Merck; MABE343	AB_2566826
anti-S6	mouse; WB 1:1000	Cell Signaling; #2317	AB_2238583
anti-pS6	rabbit; WB 1:1000	Cell Signaling; #2211	AB_331679

Primary antibodies	Host species; dilution	Manufacturer; #catalog	RRID
anti-S6K	rabbit; WB 1:2000	Cell Signaling; #2708	AB_390722
anti-pS6K	rabbit; WB 1:750	Cell Signaling; #9234	AB_2269803
anti-SMN	mouse; WB 1:3000	BD Biosciences; 610646	AB_397973
anti-Tau	mouse; IF 1:800	Santa Cruz; sc-390476	
anti-Tau	chicken; IF 1:100	Abcam; ab75714	AB_1310734
anti-Tom20	rabbit; IF 1:500	Santa Cruz; sc-11415	AB_2207533

6.1.7 Secondary antibodies

Dilutions are indicated for Western blot (WB) or immunofluorescence (IF) application.

All secondary antibodies used for WB or IF were incubated at 4 °C ON or at RT for 3 h, respectively. Coverslips for IF were incubated in a humidified chamber as described in 6.2.13.

Secondary antibodies	Host species/ dilution	Manufacturer/ #catalog	RRID
anti-mouse IgG, HRP-conjugated	goat; WB 1:3000	Dianova; 115-035-146	AB_2307392
anti-rabbit IgG, HRP-conjugated	goat; WB 1:2000	Cell Signaling; #7074	AB_2099233
anti-chicken IgG, AlexaFluor647-conjugated	goat; IF 1:350	Thermo Scientific; A21449	AB_1500594
anti-mouse IgG, AlexaFluor488-conjugated	goat; IF 1:350	Thermo Scientific; A11001	AB_2534069
anti-rabbit IgG, AlexaFluor488-conjugated	donkey; IF 1:350	Thermo Scientific; A21206	AB_2535792
anti-rabbit IgG, AlexaFluor568-conjugated	donkey; IF 1:350	Thermo Scientific; A10042	AB_2534017

6.1.8 Primers

Primers used for genotyping and qRT-PCR were purchased from Metabion. Lyophilized primers were diluted in nuclease-free water to obtain a 100 pmol/µl stock solution and a 10 pmol/µl working solution.

Name	Sequence (5‘ -3‘)	Amplicon length (bp)	Annealing temp. (°C)
Genotyping			
mSmn KO fw1	ATA ACA CCA CCA CTC TTA CTC	950	59
mSmn KO fw2	GTA GCC GTG ATG CCA TTG TCA	1050	59
mSmn KO rev	AGC CTG AAG AAC GAG ATC AGC		59
qRT-PCR			
Actb fw	AGC CAT GTA CGT AGC CAT CC	201	60
Actb rev	CTC TCA GCT GTG GTG GTG AA		60
Smn fw	ACT CCT CCA GAT CGC TCA GA	227	58
Smn rev	AGG GGG TGG CGG GAT TAT TG		58
SMN fw	ACT CCT CCA GAT CGC TCA GA	227	58
SMN rev	AGG GGG TGG AGG AAT TAT G		58

fw = forward primer; rev = reverse primer.

6.1.9 Mouse & cell lines

- **Control mice:** Inbreed WT FVBN mice were obtained from the CMMC mouse facility (University of Cologne).
- **SMA mice:** SMA mice are generated based on the Taiwanese SMA mouse model (FVB.Cg-*Smn1*^{tm1Hung}Tg(SMN2)2Hung/J, reference number 005058).

  The breeding scheme is described in 6.2.2.
- **NSC-34 cell line:** The immortalized hybrid cell line NSC-34 was produced by fusion of mouse neuroblastoma cells with motor neuron enriched, embryonic cells from mouse spinal cords (Cashman et al., 1992). Therefore, NSC-34 cells display characteristics of motor neurons, including generation of action potentials, acetylcholine synthesis, storage and release (Cashman et al., 1992).

  In this study, NSC-34 cells were used to optimize experimental setups. Conclusions were drawn from experiments with primary motor neurons derived from WT or SMA mice.

6.1.10 Solutions and media

6.1.10.1 Routinely used solutions

All chemicals used are listed in 6.1.2. If not mentioned otherwise, all solutions were stored at RT.

Name	Composition
Genotyping	

Name	Composition
Lysis buffer (500 ml)	50 ml Tris/HCl (1 M, pH 8.5); 5 ml EDTA (0.5 M); 5 ml SDS (20%); 5 ml NaCl (5 M); ddH_2O to 500 ml; add 7 µl proteinase K per 493 µl buffer before use
Resuspension buffer (50 ml)	0.5 ml Tris (1 M, pH 7.4); 0.01 ml EDTA (0.5 M); ddH_2O to 50 ml; 0.06 µl RNase per 50 µl buffer before use
IF	
Blocking solution (BSA)	3% (w/v) BSA in 1x PBS-T
Mowiol	Mix 6 g glycerin with 2.4 g mowiol 4-88 for 1 h at RT; add 6 ml ddH_2O and stir for 1 h; add 12 ml Tris/HCl (0.2 M, pH 8.5) and stir for 2 h at 50 °C
Paraformaldehyde	4% (w/v) paraformaldehyde dissolved in 1x PBS (pH 7.4) at 60 °C; raise pH with 1 M NaOH until solution clears; cool the solution and filter
Protein work	
Ammonium persulfate	1% (w/v) in ddH_2O, aliquot and stored at -20 °C
Blocking solution (BSA)	5% (w/v) BSA in TBS-T, store at 4 °C
Blocking solution (milk)	5% (w/v) non-fat milk powder in TBS-T, store at 4 °C
Laemmli buffer (3x)	2.4 ml Tris (1 M, pH 6.8); 3 ml SDS (20%); 3 ml glycerol; 1.6 ml β-mercaptoethanol; 6 mg bromophenol blue, store at 4 °C
Ponceau staining solution	1% (w/v) Ponceau S; 2% (v/v) ml acetic acid in ddH_2O
Protease and phosphatase inhibitors	1 tablet in 1 ml ddH_2O (10x)
Resolving gel (12%, 10 ml)	4.2 ml ddH_2O; 3 ml 40% (39:1) Acrylamide/ bisacrylamide mix; 2.6 ml Tris (1.5 M, pH 8.8); 0.1 ml SDS (10%); 0.1 ml APS (10%); 40 µl TEMED
SDS Electrophoresis buffer (10x, 1 L)	30.29 g Tris (Base); 144,13 g Glycin; 10 g SDS; ddH_2O to 1 L
Stacking gel (5%, 2 ml)	1.45 ml ddH_2O; 0.25 ml 40% (39:1) Acrylamide/ bisacrylamide mix; 0.26 ml Tris (1 M, pH 6.8); 20 µl SDS (10%); 20 µl APS (10%); 2 µl TEMED
TBS-T (1 L)	2.42 g Tris (20 mM); 8 g NaCl (137 mM); 5 ml Tween 20 (0.5%); H_2O; pH 7.56 (HCl)
Transfer buffer (2 L)	4.84 g Tris (Base); 22.52 g Glycin; 400 ml methanol; ddH_2O to 2 L
Tris-HCl (1 M, pH 6.8, 200 ml)	12.22 g Tris-HCl; ddH_2O to 200 ml; adjust pH to 6.8 (HCl)

Name	Composition
Tris-HCl (1.5 M, pH 8.8, 200 ml)	36.34 g Tris-HCl; ddH_2O to 200 ml; adjust pH to 8.8 (HCl)

6.1.10.2 Cell culture media

All cell culture media were prepared under sterile conditions and stored at 4 °C. Growth factors and antibiotics were stored at -20 °C.

Name	Composition
MN growth medium (500 ml)	500 ml Neurobasal™ medium; 10 ml B-27 supplement (50x); 5 ml L-Glutamine; 1% (v/v) ml Pen/Strep (10 U/ml); 250 µg/ml Amphotericin B; sterile filtered before use, 10 ng/ml BDNF; 10 ng/ml CNTF; 10 ng/ml GDNF added after filtration
MN plating medium (50 ml)	45 ml DMEM; 2.5 ml FCS; 1.5 ml Glucose (20%) (w/v); 1% (v/v) Pen/Strep; 250 µg/ml Amphotericin B; sterile filtered before use
NSC-34 freezing medium	60% NSC-34 growth medium; 20% FCS; 10% DMSO
NSC-34 growth medium (500 ml)	500 ml DMEM; 50 ml FCS; 1% (v/v) Pen/Strep (10 U/ml); 250 µg/ml Amphotericin B

6.1.11 Kits

All kits were stored and used according to manufacturer's instructions. Adjustments in volume or incubation times can be found in the appropriate section in 6.2.

Name	Manufacturer
Amicon® Ultra-0.5 Centrifugal Filter (#UFC5010)	Merck Millipore
ATP Assay Kit (#MAK190)	Sigma-Aldrich
ATP Determination Kit (#A22066)	Thermo Fischer Scientific
Complex I Enzyme Activity Microplate Assay Kit (#ab109721)	Abcam
Glucose Uptake-Glo™ Assay (#J1341)	Promega
High Capacity cDNA Reverse Transcription Kit (#4368814)	Thermo Fisher Scientific
KAPA Mouse Genotyping Kit (#KK7301)	Kapa Biosystems
mirVana™ miRNA Isolation Kit (#AM1560)	Thermo Fisher Scientific
Mitochondria Isolation Kit for Cultured Cells (#ab11070)	Abcam
Pierce BCA Protein Assay (#23225)	Thermo Fisher Scientific
Protein Carbonylation Assay Kit (#ab178020)	Abcam
Pyruvate Assay Kit (#MAK071)	Sigma-Aldrich
qPCRBIO SyGreen Mix Lo-ROX (#PB20.11)	PCR Biosystems

6.1.12 Software packages

Software	Application	Distributor
Andromeda	Proteomics analysis (CECAD)	MaxQuant
Findings 2	Electronic lab notebook	Findings Software SAS
Fiji/ImageJ	Image analysis	NIH, Open Source
ImageLab 6.0	WB analysis	BioRad
Mendeley	Reference manager	Mendeley Ltd.
Perseus	Proteomics analysis (CECAD)	MaxQuant
PyRAT	Laboratory animal management (CMMC)	Scionics
Quantity One	Image acquisition and analysis	Bio-Rad
RStudio	Statistics IDE for R	RStudio, Inc.
Spectronaut 13	Proteomics analysis (CECAD)	Biognosys
TeXShop	Text processing IDE for TeX	Open Source GPLv2
Vectornator	Vector graphics software	Linearity GmbH
ZEN	Image acquisition and analysis	Zeiss

6.1.13 Internet databases

Software	Website
Database for Annotation, Visualization and Integrated Discovery 6.7 (DAVID)	https://david-d.ncifcrf.gov
Ensembl	http://www.ensembl.org/index.html
GeneCards	http://www.genecards.com
KEGG: Kyoto Encyclopedia of Genes and Genomes	http://www.genome.jp/kegg
NCBI	http://www.ncbi.nlm.nih.gov
PRIDE PRoteomics IDEntification Database	https://www.ebi.ac.uk/pride
UniProt	http://www.uniprot.org

6.2 Methods

6.2.1 Working with laboratory mice

All experimental animals were bred and housed in accordance with the institutional animal care guidelines and the German animal welfare laws in the mouse facility of the Center for Molecular Medicine Cologne (CMMC, University of Cologne). Experimental animal protocols were approved by the "Landesamt für Natur, Umwelt und Verbraucherschutz" of North Rhine-Westfalia" (LANUV, NRW). Breedings of the mouse lines are approved under the reference number 84-02.04.2015.A378, and experimental use of animals was approved under the reference numbers UniKoeln_Anziege§4.16.020 and UniKoeln_Anziege§4.17.025. For all experiments, FVB/N wild type mice (Jackson) were used as controls.

6.2.2 SMA mouse model

Numerous mouse models have been developed to mimic the SMA phenotype in mice and understand the basic SMA pathology. Since mice do not have a second *Smn* gene in their genome, homozygous ubiquitous knockout of the murine *Smn* is embryonically lethal (Schrank et al., 1997). Among the numerous SMA mouse models, we used the 'Taiwanese' SMA mouse model on an FVB background. This model is homozygous for the Tg(SMN2)2Hung human *SMN2* transgene on a homozygous murine $Smn1^{tm1Hung}$ knock-out background (Hsieh-Li et al., 2000). The knock-out of endogenous *Smn* was accomplished by introduction of an hypoxanthine phosphoribosyltransferase (HPRT) cassette. The SMA model was established by a breeding scheme previously described (Riessland et al., 2010). Here, homozygous Taiwanese $Smn^{ko/ko}$; $SMN2^{tg/tg}$ mice carrying 4 copies of the transgene with heterozygous $Smn^{ko/wt}$ mice, resulting in 50% SMA mice, which display a Type I SMA-like phenotype and die at ~10 days of age ($Smn^{ko/ko}$; $SMN2^{tg/0}$) and 50% phenotypically normal littermates ($Smn^{ko/wt}$; $SMN2^{tg/0}$) (Riessland et al., 2010). The initial "Hung" or "Taiwanese" $Smn^{ko/ko}$; $SMN2^{tg/tg}$ mice were purchased from Jackson Laboratory (FVB.Cg-$Smn1^{tm1Hung}$ Tg(SMN2)2Hung/J, reference number 005058).

6.2.3 Cell culture work

Handling of primary cells and cell lines was done under sterile conditions. The equipment was sterilized with ethanol, and cells were handled in a laminar flow hood to avoid contamination. All cells were cultured in sterile incubators at 37 °C and with 5% CO_2. Time outside of the incubator was kept to a minimum to reduce stress on the cells. All cell media were filtered before use and supplied with antibiotics and anti-fungal agents if not otherwise stated. Cell culture plates and coverslips were coated with poly-D-lysine (PDL) to increase the attachment of primary motor neurons or NSC-34 cells. Briefly, the surface of the plates and coverslips were covered with 20 µg/ml PDL in DPBS and incubated for 1 h at RT. Afterward, plates were thoroughly rinsed with DPBS three times to remove residual PDL.

6.2.4 Counting cells

Cells were counted with a Neubauer counting chamber. Primary motor neurons were counted after trituration, and NSC-34 cells were counted after being detached using Trypsin/ EDTA and resuspended in medium. After that, a 1:10 dilution of the cell suspension was applied to the counting chamber. Cells in all four quadrants of the counting chamber were assessed to increase the precision of the counting. In attempt to visualize individual motor neurons during imaging analyses, 15,000 cells/cm^2 were plated on glass coverslips, and for all other analyses, 120,000 cells/cm^2 were plated in 12- well plates or 6-well plates containing 1 ml and 2 ml plating medium, respectively. NSC-34 cells were seeded at a density of 20,000 cells/cm^2 in normal growth medium, described in 6.2.5.

6.2.5 Cultivation of NSC-34 cells

For optimizing experimental setups, including time and dose optimization, motor neuron-like NSC-34 cells (Eggett et al., 2008) were used. Cells were cultured in Dulbecco's Modified Eagle's Medium (DMEM) with 10% fetal calf serum, 1% penicillin/streptomycin, and amphotericin B in cell culture flasks. At 80% confluency, cultures were rinsed with DPBS, detached with Trypsin/EDTA for 3 min at 37 °C, and diluted into new flasks. For biochemical assays, 20,000 cells/cm^2 were plated in PDL coated 12-well plates. Cells were differentiated for 3 days by adding 50 µM retinoic acid into the medium the day after plating.

6.2.5.1 Cryopreservation of NSC-34 cells

For long-term storage of NSC-34 cells, 80% confluent flasks were enzymatically dissociated with trypsin as noted in 6.2.5 and isolated by centrifugation at 200 x g for 10 min. The pellet was resuspended in freezing medium containing 60% growth medium, 30% FCS and 10% DMSO. A cryo-container was used to slow the freezing of the cells to -80 °C.

6.2.5.2 Isolation of murine spinal cords

Primary motor neurons were isolated from *Smn*$^{ko/ko}$; SMN2$^{tg/0}$ and WT embryos. Pregnant mice were euthanized by CO_2 at 13.5 days post-fertilization. The day of fertilization was noted by plug check. The embryos were released from the uterus and placed immediately in ice-cold PBS. Tail snips from SMA embryos were used for genotyping described in 6.2.10.1 using the KAPA mouse genotyping kit before further processing. Embryos were fixed in prone position with minutien pins on a Sylgard-coated petri dish filled with DPBS. Under the dissection microscope, the skin was removed, and the spinal meninges were opened inferior from the prebrachial region to the caudal region of the spinal cord using fine forceps. The spinal cord was separated from the spinal meninges prebrachial to extract the pure spinal cord by pulling it out using forceps. Any remaining pieces of meninges or dorsal root ganglion were carefully removed after isolation. Isolated spinal cords were transferred immediately into a reaction tube containing 500 µl DPBS and stored on ice. All subsequent steps of primary motor neuron isolation were performed under sterile conditions under a laminar flow hood.

6.2.6 Culture of primary motor neurons

All reagents and media were filtered with a 0.2 µm filter before use. Isolated spinal cords were dissociated (described in 6.2.5.2) with 1% trypsin in DPBS for 2 min. Afterward, spinal cords were triturated in plating medium (noted in 6.1.10) with DNase I (100U/ml). The single-cell suspension was collected after bigger pieces of debris have settled. Motor neurons of the same litter were merged and considered as one biological replicate to reduce technical variability. For imaging analyses, 15,000 cells/cm^2 were plated on glass coverslips coated with 20 µg/ml poly-D-lysine (PDL, Sigma) and for protein analyses or RNA extraction, 120,000 cells/cm^2 were plated on PDL coated cell culture plates with neuronal plating medium. Neuronal plating medium was replaced the following day by motor neuron maintenance medium (noted in 6.1.10)

with additional growth factors: brain-derived neurotrophic factor (BDNF, 10 ng/ml), ciliary neurotrophic factor (CNTF, 10 ng/ml), and glia cell line-derived neurotrophic factor (GDNF, 10 ng/ml). Every third day half of the medium was exchanged, and cytosine arabinoside (AraC) was added after 3 days in culture to a final concentration of 1 µM to inhibit glia cell growth. Cells were cultured for 10DIV at 37 °C in a humidified incubator with 5% CO_2.

6.2.7 Surface SEnsing of Translation assay (SUnSET)

Protein synthesis efficiency was measured by SUnSET assay (Schmidt et al., 2009). Briefly, the Tyrosyl-tRNA analog puromycin is incorporated during protein elongation and labels newly synthesized proteins. Detection of puromycin labeled proteins was achieved by western blotting or immunostaining using an anti-puromycin antibody. For immunofluorescence assay, neurites were selected with a segmented line, straightened, and divided into 20 µm bins using the concentric circles plugin. Mean puromycin intensities were quantified using plot profiles. SUnSET assay was performed on primary motor neurons at 10DIV and on three days differentiated NSC-34 cells. Cells were cultured at a density of 120,000 cells/cm^2 on PDL coated cell culture plates. ROS modifying drugs were treated for 30 min before 30 min puromycin labeling (1 µM). As a negative control, protein synthesis was inhibited by 50 µM anisomycin for 30 min before puromycin labeling (1 µM).

6.2.8 SUnSET-based Ribosome Speed of Elongation assay (SunRiSE)

To measure protein elongation speed, SunRiSE assay was used (Argüello et al., 2018). In contrast to SUnSET assay, initiation of mRNA translation was blocked by 2 µg/ml harringtonine at different time points, prior incubation with 10 µg/ml (16.7 µM) puromycin for 10 min. Puromycin labeled peptides were detected by western blotting using an anti-puromycin specific antibody.

6.2.9 Drug treatment

For drug treatment, half of the medium was removed, and drugs were diluted to twice the working concentration in freshly prepared maintenance medium. After the medium was supplied with the drug, the conditioned medium was added to the old maintenance medium on the cells in a 1:1 ratio. Cells were incubated after drug treatment for given times in a humidified chamber with 5% CO_2 at 37 °C. The supplied substances to motor neurons and NSC-34 cells are as follows and listed in 6.1.5 with given concentration in each figure legend: The cell culture supplements sodium pyruvate and sodium lactate, the antioxidant NAC, the ROS inducer menadione, the protein synthesis inhibitor anisomycin and the water-soluble mTOR inhibitor WYE-687 dihydrochloride.

6.2.10 Nucleic acid methods

6.2.10.1 Isolation of DNA

Mouse lines were routinely genotyped to ensure the correctness of stock animals for further breeding. Tail tips or ear biopsies after tagging of 10 to 14 days old stock animals were provided by the animal facility. Samples were lysed in 500 µl tissue lysis buffer, containing fresh 200 µg/ml proteinase K at 55 °C ON or at least for 4 h shaking at 1500 rpm. Samples were centrifuged at maximum speed (16,000 x g) for 5 min to remove insoluble tissue. Without disturbing the settled debris, the supernatant was transferred into new reaction tubes containing 500 µl isopropanol. By shortly mixing the samples, DNA is precipitated and isolated by centrifugation for 5 min at maximum speed. To remove salts in the samples, 300 µl of 70% ethanol was added, and samples were centrifuged at maximum speed for 5 min. As remaining ethanol could inhibit the subsequent PCR, samples were dried by centrifugation in a vacuum concentrator for 10 min. Further on, genomic DNA was dissolved by 40 µl resuspension buffer supplied with RNase.

In addition to routinely genotyped stock animals, embryos used for cell culture experiments were genotyped due to the breeding scheme of SMA, described in 6.2.2. After retrieving the embryos from the pregnant female mouse described in 6.2.5.2, ~1 mm of the tail was collected from each embryo. In order to mix primary motor neurons with the same genotype before plating, each embryo was genotyped with the KAPA Mouse Genotyping Kit. This allows for rapid lysis of the tissue and fast processing of DNA isolation. We followed the manufacturer's protocol. In brief, tail tips were lysed in a heating block at 75 °C for 10 min with subsequent inactivation of the enzyme at 95 °C for 5 min. Before use in PCR analysis, the DNA was diluted 1:10.

6.2.10.2 Isolation of RNA

To prevent degradation of RNA, all procedures were performed on ice and under RNase-free conditions. Total RNA was extracted from cells using the mirVana™ miRNA Isolation Kit, according to the manufacturer's instructions to measure mRNA expression levels. In brief, the cell culture medium was removed, and cells were rinsed with DPBS. Lysis of the cells was carried out by adding Lysis/Binding buffer of the *mirVana™* miRNA Isolation Kit directly on the cells and thoroughly pipetting up and down. Samples were either frozen at -20 °C or directly used for further processing. Cellular components and most of the DNA was removed by acid-phenol: chloroform. In the final purification step, total RNA was isolated on glass-fiber filters and eluted in RNase-free water. For long-term storage, samples were stored at -80 °C.

6.2.10.3 Quantification of RNA

The concentration and purity of RNA were determined with the NanoDrop ND-1000 spectrometer. The absorbance at 260nm was used to quantify the RNA, and the ratio of A_{260}/A_{280} was used to determine the purity. For high purity and the absence of contaminants, a value close to 2 was aimed.

6.2.10.4 Polymerase chain reaction (PCR)

The polymerase chain reaction (PCR) technique was used to identify genotypes of mice by amplifying genomic DNA isolated from mouse tails. The PCR technique enables the amplification of a distinct DNA sequence using gene-specific primers flanking the region of interest (Mullis, 1990). The temperature for the primer annealing step is experimentally optimized for each primer pair used, and a temperature of 60 °C was used for genotyping and qRT-PCR. Lyophilized primers used in the PCR were diluted in nuclease-free water to obtain a stock solution of 100 pmol/µl and a final working solution of 10 pmol/µl. In the last step, the elongation, a thermostable DNA-polymerase, synthesizes the new DNA strand. All three steps are repeated 35 times for genotyping and 40 times during qRT-PCR. For routine genotyping, the standard composition of PCR reagents listed in Table 9 were used. To speed up genotyping during MN culture preparation, the rapid PCR mix components listed in Table 9 were used. To test the primers' specificity during qRT-PCR, amplification products of the qRT-PCR were also used in PCR with the standard reagent composition.

Table 9: Components and volumes for genotyping PCR reactions.

	Rapid genotyping PCR	**Standard genotyping PCR**
Components	**Volume [µl]**	**Volume [µl]**
PCR buffer $MgCl_2$ DNA polymerase dNTPs	12.5 (2X KAPA2G Fast (HotStart) Genotyping Mix with dye)	12 (OneTaq Quick-Load Master mix)
ddH_2O	7.5	5
mSmn KO rv	1.5	3
mSmn KO fw-1	1.25	2
mSmn KO fw-2	1.25	2
Additional $MgCl_2$	0.5	-
Template DNA	0.5	1

Table 10: Thermocycler *Smn* PCR program.

Step	**Duration**	**Temperature [°C]**
1. Initial denaturation	5 min	95
2. Denaturation	30 sec	95
3. Primer annealing	30 sec	60
4. Elongation	1 min per 1 kb	72
	Repeat steps 2-4 for 35x	
5. Final elongation	10 min	72
Cooling	∞	4

6.2.10.5 cDNA synthesis

To compare expression levels of specific mRNAs by qRT-PCR analysis, RNA templates were reversely transcribed into complementary DNA (cDNA) using the High-Capacity cDNA Reverse Transcription Kit. RNA was isolated from motor neuron cell cultures as described in 6.2.10.2. In each reaction, 100 ng RNA was transcribed using random primers, and the manufacturer's protocol was followed. The full composition of the reaction is listed in Table 11 and the conditions of the PCR in the thermocycler are noted in Table 12.

Table 11: Components for cDNA synthesis

Reagent	**Amount**
10x RT Buffer	2 µl
25x dNTP Mix (100mM)	0.8 µl
10x RT Random Primers	2 µl
MultiScribe^{TM} Reverse Transcriptase (50 U/µl)	1µl
RNase Inhibitor	0.2 µl
Total RNA	100 ng
Nuclease-free H_2O to a final volume of 20 µl	

Table 12: Conditions for cDNA synthesis PCR

	Step 1	Step 2	Step 3	Step 4
Temperature [°C]	25	37	85	4
Time [min]	10	120	5	∞

6.2.10.6 Quantitative real time PCR

To measure the number of transcripts produced by a given gene, mRNA levels were quantified by qRT-PCR using gene-specific primers. Similar to the PCR reaction described in 6.2.10.4, gene-specific primers are annealed to the template DNA and multiplied by a thermostable DNA polymerase. In this case, cDNA produced from total RNA serves as a template for the reaction after 1:2 dilution. The formation of dsDNA allows the intercalating dye SYBR® green to bind nonspecifically into dsDNA products. SYBR® green binds with lower affinity and a lower fluorescence signal to ssDNA or RNA than to dsDNA and is, therefore, a suitable reporter dye in qRT-PCR. The increase of amplified products can be monitored in real-time due to a fluorescent dye's intercalation. Here, PowerSYBR® Green PCR Master Mix and 1 µM of gene-specific forward and reverse primers were used (Table 6.1.8). The reaction's full composition can be found in Table 13. The exponential increase of fluorescence signal was measured using the 7500 Real-Time PCR System. The threshold of the cycle (Ct) value, which displays the cycle number at which the fluorescence signal exceeds the background signal by exponential amplification, was used to compare different samples. Samples were normalized to

a housekeeping gene product. Relative quantification levels were obtained using an internal control, and relative changes were analyzed using the 2(-Delta Delta C(T)) method (Livak & Schmittgen, 2001). The primers' specificity was confirmed by a single peak of a dissociation curve, agarose gel electrophoresis (6.2.10.7) and Sanger sequencing.

Table 13: Components for qRT-PCR

Reagent	**Amount**
2x qPCRBIO SyGreen Mix	10 µl
1 µM forward primer	2 µl
1 µM reverse primer	2 µl
cDNA	2 µl
Nuclease-free H_2O to a final volume of 20 µl	

Table 14: Conditions for qRT-PCR

Step	**Duration**	**Temperature [°C]**
1. Hold	2 min	50
2. Initial denaturation	10 min	95
3. Denaturation	15 sec	95
4. Primer annealing	30 sec	60
5. Elongation	40 sec	72
Repeat steps 3-5 for 40x		
6. Cooling	∞	4

6.2.10.7 Agarose gel electrophoresis

Agarose gel electrophoresis was used to confirm the primers' specificity used in qRT-PCR described in 6.2.10.6, but also to verify the genotype after DNA isolation from mouse tails described in 6.2.10.1. Based on sizes separation in an 1.5% agarose gel in 1x TBE buffer due to the electric force between DNA and an electric field, a single band with the correct size of the qRT-PCR product was determined. Differences in genotypes were determined using sequence-specific primers, leading to either a single band or two bands. Single band represents the homozygously interrupted murine *Smn* by the HPRT cassette while two bands represent the heterozygous genotype containing one interrupted murine *Smn* allele and one intact *Smn* allele. PCR products were separated for 30-40 min at 100 V and visualized using the ChemiDoc XRS Imaging System.

6.2.11 Proteinbiochemistry methods

To avoid degradation or aggregation of isolated proteins, all subsequent steps were handled on ice or at 4 °C. For long term storage, proteins were kept at -20 °C, and repetitive freezing and

thawing of samples was avoided when possible.

6.2.11.1 Isolation of proteins from cells

Primary motor neurons and NSC-34 cells were carefully rinsed with DPBS twice before proteins were isolated. To lyse cells, the surface of each well was covered with RIPA buffer (Sigma) supplemented with phosphatase and protease inhibitors. After 10 min incubation on ice, samples were collected using a cell scraper and rinsing with RIPA buffer. Lysates were centrifuged at 8000 x g for 10 min in a pre-cooled centrifuge to seperate insoluble cellular compartments. Supernatants containing the soluble proteins were transferred into a new tube and stored at -20 °C until further use. Proteins used to detect phosphorylated proteins were stored in aliquots to minimize freeze and thaw cycles.

6.2.11.2 Isolation of mitochondria

To investigate the functionality of the respiratory chain in SMA motor neurons, mitochondria were isolated from primary motor neurons using the 'Mitochondria Isolation Kit' noted in 6.1.11. In brief, 3 x 10^7 cells were cultivated for 10DIV and mitochondria were collected. After cells were rinsed carefully, a cell scraper was used to collect the cells. To weaken the cell membrane, collected cells were frozen for 10 min and subsequently thawed. Cells were disrupted after 10 min incubation on ice by a pre-cooled Dounce homogenizer. The complete rupture was performed on the cell pellet after centrifugation. After an additional centrifugation step at 1000 x g, supernatants were combined and centrifuged at 12000 x g. The cell pellet was resuspended in a buffer included in the kit after addition of protease inhibitor (6.1.3). Isolated mitochondria were stored at -80 °C until further use.

6.2.11.3 Determining protein concentrations

Proteins lysed in RIPA buffer are quantified by BCA assay, but proteins used in the carbonylation assay described in 6.2.19 were quantified by Bradford due to the inhibitory effect of dithiothreitol (DTT).

BCA assay Proteins were quantified using the colorimetric detection assay Pierce™ BCA protein assay kit. This assay is based on the biuret reaction reducing Cu^{2+} to Cu^{+} by protein in an alkaline medium, combined with the chelation of bicinchoninic acid (BCA) by Cu^{+} (Smith et al., 1985). The resulting color change is quantified in a microplate reader by measurement of the absorbance at 562 nm after 30 min incubation at 37 °C. Samples are compared to an internal BSA standard in the range of 20-2000 µg/ml.

Bradford To quantify proteins used in the carbonylation assay described in 6.2.19, the Bradford assay was used. In brief, the colorimetric shift in absorbance of Coomassie Brilliant Blue G-250 upon protein binding is detected by a spectrophotometer at 595nm. Concentrations were calculated using an internal standard curve with known BSA concentrations (0.5 µg -

5 µg). To minimize the amount of protein used, 2 µl of each sample was diluted in 500 µl Bradford reagent in duplicate. Samples were incubated 5 min at RT before detection.

6.2.11.4 Sodium dodecyl polyacrylamide gel electrophoresis (SDS-PAGE) In order to measure protein expression, the widely used western blotting technique, composed of sodium dodecyl polyacrylamide gel electrophoresis (SDS-PAGE) followed by immunodetection was applied. All reagents and solutions used to perform western blot analysis in the Mini-Protean 3 cell system are listed in 6.1.3.1 and 6.1.10.1. After protein concentration was determined by BCA assay or Bradford, equal amounts between 10 µg and 20 µg of soluble protein were mixed with SDS containing Laemmli buffer (Laemmli, 1970). Negatively charged SDS binds to proteins and enables migration through a polyacrylamide gel in an electric field towards the anode. Here, proteins are primarily separated by their molecular weight (MW). Proteins were denatured by boiling at 95 °C for 5 min, and disulfide bonds are reduced by β-Mercaptoethanol. Samples were loaded into the pockets of a discontinuous SDS gel consisting of a 5% stacking gel and a separating gel. Due to a lower pH and bigger pore size in the stacking gel (pH 6.8), proteins can concentrate without separation. The actual separation of proteins by MW happens in the separating gel, which has a pH of 8.8 and smaller pore sizes. Depended on the size of the protein of interest, separating gels between 10% and 15% polyacrylamide were used. To estimate protein size, one pocket of the gel was loaded with PageRuler^{TM} Prestained Protein Ladder. Electrophoresis was initially performed at 90 V to concentrate the samples in the stacking gel and voltage was subsequently increased up to 120 V to separate proteins in the resolving gel.

6.2.11.5 Western blotting

After separation in SDS-PAGE, proteins were transferred from the gel to nitrocellulose or polyvinylidene fluoride (PVDF) membranes. Nitrocellulose membranes have the advantage of lower background signals, but PVDF membranes are capable of binding more protein. Due to PVDF membranes' hydrophobicity, incubation in methanol for 1 min before is required. All other components were first equilibrated in the transfer buffer. The appropriate membrane to use was determined for each protein empirically. For the complete transfer of proteins of all sizes, a wet transfer was performed. A transfer stack of the SDS gel and the membrane, surrounded by Whatman paper and two sponges were assembled. To ensure the negatively charged proteins migrate into the membrane, the gel was placed inside the transfer stack facing towards the cathode, and the membrane was facing towards the anode. Further on, the transfer stack was locked in a cassette and placed into the transfer chamber filled with transfer buffer. To reduce heat during transfer, a cooling pad was added, and the transfer tank was placed in the cold room at 4 °C. After 1 h of transfer at 110 V, the transfer stack was disassembled, and the transfer was confirmed by short incubation of the membrane in Ponceau S.

6.2.11.6 Detection of proteins by Western blot analysis

Once proteins are transferred to a membrane, proteins of interest were detected by antigen-specific antibodies. The information about antibodies is listed in 6.1.6 and 6.1.7. To avoid non-specific binding of antibodies, the membrane was first incubated in 5% BSA solution or 5% milk for 1 h at RT. Next, the membrane was incubated with primary antibodies diluted in blocking buffer at 4 °C ON. To remove excessive antibodies, the membrane was washed three times with PBS-T for 10 min each wash. Membranes were incubated at RT for 3 h in secondary antibodies conjugated with horseradish peroxidase (HRP). Secondary antibodies are directed against the host species of the primary antibody and diluted in a blocking solution. After membranes were washed three times, membranes were incubated for 5 min in Super Signal® West Pico Chemiluminescent Substrate. The enhanced chemiluminescent substrate is converted by the HRP conjugated to the secondary antibody. The resulting light signal is detected by the ChemiDoc XRS+ System. Signal intensities were quantified using the ImageLab 6.0 software. In order to detect multiple proteins on the same membrane, Restore Western Blot Stripping Buffer was used. Membranes were incubated for 15 - 30 min in stripping buffer and subsequently washed 3 times with PBS-T. Afterward, membranes were blocked for 30 min in a blocking buffer.

6.2.12 Proteomics

Primary MNs were treated with 50 mM pyruvate, 10 µM NAC and 100 µM menadione for 1 h, lysed in RIPA buffer with protease and phosphatase inhibitors and further processed for mass spectrometry (MS) analysis. To avoid contaminations of the samples, all subsequent steps were carried out particularly clean. MS sample preparation and analysis were accomplished in cooperation with the proteomics facility (CECAD, University of Cologne).

6.2.12.1 Sample lysis and acetone precipitation

Cells were collected and lysed in RIPA buffer with protease and phosphatase inhibitor as previously described in 6.2.11.1. To use the same amount of protein in every sample, proteins were quantified by BCA assay as described in 6.2.11.3. In total, 50 µg protein was used for acetone precipitation and subsequent MS processing. In order to precipitate samples, 4 times the volume of ice-cold acetone was added to the samples and incubated for 15 min at -80 °C, following 120 min incubation at -20 °C. After centrifugation for 5 min at 16000 x g, the supernatant was carefully discarded. Again, 500 µl of ice-cold acetone was added to the protein pellet and centrifuged for 5 min at 1600 x g. The supernatant was discarded, and the process was repeated once more. The resulting pellets were air-dried and resuspended in 50 µl of 8 M urea in 50 mM Triethylammoniumbicarbonate (TEAB) buffer supplemented with protease inhibitor.

6.2.12.2 In solution reduction, alkylation and digestion of proteins

After precipitation and resuspension in urea buffer, disulfide bonds in the samples were reduced, alkylated, and digested. Reduction of the samples was achieved using 5 mM dithio-

threitol (DTT) at RT for 1 h. Immediately after reduction, samples were alkylated using 40 mM chloroacetamide (CAA) in the dark for 30 min. The final digestion was carried out using endoproteinase Lys-C in an enzyme: substrate ratio of 1:75 for 4 h at RT and trypsin in an enzyme: substrate ratio of 1:75 ON at RT. Before digestion with trypsin, samples were diluted with 50 mM TEAB buffer to a final concentration of Urea $\leq$ 2 M. To stop enzymatic digestion, samples were acidified with 2% formic acid.

6.2.12.3 Stage Tip sample purification

Acidified samples were purified with C-18 styrenedivinylbenzene-reverse phase sulfonate (SDB-RPS) Stage Tips. Before samples were loaded, Stage Tips were activated with methanol and equilibrated using buffers containing 0.1% formic acid in water or 80% acetonitrile, respectively.

6.2.12.4 Liquid chromatography-mass spectrometry and data analysis

All samples were analyzed on a Q Exactive Plus Orbitrap mass spectrometer that was coupled to an EASY nLC at the CECAD proteomics facility (University of Cologne). Peptides were loaded with solvent A (0.1% formic acid in water) onto an in-house packed analytical column (50 cm - 75 µm I.D., filled with 2.7 µm Poroshell EC120 C18). Peptides were chromatographically separated at a constant flow rate of 250 nL/min and the following gradient: 3-5% solvent B (0.1% formic acid in 80% acetonitrile) within 1.0 min, 5-30% solvent B within 91.0 min, 30-50% solvent B within 17.0 min, 50-95% solvent B within 1.0 min, followed by washing and column equilibration. DDA library runs were acquired from distinct pools of the sample groups. The MS1 survey scan was acquired from 300-1750 m/z at a resolution of 70,000. The top 10 most abundant peptides were isolated within a 2.0 Th window and subjected to HCD fragmentation with a normalized collision energy of 27%. The AGC target was set to 5e5 charges, allowing a maximum injection time of 55 ms. Product ions were detected in the Orbitrap at a resolution of 17,500. Precursors were dynamically excluded for 20.0 s. For the acquisition of the samples, the mass spectrometer was operated in data-independent mode. For MS1 and MS/MS scans the maximum IT was restricted to 60 ms and the AGC target was set to 1e6 charges. The MS1 scan was acquired from 400-1220 m/z at a resolution of 35,000. MSMS scans were acquired in in DIA mode using 25 x 24 m/z windows covering the mass range from m/z 400 to m/z1000 at a resolution of 17,500. The default charge state for the MS2 was set to 3. Stepped normalized collision energy was set to 27%. The MS/MS spectra were acquired in centroid mode. DIA data were analyzed with assay-specific hybrid library using default settings in Spectronaut 13 (Bruderer et al., 2015). The library was generated by searching a *mus musculus* fasta library (UP000000589, 50331 entries from Swiss-Prot and TrEMBL) with DDA library runs plus all DIA sample runs using PulsarX and direct DIA. Normalized $\log_2$ intensities were exported for protein identifications with q-values below 0.01. Perseus was used for subsequent statistical analysis (Tyanova et al., 2016). The MS proteomics raw data has been deposited to the ProteomeXchange Consortium via the PRIDE (Perez-Riverol et al., 2019) partner repository with the dataset identifier PXD020403.

6.2.12.5 Gene ontology

Further gene ontology (GO) analysis was conducted by using the Database for Annotation, Visualization and Integrated Discovery 6.7 (DAVID). Statistical analysis and data visualization were performed using RStudio. The mouse MitoCarta 2.0 dataset was used to identify mitochondrial proteins (Calvo et al., 2016).

6.2.13 Immunofluorescence methods

6.2.13.1 Immunofluorescence staining of cells

Immunofluorescence is an ideal method to visualize the localization and distribution of specific proteins inside a cell. Antibodies against specific epitopes tag the desired proteins, and secondary antibodies targeted against the primary antibody are conjugated to a fluorophore, which can be visualized in a fluorescence microscope. We used the advantage of low-density neuronal cultures to determine the subcellular localization of proteins at a single-cell level. For this experiment, motor neurons were cultured on PDL coated coverslips as described in 6.2.6. After the desired days *in vitro* cultivation, the maintenance medium was removed, and cells were carefully rinsed with DPBS 3 times. Fixation of cells was accomplished using 4% PFA for 20 min at RT and subsequent washing with DPBS. To visualize intracellular proteins, cells were permeabilized using PBS containing 0.3% Tween20 for 10 min at RT and three wash steps with PBS were followed. In order to avoid unspecific binding of the antibody, coverslips were incubated for 1 h in PBS containing 0.2% Tween-20 and 3% BSA. After blocking, cells were incubated with primary antibody diluted in blocking buffer ON at 4 °C. For optimal distribution of the antibody on the coverslip surface and to reduce the amount used, coverslips were incubated inverted with the cell side down facing one drop of the antibody dilution. After coverslips were washed three times with PBS, secondary antibody conjugated with the fluorophore was applied the same way as the primary antibody. Dilution factors of primary antibodies used are listed in 6.1.6, and secondary antibodies are noted in 6.1.7. To visualize the nuclei, DNA was stained by 4',6-diamidino-2-phenylindole (DAPI) staining solution after coverslips were washed three times with PBS. Coverslips were mounted on microscope slides using mowiol with the cells facing down and stored in the dark at 4 °C until analysis.

6.2.13.2 MitoTracker® staining

The use of the mitochondria membrane intercalating dye MitoTracker® Red CMXRos gives the advantage to label mitochondria before fixation and permeabilization. Using MitoTracker, functional mitochondria can be detected based on their membrane potential, and labeling is retained in the mitochondria after fixation. Staining was accomplished by 100nM MitoTracker® Red CMXRos added directly in serum-free medium on the cells. Further on, fixation and antibody staining were performed as described in 6.2.13.

6.2.13.3 Microscopic analysis

All fluorescence images were acquired blinded with an Axio Imager.M2 fluorescence microscope equipped with an AxioCam MRm camera and an ApoTome.2 system. Images were analyzed blindly with FIJI. To quantify the number and appearance of mitochondria along neurites, a modified version of the ImageJ Mitophagy Macro by Ruben K. Dagda was used (Dagda et al., 2008).

6.2.14 Complex I activity assay

In order to test the functionality of mitochondrial respiratory chain complexes, the Complex I enzyme activity assay kit was used (noted in 6.1.11). After mitochondria were isolated (6.2.11.2), proteins were isolated by detergent extraction and loaded onto a microwell plate. To enable attachment of complex I proteins to the microplate via antibody coupling, plates were incubated for 3 h at RT. Differences of complex I activity in SMA and WT motor neurons were assessed by measuring the optical density (OD_{450} nm) after adding the assay solution on the plate. The enzyme kinetic was followed for 1 h. For tissue samples from the heart and spinal cord (SC) 300 µg of cell extracts were used, and 20 µg of mitochondrial extracts were used from motor neuron samples.

6.2.15 ATP assay

To increase the accuracy of the measures, two independent methods were used to determine the intracellular ATP concentration. One was by phosphorylating glycerol, resulting in a fluorometric ($\lambda_{ex} = 535/\lambda_{ex} = 587$ nm) product using the ATP Assay Kit. The other approach was the ATP Determination Kit using a recombinant firefly luciferase and a bioluminescence signal produced by the substrate D-luciferin. Both methods result in a signal proportional to the amount of ATP present in the sample and were normalized to soluble protein concentrations. Results of fluorescence signal were quantified using the Safire 2 microplate reader and luminescence signals were detected by GloMax® luminescence reader.

6.2.16 Glucose uptake assay

In order to compare glucose uptake efficiency between WT and SMA MNs the Glucose Uptake-Glo kit was used. In this assay, NADH is produced via glucose oxidation by glucose dehydrogenase. The production of NADH is coupled to a reduction of pro-luciferin into luciferin, which is subsequently used by luciferase to produce a light signal. Primary MNs were cultured at a density of 120,000 cells/cm^2 and manufacturer's instructions were followed. The emitted light signal was measured by the GloMax luminescence reader and normalized to protein concentration measured by BCA assay.

6.2.17 Pyruvate uptake assay

Pyruvate uptake was measured with the Pyruvate assay kit. MNs were supplied with pyruvate over 1 h and cells were lysed using assay buffer and mechanical disruption by pipetting. To reduce

the conversion of pyruvate to lactate by lactate dehydrogenase, samples were deproteinized using 10 kDa spin columns. Further on, samples were compared to standards ranging between 0 and 200 µm pyruvate. Fluorescence signal was measured at $\lambda_{ex} = 535/\ \lambda_{em} = 587$ nm with the Safire 2 microplate reader and normalized to soluble protein amount.

6.2.18 Detection of oxidative stress

To measure ROS in MNs and NSC-34 cells, CellROX^{TM} Green was used. CellROX^{TM} Green is a cell-permeant nonfluorescent probe, which exhibits fluorescence upon oxidation. The oxidized probe remains localized within the cell due to binding to DNA. In our analysis, WT and SMA MNs were incubated with 5 µM CellROX^{TM} Green reagent for 30 min. After fixation with 3.7% formaldehyde, nuclei and F-actin of the cells were co-stained with DAPI and Alexa Fluor^{TM} 568 Phalloidin respectively. To increase the reliability of measures, CellROX^{TM} signal was measured with two independent methods. CellROX^{TM} signal on coverslip images were acquired with a fluorescence microscope equipped with an ApoTome.2 system. In addition, the signal was also quantified with a Safire 2 microplate reader. Data acquired by microplate reader were normalized to soluble protein concentration after lysis with RIPA buffer. To monitor oxidative stress after manipulation of ROS levels in cells, 50 mM pyruvate, 10 µm NAC, and 100 µm Menadione were added 45 min before measurement. Those signals were quantified with the Safire 2 microplate reader.

6.2.19 Protein carbonylation assay

The amount of protein carbonyl groups was measured with the Protein carbonyl assay kit according to the manufacturer's instructions. In brief, carbonyl groups are derivatized to DNP-hydrazone by reaction with 2,4-Dinitrophenylhydrazine (DNPH). To prevent oxidation of proteins after cell lysis, 50 mM DTT was added. Protein concentration was measured by Bradford, described in 6.2.11.3. The amount of carbonylated protein was quantified by use of an anti-DNP specific antibody in western blot analysis.

6.2.20 AHA-click iT assay

L-azidohomoalanine (AHA) is incorporated into proteins during active protein synthesis and later on detected by click chemistry reaction with biotin alkyne. To deplete endogenous methionine reserves of primary motor neurons, the culture medium was exchanged for 30 min with HBSS. For AHA labeling, 500 µM L-AHA, 500 µM L-AHA in addition with 40 µM anisomycin, and L-AHA in addition with ROS modulating drugs were added for 1 h. After incubation at 37 °C, cells were washed with PBS and lysed for 20 min on ice with RIPA buffer supplemented with protease and phosphatase inhibitors. Click chemistry reaction was achieved by adding 40 µM biotin alkyne and following the manufacturer's protocol of the Click-iT® protein reaction buffer kit. Further, L-AHA labeled proteins were detected by western blotting.

6.2.21 Statistical analyses

All statistical analyses were conducted in R version 3.6.2 using RStudio (RStudio Team, 2019). Quantities of peptides in proteomics data were determined at the proteomics facility (CECAD) using Perseus. Statistical significances of quantified peptides were determined by a two-sided unpaired t-test. All graphs of experiment quantification represent the average by mean, including error bars depicting the standard deviation ($\pm$ SD). Also, individual data points from either independent biological replicates (N) or technical replicates (n) are presented. Statistical tests were applied only to biological replicates. For experiments with small sample sizes, normality tests have little power to reject the null-hypothesis and result in the assumption of normal distribution (Le Boedec, 2016). Therefore, the distribution of samples in all experiments was observed post hoc visually and by Shapiro-Wilk normality test, as it provides the highest power at small sample sizes among normality tests (Ghasemi & Zahediasl, 2012). Statistically significant differences of normally distributed means of two groups were determined by t-test (two-tailed). Multiple group comparisons where t-tests were applied were corrected with the Holm-Bonferroni method (Holm, 1979). Differences among multiple group means are determined with Tukey's honestly significant difference (HSD) test after the rejection of the null hypothesis by one-way analysis of variance (ANOVA). Normally distributed experimental results including two factors were analyzed by two-way ANOVA with Tukey HSD post-hoc analysis. In time-course and dose-response experiments, comparing multiple mean values to a single control mean, Dunnett's post hoc test was used after one-way ANOVA. Significance is indicated by asterisks as follows: n.s. = not significant, $^{*}p < 0.05$; $^{**}p < 0.01$; $^{***} < 0.001$.

7 REFERENCES

Ackermann, B., Kröber, S., Torres-benito, L., Borgmann, A., Peters, M., Hosseini barkooie, S. M., ... Wirth, B. (2013). Plastin 3 ameliorates spinal muscular atrophy via delayed axon pruning and improves neuromuscular junction functionality. *Hum. Mol. Genet.*, *22*(7), 1328–1347. doi: 10.1093/hmg/dds540

Acsadi, G., Lee, I., Li, X., Khaidakov, M., Pecinova, A., Parker, G. C., & Hüttemann, M. (2009, sep). Mitochondrial dysfunction in a neural cell model of spinal muscular atrophy. *J. Neurosci. Res.*, *87*(12), 2748–2756. Retrieved from http://onlinelibrary.wiley.com/doi/10.1002/jnr.22106/fullhttp://doi.wiley.com/10.1002/jnr.22106 doi: 10.1002/jnr.22106

Adams, M. J., Buehner, M., Chandrasekhar, K., Ford, G. C., Hackert, M. L., Liljas, A., ... Taylor, S. S. (1973, jul). Structure-Function Relationships in Lactate Dehydrogenase. *Proc. Natl. Acad. Sci.*, *70*(7), 1968–1972. Retrieved from http://www.pnas.org/cgi/doi/10.1073/pnas.70.7.1968 doi: 10.1073/pnas.70.7.1968

Adam-Vizi, V., & Starkov, A. A. (2010, jun). Calcium and Mitochondrial Reactive Oxygen Species Generation: How to Read the Facts. *J. Alzheimer's Dis.*, *20*(s2), S413–S426. Retrieved from https://www.medra.org/servlet/aliasResolver?alias=iospress{&}doi=10.3233/JAD-2010-100465 doi: 10.3233/JAD-2010-100465

Akten, B., Kye, M. J., Hao, L. T., Wertz, M. H., Singh, S., Nie, D., ... Sahin, M. (2011). Interaction of survival of motor neuron (SMN) and HuD proteins with mRNA cpg15 rescues motor neuron axonal deficits. *Proc. Natl. Acad. Sci. U. S. A.*, *108*(25), 10337–10342. doi: 10.1073/pnas.1104928108

Alam, Z. I., Jenner, A., Daniel, S. E., Lees, A. J., Cairns, N., Marsden, C. D., ... Halliwell, B. (2002, nov). Oxidative DNA Damage in the Parkinsonian Brain: An Apparent Selective Increase in 8-Hydroxyguanine Levels in Substantia Nigra. *J. Neurochem.*, *69*(3), 1196–1203. Retrieved from http://doi.wiley.com/10.1046/j.1471-4159.1997.69031196.x doi: 10.1046/j.1471-4159.1997.69031196.x

Alías, L., Bernal, S., Fuentes-Prior, P., Barceló, M. J., Also, E., Martínez-Hernández, R., ... Tizzano, E. F. (2009, feb). Mutation update of spinal muscular atrophy in Spain: molecular characterization of 745 unrelated patients and identification of four novel mutations in the SMN1 gene. *Hum. Genet.*, *125*(1), 29–39. Retrieved from http://www.ncbi.nlm.nih.gov/pubmed/19050931 doi: 10.1007/s00439-008-0598-1

Amin, N. D., Bai, G., Klug, J. R., Bonanomi, D., Pankratz, M. T., Gifford, W. D., ... Pfaff, S. L. (2015, dec). Loss of motoneuron-specific microRNA-218 causes systemic neuromuscular failure. *Science (80-.).*, *350*(6267), 1525–1529. Retrieved from https://www.sciencemag.org/lookup/doi/10.1126/science.aad2509 doi: 10.1126/science.aad2509

An, Y., Varma, V. R., Varma, S., Casanova, R., Dammer, E., Pletnikova, O., ... Thambisetty, M. (2018, mar). Evidence for brain glucose dysregulation in Alzheimer's disease. *Alzheimer's*

Dement., *14*(3), 318–329. Retrieved from http://doi.wiley.com/10.1016/j.jalz.2017.09.011 doi: 10.1016/j.jalz.2017.09.011

Andreassi, C., & Riccio, A. (2009, sep). To localize or not to localize: mRNA fate is in 3' UTR ends. *Trends Cell Biol.*, *19*(9), 465–474. Retrieved from https://linkinghub.elsevier.com/retrieve/pii/S096289240900141X doi: 10.1016/j.tcb.2009.06.001

Andreou, A. Z., Harms, U., & Klostermeier, D. (2017, jan). eIF4B stimulates eIF4A ATPase and unwinding activities by direct interaction through its 7-repeats region. *RNA Biol.*, *14*(1), 113–123. Retrieved from https://www.tandfonline.com/doi/full/10.1080/15476286.2016.1259782 doi: 10.1080/15476286.2016.1259782

Angliker, N., & Rüegg, M. A. (2013, jul). In vivo evidence for mTORC2-mediated actin cytoskeleton rearrangement in neurons. *Bioarchitecture*, *3*(4), 113–118. Retrieved from http://www.tandfonline.com/doi/abs/10.4161/bioa.26497 doi: 10.4161/bioa.26497

Arce, V., Garces, A., de Bovis, B., Filippi, P., Henderson, C., Pettmann, B., & De-Lapeyrière, O. (1999, jan). Cardiotrophin-1 requires LIFRβ to promote survival of mouse motoneurons purified by a novel technique. *J. Neurosci. Res.*, *55*(1), 119–126. Retrieved from https://onlinelibrary.wiley.com/doi/10.1002/(SICI)1097-4547(19990101)55:1{%}3C119::AID-JNR13{%}3E3.0.CO;2-6 doi: 10.1002/(SICI)1097-4547(19990101)55:1<119::AID-JNR13>3.0.CO;2-6

Argüello, R. J., Reverendo, M., Mendes, A., Camosseto, V., Torres, A. G., Ribas de Pouplana, L., ... Pierre, P. (2018, may). SunRiSE – measuring translation elongation at single-cell resolution by means of flow cytometry. *J. Cell Sci.*, *131*(10), jcs214346. Retrieved from http://jcs.biologists.org/lookup/doi/10.1242/jcs.214346 doi: 10.1242/jcs.214346

Ashok, B. T., & Ali, R. (1999, jun). The aging paradox: free radical theory of aging. *Exp. Gerontol.*, *34*(3), 293–303. Retrieved from https://linkinghub.elsevier.com/retrieve/pii/S0531556599000054 doi: 10.1016/S0531-5565(99)00005-4

Ashrafi, G., Wu, Z., Farrell, R. J., & Ryan, T. A. (2017, feb). GLUT4 Mobilization Supports Energetic Demands of Active Synapses. *Neuron*, *93*(3), 606–615.e3. Retrieved from http://dx.doi.org/10.1016/j.neuron.2016.12.020https://linkinghub.elsevier.com/retrieve/pii/S089662731630993X doi: 10.1016/j.neuron.2016.12.020

Attwell, D., & Laughlin, S. B. (2001). An energy budget for signaling in the grey matter of the brain. *J. Cereb. Blood Flow Metab.*, *21*(10), 1133–45. Retrieved from http://www.ncbi.nlm.nih.gov/pubmed/11598490 doi: 10.1097/00004647-200110000-00001

Auten, R. L., & Davis, J. M. (2009, aug). Oxygen Toxicity and Reactive Oxygen Species: The Devil Is in the Details. *Pediatr. Res.*, *66*(2), 121–127. Retrieved from http://www.nature.com/doifinder/10.1203/PDR.0b013e3181a9eafb doi: 10.1203/PDR.0b013e3181a9eafb

Baloh, R. H., Rakowicz, W., Gardner, R., & Pestronk, A. (2007, jul). Frequent atrophic groups with mixed-type myofibers is distinctive to motor neuron syndromes. *Muscle Nerve*,

36(1), 107–110. Retrieved from http://doi.wiley.com/10.1002/mus.20755 doi: 10.1002/mus.20755

Banerjee, A. K. (1980, jun). 5'-terminal cap structure in eucaryotic messenger ribonucleic acids. *Microbiol. Rev.*, *44*(2), 175 LP – 205. Retrieved from http://mmbr.asm.org/content/44/2/175.abstract

Barja, G. (1999). Mitochondrial Oxygen Radical Generation and Leak: Sites of Production in States 4 and 3, Organ Specificity, and Relation to Aging and Longevity. *J. Bioenerg. Biomembr.*, *31*(4), 347–366. Retrieved from https://doi.org/10.1023/A:1005427919188 doi: 10.1023/A:1005427919188

Barja, G., & Herrero, A. (1998). Localization at Complex I and Mechanism of the Higher Free Radical Production of Brain Nonsynaptic Mitochondria in the Short-Lived Rat Than in the Longevous Pigeon. *J. Bioenerg. Biomembr.*, *30*(3), 235–243. Retrieved from https://doi.org/10.1023/A:1020592719405 doi: 10.1023/A:1020592719405

Bäumer, D., Lee, S., Nicholson, G., Davies, J. L., Parkinson, N. J., Murray, L. M., ... Talbot, K. (2009, dec). Alternative Splicing Events Are a Late Feature of Pathology in a Mouse Model of Spinal Muscular Atrophy. *PLoS Genet.*, *5*(12), e1000773. Retrieved from https://dx.plos.org/10.1371/journal.pgen.1000773 doi: 10.1371/journal.pgen.1000773

Bebee, T. W., Dominguez, C. E., Samadzadeh-Tarighat, S., Akehurst, K. L., & Chandler, D. S. (2012, oct). Hypoxia is a modifier of SMN2 splicing and disease severity in a severe SMA mouse model. *Hum. Mol. Genet.*, *21*(19), 4301–13. Retrieved from http://www.ncbi.nlm.nih.gov/pubmed/22763238http://www.pubmedcentral.nih.gov/articlerender.fcgi?artid=PMC3441125 doi: 10.1093/hmg/dds263

Béchade, C., Rostaing, P., Cisterni, C., Kalisch, R., Bella, V. L., Pettmann, B., & Triller, A. (1999, jan). Subcellular distribution of survival motor neuron (SMN) protein: possible involvement in nucleocytoplasmic and dendritic transport. *Eur. J. Neurosci.*, *11*(1), 293–304. Retrieved from http://doi.wiley.com/10.1046/j.1460-9568.1999.00428.x doi: 10.1046/j.1460-9568.1999.00428.x

Belmonte, M. K., Cook, E. H., Anderson, G. M., Rubenstein, J. L. R., Greenough, W. T., Beckel-Mitchener, A., ... Tierney, E. (2004, jul). Autism as a disorder of neural information processing: directions for research and targets for therapy. *Mol. Psychiatry*, *9*(7), 646–663. Retrieved from http://www.nature.com/articles/4001499 doi: 10.1038/sj.mp.4001499

Bernabò, P., Tebaldi, T., Groen, E. J., Lane, F. M., Perenthaler, E., Mattedi, F., ... Viero, G. (2017, oct). In Vivo Translatome Profiling in Spinal Muscular Atrophy Reveals a Role for SMN Protein in Ribosome Biology. *Cell Rep.*, *21*(4), 953–965. Retrieved from https://linkinghub.elsevier.com/retrieve/pii/S2211124717314274 doi: 10.1016/j.celrep.2017.10.010

Birben, E., Sahiner, U. M., Sackesen, C., Erzurum, S., & Kalayci, O. (2012, jan). Oxidative Stress and Antioxidant Defense. *World Allergy Organ. J.*, *5*(1), 9–19. Retrieved from http://www.waojournal.org/content/5/1/9 doi: 10.1097/WOX.0b013e3182439613

Bogetofte, H., Jensen, P., Ryding, M., Schmidt, S. I., Okarmus, J., Ritter, L., ... Meyer, M. (2019, jul). PARK2 Mutation Causes Metabolic Disturbances and Impaired Survival of Human iPSC-Derived Neurons. *Front. Cell. Neurosci.*, *13*. Retrieved from https://www.frontiersin.org/article/10.3389/fncel.2019.00297/full doi: 10.3389/fncel.2019.00297

Boillée, S., Vande Velde, C., & Cleveland, D. W. (2006, oct). ALS: A Disease of Motor Neurons and Their Nonneuronal Neighbors. *Neuron*, *52*(1), 39–59. Retrieved from https://linkinghub.elsevier.com/retrieve/pii/S0896627306007252 doi: 10.1016/j.neuron.2006.09.018

Bömmel, H., Xie, G., Rossoll, W., Wiese, S., Jablonka, S., Boehm, T., & Sendtner, M. (2002, nov). Missense mutation in the tubulin-specific chaperone E (Tbce) gene in the mouse mutant progressive motor neuronopathy, a model of human motoneuron disease. *J. Cell Biol.*, *159*(4), 563–569. Retrieved from https://rupress.org/jcb/article/159/4/563/33093/Missense-mutation-in-the-tubulinspecific-chaperone doi: 10.1083/jcb.200208001

Bowerman, M., Michalski, J.-P., Beauvais, A., Murray, L. M., DeRepentigny, Y., & Kothary, R. (2014, jul). Defects in pancreatic development and glucose metabolism in SMN-depleted mice independent of canonical spinal muscular atrophy neuromuscular pathology. *Hum. Mol. Genet.*, *23*(13), 3432–3444. Retrieved from http://linkinghub.elsevier.com/retrieve/pii/S2211124717317990http://academic.oup.com/hmg/article/23/13/3432/659416/Defects-in-pancreatic-development-and-glucose doi: 10.1093/hmg/ddu052

Boyd, P. J., Tu, W.-Y., Shorrock, H. K., Groen, E. J. N., Carter, R. N., Powis, R. A., ... Gillingwater, T. H. (2017, apr). Bioenergetic status modulates motor neuron vulnerability and pathogenesis in a zebrafish model of spinal muscular atrophy. *PLOS Genet.*, *13*(4), e1006744. Retrieved from http://dx.plos.org/10.1371/journal.pgen.1006744https://dx.plos.org/10.1371/journal.pgen.1006744http://www.ncbi.nlm.nih.gov/pubmed/28426667 doi: 10.1371/journal.pgen.1006744

Brooks, G. A. (2002, apr). Lactate shuttles in Nature. *Biochem. Soc. Trans.*, *30*(2), 258–264. Retrieved from https://doi.org/10.1042/bst0300258 doi: 10.1042/bst0300258

Brown, E. J., Albers, M. W., Bum Shin, T., Ichikawa, K., Keith, C. T., Lane, W. S., & Schreiber, S. L. (1994, jun). A mammalian protein targeted by G1-arresting rapamycin–receptor complex. *Nature*, *369*(6483), 756–758. Retrieved from http://www.nature.com/articles/369756a0 doi: 10.1038/369756a0

Browne, S. E., Bowling, A. C., Macgarvey, U., Baik, M. J., Berger, S. C., Muquit, M. M. K., ... Beal, M. F. (1997, may). Oxidative damage and metabolic dysfunction in Huntington's disease: Selective vulnerability of the basal ganglia. *Ann. Neurol.*, *41*(5), 646–653. Retrieved from http://doi.wiley.com/10.1002/ana.410410514 doi: 10.1002/ana.410410514

Bruderer, R., Bernhardt, O. M., Gandhi, T., Miladinović, S. M., Cheng, L.-Y., Messner, S., ... Reiter, L. (2015, may). Extending the limits of quantitative proteome profiling with data-independent acquisition and application to acetaminophen-treated

three-dimensional liver microtissues. *Mol. Cell. Proteomics*, *14*(5), 1400–10. Retrieved from http://www.ncbi.nlm.nih.gov/pubmed/25724911http://www.pubmedcentral.nih.gov/articlerender.fcgi?artid=PMC4424408 doi: 10.1074/mcp.M114.044305

Brzustowicz, L. M., Lehner, T., Castilla, L. H., Penchaszadeh, G. K., Wilhelmsen, K. C., Daniels, R., ... Gilliam, T. C. (1990, apr). Genetic mapping of chronic childhood-onset spinal muscular atrophy to chromosome 5q1 1.2–13.3. *Nature*, *344*(6266), 540–541. Retrieved from http://www.nature.com/articles/344540a0 doi: 10.1038/344540a0

Buffington, S. A., Huang, W., & Costa-Mattioli, M. (2014, jul). Translational Control in Synaptic Plasticity and Cognitive Dysfunction. *Annu. Rev. Neurosci.*, *37*(1), 17–38. Retrieved from http://www.annualreviews.org/doi/10.1146/annurev-neuro-071013-014100 doi: 10.1146/annurev-neuro-071013-014100

Buhler, D., Raker, V., Luhrmann, R., & Fischer, U. (1999, dec). Essential Role for the Tudor Domain of SMN in Spliceosomal U snRNP Assembly: Implications for Spinal Muscular Atrophy. *Hum. Mol. Genet.*, *8*(13), 2351–2357. Retrieved from https://academic.oup.com/hmg/article-lookup/doi/10.1093/hmg/8.13.2351 doi: 10.1093/hmg/8.13.2351

Bürglen, L., Lefebvre, S., Clermont, O., Burlet, P., Viollet, L., Cruaud, C., ... Melki, J. (1996, mar). Structure and Organization of the Human Survival Motor Neurone (SMN) Gene. *Genomics*, *32*(3), 479–482. Retrieved from https://linkinghub.elsevier.com/retrieve/pii/S0888754396901470 doi: 10.1006/geno.1996.0147

Burkard, K. T. D., & Butler, J. S. (2000, jan). A Nuclear 3'-5' Exonuclease Involved in mRNA Degradation Interacts with Poly(A) Polymerase and the hnRNA Protein Npl3p. *Mol. Cell. Biol.*, *20*(2), 604–616. Retrieved from https://mcb.asm.org/content/20/2/604 doi: 10.1128/MCB.20.2.604-616.2000

Burlet, P., Burglen, L., Clermont, O., Lefebvre, S., Viollet, L., Munnich, A., & Melki, J. (1996, apr). Large scale deletions of the 5q13 region are specific to Werdnig-Hoffmann disease. *J. Med. Genet.*, *33*(4), 281–283. Retrieved from https://jmg.bmj.com/lookup/doi/10.1136/jmg.33.4.281 doi: 10.1136/jmg.33.4.281

Burnett, B. G., Munoz, E., Tandon, A., Kwon, D. Y., Sumner, C. J., & Fischbeck, K. H. (2009, mar). Regulation of SMN Protein Stability. *Mol. Cell. Biol.*, *29*(5), 1107–1115. Retrieved from http://mcb.asm.org/cgi/doi/10.1128/MCB.01262-08 doi: 10.1128/MCB.01262-08

Buttgereit, F., & Brand, M. D. (1995, nov). A hierarchy of ATP-consuming processes in mammalian cells. *Biochem. J.*, *312*(1), 163–167. Retrieved from https://portlandpress.com/biochemj/article/312/1/163/32435/A-hierarchy-of-ATPconsuming-processes-in-mammalian doi: 10.1042/bj3120163

Cafferkey, R., Young, P. R., McLaughlin, M. M., Bergsma, D. J., Koltin, Y., Sathe, G. M., ... Livi, G. P. (1993, oct). Dominant missense mutations in a novel yeast protein related to mammalian phosphatidylinositol 3-kinase and VPS34 abrogate rapamycin cytotoxicity. *Mol.*

Cell. Biol., *13*(10), 6012–6023. Retrieved from http://mcb.asm.org/lookup/doi/10.1128/MCB.13.10.6012 doi: 10.1128/MCB.13.10.6012

Calucho, M., Bernal, S., Alías, L., March, F., Venceslá, A., Rodríguez-Álvarez, F. J., ... Tizzano, E. F. (2018, mar). Correlation between SMA type and SMN2 copy number revisited: An analysis of 625 unrelated Spanish patients and a compilation of 2834 reported cases. *Neuromuscul. Disord.*, *28*(3), 208–215. Retrieved from https://linkinghub.elsevier.com/retrieve/pii/S096089661730490X doi: 10.1016/j.nmd.2018.01.003

Calvo, S. E., Clauser, K. R., & Mootha, V. K. (2016, jan). MitoCarta2.0: an updated inventory of mammalian mitochondrial proteins. *Nucleic Acids Res.*, *44*(D1), D1251–D1257. Retrieved from https://academic.oup.com/nar/article-lookup/doi/10.1093/nar/gkv1003 doi: 10.1093/nar/gkv1003

Carmo, C., Naia, L., Lopes, C., & Rego, A. C. (2018). Mitochondrial Dysfunction in Huntington's Disease. *Adv. Exp. Med. Biol.*, *1049*, 59–83. Retrieved from https://doi.org/10.1007/978-3-319-71779-1{_}3http://link.springer.com/10.1007/978-3-319-71779-1{_}3http://www.ncbi.nlm.nih.gov/pubmed/29427098 doi: 10.1007/978-3-319-71779-1_3

Cartegni, L., & Krainer, A. R. (2002, apr). Disruption of an SF2/ASF-dependent exonic splicing enhancer in SMN2 causes spinal muscular atrophy in the absence of SMN1. *Nat. Genet.*, *30*(4), 377–84. Retrieved from https://linkinghub.elsevier.com/retrieve/pii/S0002929707608064http://www.nature.com/articles/ng854zhttp://www.ncbi.nlm.nih.gov/pubmed/11925564 doi: 10.1038/ng854

Carvalho, T., Almeida, F., Calapez, A., Lafarga, M., Berciano, M. T., & Carmo-Fonseca, M. (1999, nov). The Spinal Muscular Atrophy Disease Gene Product, Smn. *J. Cell Biol.*, *147*(4), 715–728. Retrieved from https://rupress.org/jcb/article/147/4/715/32002/The-Spinal-Muscular-Atrophy-Disease-Gene-Product doi: 10.1083/jcb.147.4.715

Cashman, N. R., Durham, H. D., Blusztajn, J. K., Oda, K., Tabira, T., Shaw, I. T., ... Antel, J. P. (1992, jul). Neuroblastoma x spinal cord (NSC) hybrid cell lines resemble developing motor neurons. *Dev. Dyn.*, *194*(3), 209–21. Retrieved from http://www.ncbi.nlm.nih.gov/pubmed/1467557 doi: 10.1002/aja.1001940306

Catanesi, M., D'Angelo, M., Tupone, M. G., Benedetti, E., Giordano, A., Castelli, V., & Cimini, A. (2020, aug). MicroRNAs Dysregulation and Mitochondrial Dysfunction in Neurodegenerative Diseases. *Int. J. Mol. Sci.*, *21*(17), 5986. Retrieved from https://www.mdpi.com/1422-0067/21/17/5986 doi: 10.3390/ijms21175986

Chance, B., Sies, H., & Boveris, A. (1979, jul). Hydroperoxide metabolism in mammalian organs. *Physiol. Rev.*, *59*(3), 527–605. Retrieved from https://www.physiology.org/doi/10.1152/physrev.1979.59.3.527 doi: 10.1152/physrev.1979.59.3.527

Chang, H.-C. C., Hung, W.-C. C., Chuang, Y.-J. J., & Jong, Y.-J. J. (2004, dec). Degradation of survival motor neuron (SMN) protein is mediated via the ubiquitin/proteasome pathway.

Neurochem. Int., *45*(7), 1107–1112. Retrieved from https://linkinghub.elsevier.com/retrieve/pii/S0197018604000907 doi: 10.1016/j.neuint.2004.04.005

Chauvin, C., Koka, V., Nouschi, A., Mieulet, V., Hoareau-Aveilla, C., Dreazen, A., ... Pende, M. (2014, jan). Ribosomal protein S6 kinase activity controls the ribosome biogenesis transcriptional program. *Oncogene*, *33*(4), 474–483. Retrieved from http://www.nature.com/articles/onc2012606 doi: 10.1038/onc.2012.606

Chinnery, P. F., & Hudson, G. (2013, jun). Mitochondrial genetics. *Br. Med. Bull.*, *106*(1), 135–159. Retrieved from https://academic.oup.com/bmb/article-lookup/doi/10.1093/bmb/ldt017 doi: 10.1093/bmb/ldt017

Cifuentes-Diaz, C., Frugier, T., Tiziano, F. D., Lacène, E., Roblot, N., Joshi, V., ... Melki, J. (2001, mar). Deletion of Murine SMN Exon 7 Directed to Skeletal Muscle Leads to Severe Muscular Dystrophy. *J. Cell Biol.*, *152*(5), 1107–1114. Retrieved from https://doi.org/10.1083/jcb.152.5.1107https://rupress.org/jcb/article/152/5/1107/45905/Deletion-of-Murine-SMN-Exon-7-Directed-to-Skeletalhttp://www.ncbi.nlm.nih.gov/pubmed/11238465http://www.pubmedcentral.nih.gov/articlerender.fcgi?artid=PMC2198815 doi: 10.1083/jcb.152.5.1107

Cioni, J.-M., Lin, J. Q., Holtermann, A. V., Koppers, M., Jakobs, M. A., Azizi, A., ... Holt, C. E. (2019, jan). Late Endosomes Act as mRNA Translation Platforms and Sustain Mitochondria in Axons. *Cell*, *176*(1-2), 56–72.e15. Retrieved from https://doi.org/10.1016/j.cell.2018.11.030https://linkinghub.elsevier.com/retrieve/pii/S0092867418315551 doi: 10.1016/j.cell.2018.11.030

Cioni, J.-M. M., Koppers, M., & Holt, C. E. (2018, aug). Molecular control of local translation in axon development and maintenance. *Curr. Opin. Neurobiol.*, *51*, 86–94. Retrieved from https://doi.org/10.1016/j.conb.2018.02.025https://linkinghub.elsevier.com/retrieve/pii/S0959438817303252 doi: 10.1016/j.conb.2018.02.025

Cole, C. N., & Scarcelli, J. J. (2006, jun). Transport of messenger RNA from the nucleus to the cytoplasm. *Curr. Opin. Cell Biol.*, *18*(3), 299–306. Retrieved from https://linkinghub.elsevier.com/retrieve/pii/S0955067406000573 doi: 10.1016/j.ceb.2006.04.006

Contreras-Baeza, Y., Sandoval, P. Y., Alarcón, R., Galaz, A., Cortés-Molina, F., Alegría, K., ... Barros, L. F. (2019, dec). Monocarboxylate transporter 4 (MCT4) is a high affinity transporter capable of exporting lactate in high-lactate microenvironments. *J. Biol. Chem.*, *294*(52), 20135–20147. Retrieved from http://www.jbc.org/lookup/doi/10.1074/jbc.RA119.009093 doi: 10.1074/jbc.RA119.009093

Costa-Mattioli, M., Sossin, W. S., Klann, E., & Sonenberg, N. (2009, jan). Translational Control of Long-Lasting Synaptic Plasticity and Memory. *Neuron*, *61*(1), 10–26. Retrieved from https://linkinghub.elsevier.com/retrieve/pii/S0896627308010891 doi: 10.1016/j.neuron.2008.10.055

Courtney, N. L., Mole, A. J., Thomson, A. K., & Murray, L. M. (2019, jul). Reduced P53 levels ameliorate neuromuscular junction loss without affecting motor neuron pathology in a mouse model of spinal muscular atrophy. *Cell Death Dis.*, *10*(7), 515. Retrieved from http://www.nature.com/articles/s41419-019-1727-6 doi: 10.1038/s41419-019-1727-6

Cunningham, J. T., Rodgers, J. T., Arlow, D. H., Vazquez, F., Mootha, V. K., & Puigserver, P. (2007). mTOR controls mitochondrial oxidative function through a YY1-PGC-1α transcriptional complex. *Nature*, *450*(7170), 736–740. doi: 10.1038/nature06322

Custer, S. K., Gilson, T. D., Li, H., Todd, A. G., Astroski, J. W., Lin, H., ... Androphy, E. J. (2016, oct). Altered mRNA Splicing in SMN-Depleted Motor Neuron-Like Cells. *PLoS One*, *11*(10), e0163954. Retrieved from https://dx.plos.org/10.1371/journal.pone.0163954 doi: 10.1371/journal.pone.0163954

Daffis, S., Szretter, K. J., Schriewer, J., Li, J., Youn, S., Errett, J., ... Diamond, M. S. (2010, nov). 2'-O methylation of the viral mRNA cap evades host restriction by IFIT family members. *Nature*, *468*(7322), 452–456. Retrieved from http://www.nature.com/articles/nature09489 doi: 10.1038/nature09489

Dagda, R. K., Zhu, J., Kulich, S. M., & Chu, C. T. (2008, aug). Mitochondrially localized ERK2 regulates mitophagy and autophagic cell stress: implications for Parkinson's disease. *Autophagy*, *4*(6), 770–82. Retrieved from http://www.ncbi.nlm.nih.gov/pubmed/18594198http://www.pubmedcentral.nih.gov/articlerender.fcgi?artid=PMC2574804 doi: 10.4161/auto.6458

Dalle-Donne, I., Giustarini, D., Colombo, R., Rossi, R., & Milzani, A. (2003, apr). Protein carbonylation in human diseases. *Trends Mol. Med.*, *9*(4), 169–176. Retrieved from https://linkinghub.elsevier.com/retrieve/pii/S1471491403000315 doi: 10.1016/S1471-4914(03)00031-5

Davis, R. E., & Williams, M. (2012, sep). Mitochondrial Function and Dysfunction: An Update. *J. Pharmacol. Exp. Ther.*, *342*(3), 598–607. Retrieved from http://jpet.aspetjournals.org/lookup/doi/10.1124/jpet.112.192104 doi: 10.1124/jpet.112.192104

De Benedetti, A., & Graff, J. R. (2004, apr). eIF-4E expression and its role in malignancies and metastases. *Oncogene*, *23*(18), 3189–3199. Retrieved from http://www.nature.com/articles/1207545 doi: 10.1038/sj.onc.1207545

Debernardi, R., Pierre, K., Lengacher, S., Magistretti, P. J., & Pellerin, L. (2003, jul). Cell-specific expression pattern of monocarboxylate transporters in astrocytes and neurons observed in different mouse brain cortical cell cultures. *J. Neurosci. Res.*, *73*(2), 141–155. Retrieved from http://doi.wiley.com/10.1002/jnr.10660 doi: 10.1002/jnr.10660

Dennis, M. D., Jefferson, L. S., & Kimball, S. R. (2012, dec). Role of p70S6K1-mediated Phosphorylation of eIF4B and PDCD4 Proteins in the Regulation of Protein Synthesis. *J. Biol. Chem.*, *287*(51), 42890–42899. Retrieved from http://www.jbc.org/lookup/doi/10.1074/jbc.M112.404822 doi: 10.1074/jbc.M112.404822

Dennis, M. Y., Harshman, L., Nelson, B. J., Penn, O., Cantsilieris, S., Huddleston, J., ... Eichler, E. E. (2017, mar). The evolution and population diversity of human-specific segmental duplications. *Nat. Ecol. Evol.*, *1*(3), 0069. Retrieved from http://www.nature.com/articles/s41559-016-0069 doi: 10.1038/s41559-016-0069

Desagher, S., Glowinski, J., & Prémont, J. (1997). Pyruvate protects neurons against hydrogen peroxide-induced toxicity. *J. Neurosci.*, *17*(23), 9060–9067. doi: 10.1523/jneurosci.17-23-09060.1997

Díaz-García, C. M., Mongeon, R., Lahmann, C., Koveal, D., Zucker, H., & Yellen, G. (2017, aug). Neuronal Stimulation Triggers Neuronal Glycolysis and Not Lactate Uptake. *Cell Metab.*, *26*(2), 361–374.e4. Retrieved from http://linkinghub.elsevier.com/retrieve/pii/S1550413117304217 doi: 10.1016/j.cmet.2017.06.021

Díaz-García, C. M., & Yellen, G. (2019, aug). Neurons rely on glucose rather than astrocytic lactate during stimulation. *J. Neurosci. Res.*, *97*(8), 883–889. Retrieved from https://onlinelibrary.wiley.com/doi/abs/10.1002/jnr.24374 doi: 10.1002/jnr.24374

Dimmer, K. S., Friedrich, B., Lang, F., Deitmer, J. W., & Bröer, S. (2000, aug). The low-affinity monocarboxylate transporter MCT4 is adapted to the export of lactate in highly glycolytic cells. *Biochem. J.*, *350 Pt 1*(Pt 1), 219–227. Retrieved from https://pubmed.ncbi.nlm.nih.gov/10926847https://www.ncbi.nlm.nih.gov/pmc/articles/PMC1221245/

Dodd, K. M., Yang, J., Shen, M. H., Sampson, J. R., & Tee, A. R. (2015, apr). mTORC1 drives HIF-1α and VEGF-A signalling via multiple mechanisms involving 4E-BP1, S6K1 and STAT3. *Oncogene*, *34*(17), 2239–2250. Retrieved from http://www.nature.com/articles/onc2014164 doi: 10.1038/onc.2014.164

Dombert, B., Sivadasan, R., Simon, C. M., Jablonka, S., & Sendtner, M. (2014, oct). Presynaptic Localization of Smn and hnRNP R in Axon Terminals of Embryonic and Postnatal Mouse Motoneurons. *PLoS One*, *9*(10), e110846. Retrieved from https://dx.plos.org/10.1371/journal.pone.0110846 doi: 10.1371/journal.pone.0110846

Dorrello, N. V., Peschiaroli, A., Guardavaccaro, D., Colburn, N. H., Sherman, N. E., & Pagano, M. (2006, oct). S6K1- and TRCP-Mediated Degradation of PDCD4 Promotes Protein Translation and Cell Growth. *Science (80-.).*, *314*(5798), 467–471. Retrieved from https://www.sciencemag.org/lookup/doi/10.1126/science.1130276 doi: 10.1126/science.1130276

Duarte, F. V., Palmeira, C. M., & Rolo, A. P. (2014, sep). The Role of microRNAs in Mitochondria: Small Players Acting Wide. *Genes (Basel).*, *5*(4), 865–886. Retrieved from http://www.mdpi.com/2073-4425/5/4/865 doi: 10.3390/genes5040865

Dubowitz, V. (1999, jan). Very severe spinal muscular atrophy (SMA type 0): an expanding clinical phenotype. *Eur. J. Paediatr. Neurol.*, *3*(2), 49–51. Retrieved from https://linkinghub.elsevier.com/retrieve/pii/S1090379899800129 doi: 10.1016/S1090-3798(99)80012-9

Duque, S. I., Arnold, W. D., Odermatt, P., Li, X., Porensky, P. N., Schmelzer, L., ... Burghes, A. H. M. (2015, mar). A large animal model of spinal muscular atrophy and correction

of phenotype. *Ann. Neurol.*, *77*(3), 399–414. Retrieved from https://doi.org/10.1002/ana.24332http://doi.wiley.com/10.1002/ana.24332 doi: 10.1002/ana.24332

Edens, B. M., Ajroud-Driss, S., Ma, L., & Ma, Y. C. (2015). Molecular mechanisms and animal models of spinal muscular atrophy. *Biochim. Biophys. Acta - Mol. Basis Dis.*, *1852*(4), 685–692. Retrieved from http://dx.doi.org/10.1016/j.bbadis.2014.07.024 doi: 10.1016/j.bbadis.2014.07.024

Eggett, C. J., Crosier, S., Manning, P., Cookson, M. R., Menzies, F. M., McNeil, C. J., & Shaw, P. J. (2008, jul). Development and Characterisation of a Glutamate-Sensitive Motor Neurone Cell Line. *J. Neurochem.*, *74*(5), 1895–1902. Retrieved from http://www.ncbi.nlm.nih.gov/pubmed/10800932http://doi.wiley.com/10.1046/j.1471-4159.2000.0741895.x doi: 10.1046/j.1471-4159.2000.0741895.x

Elliott, B. A., Ho, H.-T., Ranganathan, S. V., Vangaveti, S., Ilkayeva, O., Abou Assi, H., ... Holley, C. L. (2019, dec). Modification of messenger RNA by 2'-O-methylation regulates gene expression in vivo. *Nat. Commun.*, *10*(1), 3401. Retrieved from http://www.nature.com/articles/s41467-019-11375-7 doi: 10.1038/s41467-019-11375-7

Engl, E., & Attwell, D. (2015, aug). Non-signalling energy use in the brain. *J. Physiol.*, *593*(16), 3417–3429. Retrieved from http://doi.wiley.com/10.1113/jphysiol.2014.282517 doi: 10.1113/jphysiol.2014.282517

Fallini, C., Donlin-Asp, P. G., Rouanet, J. P., Bassell, G. J., & Rossoll, W. (2016, mar). Deficiency of the Survival of Motor Neuron Protein Impairs mRNA Localization and Local Translation in the Growth Cone of Motor Neurons. *J. Neurosci.*, *36*(13), 3811–3820. Retrieved from http://www.ncbi.nlm.nih.gov/pubmed/27030765http://www.pubmedcentral.nih.gov/articlerender.fcgi?artid=PMC4812137http://www.jneurosci.org/lookup/doi/10.1523/JNEUROSCI.2396-15.2016 doi: 10.1523/JNEUROSCI.2396-15.2016

Fallini, C., Rouanet, J. P., Donlin-Asp, P. G., Guo, P., Zhang, H., Singer, R. H., ... Bassell, G. J. (2014, mar). Dynamics of survival of motor neuron (SMN) protein interaction with the mRNA-binding protein IMP1 facilitates its trafficking into motor neuron axons. *Dev. Neurobiol.*, *74*(3), 319–332. Retrieved from http://doi.wiley.com/10.1002/dneu.22111 doi: 10.1002/dneu.22111

Fallini, C., Zhang, H., Su, Y., Silani, V., Singer, R. H., Rossoll, W., & Bassell, G. J. (2011, mar). The Survival of Motor Neuron (SMN) Protein Interacts with the mRNA-Binding Protein HuD and Regulates Localization of Poly(A) mRNA in Primary Motor Neuron Axons. *J. Neurosci.*, *31*(10), 3914–3925. Retrieved from http://www.jneurosci.org/cgi/doi/10.1523/JNEUROSCI.3631-10.2011 doi: 10.1523/JNEUROSCI.3631-10.2011

Fan, F., & Wood, K. V. (2007, feb). Bioluminescent Assays for High-Throughput Screening. *Assay Drug Dev. Technol.*, *5*(1), 127–136. Retrieved from http://www.liebertpub.com/doi/10.1089/adt.2006.053 doi: 10.1089/adt.2006.053

Farrar, M. A., & Kiernan, M. C. (2015, apr). The Genetics of Spinal Muscular Atrophy: Progress and Challenges. *Neurotherapeutics*, *12*(2), 290–302. Retrieved from http://link.springer.com/10.1007/s13311-014-0314-x doi: 10.1007/s13311-014-0314-x

Farrar, M. A., Park, S. B., Vucic, S., Carey, K. A., Turner, B. J., Gillingwater, T. H., ... Kiernan, M. C. (2017, mar). Emerging therapies and challenges in spinal muscular atrophy. *Ann. Neurol.*, *81*(3), 355–368. Retrieved from http://doi.wiley.com/10.1002/ana.24864 doi: 10.1002/ana.24864

Farrar, M. A., Vucic, S., Johnston, H. M., du Sart, D., & Kiernan, M. C. (2013, jan). Pathophysiological Insights Derived by Natural History and Motor Function of Spinal Muscular Atrophy. *J. Pediatr.*, *162*(1), 155–159. Retrieved from https://linkinghub.elsevier.com/retrieve/pii/S0022347612006737 doi: 10.1016/j.jpeds.2012.05.067

Feldkötter, M., Schwarzer, V., Wirth, R., Wienker, T. F., & Wirth, B. (2002). Quantitative analyses of SMN1 and SMN2 based on real-time lightcycler PCR: Fast and highly reliable carrier testing and prediction of severity of spinal muscular atrophy. *Am. J. Hum. Genet.*, *70*(2), 358–368. doi: 10.1086/338627

Fernandopulle, M. S., Lippincott-Schwartz, J., & Ward, M. E. (2021, jan). RNA transport and local translation in neurodevelopmental and neurodegenerative disease. *Nat. Neurosci.*. Retrieved from http://dx.doi.org/10.1038/s41593-020-00785-2http://www.nature.com/articles/s41593-020-00785-2 doi: 10.1038/s41593-020-00785-2

Ferrante, R. J., Browne, S. E., Shinobu, L. A., Bowling, A. C., Baik, M. J., MacGarvey, U., ... Beal, M. F. (2002, nov). Evidence of Increased Oxidative Damage in Both Sporadic and Familial Amyotrophic Lateral Sclerosis. *J. Neurochem.*, *69*(5), 2064–2074. Retrieved from http://doi.wiley.com/10.1046/j.1471-4159.1997.69052064.x doi: 10.1046/j.1471-4159.1997.69052064.x

Ferri, A., Cozzolino, M., Crosio, C., Nencini, M., Casciati, A., Gralla, E. B., ... Carri, M. T. (2006, sep). Familial ALS-superoxide dismutases associate with mitochondria and shift their redox potentials. *Proc. Natl. Acad. Sci.*, *103*(37), 13860–13865. Retrieved from http://www.pnas.org/cgi/doi/10.1073/pnas.0605814103 doi: 10.1073/pnas.0605814103

Finkel, R. S., Mercuri, E., Darras, B. T., Connolly, A. M., Kuntz, N. L., Kirschner, J., ... ENDEAR Study Group (2017). Nusinersen versus Sham Control in Infantile-Onset Spinal Muscular Atrophy. *N. Engl. J. Med.*, *377*(18), 1723–1732. Retrieved from http://www.ncbi.nlm.nih.gov/pubmed/29091570 doi: 10.1056/NEJMoa1702752

Finkel, R. S., Mercuri, E., Meyer, O. H., Simonds, A. K., Schroth, M. K., Graham, R. J., ... Sejersen, T. (2018, mar). Diagnosis and management of spinal muscular atrophy: Part 2: Pulmonary and acute care; medications, supplements and immunizations; other organ systems; and ethics. *Neuromuscul. Disord.*, *28*(3), 197–207. Retrieved from https://linkinghub.elsevier.com/retrieve/pii/S0960896617312907 doi: 10.1016/j.nmd.2017.11.004

Forman, H. J., & Kennedy, J. A. (1974, oct). Role of superoxide radical in mitochondrial dehydrogenase reactions. *Biochem. Biophys. Res. Commun.*, *60*(3), 1044–1050. Retrieved from https://linkinghub.elsevier.com/retrieve/pii/0006291X74904185 doi: 10.1016/0006-291X(74)90418-5

Frugier, T., Tiziano, F. D., Cifuentes-Diaz, C., Miniou, P., Roblot, N., Dierich, A., ... Melki, J. (2000, mar). Nuclear targeting defect of SMN lacking the C-terminus in a mouse model of spinal muscular atrophy. *Hum. Mol. Genet.*, *9*(5), 849–858. Retrieved from https://doi.org/10.1093/hmg/9.5.849https://academic.oup.com/hmg/article-lookup/doi/10.1093/hmg/9.5.849http://www.ncbi.nlm.nih.gov/pubmed/10749994 doi: 10.1093/hmg/9.5.849

Fukui, H., & Moraes, C. T. (2008, may). The mitochondrial impairment, oxidative stress and neurodegeneration connection: reality or just an attractive hypothesis? *Trends Neurosci.*, *31*(5), 251–256. Retrieved from https://pubmed.ncbi.nlm.nih.gov/18403030https://www.ncbi.nlm.nih.gov/pmc/articles/PMC2731695/https://linkinghub.elsevier.com/retrieve/pii/S0166223608000957 doi: 10.1016/j.tins.2008.02.008

Gao, M., Fritz, D. T., Ford, L. P., & Wilusz, J. (2000, mar). Interaction between a Poly(A)-Specific Ribonuclease and the 5' Cap Influences mRNA Deadenylation Rates In Vitro. *Mol. Cell*, *5*(3), 479–488. Retrieved from https://linkinghub.elsevier.com/retrieve/pii/S1097276500804426 doi: 10.1016/S1097-2765(00)80442-6

Gao, X., Xu, J., Chen, H., Xue, D., Pan, W., Zhou, C., ... Ma, L. (2019, may). Defective Expression of Mitochondrial, Vacuolar H+-ATPase and Histone Genes in a C. elegans Model of SMA. *Front. Genet.*, *10*. Retrieved from https://www.frontiersin.org/article/10.3389/fgene.2019.00410/full doi: 10.3389/fgene.2019.00410

Gebauer, F., & Hentze, M. W. (2004, oct). Molecular mechanisms of translational control. *Nat. Rev. Mol. Cell Biol.*, *5*(10), 827–835. Retrieved from http://www.nature.com/articles/nrm1488 doi: 10.1038/nrm1488

Gerhart, D. Z., Broderius, M. A., Borson, N. D., & Drewes, L. R. (1992, jan). Neurons and microvessels express the brain glucose transporter protein GLUT3. *Proc. Natl. Acad. Sci.*, *89*(2), 733–737. Retrieved from http://www.pnas.org/cgi/doi/10.1073/pnas.89.2.733 doi: 10.1073/pnas.89.2.733

Ghasemi, A., & Zahediasl, S. (2012, dec). Normality Tests for Statistical Analysis: A Guide for Non-Statisticians. *Int. J. Endocrinol. Metab.*, *10*(2), 486–489. Retrieved from https://sites.kowsarpub.com/ijem/articles/71904.html doi: 10.5812/ijem.3505

Giavazzi, A., Setola, V., Simonati, A., & Battaglia, G. (2006, mar). Neuronal-Specific Roles of the Survival Motor Neuron Protein. *J. Neuropathol. Exp. Neurol.*, *65*(3), 267–277. Retrieved from https://academic.oup.com/jnen/article-lookup/doi/10.1097/01.jnen.0000205144.54457.a3 doi: 10.1097/01.jnen.0000205144.54457.a3

Gilliam, T. C., Brzustowicz, L. M., Castilla, L. H., Lehner, T., Penchaszadeh, G. K., Daniels, R. J., ... Davies, K. E. (1990, jun). Genetic homogeneity between acute and chronic forms of spinal muscular atrophy. *Nature*, *345*(6278), 823–825. Retrieved from http://www.nature.com/articles/345823a0 doi: 10.1038/345823a0

Gingras, A.-C., Gygi, S. P., Raught, B., Polakiewicz, R. D., Abraham, R. T., Hoekstra, M. F., ... Sonenberg, N. (1999, jun). Regulation of 4E-BP1 phosphorylation: a novel two-step mechanism. *Genes Dev.*, *13*(11), 1422–1437. Retrieved from http://www.genesdev.org/cgi/doi/10.1101/gad.13.11.1422 doi: 10.1101/gad.13.11.1422

Girard, C., Verheggen, C., Neel, H., Cammas, A., Vagner, S., Soret, J., ... Bordonné, R. (2008, jan). Characterization of a Short Isoform of Human Tgs1 Hypermethylase Associating with Small Nucleolar Ribonucleoprotein Core Proteins and Produced by Limited Proteolytic Processing. *J. Biol. Chem.*, *283*(4), 2060–2069. Retrieved from https://linkinghub.elsevier.com/retrieve/pii/S0021925820776398 doi: 10.1074/jbc.M704209200

Gogliotti, R. G., Quinlan, K. A., Barlow, C. B., Heier, C. R., Heckman, C. J., & DiDonato, C. J. (2012, mar). Motor Neuron Rescue in Spinal Muscular Atrophy Mice Demonstrates That Sensory-Motor Defects Are a Consequence, Not a Cause, of Motor Neuron Dysfunction. *J. Neurosci.*, *32*(11), 3818–3829. Retrieved from http://www.jneurosci.org/cgi/doi/10.1523/JNEUROSCI.5775-11.2012 doi: 10.1523/JNEUROSCI.5775-11.2012

Gonçalves, I. D. C. G., Brecht, J., Thelen, M. P., Rehorst, W. A., Peters, M., Lee, H. J., ... Kye, M. J. (2018, dec). Neuronal activity regulates DROSHA via autophagy in spinal muscular atrophy. *Sci. Rep.*, *8*(1). doi: 10.1038/s41598-018-26347-y

Granata, C., Merlini, L., Magni, E., Marini, M. L., & Stagni, S. B. (1989, jul). Spinal Muscular Atrophy: Natural History and Orthopaedic Treatment of Scoliosis. *Spine (Phila. Pa. 1976).*, *14*(7), 760–762. Retrieved from http://journals.lww.com/00007632-198907000-00019 doi: 10.1097/00007632-198907000-00019

Grimmler, M., Bauer, L., Nousiainen, M., Körner, R., Meister, G., & Fischer, U. (2005, jan). Phosphorylation regulates the activity of the SMN complex during assembly of spliceosomal U snRNPs. *EMBO Rep.*, *6*(1), 70–76. Retrieved from https://onlinelibrary.wiley.com/doi/abs/10.1038/sj.embor.7400301 doi: 10.1038/sj.embor.7400301

Groen, E. J. N., Perenthaler, E., Courtney, N. L., Jordan, C. Y., Shorrock, H. K., van der Hoorn, D., ... Gillingwater, T. H. (2018, aug). Temporal and tissue-specific variability of SMN protein levels in mouse models of spinal muscular atrophy. *Hum. Mol. Genet.*, *27*(16), 2851–2862. Retrieved from https://academic.oup.com/hmg/article/27/16/2851/5001458 doi: 10.1093/hmg/ddy195

Gross, J. D., Moerke, N. J., von der Haar, T., Lugovskoy, A. A., Sachs, A. B., McCarthy, J. E., & Wagner, G. (2003, dec). Ribosome Loading onto the mRNA Cap Is Driven by Conformational Coupling between eIF4G and eIF4E. *Cell*, *115*(6), 739–750. Retrieved from https://linkinghub.elsevier.com/retrieve/pii/S0092867403009759 doi: 10.1016/S0092-8674(03)00975-9

Gubitz, A. (2004, may). The SMN complex. *Exp. Cell Res.*, *296*(1), 51–56. Retrieved from https://linkinghub.elsevier.com/retrieve/pii/S0014482704001338 doi: 10.1016/j.yexcr.2004.03.022

Günther, R., Wurster, C. D., Cordts, I., Koch, J. C., Kamm, C., Petzold, D., ... Hermann, A. (2019, nov). Patient-Reported Prevalence of Non-motor Symptoms Is Low in Adult Patients Suffering From 5q Spinal Muscular Atrophy. *Front. Neurol.*, *10*. Retrieved from https://www.frontiersin.org/article/10.3389/fneur.2019.01098/full doi: 10.3389/fneur.2019.01098

Haghighat, A., Mader, S., Pause, A., & Sonenberg, N. (1995, nov). Repression of cap-dependent translation by 4E-binding protein 1: competition with p220 for binding to eukaryotic initiation factor-4E. *EMBO J.*, *14*(22), 5701–5709. Retrieved from http://doi.wiley.com/10.1002/j.1460-2075.1995.tb00257.x doi: 10.1002/j.1460-2075.1995.tb00257.x

Hahnen, E., Schonling, J., Rudnik-Schoneborn, S., Raschke, H., Zerres, K., & Wirth, B. (1997, may). Missense Mutations in Exon 6 of the Survival Motor Neuron Gene in Patients with Spinal Muscular Atrophy (SMA). *Hum. Mol. Genet.*, *6*(5), 821–825. Retrieved from https://academic.oup.com/hmg/article-lookup/doi/10.1093/hmg/6.5.821 doi: 10.1093/hmg/6.5.821

Halestrap, A. P. (2013, oct). Monocarboxylic Acid Transport. *Compr. Physiol.*, 1611–1643. Retrieved from https://doi.org/10.1002/cphy.c130008 doi: https://doi.org/10.1002/cphy.c130008

Halestrap, A. P., & Meredith, D. (2004). The SLC16 gene family—from monocarboxylate transporters (MCTs) to aromatic amino acid transporters and beyond. *Pflügers Arch.*, *447*(5), 619–628. Retrieved from https://doi.org/10.1007/s00424-003-1067-2 doi: 10.1007/s00424-003-1067-2

Hamilton, G., & Gillingwater, T. H. (2013, jan). Spinal muscular atrophy: going beyond the motor neuron. *Trends Mol. Med.*, *19*(1), 40–50. Retrieved from https://linkinghub.elsevier.com/retrieve/pii/S1471491412002109 doi: 10.1016/j.molmed.2012.11.002

Hamm, J., Darzynkiewicz, E., Tahara, S. M., & Mattaj, I. W. (1990, aug). The trimethylguanosine cap structure of U1 snRNA is a component of a bipartite nuclear targeting signal. *Cell*, *62*(3), 569–77. Retrieved from http://www.ncbi.nlm.nih.gov/pubmed/2143105 doi: 10.1016/0092-8674(90)90021-6

Hara, K., Yonezawa, K., Kozlowski, M. T., Sugimoto, T., Andrabi, K., Weng, Q.-P. P., ... Avruch, J. (1997, oct). Regulation of eIF-4E BP1 Phosphorylation by mTOR. *J. Biol. Chem.*, *272*(42), 26457–26463. Retrieved from http://www.jbc.org/lookup/doi/10.1074/jbc.272.42.26457 doi: 10.1074/jbc.272.42.26457

Hara, T., & Mizushima, N. (2009). Role of ULK-FIP200 complex in mammalian autophagy: FIP200, a counterpart of yeast Atg17? *Autophagy*, *5*(1), 85–87. doi: 10.4161/auto.5.1.7180

Harding, B. N., Kariya, S., Monani, U. R., Chung, W. K., Benton, M., Yum, S. W., ... Finkel, R. S. (2015, jan). Spectrum of Neuropathophysiology in Spinal Muscular Atrophy

Type I. *J. Neuropathol. Exp. Neurol.*, *74*(1), 15–24. Retrieved from https://academic.oup.com/jnen/article-lookup/doi/10.1097/NEN.0000000000000144 doi: 10.1097/NEN.0000000000000144

Harris, J. J., & Attwell, D. (2012, jan). The Energetics of CNS White Matter. *J. Neurosci.*, *32*(1), 356–371. Retrieved from http://www.jneurosci.org/cgi/doi/10.1523/JNEUROSCI.3430-11.2012 doi: 10.1523/JNEUROSCI.3430-11.2012

Harris, J. J., Jolivet, R., & Attwell, D. (2012, sep). Synaptic Energy Use and Supply. *Neuron*, *75*(5), 762–777. Retrieved from http://dx.doi.org/10.1016/j.neuron.2012.08.019http://linkinghub.elsevier.com/retrieve/pii/S0896627312007568https://linkinghub.elsevier.com/retrieve/pii/S0896627312007568 doi: 10.1016/j.neuron.2012.08.019

Hauser, D. N., & Hastings, T. G. (2013, mar). *Mitochondrial dysfunction and oxidative stress in Parkinson's disease and monogenic parkinsonism* (Vol. 51). Retrieved from http://www.sciencedirect.com/science/article/pii/S0969996112003397https://linkinghub.elsevier.com/retrieve/pii/S0969996112003397 doi: 10.1016/j.nbd.2012.10.011

Hayashi, M., Araki, S., Arai, N., Kumada, S., Itoh, M., Tamagawa, K., ... Morimatsu, Y. (2002). Oxidative stress and disturbed glutamate transport in spinal muscular atrophy. *Brain Dev.*, *24*(8), 770–5. Retrieved from http://www.ncbi.nlm.nih.gov/pubmed/12453601 doi: 10.1016/S0387-7604(02)00103-1

Hellbach, N., Peterson, S., Haehnke, D., Shankar, A., LaBarge, S., Pivaroff, C., ... Metzger, F. (2018, oct). Impaired myogenic development, differentiation and function in hESC-derived SMA myoblasts and myotubes. *PLoS One*, *13*(10), e0205589. Retrieved from https://dx.plos.org/10.1371/journal.pone.0205589 doi: 10.1371/journal.pone.0205589

Hensel, N., Kubinski, S., & Claus, P. (2020). The Need for SMN-Independent Treatments of Spinal Muscular Atrophy (SMA) to Complement SMN-Enhancing Drugs. *Front. Neurol.*, *11*, 45. Retrieved from http://www.ncbi.nlm.nih.gov/pubmed/32117013http://www.pubmedcentral.nih.gov/articlerender.fcgi?artid=PMC7009174 doi: 10.3389/fneur.2020.00045

Hernandez-Gerez, E., Dall'Angelo, S., Collinson, J. M., Fleming, I. N., & Parson, S. H. (2020). Widespread tissue hypoxia dysregulates cell and metabolic pathways in SMA. *Ann. Clin. Transl. Neurol.*, *7*(9), 1580–1593. Retrieved from http://www.ncbi.nlm.nih.gov/pubmed/32790171http://www.pubmedcentral.nih.gov/articlerender.fcgi?artid=PMC7480929 doi: 10.1002/acn3.51134

Hinnebusch, A. G. (2014, jun). The Scanning Mechanism of Eukaryotic Translation Initiation. *Annu. Rev. Biochem.*, *83*(1), 779–812. Retrieved from http://www.annualreviews.org/doi/10.1146/annurev-biochem-060713-035802 doi: 10.1146/annurev-biochem-060713-035802

Hirst, J. (2011, jul). Why does mitochondrial complex I have so many subunits? *Biochem. J.*, *437*(2), e1–e3. Retrieved from https://portlandpress.com/biochemj/article/437/2/e1/45606/Why-does-mitochondrial-complex-I-have-so-many doi: 10.1042/BJ20110918

Holm, S. (1979). A Simple Sequentially Rejective Multiple Test Procedure. *Scand. J. Stat.*, *6*(2), 65–70. Retrieved from www.jstor.org/stable/4615733

Holt, C. E., Martin, K. C., & Schuman, E. M. (2019). Local translation in neurons: visualization and function. *Nat. Struct. Mol. Biol.*, *26*(7), 557–566. Retrieved from http://dx.doi.org/10.1038/s41594-019-0263-5 doi: 10.1038/s41594-019-0263-5

Hornburg, D., Drepper, C., Butter, F., Meissner, F., Sendtner, M., & Mann, M. (2014). Deep proteomic evaluation of primary and cell line motoneuron disease models delineates major differences in neuronal characteristics. *Mol. Cell. Proteomics*, *13*(12), 3410–3420. doi: 10.1074/mcp.M113.037291

Hosseinibarkooie, S., Peters, M., Torres-Benito, L., Rastetter, R. H., Hupperich, K., Hoffmann, A., ... Wirth, B. (2016, sep). The Power of Human Protective Modifiers: PLS3 and CORO1C Unravel Impaired Endocytosis in Spinal Muscular Atrophy and Rescue SMA Phenotype. *Am. J. Hum. Genet.*, *99*(3), 647–665. Retrieved from https://linkinghub.elsevier.com/retrieve/pii/S0002929716302889 doi: 10.1016/j.ajhg.2016.07.014

Howarth, C., Gleeson, P., & Attwell, D. (2012, jul). Updated Energy Budgets for Neural Computation in the Neocortex and Cerebellum. *J. Cereb. Blood Flow Metab.*, *32*(7), 1222–1232. Retrieved from http://journals.sagepub.com/doi/10.1038/jcbfm.2012.35 doi: 10.1038/jcbfm.2012.35

Howarth, C., Peppiatt-Wildman, C. M., & Attwell, D. (2010, feb). The Energy Use Associated with Neural Computation in the Cerebellum. *J. Cereb. Blood Flow Metab.*, *30*(2), 403–414. Retrieved from http://journals.sagepub.com/doi/10.1038/jcbfm.2009.231 doi: 10.1038/jcbfm.2009.231

Hsieh-Li, H. M., Chang, J. G., Jong, Y. J., Wu, M. H., Wang, N. M., Tsai, C. H., & Li, H. (2000, jan). A mouse model for spinal muscular atrophy. *Nat. Genet.*, *24*(1), 66–70. Retrieved from http://www.nature.com/doifinder/10.1038/71709http://www.ncbi.nlm.nih.gov/pubmed/10615130 doi: 10.1038/71709

Hua, Y., Vickers, T. A., Okunola, H. L., Bennett, C. F., & Krainer, A. R. (2008, apr). Antisense Masking of an hnRNP A1/A2 Intronic Splicing Silencer Corrects SMN2 Splicing in Transgenic Mice. *Am. J. Hum. Genet.*, *82*(4), 834–848. Retrieved from https://linkinghub.elsevier.com/retrieve/pii/S0002929708001638 doi: 10.1016/j.ajhg.2008.01.014

Huber, K. M., Klann, E., Costa-Mattioli, M., & Zukin, R. S. (2015, oct). Dysregulation of Mammalian Target of Rapamycin Signaling in Mouse Models of Autism. *J. Neurosci.*, *35*(41), 13836–13842. Retrieved from http://www.jneurosci.org/cgi/doi/10.1523/JNEUROSCI.2656-15.2015 doi: 10.1523/JNEUROSCI.2656-15.2015

Hubers, L., Valderrama-Carvajal, H., Laframboise, J., Timbers, J., Sanchez, G., & Côté, J. (2011, feb). HuD interacts with survival motor neuron protein and can rescue spinal muscular atrophy-like neuronal defects. *Hum. Mol. Genet.*, *20*(3), 553–579. Retrieved from

https://academic.oup.com/hmg/article-lookup/doi/10.1093/hmg/ddq500 doi: 10.1093/hmg/ddq500

Hüttelmaier, S., Zenklusen, D., Lederer, M., Dictenberg, J., Lorenz, M., Meng, X., ... Singer, R. H. (2005, nov). Spatial regulation of β-actin translation by Src-dependent phosphorylation of ZBP1. *Nature*, *438*(7067), 512–515. Retrieved from http://www.nature.com/articles/nature04115 doi: 10.1038/nature04115

Iadevaia, V., Caldarola, S., Tino, E., Amaldi, F., & Loreni, F. (2008, jul). All translation elongation factors and the e, f, and h subunits of translation initiation factor 3 are encoded by 5'-terminal oligopyrimidine (TOP) mRNAs. *RNA*, *14*(9), 1730–1736. Retrieved from http://www.rnajournal.org/cgi/doi/10.1261/rna.1037108 doi: 10.1261/rna.1037108

Iyer, C. C., McGovern, V. L., Murray, J. D., Gombash, S. E., Zaworski, P. G., Foust, K. D., ... Burghes, A. H. (2015, nov). Low levels of Survival Motor Neuron protein are sufficient for normal muscle function in the SMNΔ7 mouse model of SMA. *Hum. Mol. Genet.*, *24*(21), 6160–6173. Retrieved from https://academic.oup.com/hmg/article-lookup/doi/10.1093/hmg/ddv332 doi: 10.1093/hmg/ddv332

Jablonka, S., Beck, M., Lechner, B. D., Mayer, C., & Sendtner, M. (2007, oct). Defective Ca2+ channel clustering in axon terminals disturbs excitability in motoneurons in spinal muscular atrophy. *J. Cell Biol.*, *179*(1), 139–149. Retrieved from https://rupress.org/jcb/article/179/1/139/34887/Defective-Ca2-channel-clustering-in-axon-terminals doi: 10.1083/jcb.200703187

Jablonka, S., & Sendtner, M. (2017, sep). Developmental regulation of SMN expression: pathophysiological implications and perspectives for therapy development in spinal muscular atrophy. *Gene Ther.*, *24*(9), 506–513. Retrieved from http://www.nature.com/articles/gt201746 doi: 10.1038/gt.2017.46

Jacinto, E., Loewith, R., Schmidt, A., Lin, S., Rüegg, M. A., Hall, A., & Hall, M. N. (2004, nov). Mammalian TOR complex 2 controls the actin cytoskeleton and is rapamycin insensitive. *Nat. Cell Biol.*, *6*(11), 1122–1128. Retrieved from http://www.nature.com/articles/ncb1183 doi: 10.1038/ncb1183

Jackson, R. J. (1991, sep). The ATP requirement for initiation of eukaryotic translation varies according to the mRNA species. *Eur. J. Biochem.*, *200*(2), 285–294. Retrieved from http://doi.wiley.com/10.1111/j.1432-1033.1991.tb16184.x doi: 10.1111/j.1432-1033.1991.tb16184.x

Jackson, R. J., Hellen, C. U. T., & Pestova, T. V. (2010, feb). The mechanism of eukaryotic translation initiation and principles of its regulation. *Nat. Rev. Mol. Cell Biol.*, *11*(2), 113–127. Retrieved from http://www.nature.com/articles/nrm2838 doi: 10.1038/nrm2838

Jambhekar, A., & DeRisi, J. L. (2007, may). Cis-acting determinants of asymmetric, cytoplasmic RNA transport. *RNA*, *13*(5), 625–642. Retrieved from http://www.rnajournal.org/cgi/doi/10.1261/rna.262607 doi: 10.1261/rna.262607

Jang, S. R., Nelson, J. C., Bend, E. G., Rodríguez-Laureano, L., Tueros, F. G., Cartagenova, L., ... Colón-Ramos, D. A. (2016). Glycolytic Enzymes Localize to Synapses under Energy Stress to Support Synaptic Function. *Neuron*, *90*(2), 278–291. doi: 10.1016/j.neuron.2016.03.011

Janzen, E., Mendoza-Ferreira, N., Hosseinibarkooie, S., Schneider, S., Hupperich, K., Tschanz, T., ... Wirth, B. (2018, aug). CHP1 reduction ameliorates spinal muscular atrophy pathology by restoring calcineurin activity and endocytosis. *Brain*, *141*(8), 2343–2361. Retrieved from https://academic.oup.com/brain/article/141/8/2343/5046343 doi: 10.1093/brain/awy167

Jędrzejowska, M., Gos, M., Zimowski, J. G., Kostera-Pruszczyk, A., Ryniewicz, B., & Hausmanowa-Petrusewicz, I. (2014, jul). Novel point mutations in survival motor neuron 1 gene expand the spectrum of phenotypes observed in spinal muscular atrophy patients. *Neuromuscul. Disord.*, *24*(7), 617–623. Retrieved from https://linkinghub.elsevier.com/retrieve/pii/S0960896614001059 doi: 10.1016/j.nmd.2014.04.003

Jensen, P. (1966, aug). Antimycin-insensitive oxidation of succinate and reduced nicotinamide-adenine dinucleotide in electron-transport particles I. pH dependency and hydrogen peroxide formation. *Biochim. Biophys. Acta - Enzymol. Biol. Oxid.*, *122*(2), 157–166. Retrieved from https://linkinghub.elsevier.com/retrieve/pii/0926659366900579 doi: 10.1016/0926-6593(66)90057-9

John, A., Kubosumi, A., & Reddy, P. H. (2020, may). Mitochondrial MicroRNAs in Aging and Neurodegenerative Diseases. *Cells*, *9*(6), 1345. Retrieved from https://www.mdpi.com/2073-4409/9/6/1345 doi: 10.3390/cells9061345

Johri, A., & Beal, M. F. (2012, sep). Mitochondrial Dysfunction in Neurodegenerative Diseases. *J. Pharmacol. Exp. Ther.*, *342*(3), 619–630. Retrieved from http://jpet.aspetjournals.org/lookup/doi/10.1124/jpet.112.192138 doi: 10.1124/jpet.112.192138

Jung, H., & Holt, C. E. (2011, jan). Local translation of mRNAs in neural development. *Wiley Interdiscip. Rev. RNA*, *2*(1), 153–165. Retrieved from http://www.ncbi.nlm.nih.gov/pubmed/21956974http://www.pubmedcentral.nih.gov/articlerender.fcgi?artid=PMC3683645http://doi.wiley.com/10.1002/wrna.53 doi: 10.1002/wrna.53

Kahvejian, A., Svitkin, Y. V., Sukarieh, R., M'Boutchou, M.-N., & Sonenberg, N. (2005, jan). Mammalian poly(A)-binding protein is a eukaryotic translation initiation factor, which acts via multiple mechanisms. *Genes Dev.*, *19*(1), 104–113. Retrieved from http://genesdev.cshlp.org/content/19/1/104.abstract doi: 10.1101/gad.1262905

Kaizuka, T., Hara, T., Oshiro, N., Kikkawa, U., Yonezawa, K., Takehana, K., ... Mizushima, N. (2010, jun). Tti1 and Tel2 Are Critical Factors in Mammalian Target of Rapamycin Complex Assembly. *J. Biol. Chem.*, *285*(26), 20109–20116. Retrieved from http://www.jbc.org/lookup/doi/10.1074/jbc.M110.121699 doi: 10.1074/jbc.M110.121699

Kanehisa, M. (2000, jan). KEGG: Kyoto Encyclopedia of Genes and Genomes. *Nucleic Acids Res.*, *28*(1), 27–30. Retrieved from https://academic.oup.com/nar/article-lookup/doi/10.1093/nar/28.1.27 doi: 10.1093/nar/28.1.27

Kapahi, P., Chen, D., Rogers, A. N., Katewa, S. D., Li, P. W.-L., Thomas, E. L., & Kockel, L. (2010, jun). With TOR, Less Is More: A Key Role for the Conserved Nutrient-Sensing TOR Pathway in Aging. *Cell Metab.*, *11*(6), 453–465. Retrieved from https://linkinghub.elsevier.com/retrieve/pii/S1550413110001531 doi: 10.1016/j.cmet.2010.05.001

Kapur, M., Monaghan, C. E., & Ackerman, S. L. (2017, nov). Regulation of mRNA Translation in Neurons—A Matter of Life and Death. *Neuron*, *96*(3), 616–637. Retrieved from https://doi.org/10.1016/j.neuron.2017.09.057https://linkinghub.elsevier.com/retrieve/pii/S0896627317309261 doi: 10.1016/j.neuron.2017.09.057

Kariya, S., Obis, T., Garone, C., Akay, T., Sera, F., Iwata, S., ... Monani, U. R. (2014, feb). Requirement of enhanced Survival Motoneuron protein imposed during neuromuscular junction maturation. *J. Clin. Invest.*, *124*(2), 785–800. Retrieved from http://www.jci.org/articles/view/72017 doi: 10.1172/JCI72017

Kashima, T., & Manley, J. L. (2003, aug). A negative element in SMN2 exon 7 inhibits splicing in spinal muscular atrophy. *Nat. Genet.*, *34*(4), 460–463. Retrieved from http://www.nature.com/articles/ng1207 doi: 10.1038/ng1207

Kennedy, W. R., Alter, M., & Sung, J. H. (1968, jul). Progressive proximal spinal and bulbar muscular atrophy of late onset: A sex-linked recessive trait. *Neurology*, *18*(7), 671–671. Retrieved from http://www.neurology.org/cgi/doi/10.1212/WNL.18.7.671 doi: 10.1212/WNL.18.7.671

Kety, S. S., & Schmidt, C. F. (1948, jul). The Nitrous Oxide Method for the Quantitative Determination of Cerebral Blood Flow in Man: Theory, Procedure and Normal Values. *J. Clin. Invest.*, *27*(4), 476–483. Retrieved from http://www.jci.org/articles/view/101994 doi: 10.1172/JCI101994

Kiebler, M. A., & Bassell, G. J. (2006, sep). Neuronal RNA Granules: Movers and Makers. *Neuron*, *51*(6), 685–690. Retrieved from https://linkinghub.elsevier.com/retrieve/pii/S089662730600643X doi: 10.1016/j.neuron.2006.08.021

Kim, D.-H., Sarbassov, D. D., Ali, S. M., Latek, R. R., Guntur, K. V., Erdjument-Bromage, H., ... Sabatini, D. M. (2003, apr). GβL, a Positive Regulator of the Rapamycin-Sensitive Pathway Required for the Nutrient-Sensitive Interaction between Raptor and mTOR. *Mol. Cell*, *11*(4), 895–904. Retrieved from https://linkinghub.elsevier.com/retrieve/pii/S109727650300114X doi: 10.1016/S1097-2765(03)00114-X

Kim, H. J., Kim, N. C., Wang, Y.-D., Scarborough, E. A., Moore, J., Diaz, Z., ... Taylor, J. P. (2013, mar). Mutations in prion-like domains in hnRNPA2B1 and hnRNPA1 cause multisystem proteinopathy and ALS. *Nature*, *495*(7442), 467–473. Retrieved from http://www.nature.com/articles/nature11922 doi: 10.1038/nature11922

Kim, J.-K., Caine, C., Awano, T., Herbst, R., & Monani, U. R. (2017, jul). Motor neuronal repletion of the NMJ organizer, Agrin, modulates the severity of the spinal muscular atrophy

disease phenotype in model mice. *Hum. Mol. Genet.*, *26*(13), 2377–2385. Retrieved from https://academic.oup.com/hmg/article/26/13/2377/3098164 doi: 10.1093/hmg/ddx124

Kislauskis, E., & Singer, R. (1992, dec). Determinants of mRNA localization. *Curr. Opin. Cell Biol.*, *4*(6), 975–978. Retrieved from https://linkinghub.elsevier.com/retrieve/pii/095506749290128Y doi: 10.1016/0955-0674(92)90128-Y

Kitaoka, H., Shitara, Y., Uchida, Y., Kondo, U., & Omori, I. (2020, jan). Case of spinal muscular atrophy type 0 with mild prognosis. *Pediatr. Int.*, *62*(1), 106–107. Retrieved from https://onlinelibrary.wiley.com/doi/abs/10.1111/ped.14047 doi: 10.1111/ped.14047

Kładna, A., Marchlewicz, M., Piechowska, T., Kruk, I., & Aboul-Enein, H. Y. (2015, nov). Reactivity of pyruvic acid and its derivatives towards reactive oxygen species. *Luminescence*, *30*(7), 1153–1158. Retrieved from http://doi.wiley.com/10.1002/bio.2879 doi: 10.1002/bio.2879

Klöppel, C., Michels, C., Zimmer, J., Herrmann, J. M., & Riemer, J. (2010, dec). In yeast redistribution of Sod1 to the mitochondrial intermembrane space provides protection against respiration derived oxidative stress. *Biochem. Biophys. Res. Commun.*, *403*(1), 114–119. Retrieved from https://linkinghub.elsevier.com/retrieve/pii/S0006291X10020279 doi: 10.1016/j.bbrc.2010.10.129

Knull, H. R., Bronstein, W. W., DesJardins, P., & Niehaus, W. G. (1980, jan). Interaction of Selected Brain Glycolytic Enzymes with an F-Actin-Tropomyosin Complex. *J. Neurochem.*, *34*(1), 222–225. Retrieved from http://doi.wiley.com/10.1111/j.1471-4159.1980.tb04646.x doi: 10.1111/j.1471-4159.1980.tb04646.x

Kohen, R., & Nyska, A. (2002, oct). Invited Review: Oxidation of Biological Systems: Oxidative Stress Phenomena, Antioxidants, Redox Reactions, and Methods for Their Quantification. *Toxicol. Pathol.*, *30*(6), 620–650. Retrieved from http://journals.sagepub.com/doi/10.1080/01926230290166724 doi: 10.1080/01926230290166724

Korshunov, S. S., Skulachev, V. P., & Starkov, A. A. (1997, oct). High protonic potential actuates a mechanism of production of reactive oxygen species in mitochondria. *FEBS Lett.*, *416*(1), 15–18. Retrieved from http://doi.wiley.com/10.1016/S0014-5793{%}2897{%}2901159-9 doi: 10.1016/S0014-5793(97)01159-9

Krichevsky, A. M., & Kosik, K. S. (2001, nov). Neuronal RNA Granules. *Neuron*, *32*(4), 683–696. Retrieved from https://linkinghub.elsevier.com/retrieve/pii/S0896627301005086 doi: 10.1016/S0896-6273(01)00508-6

Kugelberg, E., & Welander, L. (1956, may). Heredofamilial juvenile muscular atrophy simulating muscular dystrophy. *AMA. Arch. Neurol. Psychiatry*, *75*(5), 500–9. Retrieved from http://www.ncbi.nlm.nih.gov/pubmed/13312732 doi: 10.1001/archneurpsyc.1956.02330230050005

Kunz, J., Henriquez, R., Schneider, U., Deuter-Reinhard, M., Movva, N., & Hall, M. N. (1993, may). Target of rapamycin in yeast, TOR2, is an essential phosphatidylinositol kinase homolog

required for G1 progression. *Cell*, *73*(3), 585–596. Retrieved from https://linkinghub.elsevier.com/retrieve/pii/009286749390144F doi: 10.1016/0092-8674(93)90144-F

Kuzniewska, B., Cysewski, D., Wasilewski, M., Sakowska, P., Milek, J., Kulinski, T. M., ... Dziembowska, M. (2020, aug). Mitochondrial protein biogenesis in the synapse is supported by local translation. *EMBO Rep.*, *21*(8). Retrieved from https://onlinelibrary.wiley.com/doi/10.15252/embr.201948882 doi: 10.15252/embr.201948882

Kye, M. J., & Gonçalves, I. d. C. G. (2014). The role of miRNA in motor neuron disease. *Front. Cell. Neurosci.*, *8*(January), 1–8. Retrieved from http://journal.frontiersin.org/article/10.3389/fncel.2014.00015/abstract doi: 10.3389/fncel.2014.00015

Kye, M. J., Niederst, E. D., Wertz, M. H., Gonçalves, I. d. C. G., Akten, B., Dover, K. Z., ... Sahin, M. (2014, dec). SMN regulates axonal local translation via miR-183/mTOR pathway. *Hum. Mol. Genet.*, *23*(23), 6318–6331. Retrieved from https://academic.oup.com/hmg/article-lookup/doi/10.1093/hmg/ddu350 doi: 10.1093/hmg/ddu350

Lacerda, R., Menezes, J., & Romão, L. (2017, may). More than just scanning: the importance of cap-independent mRNA translation initiation for cellular stress response and cancer. *Cell. Mol. Life Sci.*, *74*(9), 1659–1680. Retrieved from http://link.springer.com/10.1007/s00018-016-2428-2 doi: 10.1007/s00018-016-2428-2

Laemmli, U. K. (1970, aug). Cleavage of Structural Proteins during the Assembly of the Head of Bacteriophage T4. *Nature*, *227*(5259), 680–685. Retrieved from http://www.ncbi.nlm.nih.gov/pubmed/5432063http://www.nature.com/articles/227680a0 doi: 10.1038/227680a0

Lally, C., Jones, C., Farwell, W., Reyna, S. P., Cook, S. F., & Flanders, W. D. (2017, dec). Indirect estimation of the prevalence of spinal muscular atrophy Type I, II, and III in the United States. *Orphanet J. Rare Dis.*, *12*(1), 175. Retrieved from https://ojrd.biomedcentral.com/articles/10.1186/s13023-017-0724-z doi: 10.1186/s13023-017-0724-z

Laplante, M., & Sabatini, D. M. (2012, apr). mTOR Signaling in Growth Control and Disease. *Cell*, *149*(2), 274–293. Retrieved from http://dx.doi.org/10.1016/j.cell.2012.03.017https://linkinghub.elsevier.com/retrieve/pii/S0092867412003510 doi: 10.1016/j.cell.2012.03.017

Lauria, F., Bernabò, P., Tebaldi, T., Groen, E. J. N., Perenthaler, E., Maniscalco, F., ... Viero, G. (2020, sep). SMN-primed ribosomes modulate the translation of transcripts related to spinal muscular atrophy. *Nat. Cell Biol.*. Retrieved from http://www.nature.com/articles/s41556-020-00577-7 doi: 10.1038/s41556-020-00577-7

Le, T. T., Pham, L. T., Butchbach, M. E., Zhang, H. L., Monani, U. R., Coovert, D. D., ... Burghes, A. H. (2005, mar). SMNΔ7, the major product of the centromeric survival motor neuron (SMN2) gene, extends survival in mice with spinal muscular atrophy and associates with full-length SMN. *Hum. Mol. Genet.*, *14*(6), 845–857. Retrieved from https://doi.org/10.1093/hmg/ddi078https://academic.oup.com/hmg/article-lookup/doi/10.1093/hmg/ddi078 doi: 10.1093/hmg/ddi078

Le Boedec, K. (2016, dec). Sensitivity and specificity of normality tests and consequences on reference interval accuracy at small sample size: a computer-simulation study. *Vet. Clin. Pathol.*, *45*(4), 648–656. doi: 10.1111/vcp.12390

Lee, E. B., Lee, V. M.-Y., & Trojanowski, J. Q. (2011, nov). Gains or losses: molecular mechanisms of TDP43-mediated neurodegeneration. *Nat. Rev. Neurosci.*, *13*(1), 38–50. Retrieved from http://www.ncbi.nlm.nih.gov/pubmed/22127299http://www.pubmedcentral.nih.gov/articlerender.fcgi?artid=PMC3285250 doi: 10.1038/nrn3121

Lefebvre, S., Bürglen, L., Reboullet, S., Clermont, O., Burlet, P., Viollet, L., ... Melki, J. (1995, jan). Identification and characterization of a spinal muscular atrophy-determining gene. *Cell*, *80*(1), 155–165. doi: 10.1016/0092-8674(95)90460-3

Lehmkuhl, E. M., & Zarnescu, D. C. (2018). Lost in translation: Evidence for protein synthesis deficits in ALS/FTD and related neurodegenerative diseases. *Adv. Neurobiol.*, *20*, 283–301. doi: 10.1007/978-3-319-89689-2_11

León, K., Boulo, T., Musnier, A., Morales, J., Gauthier, C., Dupuy, L., ... Crepieux, P. (2014, jun). Activation of a GPCR leads to eIF4G phosphorylation at the 5' cap and to IRES-dependent translation. *J. Mol. Endocrinol.*, *52*(3), 373–382. Retrieved from https://jme.bioscientifica.com/view/journals/jme/52/3/373.xml doi: 10.1530/JME-14-0009

Leung, D. W., & Amarasinghe, G. K. (2016, feb). When your cap matters: structural insights into self vs non-self recognition of 5' RNA by immunomodulatory host proteins. *Curr. Opin. Struct. Biol.*, *36*, 133–141. Retrieved from https://linkinghub.elsevier.com/retrieve/pii/S0959440X1630001X doi: 10.1016/j.sbi.2016.02.001

Leung, K.-M., van Horck, F. P., Lin, A. C., Allison, R., Standart, N., & Holt, C. E. (2006, oct). Asymmetrical β-actin mRNA translation in growth cones mediates attractive turning to netrin-1. *Nat. Neurosci.*, *9*(10), 1247–1256. Retrieved from http://www.nature.com/articles/nn1775 doi: 10.1038/nn1775

Levine, R. L. (2002, may). Carbonyl modified proteins in cellular regulation, aging, and disease2,3 2Guest Editor: Earl Stadtman 3This article is part of a series of reviews on "Oxidatively Modified Proteins in Aging and Disease." The full list of papers may be found on the homepag. *Free Radic. Biol. Med.*, *32*(9), 790–796. Retrieved from https://linkinghub.elsevier.com/retrieve/pii/S0891584902007657 doi: 10.1016/S0891-5849(02)00765-7

Lewelt, A., Newcomb, T. M., & Swoboda, K. J. (2012, feb). New Therapeutic Approaches to Spinal Muscular Atrophy. *Curr. Neurol. Neurosci. Rep.*, *12*(1), 42–53. Retrieved from http://link.springer.com/10.1007/s11910-011-0240-9 doi: 10.1007/s11910-011-0240-9

Lewén, A., Matz, P., & Chan, P. H. (2000, oct). Free radical pathways in CNS injury. *J. Neurotrauma*, *17*(10), 871–90. Retrieved from http://www.liebertpub.com/doi/10.1089/neu.2000.17.871http://www.ncbi.nlm.nih.gov/pubmed/11063054 doi: 10.1089/neu.2000.17.871

Lewis, J. D., & Izaurflde, E. (1997, jul). The Role of the Cap Structure in RNA Processing and Nuclear Export. *Eur. J. Biochem.*, *247*(2), 461–469. Retrieved from http://doi.wiley.com/10.1111/j.1432-1033.1997.00461.x doi: 10.1111/j.1432-1033.1997.00461.x

Li, B. B., Qian, C., Gameiro, P. A., Liu, C. C., Jiang, T., Roberts, T. M., ... Zhao, J. J. (2018). Targeted profiling of RNA translation reveals mTOR- 4EBP1/2-independent translation regulation of mRNAs encoding ribosomal proteins. *Proc. Natl. Acad. Sci. U. S. A.*, *115*(40), E9325–E9332. doi: 10.1073/pnas.1805782115

Li, D. K., Tisdale, S., Lotti, F., & Pellizzoni, L. (2014, aug). SMN control of RNP assembly: From post-transcriptional gene regulation to motor neuron disease. *Semin. Cell Dev. Biol.*, *32*, 22–29. Retrieved from https://linkinghub.elsevier.com/retrieve/pii/S1084952114000974 doi: 10.1016/j.semcdb.2014.04.026

Li, M., Zhao, L., Liu, J., Liu, A., Jia, C., Ma, D., ... Bai, X. (2010, oct). Multi-mechanisms are involved in reactive oxygen species regulation of mTORC1 signaling. *Cell. Signal.*, *22*(10), 1469–1476. Retrieved from http://dx.doi.org/10.1016/j.cellsig.2010.05.015https://linkinghub.elsevier.com/retrieve/pii/S0898656810001452 doi: 10.1016/j.cellsig.2010.05.015

Li, X., & Gao, T. (2014, feb). mTORC2 phosphorylates protein kinase Cζ to regulate its stability and activity. *EMBO Rep.*, *15*(2), 191–198. Retrieved from https://onlinelibrary.wiley.com/doi/abs/10.1002/embr.201338119 doi: 10.1002/embr.201338119

Ligon, L. A., & Steward, O. (2000, nov). Role of microtubules and actin filaments in the movement of mitochondria in the axons and dendrites of cultured hippocampal neurons. *J. Comp. Neurol.*, *427*(3), 351–361. Retrieved from https://onlinelibrary.wiley.com/doi/10.1002/1096-9861(20001120)427:3{%}3C351::AID-CNE3{%}3E3.0.CO;2-R doi: 10.1002/1096-9861(20001120)427:3<351::AID-CNE3>3.0.CO;2-R

Lin, R.-Y., Vera, J. C., Chaganti, R. S. K., & Golde, D. W. (1998, oct). Human Monocarboxylate Transporter 2 (MCT2) Is a High Affinity Pyruvate Transporter. *J. Biol. Chem.*, *273*(44), 28959–28965. Retrieved from http://www.jbc.org/lookup/doi/10.1074/jbc.273.44.28959 doi: 10.1074/jbc.273.44.28959

Liu, H., Lu, J., Chen, H., Du, Z., Li, X.-J., & Zhang, S.-C. (2015, dec). Spinal muscular atrophy patient-derived motor neurons exhibit hyperexcitability. *Sci. Rep.*, *5*(1), 12189. Retrieved from http://www.nature.com/articles/srep12189http://www.nature.com/srep/2015/150720/srep12189/full/srep12189.htmlhttps://linkinghub.elsevier.com/retrieve/pii/S1550413113004130https://academic.oup.com/nar/article-lookup/doi/10.1093/nar/gkv1003 doi: 10.1038/srep12189

Liu, Q., & Dreyfuss, G. (1996, jul). A novel nuclear structure containing the survival of motor neurons protein. *EMBO J.*, *15*(14), 3555–3565. Retrieved from http://doi.wiley.com/10.1002/j.1460-2075.1996.tb00725.x doi: 10.1002/j.1460-2075.1996.tb00725.x

Liu, Q., Fischer, U., Wang, F., & Dreyfuss, G. (1997, sep). The Spinal Muscular Atrophy Disease Gene Product, SMN, and Its Associated Protein SIP1 Are in a Complex with Spliceosomal snRNP Proteins. *Cell*, *90*(6), 1013–1021. Retrieved from https://linkinghub.elsevier.com/retrieve/pii/S0092867400803670 doi: 10.1016/S0092-8674(00)80367-0

Liu, S.-s. (1999). Cooperation of a "Reactive Oxygen Cycle" with The Q Cycle and The Proton Cycle in the Respiratory Chain—Superoxide Generating and Cycling Mechanisms in Mitochondria. *J. Bioenerg. Biomembr.*, *31*(4), 367–376. Retrieved from https://doi.org/10.1023/A:1018650103259 doi: 10.1023/A:1018650103259

Liu, Y., Fiskum, G., & Schubert, D. (2002, mar). Generation of reactive oxygen species by the mitochondrial electron transport chain. *J. Neurochem.*, *80*(5), 780–7. Retrieved from http://www.ncbi.nlm.nih.gov/pubmed/11948241 doi: 10.1046/j.0022-3042.2002.00744.x

Livak, K. J., & Schmittgen, T. D. (2001, dec). Analysis of relative gene expression data using real-time quantitative PCR and the 2(-Delta Delta C(T)) Method. *Methods*, *25*(4), 402–8. Retrieved from http://www.ncbi.nlm.nih.gov/pubmed/11846609 doi: 10.1006/meth.2001.1262

Loor, G., Kondapalli, J., Schriewer, J. M., Chandel, N. S., Vanden Hoek, T. L., & Schumacker, P. T. (2010). Menadione triggers cell death through ROS-dependent mechanisms involving PARP activation without requiring apoptosis. *Free Radic. Biol. Med.*, *49*(12), 1925–1936. Retrieved from http://dx.doi.org/10.1016/j.freeradbiomed.2010.09.021 doi: 10.1016/j.freeradbiomed.2010.09.021

Lorson, C. L., Hahnen, E., Androphy, E. J., & Wirth, B. (1999, may). A single nucleotide in the SMN gene regulates splicing and is responsible for spinal muscular atrophy. *Proc. Natl. Acad. Sci.*, *96*(11), 6307–6311. Retrieved from http://www.pnas.org/cgi/doi/10.1073/pnas.96.11.6307 doi: 10.1073/pnas.96.11.6307

Lorson, C. L., Strasswimmer, J., Yao, J.-M., Baleja, J. D., Hahnen, E., Wirth, B., ... Androphy, E. J. (1998, may). SMN oligomerization defect correlates with spinal muscular atrophy severity. *Nat. Genet.*, *19*(1), 63–66. Retrieved from http://www.nature.com/articles/ng0598-63 doi: 10.1038/ng0598-63

Loschen, G., Azzi, A., Richter, C., & Flohé, L. (1974, may). Superoxide radicals as precursors of mitochondrial hydrogen peroxide. *FEBS Lett.*, *42*(1), 68–72. Retrieved from http://doi.wiley.com/10.1016/0014-5793{%}2874{%}2980281-4 doi: 10.1016/0014-5793(74)80281-4

Lynch, C. J., Xu, Y., Hajnal, A., Salzberg, A. C., & Kawasawa, Y. I. (2015, apr). RNA Sequencing Reveals a Slow to Fast Muscle Fiber Type Transition after Olanzapine Infusion in Rats. *PLoS One*, *10*(4), e0123966. Retrieved from https://dx.plos.org/10.1371/journal.pone.0123966 doi: 10.1371/journal.pone.0123966

MacAskill, A. F., Atkin, T. A., & Kittler, J. T. (2010, jul). Mitochondrial trafficking and the provision of energy and calcium buffering at excitatory synapses. *Eur. J. Neurosci.*, *32*(2),

231–240. Retrieved from http://doi.wiley.com/10.1111/j.1460-9568.2010.07345.x doi: 10.1111/j.1460-9568.2010.07345.x

Maccallini, P., Bavasso, F., Scatolini, L., Bucciarelli, E., Noviello, G., Lisi, V., ... Raffa, G. D. (2020). Intimate functional interactions between TGS1 and the Smn complex revealed by an analysis of the Drosophila eye development. *PLoS Genet.*, *16*(5), 1–24. Retrieved from http://dx.doi.org/10.1371/journal.pgen.1008815 doi: 10.1371/journal.pgen.1008815

Mächler, P., Wyss, M. T., Elsayed, M., Stobart, J., Gutierrez, R., von Faber-Castell, A., ... Weber, B. (2016, jan). In Vivo Evidence for a Lactate Gradient from Astrocytes to Neurons. *Cell Metab.*, *23*(1), 94–102. Retrieved from http://linkinghub.elsevier.com/retrieve/pii/S1550413115005264 doi: 10.1016/j.cmet.2015.10.010

Macleod, M. J., Taylor, J. E., Lunt, P. W., Mathew, C. G., & Robb, S. A. (1999, jan). Prenatal onset spinal muscular atrophy. *Eur. J. Paediatr. Neurol.*, *3*(2), 65–72. Retrieved from https://linkinghub.elsevier.com/retrieve/pii/S1090379899800154 doi: 10.1016/S1090-3798(99)80015-4

Maher, F., & Simpson, I. A. (1994, jul). The GLUT3 glucose transporter is the predominant isoform in primary cultured neurons: assessment by biosynthetic and photoaffinity labelling. *Biochem. J.*, *301*(2), 379–384. Retrieved from https://portlandpress.com/biochemj/article/301/2/379/31138/The-GLUT3-glucose-transporter-is-the-predominant doi: 10.1042/bj3010379

Maiti, P., Singh, S. B., Sharma, A. K., Muthuraju, S., Banerjee, P. K., & Ilavazhagan, G. (2006, dec). Hypobaric hypoxia induces oxidative stress in rat brain. *Neurochem. Int.*, *49*(8), 709–16. Retrieved from http://www.ncbi.nlm.nih.gov/pubmed/16911847 doi: 10.1016/j.neuint.2006.06.002

Malinovska, L., Kroschwald, S., & Alberti, S. (2013, may). Protein disorder, prion propensities, and self-organizing macromolecular collectives. *Biochim. Biophys. Acta - Proteins Proteomics*, *1834*(5), 918–931. Retrieved from https://linkinghub.elsevier.com/retrieve/pii/S1570963913000083 doi: 10.1016/j.bbapap.2013.01.003

Mangia, S., Simpson, I. A., Vannucci, S. J., & Carruthers, A. (2009, may). The in vivo neuron-to-astrocyte lactate shuttle in human brain: evidence from modeling of measured lactate levels during visual stimulation. *J. Neurochem.*, *109*, 55–62. Retrieved from http://doi.wiley.com/10.1111/j.1471-4159.2009.06003.x doi: 10.1111/j.1471-4159.2009.06003.x

Manzo, E., Lorenzini, I., Barrameda, D., O'Conner, A. G., Barrows, J. M., Starr, A., ... Zarnescu, D. C. (2019, jun). Glycolysis upregulation is neuroprotective as a compensatory mechanism in ALS. *Elife*, *8*, 517649. Retrieved from https://www.biorxiv.org/content/10.1101/517649v1https://elifesciences.org/articles/45114 doi: 10.7554/eLife.45114

Matera, A. G., Terns, R. M., & Terns, M. P. (2007). Non-coding RNAs: lessons from the small nuclear and small nucleolar RNAs. *Nat. Rev. Mol. Cell Biol.*, *8*(3), 209–20. Retrieved from http://www.ncbi.nlm.nih.gov/pubmed/17318225 doi: 10.1038/nrm2124

Matesanz, S. E., Curry, C., Gross, B., Rubin, A. I., Linn, R., Yum, S. W., & Kichula, E. A. (2020, oct). Clinical Course in a Patient With Spinal Muscular Atrophy Type 0 Treated With Nusinersen and Onasemnogene Abeparvovec. *J. Child Neurol.*, *35*(11), 717–723. Retrieved from http://journals.sagepub.com/doi/10.1177/0883073820928784 doi: 10.1177/0883073820928784

McBride, H. M., Neuspiel, M., & Wasiak, S. (2006, jul). Mitochondria: More Than Just a Powerhouse. *Curr. Biol.*, *16*(14), R551–R560. Retrieved from https://linkinghub.elsevier.com/retrieve/pii/S0960982206017817 doi: 10.1016/j.cub.2006.06.054

McGivern, J. V., Patitucci, T. N., Nord, J. A., Barabas, M.-E. A., Stucky, C. L., & Ebert, A. D. (2013, sep). Spinal muscular atrophy astrocytes exhibit abnormal calcium regulation and reduced growth factor production. *Glia*, *61*(9), 1418–1428. Retrieved from http://doi.wiley.com/10.1002/glia.22522 doi: 10.1002/glia.22522

Mecocci, P., MacGarvey, U., & Beal, M. F. (1994, nov). Oxidative damage to mitochondrial DNA is increased in Alzheimer's disease. *Ann. Neurol.*, *36*(5), 747–751. Retrieved from http://doi.wiley.com/10.1002/ana.410360510 doi: 10.1002/ana.410360510

Melki, J., Lefebvre, S., Burglen, L., Burlet, P., Clermont, O., Millasseau, P., ... Et, A. (1994, jun). De novo and inherited deletions of the 5q13 region in spinal muscular atrophies. *Science (80-.).*, *264*(5164), 1474–1477. Retrieved from https://www.sciencemag.org/lookup/doi/10.1126/science.7910982 doi: 10.1126/science.7910982

Melki, J., Sheth, P., Abdelhak, S., Burlet, P., Bachelot, M., Frézal, J., ... Lathrop, M. (1990, aug). Mapping of acute (type I) spinal muscular atrophy to chromosome 5q12-q14. *Lancet*, *336*(8710), 271–273. Retrieved from https://linkinghub.elsevier.com/retrieve/pii/014067369091803Ihttp://www.ncbi.nlm.nih.gov/pubmed/1973971 doi: 10.1016/0140-6736(90)91803-I

Mellins, R. B., Hays, A. P., Gold, A. P., Berdon, W. E., & Bowdler, J. D. (1974, jan). Respiratory distress as the initial manifestation of Werdnig-Hoffmann disease. *Pediatrics*, *53*(1), 33 LP – 40. Retrieved from http://pediatrics.aappublications.org/content/53/1/33.abstract

Mendell, J. R., Al-Zaidy, S., Shell, R., Arnold, W. D., Rodino-Klapac, L. R., Prior, T. W., ... Kaspar, B. K. (2017). Single-Dose Gene-Replacement Therapy for Spinal Muscular Atrophy. *N. Engl. J. Med.*, *377*(18), 1713–1722. Retrieved from http://www.ncbi.nlm.nih.gov/pubmed/29091557 doi: 10.1056/NEJMoa1706198

Mentis, G. Z., Blivis, D., Liu, W., Drobac, E., Crowder, M. E., Kong, L., ... O'Donovan, M. J. (2011, feb). Early Functional Impairment of Sensory-Motor Connectivity in a Mouse Model of Spinal Muscular Atrophy. *Neuron*, *69*(3), 453–467. Retrieved from https://linkinghub.elsevier.com/retrieve/pii/S0896627310010809http://dx.doi.org/10.1016/j.neuron.2010.12.032 doi: 10.1016/j.neuron.2010.12.032

Mercuri, E., Darras, B. T., Chiriboga, C. A., Day, J. W., Campbell, C., Connolly, A. M., ... CHERISH Study Group (2018). Nusinersen versus Sham Control in Later-Onset

Spinal Muscular Atrophy. *N. Engl. J. Med.*, *378*(7), 625–635. Retrieved from http://www.ncbi.nlm.nih.gov/pubmed/29443664 doi: 10.1056/NEJMoa1710504

Mercuri, E., Finkel, R. S., Muntoni, F., Wirth, B., Montes, J., Main, M., ... Szlagatys-Sidorkiewicz, A. (2018, feb). Diagnosis and management of spinal muscular atrophy: Part 1: Recommendations for diagnosis, rehabilitation, orthopedic and nutritional care. *Neuromuscul. Disord.*, *28*(2), 103–115. Retrieved from https://linkinghub.elsevier.com/retrieve/pii/S0960896617312841 doi: 10.1016/j.nmd.2017.11.005

Mérette, C., Brzustowicz, L., Daniels, R., Davies, K., Gilliam, T., Melki, J., ... Ott, J. (1994, may). An Investigation of Genetic Heterogeneity and Linkage Disequilibrium in 161 Families with Spinal Muscular Atrophy. *Genomics*, *21*(1), 27–33. Retrieved from https://linkinghub.elsevier.com/retrieve/pii/S0888754384712201 doi: 10.1006/geno.1994.1220

Meyuhas, O., & Kahan, T. (2015, jul). The race to decipher the top secrets of TOP mRNAs. *Biochim. Biophys. Acta - Gene Regul. Mech.*, *1849*(7), 801–811. Retrieved from http://dx.doi.org/10.1016/j.bbagrm.2014.08.015https://linkinghub.elsevier.com/retrieve/pii/S1874939914002466 doi: 10.1016/j.bbagrm.2014.08.015

Miller, N., Shi, H., Zelikovich, A. S., & Ma, Y.-C. (2016, aug). Motor neuron mitochondrial dysfunction in spinal muscular atrophy. *Hum. Mol. Genet.*, *25*(16), 3395–3406. Retrieved from http://www.ncbi.nlm.nih.gov/pubmed/27488123https://academic.oup.com/hmg/article-lookup/doi/10.1093/hmg/ddw262 doi: 10.1093/hmg/ddw262

Mink, J. W., Blumenschine, R. J., & Adams, D. B. (1981, sep). Ratio of central nervous system to body metabolism in vertebrates: its constancy and functional basis. *Am. J. Physiol.*, *241*(3), R203–12. Retrieved from http://www.ncbi.nlm.nih.gov/pubmed/7282965

Monani, U. R., Sendtner, M., Coovert, D. D., Parsons, D. W., Andreassi, C., Le, T. T., ... Burghes, A. H. (2000, feb). The human centromeric survival motor neuron gene (SMN2) rescues embryonic lethality in Smn-/- mice and results in a mouse with spinal muscular atrophy. *Hum. Mol. Genet.*, *9*(3), 333–339. Retrieved from https://academic.oup.com/hmg/article-lookup/doi/10.1093/hmg/9.3.333http://www.ncbi.nlm.nih.gov/pubmed/10655541http://www.hmg.oupjournals.org/cgi/doi/10.1093/hmg/9.3.333 doi: 10.1093/hmg/9.3.333

Moore, M. J. (2005, sep). From Birth to Death: The Complex Lives of Eukaryotic mRNAs. *Science (80-.).*, *309*(5740), 1514–1518. Retrieved from https://www.sciencemag.org/lookup/doi/10.1126/science.1111443 doi: 10.1126/science.1111443

Morita, M., Gravel, S.-P., Chénard, V., Sikström, K., Zheng, L., Alain, T., ... Sonenberg, N. (2013, nov). mTORC1 Controls Mitochondrial Activity and Biogenesis through 4E-BP-Dependent Translational Regulation. *Cell Metab.*, *18*(5), 698–711. Retrieved from https://linkinghub.elsevier.com/retrieve/pii/S1550413113004130 doi: 10.1016/j.cmet.2013.10.001

Mouaikel, J., Narayanan, U., Verheggen, C., Matera, A. G., Bertrand, E., Tazi, J., & Bordonné, R. (2003, jun). Interaction between the small-nuclear-RNA cap hypermethylase and the spinal

muscular atrophy protein, survival of motor neuron. *EMBO Rep.*, *4*(6), 616–22. Retrieved from http://www.ncbi.nlm.nih.gov/pubmed/12776181http://www.pubmedcentral.nih.gov/articlerender.fcgi?artid=PMC1319203 doi: 10.1038/sj.embor.embor863

Mouaikel, J., Verheggen, C., Bertrand, E., Tazi, J., & Bordonné, R. (2002, apr). Hypermethylation of the cap structure of both yeast snRNAs and snoRNAs requires a conserved methyltransferase that is localized to the nucleolus. *Mol. Cell*, *9*(4), 891–901. Retrieved from http://www.ncbi.nlm.nih.gov/pubmed/11983179 doi: 10.1016/s1097-2765(02)00484-7

Mourelatos, Z. (2001, oct). SMN interacts with a novel family of hnRNP and spliceosomal proteins. *EMBO J.*, *20*(19), 5443–5452. Retrieved from http://emboj.embopress.org/cgi/doi/10.1093/emboj/20.19.5443 doi: 10.1093/emboj/20.19.5443

Mourelatos, Z. (2002, mar). miRNPs: a novel class of ribonucleoproteins containing numerous microRNAs. *Genes Dev.*, *16*(6), 720–728. Retrieved from http://www.genesdev.org/cgi/doi/10.1101/gad.974702 doi: 10.1101/gad.974702

Mullis, K. B. (1990). Target amplification for DNA analysis by the polymerase chain reaction. *Ann. Biol. Clin. (Paris).*, *48*(8), 579–82. Retrieved from http://www.ncbi.nlm.nih.gov/pubmed/2288446

Munro, D., & Treberg, J. R. (2017, apr). A radical shift in perspective: mitochondria as regulators of reactive oxygen species. *J. Exp. Biol.*, *220*(7), 1170–1180. Retrieved from http://jeb.biologists.org/lookup/doi/10.1242/jeb.132142 doi: 10.1242/jeb.132142

Munsat, T. L., & Davies, K. E. (1992, jan). International SMA consortium meeting. (26-28 June 1992, Bonn, Germany). *Neuromuscul. Disord.*, *2*(5-6), 423–8. Retrieved from https://linkinghub.elsevier.com/retrieve/pii/S0960896606800155http://www.ncbi.nlm.nih.gov/pubmed/1300191 doi: 10.1016/s0960-8966(06)80015-5

Murphy, M. P. (2009, jan). How mitochondria produce reactive oxygen species. *Biochem. J.*, *417*(1), 1–13. Retrieved from https://portlandpress.com/biochemj/article/417/1/1/45114/How-mitochondria-produce-reactive-oxygen-species doi: 10.1042/BJ20081386

Murray, L. M., Thomson, D., Conklin, A., Wishart, T. M., & Gillingwater, T. H. (2008, dec). Loss of translation elongation factor (eEF1A2) expression in vivo differentiates between Wallerian degeneration and dying-back neuronal pathology. *J. Anat.*, *213*(6), 633–645. Retrieved from http://doi.wiley.com/10.1111/j.1469-7580.2008.01007.x doi: 10.1111/j.1469-7580.2008.01007.x

Nakamoto, T. (2011, feb). Mechanisms of the initiation of protein synthesis: in reading frame binding of ribosomes to mRNA. *Mol. Biol. Rep.*, *38*(2), 847–855. Retrieved from http://link.springer.com/10.1007/s11033-010-0176-1 doi: 10.1007/s11033-010-0176-1

Nangaku, M., Sato-Yoshitake, R., Okada, Y., Noda, Y., Takemura, R., Yamazaki, H., & Hirokawa, N. (1994, dec). KIF1B, a novel microtubule plus end-directed monomeric motor protein for transport of mitochondria. *Cell*, *79*(7), 1209–1220. Retrieved from https://

linkinghub.elsevier.com/retrieve/pii/0092867494900124 doi: 10.1016/0092-8674(94)90012-4

Naryshkin, N. A., Weetall, M., Dakka, A., Narasimhan, J., Zhao, X., Feng, Z., ... Metzger, F. (2014, aug). SMN2 splicing modifiers improve motor function and longevity in mice with spinal muscular atrophy. *Science (80-.).*, *345*(6197), 688–693. Retrieved from http://www.ncbi.nlm.nih.gov/pubmed/25104390http://www.sciencemag.org/cgi/doi/10.1126/science.1250127https://www.sciencemag.org/lookup/doi/10.1126/science.1250127 doi: 10.1126/science.1250127

Nedelec, S., Foucher, I., Brunet, I., Bouillot, C., Prochiantz, A., & Trembleau, A. (2004, jul). Emx2 homeodomain transcription factor interacts with eukaryotic translation initiation factor 4E (eIF4E) in the axons of olfactory sensory neurons. *Proc. Natl. Acad. Sci.*, *101*(29), 10815–10820. Retrieved from http://www.pnas.org/cgi/doi/10.1073/pnas.0403824101 doi: 10.1073/pnas.0403824101

Neil, E. E., & Bisaccia, E. K. (2019, may). Nusinersen: A Novel Antisense Oligonucleotide for the Treatment of Spinal Muscular Atrophy. *J. Pediatr. Pharmacol. Ther.*, *24*(3), 194–203. Retrieved from https://meridian.allenpress.com/jppt/article/24/3/194/433570/Nusinersen-A-Novel-Antisense-Oligonucleotide-for doi: 10.5863/1551-6776-24.3.194

Noda, T., & Ohsumi, Y. (1998). Tor, a phosphatidylinositol kinase homologue, controls autophagy in yeast. *J. Biol. Chem.*, *273*(7), 3963–3966. doi: 10.1074/jbc.273.7.3963

Nürenberg-Goloub, E., & Tampé, R. (2019, dec). Ribosome recycling in mRNA translation, quality control, and homeostasis. *Biol. Chem.*, *401*(1), 47–61. Retrieved from http://www.degruyter.com/view/j/bchm.2020.401.issue-1/hsz-2019-0279/hsz-2019-0279.xml doi: 10.1515/hsz-2019-0279

Nussbacher, J. K., Tabet, R., Yeo, G. W., & Lagier-Tourenne, C. (2019, apr). Disruption of RNA Metabolism in Neurological Diseases and Emerging Therapeutic Interventions. *Neuron*, *102*(2), 294–320. Retrieved from https://linkinghub.elsevier.com/retrieve/pii/S0896627319302776https://doi.org/10.1016/j.neuron.2019.03.014 doi: 10.1016/j.neuron.2019.03.014

Nyström, T. (2005). Role of oxidative carbonylation in protein quality control and senescence. *EMBO J.*, *24*(7), 1311–1317. doi: 10.1038/sj.emboj.7600599

Oh, W. J., Wu, C.-c., Kim, S. J., Facchinetti, V., Julien, L. A., Finlan, M., ... Jacinto, E. (2010, dec). mTORC2 can associate with ribosomes to promote cotranslational phosphorylation and stability of nascent Akt polypeptide. *EMBO J.*, *29*(23), 3939–3951. Retrieved from http://emboj.embopress.org/cgi/doi/10.1038/emboj.2010.271 doi: 10.1038/emboj.2010.271

Oprea, G. E., Krober, S., McWhorter, M. L., Rossoll, W., Muller, S., Krawczak, M., ... Wirth, B. (2008, apr). Plastin 3 Is a Protective Modifier of Autosomal Recessive Spinal Muscular Atrophy. *Science (80-.).*, *320*(5875), 524–527. Retrieved from https://www.sciencemag.org/lookup/doi/10.1126/science.1155085 doi: 10.1126/science.1155085

Otter, S., Grimmler, M., Neuenkirchen, N., Chari, A., Sickmann, A., & Fischer, U. (2007, feb). A Comprehensive Interaction Map of the Human Survival of Motor Neuron (SMN) Complex. *J. Biol. Chem.*, *282*(8), 5825–5833. Retrieved from http://www.jbc.org/lookup/doi/10.1074/jbc.M608528200 doi: 10.1074/jbc.M608528200

Pagliardini, S. (2000, jan). Subcellular localization and axonal transport of the survival motor neuron (SMN) protein in the developing rat spinal cord. *Hum. Mol. Genet.*, *9*(1), 47–56. Retrieved from https://academic.oup.com/hmg/article-lookup/doi/10.1093/hmg/9.1.47 doi: 10.1093/hmg/9.1.47

Patitucci, T. N., & Ebert, A. D. (2016). SMN deficiency does not induce oxidative stress in SMA iPSC-derived astrocytes or motor neurons. *Hum. Mol. Genet.*, *25*(3), 514–523. doi: 10.1093/hmg/ddv489

Pause, A., Belsham, G. J., Gingras, A.-C., Donzé, O., Lin, T.-A., Lawrence, J. C., & Sonenberg, N. (1994, oct). Insulin-dependent stimulation of protein synthesis by phosphorylation of a regulator of 5'-cap function. *Nature*, *371*(6500), 762–767. Retrieved from http://www.nature.com/articles/371762a0 doi: 10.1038/371762a0

Pearn, J. (1978). Incidence, prevalence, and gene frequency studies of chronic childhood spinal muscular atrophy. *J. Med. Genet.*, *15*, 409–413. doi: 10.1136/jmg.15.6.409

Pearn, J. (1980, apr). Classification of spinal muscular atrophies. *Lancet*, *315*(8174), 919–922. Retrieved from https://linkinghub.elsevier.com/retrieve/pii/S0140673680908478 doi: 10.1016/S0140-6736(80)90847-8

Pellerin, L., & Magistretti, P. J. (1994, oct). Glutamate uptake into astrocytes stimulates aerobic glycolysis: a mechanism coupling neuronal activity to glucose utilization. *Proc. Natl. Acad. Sci.*, *91*(22), 10625–10629. Retrieved from http://www.pnas.org/cgi/doi/10.1073/pnas.91.22.10625 doi: 10.1073/pnas.91.22.10625

Pellizzoni, L. (2002, nov). Essential Role for the SMN Complex in the Specificity of snRNP Assembly. *Science (80-.).*, *298*(5599), 1775–1779. Retrieved from https://www.sciencemag.org/lookup/doi/10.1126/science.1074962 doi: 10.1126/science.1074962

Pellizzoni, L. (2007, apr). Chaperoning ribonucleoprotein biogenesis in health and disease. *EMBO Rep.*, *8*(4), 340–345. Retrieved from https://onlinelibrary.wiley.com/doi/abs/10.1038/sj.embor.7400941 doi: 10.1038/sj.embor.7400941

Perez-Riverol, Y., Csordas, A., Bai, J., Bernal-Llinares, M., Hewapathirana, S., Kundu, D. J., ... Vizcaíno, J. A. (2019, jan). The PRIDE database and related tools and resources in 2019: improving support for quantification data. *Nucleic Acids Res.*, *47*(D1), D442–D450. Retrieved from http://www.ncbi.nlm.nih.gov/pubmed/30395289http://www.pubmedcentral.nih.gov/articlerender.fcgi?artid=PMC6323896https://academic.oup.com/nar/article/47/D1/D442/5160986 doi: 10.1093/nar/gky1106

Peterson, T. R., Laplante, M., Thoreen, C. C., Sancak, Y., Kang, S. A., Kuehl, W. M., ... Sabatini, D. M. (2009, may). DEPTOR Is an mTOR Inhibitor Frequently Overexpressed in

Multiple Myeloma Cells and Required for Their Survival. *Cell*, *137*(5), 873–886. Retrieved from https://linkinghub.elsevier.com/retrieve/pii/S0092867409003894 doi: 10.1016/j.cell.2009.03.046

Pfeiffer, T., Schuster, S., & Bonhoeffer, S. (2001, apr). Cooperation and Competition in the Evolution of ATP-Producing Pathways. *Science (80-.).*, *292*(5516), 504–507. Retrieved from https://www.sciencemag.org/lookup/doi/10.1126/science.1058079 doi: 10.1126/science.1058079

Phaniendra, A., Jestadi, D. B., & Periyasamy, L. (2015, jan). Free Radicals: Properties, Sources, Targets, and Their Implication in Various Diseases. *Indian J. Clin. Biochem.*, *30*(1), 11–26. Retrieved from http://link.springer.com/10.1007/s12291-014-0446-0 doi: 10.1007/s12291-014-0446-0

Pickering, B. M., & Willis, A. E. (2005, feb). The implications of structured 5' untranslated regions on translation and disease. *Semin. Cell Dev. Biol.*, *16*(1), 39–47. Retrieved from https://linkinghub.elsevier.com/retrieve/pii/S1084952104001107 doi: 10.1016/j.semcdb.2004.11.006

Pierre, K., Magistretti, P. J., & Pellerin, L. (2002, may). MCT2 is a Major Neuronal Monocarboxylate Transporter in the Adult Mouse Brain. *J. Cereb. Blood Flow Metab.*, *22*(5), 586–595. Retrieved from http://journals.sagepub.com/doi/10.1097/00004647-200205000-00010 doi: 10.1097/00004647-200205000-00010

Pilling, A. D., Horiuchi, D., Lively, C. M., & Saxton, W. M. (2006, apr). Kinesin-1 and Dynein Are the Primary Motors for Fast Transport of Mitochondria in Drosophila Motor Axons. *Mol. Biol. Cell*, *17*(4), 2057–2068. Retrieved from https://www.molbiolcell.org/doi/10.1091/mbc.e05-06-0526 doi: 10.1091/mbc.e05-06-0526

Poirier, A., Weetall, M., Heinig, K., Bucheli, F., Schoenlein, K., Alsenz, J., ... Mueller, L. (2018, dec). Risdiplam distributes and increases SMN protein in both the central nervous system and peripheral organs. *Pharmacol. Res. Perspect.*, *6*(6), e00447. Retrieved from https://onlinelibrary.wiley.com/doi/abs/10.1002/prp2.447 doi: 10.1002/prp2.447

Prior, R., Van Helleputte, L., Benoy, V., & Van Den Bosch, L. (2017, sep). Defective axonal transport: A common pathological mechanism in inherited and acquired peripheral neuropathies. *Neurobiol. Dis.*, *105*, 300–320. Retrieved from https://linkinghub.elsevier.com/retrieve/pii/S0969996117300323 doi: 10.1016/j.nbd.2017.02.009

Rangaraju, V., Calloway, N., & Ryan, T. A. (2014, feb). Activity-Driven Local ATP Synthesis Is Required for Synaptic Function. *Cell*, *156*(4), 825–835. Retrieved from http://www.ncbi.nlm.nih.gov/pubmed/24529383http://www.pubmedcentral.nih.gov/articlerender.fcgi?artid=PMC3955179http://linkinghub.elsevier.com/retrieve/pii/S0092867414000130 doi: 10.1016/j.cell.2013.12.042

Rangaraju, V., Lauterbach, M., & Schuman, E. M. (2019). Spatially Stable Mitochondrial Compartments Fuel Local Translation during Plasticity. *Cell*, *176*(1-2), 73–84.e15. Retrieved from https://doi.org/10.1016/j.cell.2018.12.013 doi: 10.1016/j.cell.2018.12.013

Ratti, A., & Buratti, E. (2016, aug). Physiological functions and pathobiology of TDP-43 and FUS/TLS proteins. *J. Neurochem.*, *138*, 95–111. Retrieved from http://doi.wiley.com/10.1111/jnc.13625 doi: 10.1111/jnc.13625

Rehorst, W. A., Thelen, M. P., Nolte, H., Türk, C., Cirak, S., Peterson, J. M., ... Kye, M. J. (2019, oct). Muscle regulates mTOR dependent axonal local translation in motor neurons via CTRP3 secretion: implications for a neuromuscular disorder, spinal muscular atrophy. *Acta Neuropathol. Commun.*, *7*(1), 154. Retrieved from https://actaneurocomms.biomedcentral.com/articles/10.1186/s40478-019-0806-3http://www.ncbi.nlm.nih.gov/pubmed/31615574 doi: 10.1186/s40478-019-0806-3

Renvoisé, B., Quérol, G., Verrier, E. R., Burlet, P., & Lefebvre, S. (2012, jun). A role for protein phosphatase PP1γ in SMN complex formation and subnuclear localization to Cajal bodies. *J. Cell Sci.*, *125*(12), 2862–2874. Retrieved from http://jcs.biologists.org/lookup/doi/10.1242/jcs.096255 doi: 10.1242/jcs.096255

Richter, J. D., & Coller, J. (2015, oct). Pausing on Polyribosomes: Make Way for Elongation in Translational Control. *Cell*, *163*(2), 292–300. Retrieved from https://linkinghub.elsevier.com/retrieve/pii/S0092867415012581 doi: 10.1016/j.cell.2015.09.041

Richter, J. D., & Sonenberg, N. (2005, feb). Regulation of cap-dependent translation by eIF4E inhibitory proteins. *Nature*, *433*(7025), 477–480. Retrieved from http://www.nature.com/articles/nature03205 doi: 10.1038/nature03205

Riessland, M., Ackermann, B., Förster, A., Jakubik, M., Hauke, J., Garbes, L., ... Wirth, B. (2010, apr). SAHA ameliorates the SMA phenotype in two mouse models for spinal muscular atrophy. *Hum. Mol. Genet.*, *19*(8), 1492–1506. Retrieved from https://academic.oup.com/hmg/article-lookup/doi/10.1093/hmg/ddq023 doi: 10.1093/hmg/ddq023

Riessland, M., Kaczmarek, A., Schneider, S., Swoboda, K. J., Löhr, H., Bradler, C., ... Wirth, B. (2017, feb). Neurocalcin Delta Suppression Protects against Spinal Muscular Atrophy in Humans and across Species by Restoring Impaired Endocytosis. *Am. J. Hum. Genet.*, *100*(2), 297–315. Retrieved from https://linkinghub.elsevier.com/retrieve/pii/S0002929717300058 doi: 10.1016/j.ajhg.2017.01.005

Ripolone, M., Ronchi, D., Violano, R., Vallejo, D., Fagiolari, G., Barca, E., ... Moggio, M. (2015, jun). Impaired Muscle Mitochondrial Biogenesis and Myogenesis in Spinal Muscular Atrophy. *JAMA Neurol.*, *72*(6), 1–10. Retrieved from http://archneur.jamanetwork.com/article.aspx?doi=10.1001/jamaneurol.2015.0178http://www.ncbi.nlm.nih.gov/pubmed/25844556 doi: 10.1001/jamaneurol.2015.0178

Robak, J., & Marcinkiewicz, E. (1995, mar). Scavenging of reactive oxygen species as the mechanism of drug action. *Pol. J. Pharmacol.*, *47*(2), 89–98. Retrieved from http://www.ncbi.nlm.nih.gov/pubmed/8688896

Ro-Choi, T. S. (1999). Nuclear snRNA and nuclear function (discovery of 5' cap structures in RNA). *Crit. Rev. Eukaryot. Gene Expr.*, *9*(2), 107–58. Retrieved from http://www.ncbi.nlm.nih.gov/pubmed/10445153 doi: 10.1615/critreveukargeneexpr.v9.i2.20

Rolfe, D. F., & Brown, G. C. (1997, jul). Cellular energy utilization and molecular origin of standard metabolic rate in mammals. *Physiol. Rev.*, *77*(3), 731–758. Retrieved from https://www.physiology.org/doi/10.1152/physrev.1997.77.3.731 doi: 10.1152/physrev.1997.77.3.731

Roosterman, D., & S. Cottrell, G. (2020). Astrocytes and neurons communicate via a monocarboxylic acid shuttle. *AIMS Neurosci.*, *7*(2), 94–106. Retrieved from http://www.aimspress.com/article/10.3934/Neuroscience.2020007 doi: 10.3934/Neuroscience.2020007

Rosen, D. R., Siddique, T., Patterson, D., Figlewicz, D. A., Sapp, P., Hentati, A., ... Brown, R. H. (1993, mar). Mutations in Cu/Zn superoxide dismutase gene are associated with familial amyotrophic lateral sclerosis. *Nature*, *362*(6415), 59–62. Retrieved from http://www.nature.com/articles/362059a0 doi: 10.1038/362059a0

Rossoll, W., & Bassell, G. J. (2019). Crosstalk of Local Translation and Mitochondria: Powering Plasticity in Axons and Dendrites. *Neuron*, *101*(2), 204–206. Retrieved from https://doi.org/10.1016/j.neuron.2018.12.027 doi: 10.1016/j.neuron.2018.12.027

Rossoll, W., Jablonka, S., Andreassi, C., Kröning, A. K., Karle, K., Monani, U. R., & Sendtner, M. (2003). Smn, the spinal muscular atrophy-determining gene product, modulates axon growth and localization of β-actin mRNA in growth cones of motoneurons. *J. Cell Biol.*, *163*(4), 801–812. doi: 10.1083/jcb.200304128

RStudio Team. (2019). *RStudio: Integrated Development Environment for R*. Boston, MA. Retrieved from http://www.rstudio.com/

Rudnik-Schoneborn, S., Goebel, H., Schlote, W., Molaian, S., Omran, H., Ketelsen, U., ... Zerres, K. (2003, mar). Classical infantile spinal muscular atrophy with SMN deficiency causes sensory neuronopathy. *Neurology*, *60*(6), 983–987. Retrieved from http://www.neurology.org/cgi/doi/10.1212/01.WNL.0000052788.39340.45 doi: 10.1212/01.WNL.0000052788.39340.45

Rudnik-Schoneborn, S., Heller, R., Berg, C., Betzler, C., Grimm, T., Eggermann, T., ... Zerres, K. (2008, jun). Congenital heart disease is a feature of severe infantile spinal muscular atrophy. *J. Med. Genet.*, *45*(10), 635–638. Retrieved from https://jmg.bmj.com/lookup/doi/10.1136/jmg.2008.057950 doi: 10.1136/jmg.2008.057950

Sakata, J. T., & Jones, T. A. (2003, feb). Synaptic mitochondrial changes in the motor cortex following unilateral cortical lesions and motor skills training in adult male rats. *Neurosci. Lett.*, *337*(3), 159–162. Retrieved from https://linkinghub.elsevier.com/retrieve/pii/S0304394002013289 doi: 10.1016/S0304-3940(02)01328-9

Sanchez, G., Dury, A. Y., Murray, L. M., Biondi, O., Tadesse, H., El fatimy, R., ... Côté, J. (2013). A novel function for the survival motoneuron protein as a translational regulator. *Hum. Mol. Genet.*, *22*(4), 668–684. doi: 10.1093/hmg/dds474

Sangaré, M., Hendrickson, B., Sango, H. A., Chen, K., Nofziger, J., Amara, A., ... Fischbeck, K. H. (2014, apr). Genetics of low spinal muscular atrophy carrier frequency in sub-Saharan

Africa. *Ann. Neurol.*, *75*(4), 525–532. Retrieved from https://onlinelibrary.wiley.com/doi/10.1002/ana.24114 doi: 10.1002/ana.24114

Sarbassov, D. D., Ali, S. M., Sengupta, S., Sheen, J.-H., Hsu, P. P., Bagley, A. F., ... Sabatini, D. M. (2006, apr). Prolonged Rapamycin Treatment Inhibits mTORC2 Assembly and Akt/PKB. *Mol. Cell*, *22*(2), 159–168. Retrieved from https://linkinghub.elsevier.com/retrieve/pii/S1097276506002188 doi: 10.1016/j.molcel.2006.03.029

Sarbassov, D. D., & Sabatini, D. M. (2005, nov). Redox Regulation of the Nutrient-sensitive Raptor-mTOR Pathway and Complex. *J. Biol. Chem.*, *280*(47), 39505–39509. Retrieved from http://www.jbc.org/lookup/doi/10.1074/jbc.M506096200 doi: 10.1074/jbc.M506096200

Sauterer, R. A., Feeney, R. J., & Zieve, G. W. (1988, jun). Cytoplasmic assembly of snRNP particles from stored proteins and newly transcribed snRNA's in L929 mouse fibroblasts. *Exp. Cell Res.*, *176*(2), 344–359. Retrieved from https://linkinghub.elsevier.com/retrieve/pii/0014482788903369 doi: 10.1016/0014-4827(88)90336-9

Schmidt, E. K., Clavarino, G., Ceppi, M., & Pierre, P. (2009, apr). SUnSET, a nonradioactive method to monitor protein synthesis. *Nat. Methods*, *6*(4), 275–277. Retrieved from http://www.nature.com/articles/nmeth.1314 doi: 10.1038/nmeth.1314

Schmutz, J., Martin, J., Terry, A., Couronne, O., Grimwood, J., Lowry, S., ... Rubin, E. M. (2004, sep). The DNA sequence and comparative analysis of human chromosome 5. *Nature*, *431*(7006), 268–274. Retrieved from http://www.nature.com/articles/nature02919 doi: 10.1038/nature02919

Schrank, B., Götz, R., Gunnersen, J. M., Ure, J. M., Toyka, K. V., Smith, A. G., & Sendtner, M. (1997, sep). Inactivation of the survival motor neuron gene, a candidate gene for human spinal muscular atrophy, leads to massive cell death in early mouse embryos. *Proc. Natl. Acad. Sci. U. S. A.*, *94*(18), 9920–9925. Retrieved from https://www.pnas.org/content/94/18/9920 doi: 10.1073/pnas.94.18.9920

Schuberth-Wagner, C., Ludwig, J., Bruder, A. K., Herzner, A.-M., Zillinger, T., Goldeck, M., ... Schlee, M. (2015, jul). A Conserved Histidine in the RNA Sensor RIG-I Controls Immune Tolerance to N1-2'O-Methylated Self RNA. *Immunity*, *43*(1), 41–51. Retrieved from https://linkinghub.elsevier.com/retrieve/pii/S1074761315002599 doi: 10.1016/j.immuni.2015.06.015

Schulz, J. B., & Beal, M. F. (1994, aug). Mitochondrial dysfunction in movement disorders. *Curr. Opin. Neurol.*, *7*(4), 333–339. Retrieved from http://journals.lww.com/00019052-199408000-00010 doi: 10.1097/00019052-199408000-00010

Schurr, A. (2002, aug). Lactate, glucose and energy metabolism in the ischemic brain (Review). *Int. J. Mol. Med.*. Retrieved from http://www.spandidos-publications.com/10.3892/ijmm.10.2.131 doi: 10.3892/ijmm.10.2.131

Schwab, A. J., & Ebert, A. D. (2014, jul). Sensory Neurons Do Not Induce Motor Neuron Loss in a Human Stem Cell Model of Spinal Muscular Atrophy. *PLoS One*, *9*(7), e103112.

Retrieved from https://dx.plos.org/10.1371/journal.pone.0103112 doi: 10.1371/journal.pone.0103112

Scott, R. C., Schuldiner, O., & Neufeld, T. P. (2004). Role and regulation of starvation-induced autophagy in the Drosophila fat body. *Dev. Cell*, *7*(2), 167–178. doi: 10.1016/j.devcel.2004.07.009

Seo, J., Singh, N. N., Ottesen, E. W., Lee, B. M., & Singh, R. N. (2016, aug). A novel human-specific splice isoform alters the critical C-terminus of Survival Motor Neuron protein. *Sci. Rep.*, *6*(1), 30778. Retrieved from http://www.nature.com/articles/srep30778 doi: 10.1038/srep30778

Shanbhogue, L. K. R., Sikdar, T., Jackson, M., & Lloyd, D. A. (1992, mar). Serum electrolytes and capillary blood gases in the management of hypertrophic pyloric stenosis. *Br. J. Surg.*, *79*(3), 251–253. Retrieved from http://doi.wiley.com/10.1002/bjs.1800790322 doi: 10.1002/bjs.1800790322

Sharma, L., Lu, J., & Bai, Y. (2009). Mitochondrial Respiratory Complex I: Structure, Function and Implication in Human Diseases. *Curr. Med. Chem.*, *16*(10), 1266–1277. doi: 10.2174/092986709787846578

Sharma, S., & Lu, H. C. (2018). microRNAs in Neurodegeneration: Current Findings and Potential Impacts. *J. Alzheimer's Dis. Park.*, *08*(01). Retrieved from https://www.omicsonline.org/open-access/micrornas-in-neurodegeneration-current-findings-and-potential-impacts-2161-0460-1000420-99050.html doi: 10.4172/2161-0460.1000420

Shatkin, A. (1976, dec). Capping of eucaryotic mRNAs. *Cell*, *9*(4), 645–653. Retrieved from https://linkinghub.elsevier.com/retrieve/pii/0092867476901288 doi: 10.1016/0092-8674(76)90128-8

Sheng, Z.-H., & Cai, Q. (2012, feb). Mitochondrial transport in neurons: impact on synaptic homeostasis and neurodegeneration. *Nat. Rev. Neurosci.*, *13*(2), 77–93. Retrieved from http://www.nature.com/articles/nrn3156 doi: 10.1038/nrn3156

Shorrock, H. K., Gillingwater, T. H., & Groen, E. J. N. (2019, mar). Molecular Mechanisms Underlying Sensory-Motor Circuit Dysfunction in SMA. *Front. Mol. Neurosci.*, *12*(March), 59. Retrieved from https://www.frontiersin.org/article/10.3389/fnmol.2019.00059/fullhttp://www.ncbi.nlm.nih.gov/pubmed/30886572http://www.pubmedcentral.nih.gov/articlerender.fcgi?artid=PMC6409332 doi: 10.3389/fnmol.2019.00059

Shukla, S., & Parker, R. (2016, jul). Hypo- and Hyper-Assembly Diseases of RNA–Protein Complexes. *Trends Mol. Med.*, *22*(7), 615–628. Retrieved from https://linkinghub.elsevier.com/retrieve/pii/S1471491416300399 doi: 10.1016/j.molmed.2016.05.005

Singh, N. K., Singh, N. N., Androphy, E. J., & Singh, R. N. (2006, feb). Splicing of a Critical Exon of Human Survival Motor Neuron Is Regulated by a Unique Silencer Element Located

in the Last Intron. *Mol. Cell. Biol.*, *26*(4), 1333–1346. Retrieved from https://mcb.asm.org/content/26/4/1333 doi: 10.1128/MCB.26.4.1333-1346.2006

Sleigh, J. N., Gillingwater, T. H., & Talbot, K. (2011, jul). The contribution of mouse models to understanding the pathogenesis of spinal muscular atrophy. *Dis. Model. Mech.*, *4*(4), 457–467. Retrieved from http://dmm.biologists.org/cgi/doi/10.1242/dmm.007245 doi: 10.1242/dmm.007245

Smith, P. K., Krohn, R. I., Hermanson, G. T., Mallia, A. K., Gartner, F. H., Provenzano, M. D., ... Klenk, D. C. (1985, oct). Measurement of protein using bicinchoninic acid. *Anal. Biochem.*, *150*(1), 76–85. Retrieved from http://www.ncbi.nlm.nih.gov/pubmed/3843705 doi: 10.1016/0003-2697(85)90442-7

Sobol, A., Askonas, C., Alani, S., Weber, M. J., Ananthanarayanan, V., Osipo, C., & Bocchetta, M. (2017, feb). Deubiquitinase OTUD6B Isoforms Are Important Regulators of Growth and Proliferation. *Mol. Cancer Res.*, *15*(2), 117–127. Retrieved from http://mcr.aacrjournals.org/lookup/doi/10.1158/1541-7786.MCR-16-0281-T doi: 10.1158/1541-7786.MCR-16-0281-T

Somers, E., Lees, R. D., Hoban, K., Sleigh, J. N., Zhou, H., Muntoni, F., ... Parson, S. H. (2016, feb). Vascular Defects and Spinal Cord Hypoxia in Spinal Muscular Atrophy. *Ann. Neurol.*, *79*(2), 217–30. Retrieved from http://www.ncbi.nlm.nih.gov/pubmed/26506088 doi: 10.1002/ana.24549

Son, E. Y., Ichida, J. K., Wainger, B. J., Toma, J. S., Rafuse, V. F., Woolf, C. J., & Eggan, K. (2011, sep). Conversion of mouse and human fibroblasts into functional spinal motor neurons. *Cell Stem Cell*, *9*(3), 205–18. Retrieved from http://www.ncbi.nlm.nih.gov/pubmed/21852222http://www.pubmedcentral.nih.gov/articlerender.fcgi?artid=PMC3188987 doi: 10.1016/j.stem.2011.07.014

Sonenberg, N., & Gingras, A.-C. (1998, apr). The mRNA 5' cap-binding protein eIF4E and control of cell growth. *Curr. Opin. Cell Biol.*, *10*(2), 268–275. Retrieved from https://linkinghub.elsevier.com/retrieve/pii/S0955067498801506 doi: 10.1016/S0955-0674(98)80150-6

Sonenberg, N., & Hinnebusch, A. G. (2009, feb). Regulation of Translation Initiation in Eukaryotes: Mechanisms and Biological Targets. *Cell*, *136*(4), 731–745. Retrieved from https://linkinghub.elsevier.com/retrieve/pii/S0092867409000907http://dx.doi.org/10.1016/j.cell.2009.01.042 doi: 10.1016/j.cell.2009.01.042

Soubrouillard, C., Pellissier, J., Lepidi, H., Mancini, J., Rougon, G., & Figarella-Branger, D. (1995, nov). Expression of developmentally regulated cytoskeleton and cell surface proteins in childhood spinal muscular atrophies. *J. Neurol. Sci.*, *133*(1-2), 155–163. Retrieved from https://linkinghub.elsevier.com/retrieve/pii/0022510X95001822 doi: 10.1016/0022-510X(95)00182-2

Spillane, M., Ketschek, A., Merianda, T. T., Twiss, J. L., & Gallo, G. (2013, dec). Mitochondria Coordinate Sites of Axon Branching through Localized Intra-axonal Protein Synthesis.

Cell Rep., *5*(6), 1564–1575. Retrieved from https://linkinghub.elsevier.com/retrieve/pii/S221112471300689X doi: 10.1016/j.celrep.2013.11.022

Stadtman, E. R. (1990). Metal ion-catalyzed oxidation of proteins: Biochemical mechanism and biological consequences. *Free Radic. Biol. Med.*, *9*(4), 315–325. doi: 10.1016/0891-5849(90)90006-5

Sumner, C. J., & Crawford, T. O. (2018, aug). Two breakthrough gene-targeted treatments for spinal muscular atrophy: challenges remain. *J. Clin. Invest.*, *128*(8), 3219–3227. Retrieved from https://www.jci.org/articles/view/121658 doi: 10.1172/JCI121658

Surin, A. M., Khiroug, S., Gorbacheva, L. R., Khodorov, B. I., Pinelis, V. G., & Khiroug, L. (2013). Comparative analysis of cytosolic and mitochondrial ATP synthesis in embryonic and postnatal hippocampal neuronal cultures. *Front. Mol. Neurosci.*, *5*(March 2014). Retrieved from http://journal.frontiersin.org/article/10.3389/fnmol.2012.00102/abstract doi: 10.3389/fnmol.2012.00102

Suzuki, Y. J., Carini, M., & Butterfield, D. A. (2010, feb). Protein Carbonylation. *Antioxid. Redox Signal.*, *12*(3), 323–325. Retrieved from http://www.liebertpub.com/doi/10.1089/ars.2009.2887 doi: 10.1089/ars.2009.2887

Tadesse, H., Deschenes-Furry, J., Boisvenue, S., & Cote, J. (2007, nov). KH-type splicing regulatory protein interacts with survival motor neuron protein and is misregulated in spinal muscular atrophy. *Hum. Mol. Genet.*, *17*(4), 506–524. Retrieved from https://academic.oup.com/hmg/article-lookup/doi/10.1093/hmg/ddm327 doi: 10.1093/hmg/ddm327

Tanaka, Y., Kanai, Y., Okada, Y., Nonaka, S., Takeda, S., Harada, A., & Hirokawa, N. (1998, jun). Targeted Disruption of Mouse Conventional Kinesin Heavy Chain kif5B, Results in Abnormal Perinuclear Clustering of Mitochondria. *Cell*, *93*(7), 1147–1158. Retrieved from https://linkinghub.elsevier.com/retrieve/pii/S0092867400814592 doi: 10.1016/S0092-8674(00)81459-2

Tauffenberger, A., Fiumelli, H., Almustafa, S., & Magistretti, P. J. (2019, sep). Lactate and pyruvate promote oxidative stress resistance through hormetic ROS signaling. *Cell Death Dis.*, *10*(9), 653. Retrieved from http://www.nature.com/articles/s41419-019-1877-6 doi: 10.1038/s41419-019-1877-6

Tefera, T. W., & Borges, K. (2019, sep). Neuronal glucose metabolism is impaired while astrocytic TCA cycling is unaffected at symptomatic stages in the hSOD1 G93A mouse model of amyotrophic lateral sclerosis. *J. Cereb. Blood Flow Metab.*, *39*(9), 1710–1724. Retrieved from http://journals.sagepub.com/doi/10.1177/0271678X18764775 doi: 10.1177/0271678X18764775

Temperley, R. J., Wydro, M., Lightowlers, R. N., & Chrzanowska-Lightowlers, Z. M. (2010, jun). Human mitochondrial mRNAs—like members of all families, similar but different. *Biochim. Biophys. Acta - Bioenerg.*, *1797*(6-7), 1081–1085. Retrieved from https://linkinghub.elsevier.com/retrieve/pii/S0005272810000915 doi: 10.1016/j.bbabio.2010.02.036

Thelen, M. P., & Kye, M. J. (2020, jan). The Role of RNA Binding Proteins for Local mRNA Translation: Implications in Neurological Disorders. *Front. Mol. Biosci.*, *6*(January), 161. Retrieved from https://www.frontiersin.org/article/10.3389/fmolb.2019.00161/fullhttp://www.ncbi.nlm.nih.gov/pubmed/32010708http://www.pubmedcentral.nih.gov/articlerender.fcgi?artid=PMC6974540 doi: 10.3389/fmolb.2019.00161

Thelen, M. P., Wirth, B., & Kye, M. J. (2020, dec). Mitochondrial defects in the respiratory complex I contribute to impaired translational initiation via ROS and energy homeostasis in SMA motor neurons. *Acta Neuropathol. Commun.*, *8*(1), 223. Retrieved from https://doi.org/10.1186/s40478-020-01101-6https://actaneurocomms.biomedcentral.com/articles/10.1186/s40478-020-01101-6http://www.ncbi.nlm.nih.gov/pubmed/33353564http://www.pubmedcentral.nih.gov/articlerender.fcgi?artid=PMC7754598 doi: 10.1186/s40478-020-01101-6

Thoreen, C. C. (2017, feb). The molecular basis of mTORC1-regulated translation. *Biochem. Soc. Trans.*, *45*(1), 213–221. Retrieved from https://portlandpress.com/biochemsoctrans/article/45/1/213/66393/The-molecular-basis-of-mTORC1regulated-translation doi: 10.1042/BST20160072

Tiberi, E., Costa, S., Pane, M., Priolo, F., Sanctis, R., Romeo, D., ... Mercuri, E. (2020, dec). Nusinersen in type 0 spinal muscular atrophy: should we treat? *Ann. Clin. Transl. Neurol.*, *7*(12), 2481–2483. Retrieved from https://onlinelibrary.wiley.com/doi/10.1002/acn3.51126 doi: 10.1002/acn3.51126

Topf, U., Suppanz, I., Samluk, L., Wrobel, L., Böser, A., Sakowska, P., ... Warscheid, B. (2018, dec). Quantitative proteomics identifies redox switches for global translation modulation by mitochondrially produced reactive oxygen species. *Nat. Commun.*, *9*(1), 324. Retrieved from http://dx.doi.org/10.1038/s41467-017-02694-8http://www.nature.com/articles/s41467-017-02694-8 doi: 10.1038/s41467-017-02694-8

Topisirovic, I., Culjkovic, B., Cohen, N., Perez, J. M., Skrabanek, L., & Borden, K. L. B. (2003, feb). The proline-rich homeodomain protein, PRH, is a tissue-specific inhibitor of eIF4E-dependent cyclin D1 mRNA transport and growth. *EMBO J.*, *22*(3), 689–703. Retrieved from http://emboj.embopress.org/cgi/doi/10.1093/emboj/cdg069http://www.ncbi.nlm.nih.gov/pubmed/12554669http://www.pubmedcentral.nih.gov/articlerender.fcgi?artid=PMC140753 doi: 10.1093/emboj/cdg069

Turrens, J. F. (2003, oct). Mitochondrial formation of reactive oxygen species. *J. Physiol.*, *552*(2), 335–344. Retrieved from http://www.jphysiol.org/cgi/doi/10.1113/jphysiol.2003.049478 doi: 10.1113/jphysiol.2003.049478

Tyanova, S., Temu, T., Sinitcyn, P., Carlson, A., Hein, M. Y., Geiger, T., ... Cox, J. (2016). The Perseus computational platform for comprehensive analysis of (prote)omics data. *Nat. Methods*, *13*(9), 731–40. Retrieved from http://www.ncbi.nlm.nih.gov/pubmed/27348712 doi: 10.1038/nmeth.3901

Vannucci, S. J., Maher, F., & Simpson, I. A. (1997, sep). Glucose transporter proteins in brain: Delivery of glucose to neurons and glia. *Glia*, *21*(1), 2–21. Retrieved from https://onlinelibrary.wiley.com/doi/10.1002/(SICI)1098-1136(199709)21:1{%}3C2::AID-GLIA2{%}3E3.0.CO;2-Chttp://www.ncbi.nlm.nih.gov/pubmed/9298843 doi: 10.1002/(sici)1098-1136(199709)21:1<2::aid-glia2>3.0.co;2-c

Veo, B. L., & Krushel, L. A. (2009, feb). Translation Initiation of the Human Tau mRNA Through an Internal Ribosomal Entry Site. *J. Alzheimer's Dis.*, *16*(2), 271–275. Retrieved from https://www.medra.org/servlet/aliasResolver?alias=iospress{&}doi=10.3233/JAD-2009-0978 doi: 10.3233/JAD-2009-0978

Vergara, R. C., Jaramillo-Riveri, S., Luarte, A., Moënne-Loccoz, C., Fuentes, R., Couve, A., & Maldonado, P. E. (2019, jul). The Energy Homeostasis Principle: Neuronal Energy Regulation Drives Local Network Dynamics Generating Behavior. *Front. Comput. Neurosci.*, *13*. Retrieved from https://www.frontiersin.org/articles/10.3389/fncom.2019.00049/full doi: 10.3389/fncom.2019.00049

Verhaart, I. E. C., Robertson, A., Leary, R., McMacken, G., König, K., Kirschner, J., ... Lochmüller, H. (2017, jul). A multi-source approach to determine SMA incidence and research ready population. *J. Neurol.*, *264*(7), 1465–1473. Retrieved from http://link.springer.com/10.1007/s00415-017-8549-1 doi: 10.1007/s00415-017-8549-1

Vidal-Folch, N., Milosevic, D., Majumdar, R., Gavrilov, D., Matern, D., Raymond, K., ... Oglesbee, D. (2017, sep). A Droplet Digital PCR Method for Severe Combined Immunodeficiency Newborn Screening. *J. Mol. Diagnostics*, *19*(5), 755–765. Retrieved from https://linkinghub.elsevier.com/retrieve/pii/S1525157817301617 doi: 10.1016/j.jmoldx.2017.05.011

Vijayvergiya, C. (2005, mar). Mutant Superoxide Dismutase 1 Forms Aggregates in the Brain Mitochondrial Matrix of Amyotrophic Lateral Sclerosis Mice. *J. Neurosci.*, *25*(10), 2463–2470. Retrieved from http://www.jneurosci.org/cgi/doi/10.1523/JNEUROSCI.4385-04.2005 doi: 10.1523/JNEUROSCI.4385-04.2005

Vill, K., Kölbel, H., Schwartz, O., Blaschek, A., Olgemöller, B., Harms, E., ... Müller-Felber, W. (2019, oct). One Year of Newborn Screening for SMA – Results of a German Pilot Project. *J. Neuromuscul. Dis.*, *6*(4), 503–515. Retrieved from https://www.medra.org/servlet/aliasResolver?alias=iospress{&}doi=10.3233/JND-190428 doi: 10.3233/JND-190428

Visa, N., Izaurralde, E., Ferreira, J., Daneholt, B., & Mattaj, I. W. (1996, apr). A nuclear cap-binding complex binds Balbiani ring pre-mRNA cotranscriptionally and accompanies the ribonucleoprotein particle during nuclear export. *J. Cell Biol.*, *133*(1), 5–14. Retrieved from https://rupress.org/jcb/article/133/1/5/59104/A-nuclear-capbinding-complex-binds-Balbiani-ring doi: 10.1083/jcb.133.1.5

Vitte, J. M., Davoult, B., Roblot, N., Mayer, M., Joshi, V., Courageot, S., ... Melki, J. (2004, nov). Deletion of Murine Smn Exon 7 Directed to Liver Leads to Severe Defect

of Liver Development Associated with Iron Overload. *Am. J. Pathol.*, *165*(5), 1731–1741. Retrieved from https://linkinghub.elsevier.com/retrieve/pii/S0002944010634281 doi: 10.1016/S0002-9440(10)63428-1

Wan, L., Ottinger, E., Cho, S., & Dreyfuss, G. (2008, jul). Inactivation of the SMN complex by oxidative stress. *Mol. Cell*, *31*(2), 244–54. Retrieved from https://linkinghub.elsevier.com/retrieve/pii/S1097276508003936http://www.ncbi.nlm.nih.gov/pubmed/18657506http://www.pubmedcentral.nih.gov/articlerender.fcgi?artid=PMC2867055 doi: 10.1016/j.molcel.2008.06.004

Wang, C., & Youle, R. J. (2009, dec). The Role of Mitochondria in Apoptosis. *Annu. Rev. Genet.*, *43*(1), 95–118. Retrieved from http://www.annualreviews.org/doi/10.1146/annurev-genet-102108-134850 doi: 10.1146/annurev-genet-102108-134850

Wang, J., Xiong, S., Xie, C., Markesbery, W. R., & Lovell, M. A. (2005, may). Increased oxidative damage in nuclear and mitochondrial DNA in Alzheimer's disease. *J. Neurochem.*, *93*(4), 953–962. Retrieved from http://doi.wiley.com/10.1111/j.1471-4159.2005.03053.x doi: 10.1111/j.1471-4159.2005.03053.x

Wang, X., & Schwarz, T. L. (2009, jan). The Mechanism of Ca2+-Dependent Regulation of Kinesin-Mediated Mitochondrial Motility. *Cell*, *136*(1), 163–174. Retrieved from https://linkinghub.elsevier.com/retrieve/pii/S0092867408015213 doi: 10.1016/j.cell.2008.11.046

Wang, Z.-B., Zhang, X., & Li, X.-J. (2013, mar). Recapitulation of spinal motor neuron-specific disease phenotypes in a human cell model of spinal muscular atrophy. *Cell Res.*, *23*(3), 378–393. Retrieved from http://www.nature.com/articles/cr2012166 doi: 10.1038/cr.2012.166

Waterlow, J. C. (1984, jul). PROTEIN TURNOVER WITH SPECIAL REFERENCE TO MAN. *Q. J. Exp. Physiol.*, *69*(3), 409–438. Retrieved from http://doi.wiley.com/10.1113/expphysiol.1984.sp002829 doi: 10.1113/expphysiol.1984.sp002829

Weisiger, R. A., & Fridovich, I. (1973, may). Superoxide dismutase. Organelle specificity. *J. Biol. Chem.*, *248*(10), 3582–3592. Retrieved from http://europepmc.org/abstract/MED/4702877

Wiese, S., Herrmann, T., Drepper, C., Jablonka, S., Funk, N., Klausmeyer, A., ... Sendtner, M. (2010, jan). Isolation and enrichment of embryonic mouse motoneurons from the lumbar spinal cord of individual mouse embryos. *Nat Protoc*, *5*(1), 31–38. Retrieved from http://www.nature.com/doifinder/10.1038/nprot.2009.193http://www.ncbi.nlm.nih.gov/pubmed/20057379{%}5Cnhttp://www.nature.com/nprot/journal/v5/n1/pdf/nprot.2009.193.pdf doi: 10.1038/nprot.2009.193

Wiese, S., Metzger, F., Holtmann, B., & Sendtner, M. (1999, may). The role of p75 NTR in modulating neurotrophin survival effects in developing motoneurons. *Eur. J. Neurosci.*, *11*(5), 1668–1676. Retrieved from http://doi.wiley.com/10.1046/j.1460-9568.1999.00585.x doi: 10.1046/j.1460-9568.1999.00585.x

Will, C. L., & Lührmann, R. (2001, jun). Spliceosomal UsnRNP biogenesis, structure and function. *Curr. Opin. Cell Biol.*, *13*(3), 290–301. Retrieved from https://linkinghub.elsevier.com/retrieve/pii/S0955067400002118 doi: 10.1016/S0955-0674(00)00211-8

Winkler, C. (2005, oct). Reduced U snRNP assembly causes motor axon degeneration in an animal model for spinal muscular atrophy. *Genes Dev.*, *19*(19), 2320–2330. Retrieved from http://www.genesdev.org/cgi/doi/10.1101/gad.342005 doi: 10.1101/gad.342005

Wirth, B. (2000, mar). An update of the mutation spectrum of the survival motor neuron gene (SMN1) in autosomal recessive spinal muscular atrophy (SMA). *Hum. Mutat.*, *15*(3), 228–237. Retrieved from https://onlinelibrary.wiley.com/doi/10.1002/(SICI)1098-1004(200003)15:3{%}3C228::AID-HUMU3{%}3E3.0.CO;2-9 doi: 10.1002/(SICI)1098-1004(200003)15:3<228::AID-HUMU3>3.0.CO;2-9

Wirth, B. (2021). Spinal Muscular Atrophy: In the Challenge Lies a Solution. *Trends Neurosci.*, 1–17. Retrieved from https://doi.org/10.1016/j.tins.2020.11.009 doi: 10.1016/j.tins.2020.11.009

Wirth, B., Brichta, L., Schrank, B., Lochmüller, H., Blick, S., Baasner, A., & Heller, R. (2006, may). Mildly affected patients with spinal muscular atrophy are partially protected by an increased SMN2 copy number. *Hum. Genet.*, *119*(4), 422–428. Retrieved from http://link.springer.com/10.1007/s00439-006-0156-7 doi: 10.1007/s00439-006-0156-7

Wirth, B., Garbes, L., & Riessland, M. (2013, jun). How genetic modifiers influence the phenotype of spinal muscular atrophy and suggest future therapeutic approaches. *Curr. Opin. Genet. Dev.*, *23*(3), 330–338. Retrieved from https://linkinghub.elsevier.com/retrieve/pii/S0959437X13000464 doi: 10.1016/j.gde.2013.03.003

Wirth, B., Karakaya, M., Kye, M. J., & Mendoza-Ferreira, N. (2020, aug). Twenty-Five Years of Spinal Muscular Atrophy Research: From Phenotype to Genotype to Therapy, and What Comes Next. *Annu. Rev. Genomics Hum. Genet.*, *21*(1), annurev–genom–102319–103602. Retrieved from https://www.annualreviews.org/doi/10.1146/annurev-genom-102319-103602 doi: 10.1146/annurev-genom-102319-103602

Wirth, B., Schmidt, T., Hahnen, E., Rudnik-Schöneborn, S., Krawczak, M., Müller-Myhsok, B., ... Zerres, K. (1997, nov). De novo rearrangements found in 2% of index patients with spinal muscular atrophy: mutational mechanisms, parental origin, mutation rate, and implications for genetic counseling. *Am. J. Hum. Genet.*, *61*(5), 1102–11. Retrieved from http://www.ncbi.nlm.nih.gov/pubmed/9345102http://www.pubmedcentral.nih.gov/articlerender.fcgi?artid=PMC1716038 doi: 10.1086/301608

Wozniak, M. J., Melzer, M., Dorner, C., Haring, H.-U., & Lammers, R. (2005). The novel protein KBP regulates mitochondria localization by interaction with a kinesin-like protein. *BMC Cell Biol.*, *6*(1), 35. Retrieved from https://doi.org/10.1186/1471-2121-6-35 doi: 10.1186/1471-2121-6-35

Wu, K. Y., Hengst, U., Cox, L. J., Macosko, E. Z., Jeromin, A., Urquhart, E. R., & Jaffrey, S. R. (2005, aug). Local translation of RhoA regulates growth cone collapse. *Nature*, *436*(7053), 1020–1024. Retrieved from http://www.nature.com/articles/nature03885 doi: 10.1038/nature03885

Wurth, L., Gribling-Burrer, A.-S., Verheggen, C., Leichter, M., Takeuchi, A., Baudrey, S., ... Allmang, C. (2014, jul). Hypermethylated-capped selenoprotein mRNAs in mammals. *Nucleic Acids Res.*, *42*(13), 8663–77. Retrieved from http://www.ncbi.nlm.nih.gov/pubmed/25013170http://www.pubmedcentral.nih.gov/articlerender.fcgi?artid=PMC4117793 doi: 10.1093/nar/gku580

Wyss, M. T., Jolivet, R., Buck, A., Magistretti, P. J., & Weber, B. (2011, may). In Vivo Evidence for Lactate as a Neuronal Energy Source. *J. Neurosci.*, *31*(20), 7477–7485. Retrieved from http://www.jneurosci.org/cgi/doi/10.1523/JNEUROSCI.0415-11.2011 doi: 10.1523/JNEUROSCI.0415-11.2011

Xu, C. C., Denton, K. R., Wang, Z. B., Zhang, X., & Li, X. J. (2016). Abnormal mitochondrial transport and morphology as early pathological changes in human models of spinal muscular atrophy. *DMM Dis. Model. Mech.*, *9*(1), 39–49. doi: 10.1242/dmm.021766

Xu, Z., Zheng, Y., Zhu, Y., Kong, X., & Hu, L. (2011, jan). Evidence for OTUD-6B Participation in B Lymphocytes Cell Cycle after Cytokine Stimulation. *PLoS One*, *6*(1), e14514. Retrieved from https://dx.plos.org/10.1371/journal.pone.0014514 doi: 10.1371/journal.pone.0014514

Yamashita, R., Suzuki, Y., Takeuchi, N., Wakaguri, H., Ueda, T., Sugano, S., & Nakai, K. (2008, jun). Comprehensive detection of human terminal oligo-pyrimidine (TOP) genes and analysis of their characteristics. *Nucleic Acids Res.*, *36*(11), 3707–3715. Retrieved from https://academic.oup.com/nar/article-lookup/doi/10.1093/nar/gkn248 doi: 10.1093/nar/gkn248

Yanagiya, A., Suyama, E., Adachi, H., Svitkin, Y. V., Aza-Blanc, P., Imataka, H., ... Sonenberg, N. (2012, jun). Translational Homeostasis via the mRNA Cap-Binding Protein, eIF4E. *Mol. Cell*, *46*(6), 847–858. Retrieved from http://dx.doi.org/10.1016/j.molcel.2012.04.004https://linkinghub.elsevier.com/retrieve/pii/S1097276512003000 doi: 10.1016/j.molcel.2012.04.004

Yecies, J. L., & Manning, B. D. (2011, apr). Transcriptional Control of Cellular Metabolism by mTOR Signaling. *Cancer Res.*, *71*(8), 2815–2820. Retrieved from http://cancerres.aacrjournals.org/cgi/doi/10.1158/0008-5472.CAN-10-4158 doi: 10.1158/0008-5472.CAN-10-4158

Yellen, G. (2018, jul). Fueling thought: Management of glycolysis and oxidative phosphorylation in neuronal metabolism. *J. Cell Biol.*, *217*(7), 2235–2246. Retrieved from https://rupress.org/jcb/article/217/7/2235/39109/Fueling-thought-Management-of-glycolysis-and doi: 10.1083/jcb.201803152

Yeo, C. J. J., & Darras, B. T. (2021, jan). Yeo and Darras: Extraneuronal Phenotypes of Spinal Muscular Atrophy. *Ann. Neurol.*, *89*(1), 24–26. Retrieved from https://onlinelibrary.wiley.com/doi/10.1002/ana.25930 doi: 10.1002/ana.25930

Zappulo, A., van den Bruck, D., Ciolli Mattioli, C., Franke, V., Imami, K., McShane, E., ... Chekulaeva, M. (2017, dec). RNA localization is a key determinant of neurite-enriched proteome. *Nat. Commun.*, *8*(1), 583. Retrieved from http://www.nature.com/articles/s41467-017-00690-6 doi: 10.1038/s41467-017-00690-6

Zerres, K. (1995, may). Natural History in Proximal Spinal Muscular Atrophy. *Arch. Neurol.*, *52*(5), 518. Retrieved from http://archneur.jamanetwork.com/article.aspx?doi=10.1001/archneur.1995.00540290108025 doi: 10.1001/archneur.1995.00540290108025

Zerres, K. (1997, may). Spinal muscular atrophy—clinical and genetic correlations. *Neuromuscul. Disord.*, *7*(3), 202–207. Retrieved from https://linkinghub.elsevier.com/retrieve/pii/S0960896697004598 doi: 10.1016/S0960-8966(97)00459-8

Zerres, K., Rudnik-Schöneborn, S., Forkert, R., & Wirth, B. (1995, oct). Genetic basis of adult-onset spinal muscular atrophy. *Lancet*, *346*(8983), 1162. Retrieved from https://linkinghub.elsevier.com/retrieve/pii/S0140673695918353 doi: 10.1016/S0140-6736(95)91835-3

Zerres, K., Rudnik-Schöneborn, S., Forrest, E., Lusakowska, A., Borkowska, J., & Hausmanowa-Petrusewicz, I. (1997, feb). A collaborative study on the natural history of childhood and juvenile onset proximal spinal muscular atrophy (type II and III SMA): 569 patients. *J. Neurol. Sci.*, *146*(1), 67–72. Retrieved from https://linkinghub.elsevier.com/retrieve/pii/S0022510X96002845 doi: 10.1016/S0022-510X(96)00284-5

Zhang, C. L., Ho, P. L., Kintner, D. B., Sun, D., & Chiu, S. Y. (2010, mar). Activity-Dependent Regulation of Mitochondrial Motility by Calcium and Na/K-ATPase at Nodes of Ranvier of Myelinated Nerves. *J. Neurosci.*, *30*(10), 3555–3566. Retrieved from http://www.jneurosci.org/cgi/doi/10.1523/JNEUROSCI.4551-09.2010 doi: 10.1523/JNEUROSCI.4551-09.2010

Zhang, H. L., Pan, F., Hong, D., Shenoy, S. M., Singer, R. H., & Bassell, G. J. (2003, jul). Active Transport of the Survival Motor Neuron Protein and the Role of Exon-7 in Cytoplasmic Localization. *J. Neurosci.*, *23*(16), 6627–6637. Retrieved from http://www.jneurosci.org/lookup/doi/10.1523/JNEUROSCI.23-16-06627.2003 doi: 10.1523/JNEUROSCI.23-16-06627.2003

Zhang, J., Wang, X., Vikash, V., Ye, Q., Wu, D., Liu, Y., & Dong, W. (2016). ROS and ROS-Mediated Cellular Signaling. *Oxid. Med. Cell. Longev.*, *2016*, 1–18. Retrieved from https://linkinghub.elsevier.com/retrieve/pii/B9780124058811000021http://www.hindawi.com/journals/omcl/2016/4350965/ doi: 10.1155/2016/4350965

Zheng, X., Boyer, L., Jin, M., Mertens, J., Kim, Y., Ma, L., ... Hunter, T. (2016). Metabolic reprogramming during neuronal differentiation from aerobic glycolysis to neuronal oxidative phosphorylation. *Elife*, *5*(JUN2016). doi: 10.7554/eLife.13374

Zinzalla, V., Stracka, D., Oppliger, W., & Hall, M. N. (2011, mar). Activation of mTORC2 by Association with the Ribosome. *Cell*, *144*(5), 757–768. Retrieved from https://linkinghub.elsevier.com/retrieve/pii/S0092867411001280 doi: 10.1016/j.cell.2011.02.014

8 PUBLICATIONS AND PRESENTATIONS

Publications

Thelen, M.P., Wirth, B., Kye, M.J., Mitochondrial Defects in the Respiratory Complex I Contribute to Impaired Translational Initiation via ROS and Energy Homeostasis in SMA Motor Neurons. *Acta Neuropathologica Communications* (2020) doi: 10.1186/s40478-020-01101-6 - Research article

Mendoza-Ferreira, M., Karakaya, M., Cengiz, N., Beijer, D., Brigatti, K.R., Gonzaga-Jauregui, C., Fuhrmann, N., Hölker, I., **Thelen, M.P.**, Zetsche, S., Rombo, R., Puffenberger, E.G., Jonghe, P.D., Deconinck, T., Zuchner, S., Strauss, K.A., Carson, V., Schrank, B., Wunderlich, G., Baets, J., Wirth, B., De Novo and Inherited Variants in GBF1 are Associated with Axonal Neuropathy Caused by Golgi Fragmentation. *The American Journal of Human Genetics* (2020) doi: 10.1016/j.ajhg.2020.08.018 - Report

Thelen, M.P. & Kye, M.J., The Role of RNA Binding Proteins for Local mRNA Translation: Implications in Neurological Disorders. *Frontiers in Molecular Biosciences* (2020) doi: 10.3389/fmolb.2019.00161 - Review

Rehorst, W.A., **Thelen, M.P.**, Nolte, H., Türk, C., Cirak, S., Peterson J.M., Wong, G.W., Wirth, B., Krüger, M., Winter, D., Kye, M.J., Muscle regulates mTOR dependent axonal local translation in motor neurons via CTRP3 secretion: Implications for a neuromuscular disorder, spinal muscular atrophy. *Acta Neuropathologica Communications* (2019) doi: 10.1186/s40478-019-0806-3 - Research article

Gonçalves, I., Brecht, J., **Thelen, M.P.**, Rehorst, W.A., Terers, M., Lee, H.J., Motameny, S., Torres-Benito, L., Ebrahimi-Fakhari, D., Kononenko, N.L., Altmüller, J., Vilchez, D., Sahin, M., Wirth, B., Kye, M.J., Neuronal activity regulates DROSHA via autophagy in spinal muscular atrophy. *Scientific Reports* (2018) doi: 10.1038/s41598-018-26347-y - Research article

Poster presentations

Thelen MP, Kye MJ. „ROS and ATP regulate SMN protein synthesis via mTOR pathway in motor neurons“. SMA Europe (2020), Paris, France

Thelen MP, Kye MJ, „Interplay among energy homeostasis, reactive oxygen species and protein synthesis in a genetic neuromuscular disorder, Spinal Muscular Atrophy“. Crossroads in Biology (2019), Cologne, Germany

Thelen MP, Kye MJ, „Interplay among energy homeostasis, reactive oxygen species and protein synthesis in a genetic neuromuscular disorder, Spinal Muscular Atrophy“. Cure SMA (2019), Anaheim, CA, USA

Thelen MP, Kye MJ. “Restoring Distrurbed Energy Homeostasis in Spinal Muscular Atrophy”. Society for Neuroscience (2018), San Diego, CA, USA

Thelen MP, Kye MJ. “Restoring Distrurbed Energy Homeostasis in Spinal Muscular Atrophy”. SMA Europe (2018), Krakow, Poland

APPENDIX

Appendix A Thelen *et al.*, (2020) *Acta Neuropathologica Communications*

Results embedded in this doctoral thesis were published in the research article **"Mitochondrial defects in respiratory complex I contribute to impaired translational initiation via ROS and energy homeostasis in SMA motor neurons"** in the journal *Acta Neuropathologica Communications* in December 2020. The authors' contributions are listed in the article.

Thelen et al. acta neuropathol commun (2020) 8:223
https://doi.org/10.1186/s40478-020-01101-6

Acta Neuropathologica Communications

RESEARCH Open Access

Mitochondrial defects in the respiratory complex I contribute to impaired translational initiation via ROS and energy homeostasis in SMA motor neurons

Maximilian Paul Thelen[1,2], Brunhilde Wirth[1,2,3] and Min Jeong Kye[1,2*]

Abstract

Spinal muscular atrophy (SMA) is a neuromuscular disease characterized by loss of lower motor neurons, which leads to proximal muscle weakness and atrophy. SMA is caused by reduced survival motor neuron (SMN) protein levels due to biallelic deletions or mutations in the *SMN1* gene. When SMN levels fall under a certain threshold, a plethora of cellular pathways are disturbed, including RNA processing, protein synthesis, metabolic defects, and mitochondrial function. Dysfunctional mitochondria can harm cells by decreased ATP production and increased oxidative stress due to elevated cellular levels of reactive oxygen species (ROS). Since neurons mainly produce energy via mitochondrial oxidative phosphorylation, restoring metabolic/oxidative homeostasis might rescue SMA pathology. Here, we report, based on proteome analysis, that SMA motor neurons show disturbed energy homeostasis due to dysfunction of mitochondrial complex I. This results in a lower basal ATP concentration and higher ROS production that causes an increase of protein carbonylation and impaired protein synthesis in SMA motor neurons. Counteracting these cellular impairments with pyruvate reduces elevated ROS levels, increases ATP and SMN protein levels in SMA motor neurons. Furthermore, we found that pyruvate-mediated SMN protein synthesis is mTOR-dependent. Most importantly, we showed that ROS regulates protein synthesis at the translational initiation step, which is impaired in SMA. As many neuropathies share pathological phenotypes such as dysfunctional mitochondria, excessive ROS, and impaired protein synthesis, our findings suggest new molecular interactions among these pathways. Additionally, counteracting these impairments by reducing ROS and increasing ATP might be beneficial for motor neuron survival in SMA patients.

Keywords: Spinal muscular atrophy, SMN, *SMN1*, *SMN2*, Mitochondria, Reactive oxygen species, Translation initiation

Background

Spinal muscular atrophy (SMA) is an inherited neuromuscular disease that is characterized by loss of lower motor neurons (MNs) due to reduced levels of the ubiquitously expressed survival motor neuron (SMN) protein [1]. The incidence of SMA varies between 1 per 6000–10,000 newborns in the human population [2]. In 96% of SMA patients, homozygous deletions, or mutations in *SMN1*, the gene encoding for full-length SMN, have been described [2]. Interestingly, the human genome contains an almost identical gene - *SMN2* -, that mainly produces a transcript lacking exon 7 due to a single silent mutation [3]. Hence, *SMN2* produces approximately 10% of the full-length SMN protein compared to *SMN1*. As the amount of SMN protein inversely correlates with

*Correspondence: min.kye@uk-koeln.de
[1] Institute of Human Genetics, University of Cologne, Kerpener Str. 34, 50931 Cologne, Germany
Full list of author information is available at the end of the article

disease severity [4], the copy number of *SMN2* is often used as a good predictor of SMA severity. SMN forms a stable complex with other proteins such as Gemin2-8 [5]. Additionally, SMN is an RNA binding protein that is involved in multiple essential cellular functions, including biogenesis of spliceosomal small nuclear ribonucleoproteins (snRNPs) [6] and trafficking of mRNAs to axon terminals [7–10]. Furthermore, SMN deficient cells show dysregulated splicing and miRNA processing [11, 12], hyperexcitability and impaired Ca^{2+} homeostasis [13–15], decreased translation [8, 16, 17], and also results in impaired axon growth [9]. These findings suggest SMN as a multifunctional protein.

Recent evidence suggests that energy metabolism is impaired in SMA, including mitochondria and glucose metabolism [18–20]. In the mitochondrial oxidative phosphorylation (OXPHOS), the NADH:ubiquinone oxidoreductase (complex I) of the electron transport chain is the rate-limiting enzyme in respiration and the major producer of reactive oxygen species (ROS) [21, 22]. Therefore, a dysfunctional complex I could impair energy production as well as ROS homeostasis. ROS can function as signaling molecules by activating various pathways, including MAPK, PI3K, and Ca^{2+} signaling [21], and harm cells by irreversible protein modifications such as carbonylation [23, 24]. For example, oxidative stress can hinder the SMN complex formation [25].

Various cellular mechanisms regulate neuronal protein synthesis, including trafficking of molecules, axonal local translation, and local protein degradation. Notably, impaired protein synthesis has been reported in various neurodegenerative disorders, including Alzheimer's disease (AD) and SMA. The mammalian target of rapamycin (mTOR) is the master regulator of protein synthesis in neurons. Lost balance in the mTOR pathway causes neuronal dysfunction from Tuberous sclerosis complex (TSC) to Rett syndrome [26]. mTOR can form two complexes based on its binding partners, mTORC1 and mTORC2. mTORC1 acts as an integral node between cellular energy production and consumption. It promotes anabolic processes but also restricts catabolic processes such as autophagy [27–29]. Anabolic processes promoted by active mTORC1 include mitochondrial biogenesis [30] and protein synthesis [31]. Cap-dependent translation initiation is promoted by mTORC1 via phosphorylation of 4E-BP1 or S6 kinase (S6K) [32–34].

Here, we first report the molecular mechanism explaining how mitochondria regulate protein synthesis via ATP and ROS production in spinal MNs. Furthermore, when this pathway is disturbed, it contributes to the MN disease, SMA. Particularly, cellular ATP and ROS signaling regulate protein synthesis at the translational initiation step, which is impaired in SMA MNs. Our findings imply that mitochondria control neuronal energy and ROS homeostasis, and protein synthesis via the mTOR pathway.

Materials and methods

Animal model

An SMA mouse model carrying two *SMN2* copies on one allele and a murine *Smn* null, FVB/N background was used [35]. It was established by breeding $Smn^{KO/KO}$; $SMN2^{tg/tg}$ mice with $Smn^{KO/WT}$ mice resulting in 50% SMA mice ($Smn^{KO/KO}$; $SMN2^{tg/0}$) and 50% phenotypically normal heterozygous littermates ($Smn^{KO/WT}$; $SMN2^{tg/0}$) [36]. FVB/N wild type mice were used as controls (Charles River).

Primary MN culture

E13.5 embryos were used for primary MN culture. SMA embryos were genotyped (KAPA mouse genotyping kit, Sigma) and cultured as previously described [36]. Briefly, spinal cords were isolated and dissociated with 1% trypsin (Worthington) in PBS. Single cell suspension was achieved by trituration with DNase I (Applichem) in plating medium (Dulbecco's Modified Eagle's Medium (DMEM) with 5% fetal calf serum (Biochrom), 0.6% glucose, penicillin/streptomycin (Thermo Fisher Scientific), and amphotericin B (Promocell)). For imaging analyses, 15,000 cells/cm^2 were plated on poly-D-lysine (PDL, 10 µg/ml, Sigma) coated coverslips, and for biochemical analyses, 120,000 cells/cm^2 were plated on PDL coated plates with plating media. Plating media was replaced by MN maintenance medium (Neurobasal medium with B27 supplement (Thermo Fisher Scientific), 2 mM L-glutamine, 1% penicillin/streptomycin and 0.25% amphotericin B with additional growth factors: brain derived neurotrophic factor (BDNF, 10 ng/ml), ciliary neurotrophic factor (CNTF, 10 ng/ml), and glia cell line derived neurotrophic factor (GDNF, 10 ng/ml, all purchased from PeproTech)). Half of the medium was exchanged every third day, and cytosine arabinoside (AraC) was added continuously after 3 days to a final concentration of 1 µM. Cells were cultured at 37 °C in a humidified incubator with 5% CO_2.

Culture of cell lines

MN-like NSC-34 [37] cells were cultured in DMEM with 10% fetal calf serum, 1% penicillin/streptomycin, and amphotericin B. 20,000 cells/cm^2 were plated onto PDL coated 12- well plates. Differentiation was induced by 50 µM retinoic acid (Sigma) for 3 days. Cells were maintained at 37 °C in a humidified incubator with 5% CO_2.

RNA isolation, cDNA synthesis and real-time PCR

Total RNA was extracted from cells using the mirVana miRNA Isolation Kit (Thermo Fisher Scientific) according to the manufacturer's instructions. cDNA was produced from total RNA using the High-Capacity cDNA Reverse Transcription Kit (Thermo Fisher Scientific) with random primers. mRNA expression levels were quantified with PowerSYBR Green PCR Master Mix (Thermo Fisher Scientific) and 1 µM of gene-specific primers using real-time PCR (7500 Real-Time PCR System, Thermo Fisher Scientific). Specificity of the primers was confirmed by Sanger's sequencing. Sequences of primers are listed in Additional file 1: Supplementary Table 1.

Protein isolation and Western blot analysis

Proteins were extracted with RIPA buffer (Sigma) with protease and phosphatase inhibitors (Thermo Fisher Scientific), and protein concentration was determined by Pierce BCA protein assay kit (Thermo Fisher Scientific). Western blot analysis was performed with a standard protocol. The information about antibodies is listed in Additional file 1: Supplementary Table 2. Signals were detected with ChemiDoc XRS + System (BioRad) using ECL chemiluminescence (Thermo Scientific) and quantified using the ImageLab 6.0 software (BioRad).

MitoTracker and immunostaining of MNs

Cells were incubated with MitoTracker Red CMXRos (Thermo Fisher Scientific) at a final concentration of 100 nM for 15 min and fixed with 4% paraformaldehyde (PFA). The information about dyes can be found in Additional file 1: Supplementary Table 3. Images were acquired with a fluorescence microscope (Zeiss Axio Imager.M2) equipped with an AxioCam MR camera and an ApoTome.2 system and analyzed with FIJI. All image analyses were performed blindly.

Drug treatment

Primary MNs and NSC34 cells were supplemented in culture with the following substances at given concentrations in each figure legend and Additional file 1: Supplementary Table 4: The supplements sodium pyruvate and sodium lactate, the antioxidant N-acetylcysteine (NAC), the ROS inducer menadione, the protein synthesis inhibitor anisomycin (all purchased from Sigma) and the water-soluble mTOR inhibitor WYE-687 dihydrochloride (Tocris).

Proteomics of primary MNs

Primary MNs were treated with 50 mM pyruvate, 10 µM NAC, and 100 µM menadione for 1 h, lysed in RIPA buffer with protease and phosphatase inhibitors, and further processed for mass spectrometry (MS) analysis. Proteins were precipitated using ice-cold acetone at −80 °C for 15 min and at − 20 °C for 2 h. Next, proteins were resuspended in 8 M urea buffer with protease inhibitor, reduced in-solution using 5 mM dithiothreitol (DTT) at room temperature (RT) for 1 h, alkylated with 40 mM chloroacetamide (CAA) in the dark for 30 min, and digested with endo-proteinase Lys-C at RT for 4 h. Samples were diluted with 50 mM triethylammoniumbicarbonate (TEAB) to a final concentration of urea ≤ 2 M and digested with trypsin at RT for 8 h. After digestion was completed, samples were acidified with 1% formic acid and purified with styrenedivinylbenzene-reverse phase sulfonate (SDB-RPS) Stage Tips. Proteomic analysis was performed with ultra-high-performance liquid chromatography (UHPLC) coupled to a Quadrupole-Orbitrap mass spectrometer (CECAD/CMMC Proteomics core facility, University of Cologne). Raw data were analyzed by MaxQuant. As a reference, a canonical mouse database from Uniprot (22.08.19) was used. For gene ontology (GO) analysis, the Database for Annotation, Visualization and Integrated Discovery 6.7 (DAVID) was used. Statistical analysis and data visualization were performed using RStudio and R version 3.6.2. We used the mouse MitoCarta2.0 dataset to identify mitochondrial proteins [38]. Additional data about identified proteins and GO analysis are listed in Additional file 2: MS Source data.

(See figure on next page.)

Fig. 1 Mitochondria are defective in SMA MNs. **a**, **b** Volcano plot (**a**) and pie chart (**b**) of whole proteome analysis comparing WT and SMA MNs; plotted *p* values ($-\log_{10}$) against fold changes ($\log_2$, SMA/WT). Four independent samples of WT MNs and three independent samples of SMA MNs were used for analysis. *p* values were determined using unpaired two-sided t-test. Proteins with $p < 0.05$ are highlighted in blue (313 down-regulated) and red (120 up-regulated), and proteins with localization in mitochondria are marked in purple (32 down-regulated and 29 up-regulated). **c**, **d** Gene ontology (GO) analysis of 345 down-regulated (**c**) and 149 up-regulated proteins (**d**) in SMA MNs. The 5 most significant terms of each category are shown. **e** Representative images and quantification of mitochondria in 100 µm long primary axons of WT and SMA MNs labeled with anti-Tau antibody (green), DAPI (blue), and anti-TOM20 antibody or MitoTracker (white). Scale bars: 20 µm. Each dot represents the average number of mitochondria in each neuron (n = 30; biological replicates N = 3). Two-way ANOVA with Tukey HSD post hoc analysis was used to determine statistical significance for multiple comparisons. Bar graphs depict the mean ± S.D. ***$p < 0.001$

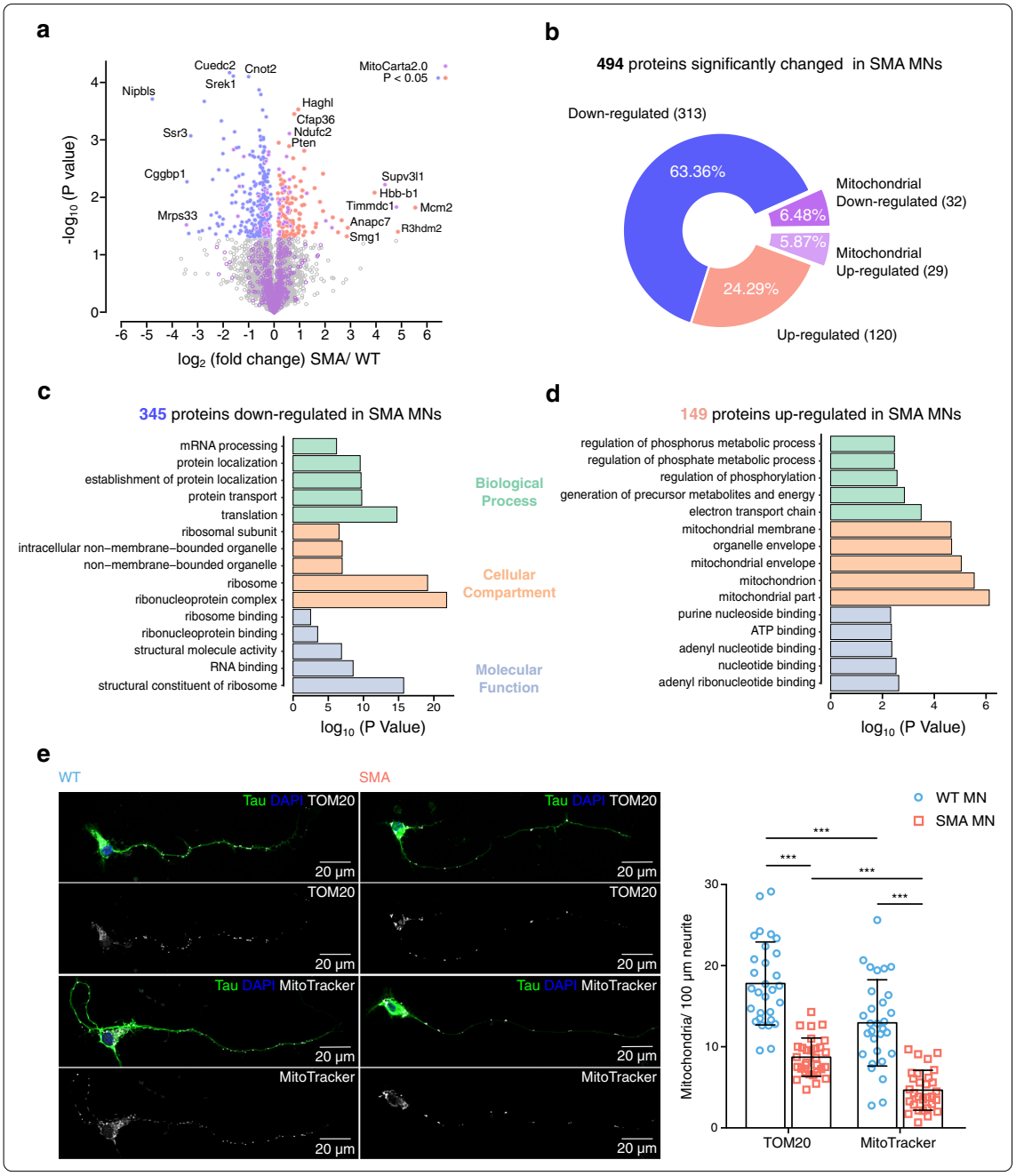

Isolation of mitochondria and complex I activity assay

Mitochondria were isolated from cultured primary MNs using the Mitochondria Isolation Kit (Abcam) according to the manufacturer's instructions. In brief, 3×10^7 10 days in vitro (DIV) cultured MNs were collected, frozen for 10 min, and subsequently thawed. Cells were disrupted by a pre-cooled Dounce homogenizer after 10 min incubation on ice. After additional centrifugation at 1000 x g, the supernatant was collected and centrifuged again at 12,000 x g. Finally,

isolated mitochondria were resuspended in a storage buffer and kept at −80 °C until further use. To test the functionality of mitochondrial respiratory chain complexes, complex I enzyme activity assay kit (Abcam) was used. In brief, proteins extracted from the isolated mitochondria were loaded onto a microwell plate and complex I proteins were attached to the microplate via antibody coupling. Complex I activity was measured by the optical density (OD_{450} nm) after adding substrates. The enzyme kinetic was followed for 1 h. We used 300 µg of cell extracts for tissue samples from heart and 20 µg of mitochondrial extracts for MN samples.

SUnSET assay (surface sensing of translation)

Protein synthesis was measured by SUnSET assay [39]. Cells were treated with ROS modifying drugs or 50 µM anisomycin as negative control. Afterward, the cells were incubated with 1 µM puromycin for 30 min. Finally, puromycin labeled peptides were detected by western blotting or immunostaining using an anti-puromycin antibody. Axons were selected with a segmented line, straightened, and divided into 20 µm bins using the concentric circles plugin. Mean puromycin intensities were quantified using plot profiles.

SunRiSE (SUnSET-based Ribosome Speed of Elongation)

SunRiSE assay was used to monitor protein elongation speed [40]. Initiation of mRNA translation was blocked by 2 µg/ml harringtonine (Abcam) at different time points, and all samples were incubated with 10 µg/ml (16.7 µM) puromycin for 10 min. Puromycin labeled peptides were detected by western blotting.

ATP assay

Intracellular ATP concentrations were measured with the ATP determination kit (Thermo Fisher Scientific) based on bioluminescence signal detection by the GloMax luminescence reader (Promega). ATP levels were normalized to the amounts of soluble proteins determined by BCA assay.

Glucose uptake assay

Glucose Uptake-Glo kit (Promega) was used to measure glucose uptake efficiency using 120,000 cells/cm^2. We mainly followed the manufacturer's instruction and luminescence was detected by the GloMax luminescence reader. Signal was normalized to protein concentration measured by BCA assay.

Pyruvate uptake assay

Pyruvate uptake was measured with the Pyruvate assay kit (Sigma). Fluorescence signal was measured with a Safire 2 microplate reader (Tecan) and normalized to soluble protein amount.

Detection of oxidative stress

CellROX Green reagent (Thermo Fisher Scientific) was used to measure oxidative stress. Cells were incubated with 5 µM CellROX Green reagent for 30 min, fixed with 3.7% formaldehyde, nuclei, and F-actin were labeled with DAPI and Alexa Fluor 568 Phalloidin (Thermo Fisher Scientific), respectively. Images were acquired with a fluorescence microscope equipped with an ApoTome.2 system. CellROX signal was quantified with a Safire 2 microplate reader (Tecan). Signals of the microplate reader were normalized to soluble protein concentration after lysis with RIPA buffer.

Protein carbonylation assay

The amount of protein carbonyl groups was measured with the Protein carbonyl assay kit (Abcam). Proteins were quantified by Bradford.

(See figure on next page.)

Fig. 2 Defective mitochondrial complex I causes cellular dysfunction in SMA MNs. **a** Complex I activity using 20 µg mitochondria extract isolated from WT and SMA MNs (10DIV) (N = 4). Quantification represents the increase in mean OD_{450} nm/h. **b** Representative images and quantification of WT and SMA MNs labeled with CellROX (green and rainbow color) for ROS detection, DAPI (blue), and Phalloidin (red). Rainbow color indicates the intensity of CellROX signal. Quantification of mean fluorescence intensity of the CellROX signal in WT and SMA MN (red squares) (n = 40, N = 4). Scale bars are written on individual images. **c** Quantification of CellROX signal of WT and SMA MNs measured with a microplate reader (N = 5). **d** Western blot analysis and quantification of carbonylated proteins (DNP = 2,4-dinitrophenyl) in 10DIV WT and SMA MNs (N = 4). Bar graph represents the quantification of the DNP signal. ACTB was used as a loading control. **e** ATP levels in WT (N = 7) and SMA MNs (N = 8). Data are normalized to solubilized protein amounts. **f** ATP levels in WT and SMA MNs (N = 6) after 50 mM pyruvate treatment for 1 h. Data are normalized to solubilized protein amounts. Individual data (circle or square) represent biological replicates. **g** ROS levels of SMA MNs after 50 mM pyruvate or 100 µM menadione treatment for 1 h. Two-tailed unpaired t-tests with Holm-Bonferroni correction for multiple comparisons were used on independent biological replicates (N = 6) to determine statistical significance. *$p < 0.05$, **$p < 0.01$. **a–f** Blue circles represent data from WT and red squares represent SMA MNs. 10DIV MNs were used. Each dot represents the quantification of individual biological replicates. A two-tailed unpaired t-test was used on independent biological replicates to determine statistical significance. Bar graphs depict the mean ± S.D., n.s. $p > 0.05$, *$p < 0.05$, **$p < 0.01$

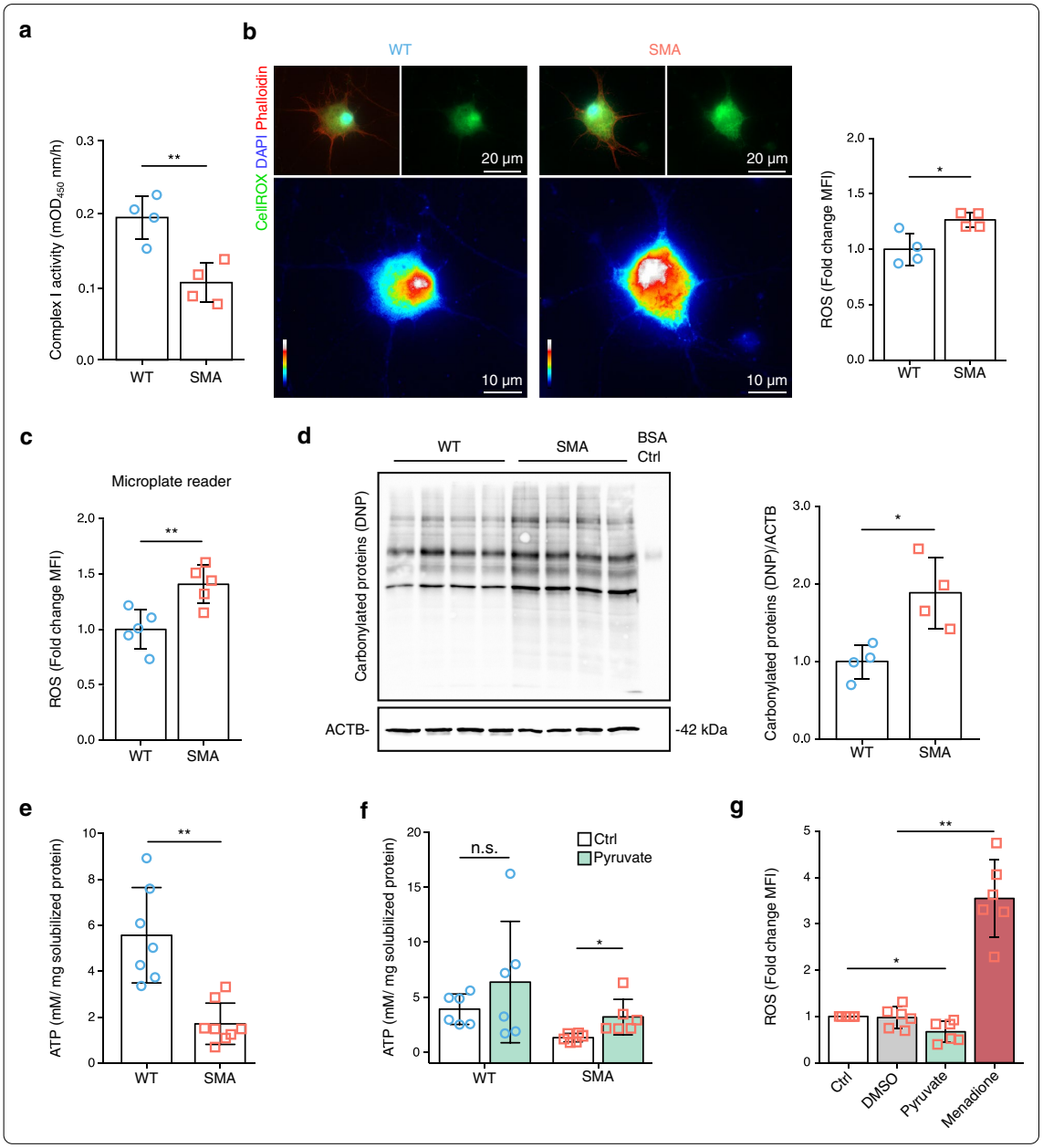

Click-iT AHA assay

To deplete endogenous methionine reserves, cells were incubated with HBSS for 30 min. 500 µM L-azidohomoalanine (AHA, Thermo Fisher Scientific) was treated to cells at 37 °C for 1 h. Cells were washed and lysed with RIPA buffer supplemented with protease and phosphatase inhibitors on ice. Click chemistry reaction was performed with Click-iT protein reaction buffer kit (Thermo Fisher Scientific), using manufacturer's protocol.

Statistical analysis

Statistical analysis was conducted in R version 3.6.2 using RStudio [41]. All graphs for cell biological experiments are presented as mean ± S.D. For normally distributed

variables, statistical significance was analyzed with an unpaired, two-tailed Student's t-test. Multiple comparisons are corrected with the Holm-Bonferroni method. Differences among group means are determined with Tukey's honestly significant difference (HSD) test after rejection of the null hypothesis by one-way analysis of variance (ANOVA). Normally distributed experimental results with two factors are analyzed by two-way ANOVA with Tukey HSD post hoc analysis. To compare multiple mean values to the mean from a single control, especially for time-course and dose–response experiments, Dunnett's post hoc test was used after one-way ANOVA. Statistical tests were applied only to biological replicates, even when data is presented as individual measurement counts. Statistical methods are listed in the figure legends of individual experiments. Significance is indicated by stars ($*p < 0.05$; $**p < 0.01$; $*** < 0.001$, n.s. = not significant).

Results

Mitochondria are defective in SMA MNs

To discover dysregulated pathways in SMA, we investigated differentially expressed proteins in primary MNs isolated from an SMA mouse model compared to wild-type mice [35]. It has been shown that around 8101 proteins are expressed in MNs from E12.5 mouse embryos [42]. We detected 5165 proteins using whole proteome analysis of 10DIV-cultured MNs, isolated from E13.5 embryos (Fig. 1a). 494 proteins are significantly changed in SMA MNs compared to WT MNs, and 61 proteins are localized to mitochondria based on the MitoCarta2.0 database containing 1158 proteins (Fig. 1b and Additional file 3: Figure S1a). From 44 known proteins of the respiratory complex I, we identified 35 proteins in our dataset, and 9 of them were significantly altered in SMA MNs (Additional file 3: Figure S1a, S2a). To understand the biological meaning of SMA affected proteins, we performed gene ontology (GO) analysis of 345 significantly down-regulated and 149 significantly up-regulated proteins in SMA (Fig. 1c and d). Among the down-regulated proteins, we identified previously reported dysfunctional processes in SMA such as mRNA processing, protein transport, and protein synthesis, confirming the reliability of the data set (Fig. 1c) [6–9, 16]. Data from the 149 up-regulated proteins strongly suggested mitochondrial dysfunction (Fig. 1d). Therefore, we further investigated the function and localization of mitochondria in MNs by staining with MitoTracker (functional mitochondria) and TOM20 (total mitochondria). Indeed, numbers of total and functional mitochondria are reduced in SMA axons (Fig. 1e). The finding of mitochondrial mislocalization is strengthened by reduced levels of mitochondrial motor proteins KIF1B and KIF1BP in SMA MNs in our whole proteome analysis (Additional file 3: Figure S1a and Additional file 2: MS source data). In addition, we found that mitochondria are smaller and fragmented in SMA MNs (Additional file 3: Figure S1b). Together, these results suggest that mitochondria are defective in SMA MNs.

Defective complex I can induce higher ROS levels and lower ATP levels in SMA MNs

As our proteomics results indicated defects in complex I of the electron transport chain, we biochemically measured the activity of complex I in WT and SMA MNs (Additional file 3: Figure S2a and S2b). Indeed, complex I activity was 50% lower in SMA MNs (Fig. 2a and Additional file 3: Figure S2c). Additionally, we measured complex I activity in the heart, another metabolically active tissue, and found no difference between WT and SMA MNs (Additional file 3: Figure S2d). This data suggested that complex I dysfunction in SMA is MN specific. Next, as complex I is a known source of reactive oxygen species (ROS) in mitochondria [22], we measured intracellular ROS levels using CellROX. As expected, ROS levels were increased in SMA MNs compared to WT ones (Fig. 2b and Fig. 2c). Furthermore, as excessive ROS can cause carbonylation of proteins [43], we measured the levels of carbonylated proteins in SMA MNs. Indeed, higher amounts of proteins were carbonylated in SMA (Fig. 2d). These data confirmed our finding that SMA MNs are under oxidative stress.

Since mitochondrial OXPHOS besides the tricarboxylic acid (TCA) cycle is the main source of energy in neurons, we measured the intracellular ATP

(See figure on next page.)

Fig. 3 Effect of ROS on protein synthesis in neurons. **a** Schematic drawing of the SUnSET method. Puromycin labels newly synthesized proteins. Puromycin is detected by anti-puromycin antibody. **b** SUnSET assay in WT and SMA MNs (N = 5). ACTB was used as loading control. **c** Schematic drawing of the Click-iT AHA method. L-azidohomoalanine (L-AHA) is incorporated into newly synthesized proteins, followed by click chemistry reaction with biotin alkyne. Biotin-labeled proteins can be detected by western blot analysis. **d** Click-iT AHA assay in WT and SMA MNs (N = 4). ACTB was used as loading control. **e** Scheme of experimental design. 10DIV MNs were treated with 10 µM NAC or 50 mM pyruvate for 1 h. Cells were incubated with 1 µM puromycin for 30 min before analysis. **f**, **g** SUnSET assay after ROS modification in (**f**) WT MNs (N = 5) and (**g**) SMA MNs (N = 5). Blue circles represent data from WT and red squares represent SMA MNs. Two-tailed unpaired t-tests with Holm-Bonferroni correction for multiple comparisons were used to determine statistical significance. All bar graphs depict the mean ± S.D., n.s. $p > 0.05$, $*p < 0.05$, $**p < 0.01$, $***p < 0.001$

Thelen et al. acta neuropathol commun (2020) 8:223

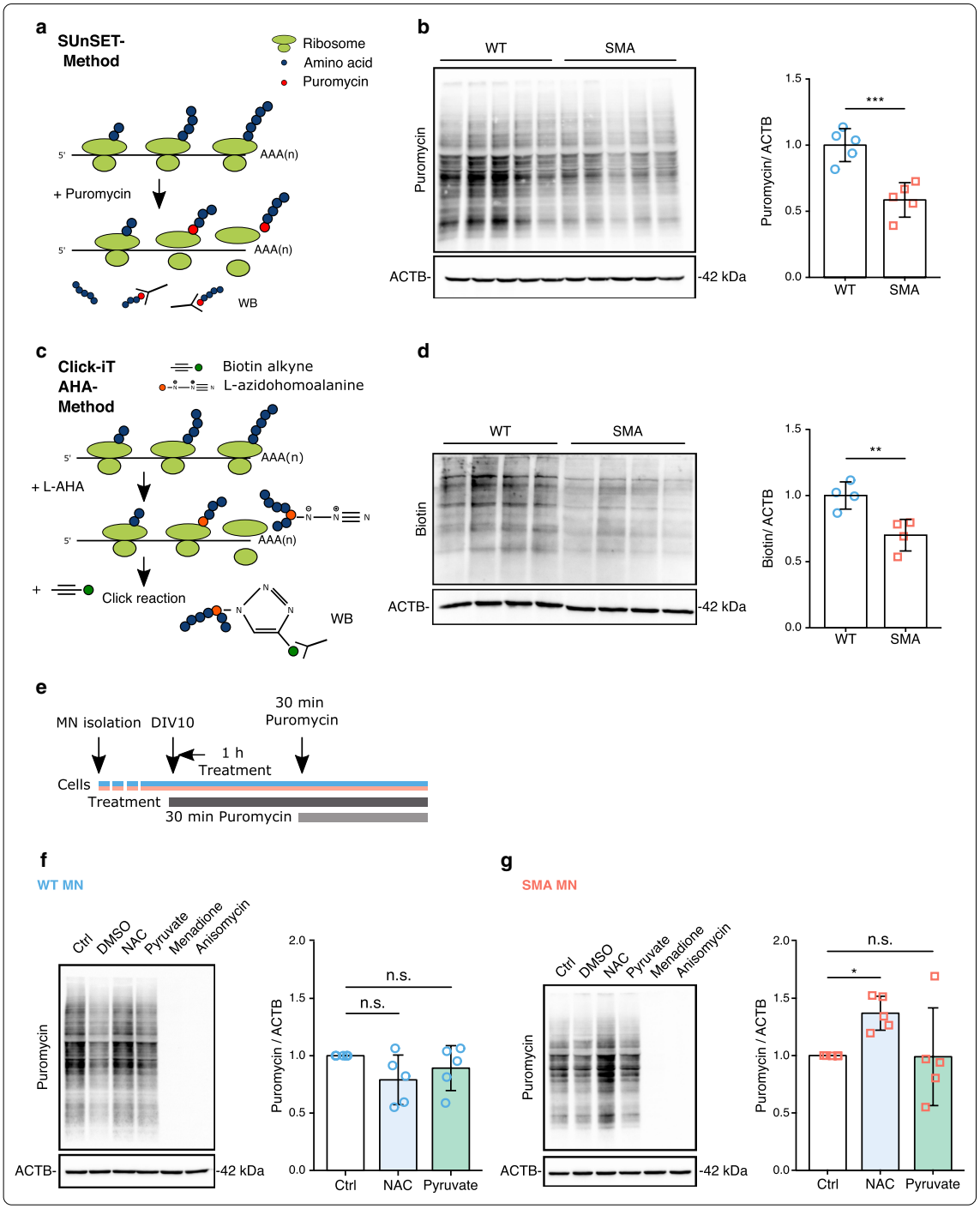

concentrations in WT and SMA MNs. ATP concentration is up to threefold lower in SMA compared to WT MNs (Fig. 2e). Furthermore, as ATP can also be produced by glycolysis to compensate for high energy demand in neurons [44], glucose uptake was monitored. Interestingly, glucose uptake is also impaired in SMA MNs (Additional file 3: Figure S2e). These data indicate that SMA MNs are in an energy-deprived status. Next, we pursued to restore the effects of defective mitochondria in SMA. Since pyruvate is known to reduce ROS in a non-enzymatic way and is also a known substrate of the TCA cycle [45], we supplemented MNs with sodium pyruvate. First, we confirmed that MNs can take up pyruvate within 5 min after treatment (Additional file 3: Figure S2f). While 10 mM pyruvate showed no clear effect, 50 mM pyruvate treatment for 1 h could increase ATP concentration significantly in SMA MNs (Fig. 2f and Additional file 3: Figure S2 g). However, lactate, which can be converted to pyruvate by lactate dehydrogenase in the cytoplasm [46], did not alter ATP levels in primary MNs (Additional file 3: Figure S2g). In addition, as pyruvate has been suggested to be a ROS scavenger [47], we treated SMA MNs with pyruvate and subsequently measured ROS levels. Indeed, pyruvate could successfully reduce ROS levels in SMA MNs (Fig. 2g). Further, we confirmed ROS reduction by treatment with 50 mM pyruvate or 10 µM of the antioxidant NAC in menadione mediated ROS induced NSC-34 cells (Additional file 3: Figure S2h). These results suggest that pyruvate is a valuable supplement to restore ATP levels and simultaneously balance intracellular ROS levels in MNs.

Effect of ROS on protein synthesis in neurons

Carbonylation of proteins can alter their conformation and hinder protein synthesis [23, 48]. Furthermore, as levels of ribosomes and proteins associated with translation are also changed in SMA according to our MS data, we measured protein synthesis efficiency with Surface sensing of translation (SUnSET) and Click-iT AHA assay in WT and SMA MNs. Indeed, we confirmed that SMA MNs show a reduced protein synthesis efficiency compared to WT ones (Fig. 3a-d). Based on these data, we hypothesized that the elevated ROS levels hinder protein synthesis, therefore, reducing elevated ROS might restore impaired protein synthesis in SMA MNs. To further understand the effect of ROS on protein synthesis, we modified cellular ROS levels and measured protein synthesis efficiency. We treated MNs with 10 µM NAC, 50 mM pyruvate or 100 µM menadione and performed SUnSET analysis (Scheme in Fig. 3e). While protein synthesis efficiency was unaltered by pyruvate or NAC, menadione-induced ROS clearly inhibited protein synthesis in NSC-34 cells and WT MNs. As a negative control, 50 µM of the translation inhibitor anisomycin was used (Fig. 3f and Additional file 3: Figure S3a, b). Interestingly, NAC treatment could increase protein synthesis in SMA MNs, where cellular ROS levels are higher (Fig. 3g). However, pyruvate treatment failed to increase protein synthesis in SMA MNs (Fig. 3g). Taken together, our data strongly suggests that intracellular ROS levels influence protein synthesis in MNs.

ROS regulates axonal local translation in MNs

Next, we investigated whether ROS regulates axonal local protein synthesis in MNs. We performed a SUnSET assay, but MNs were analyzed individually through imaging analysis. We are aware that local protein synthesis is lower in 10DIV-cultured MNs than in actively growing neurons [49, 50]. Therefore, we examined newly synthesized proteins in different axonal compartments. First, we measured anti-puromycin signals in 20 µm fractions and analyzed 100 µm fractions starting from the soma, comparing WT and SMA MNs. As expected, proximal fractions have higher anti-puromycin signals compared to distal parts. Importantly, the anti-puromycin signal in both soma and axonal part is lower in SMA MNs compared

(See figure on next page.)

Fig. 4 ROS regulates axonal local translation in MNs. **a** SUnSET assay. Representative images of WT and SMA MNs. Neurites were selected with a segmented line, straightened, and divided into 20 µm bins using the concentric circles plugin. Quantification of mean puromycin intensity profiles confirms that protein synthesis is reduced in the soma and axonal compartment of SMA MNs. **b** SUnSET assay. Representative images of SMA MNs after ROS modification. Tau staining shows whole neuronal morphology and puromycin signal represents newly synthesized proteins after 1 h treatment. 10 µM NAC, 100 µM menadione or 50 µM anisomycin were treated. Each dot represents the average intensity of 15 neurons (N = 5). One-way ANOVA with Tukey HSD post hoc analysis was used to determine statistical significance for multiple comparisons. Bar graphs depict the mean ± S.D. n.s. $p > 0.05$, ***$p < 0.001$. **c** SUnSET assay. Representative images of SMA axons. MNs were treated with 10 µM NAC, 50 mM pyruvate, 100 µM menadione, or 50 µM anisomycin for 1 h. **a–c** Intensity of incorporated puromycin signal is represented in rainbow scale. Scale bar: 20 µm. **a**, **c** Each dot represents the average quantification of 10 neurons of 5 individual biological replicates (N = 5). Bar graphs depict the mean ± S.D. Two-tailed unpaired t-test with Holm-Bonferroni correction for multiple comparisons was used to determine statistical significance. n.s. $p > 0.05$, *$p < 0.05$, **$p < 0.01$

Thelen et al. acta neuropathol commun (2020) 8:223

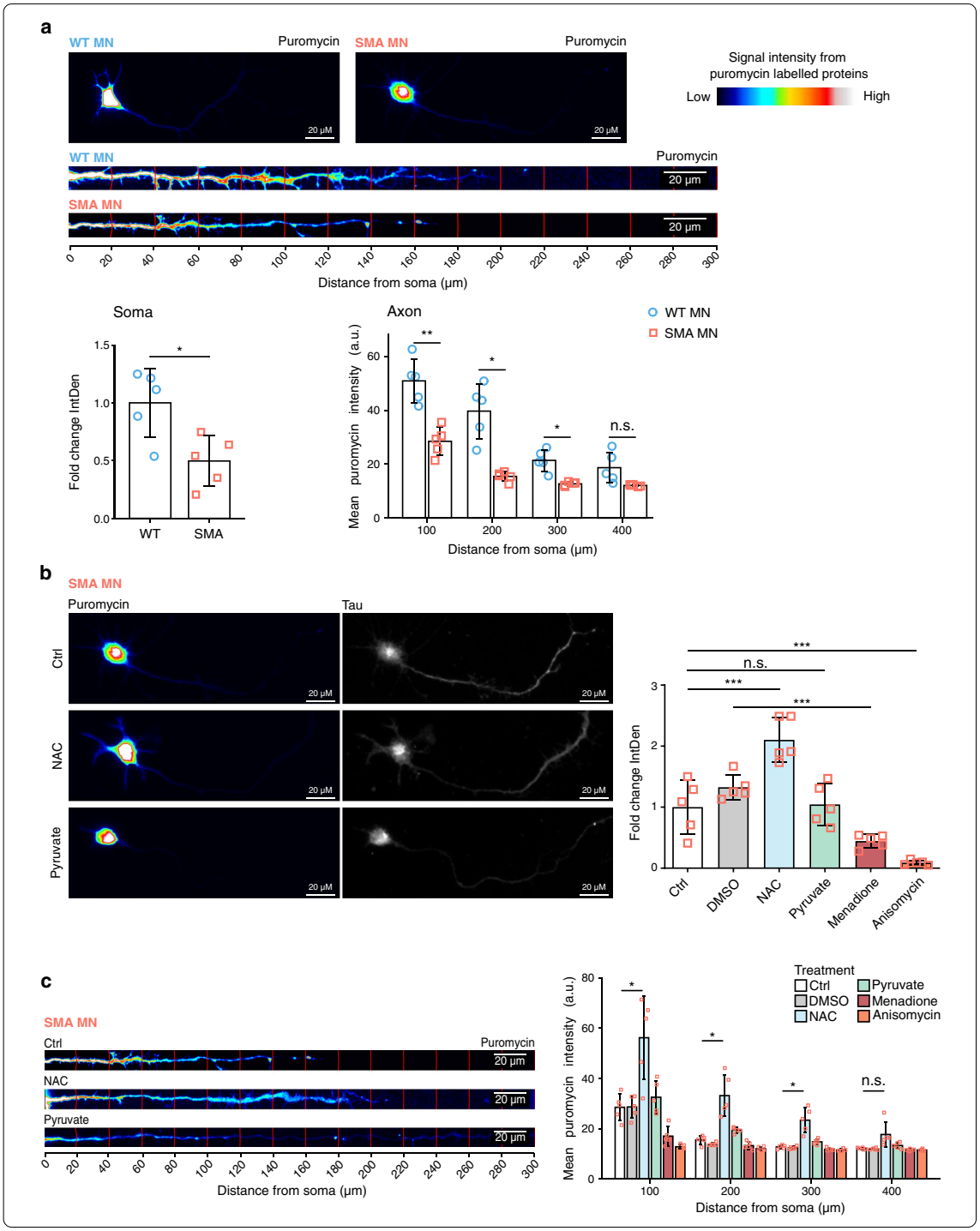

to WT ones (Fig. 4a). Next, we treated SMA MNs with NAC, pyruvate, menadione, and anisomycin and performed the same experiment. As expected, while NAC treatment increased protein synthesis, menadione or anisomycin inhibited protein synthesis in the soma as well as in the axonal compartment of SMA MNs (Fig. 4b, c and Additional file 3: Figure S4a). Consistent with the results in Fig. 3f, WT MNs did not show clear differences following NAC treatment (Additional file 3: Figure S4a and b).

Whole proteome analysis of MNs with ROS manipulation

Next, we tried to obtain a systemic view of the whole proteome regulated by ROS in MNs. First, cells were incubated with 50 mM pyruvate for 1 h and the whole proteome was analyzed by MS. We found that the levels of 122 proteins were altered in SMA MNs (Fig. 5a). GO analysis of altered proteins suggests that pyruvate regulates proteins related to mitochondria (Fig. 5b). The biological process of oxidative phosphorylation was enriched, and the cellular compartment of mitochondria was affected by pyruvate supplementation (Fig. 5b). In addition, molecular functions involved in ribonucleotide binding, cellular compartments of the spliceosome, or biological processes such as RNA splicing and mRNA processing were also affected by pyruvate. Interestingly, these terms have previously been reported as altered pathways in SMA. Among the 494 proteins significantly changed in SMA MNs compared to WT MNs, 22 were also significantly changed by pyruvate in WT MNs, and 28 were significantly altered in pyruvate-treated SMA MNs (Fig. 5c). Intriguingly, when we compare proteins altered in SMA to pyruvate-affected proteins in WT or SMA MNs, we found that the effect of pyruvate was more apparent in SMA MNs (Fig. 5d and Additional file 3: Figure S5a). Among these 28 proteins, 21 proteins were down-regulated in SMA compared to WT and up-regulated by pyruvate in SMA (Fig. 5d). In contrast, pyruvate changed levels of 144 proteins in WT MNs, and among those, 22 proteins were also altered in SMA compared to WT (Fig. 5c and Additional file 3: Figure S5a, b). However, these 22 proteins showed far fewer changes after pyruvate treatment (Additional file 3: Figure S5a). Only two proteins, DLG-associated protein 1 (DLGAP1) and Islet cell autoantigen 1 (ICA1), were commonly changed by pyruvate treatment between WT and SMA MNs (Fig. 5a and Additional file 3: Figure S5b, c).

Subsequently, to obtain an overview of the antioxidant effect on the MN proteome, SMA MNs were treated with 10 μM NAC for 1 h. Whole proteome analysis identified that 143 proteins were significantly changed by NAC treatment (Fig. 5e). GO analysis suggested these proteins have multiple functions, including nucleotide-binding and RNA processing (Fig. 5f). Compared with differentially expressed proteins between WT and SMA MNs, 31 proteins were common with NAC treatment in SMA MNs (Fig. 5g). Among them, 17 proteins were down-regulated in SMA compared to WT, and up-regulated by NAC treatment in SMA (Fig. 5h). Again, NAC treatment showed little effect on WT MNs (Additional file 3: Figure S5d, e). NAC treatment altered only one protein, namely the deubiquitinase OTUD6B, in both WT and SMA MNs (Fig. 5e and Additional file 3: Figure S5e, f). ROS induction by 100 μM menadione for 1 h in WT MNs had the biggest effect on the proteome with 344 significantly altered proteins (Additional file 3: Figure S5g). In addition, menadione showed with 56 proteins the biggest overlap of altered proteins with proteins changed in SMA (Additional file 3: Figure S5h, i). It is worth mentioning that pyruvate and NAC had only a small effect on WT MNs, whereas they can induce a considerable up-regulation of proteins in SMA MNs. A possible explanation could be that the basal amounts of these proteins are lower in SMA MNs compared to WT MNs.

ROS regulates initiation of mRNA translation

Whole proteome analysis suggested that mRNA translation is dysregulated in SMA MNs (Fig. 1c). The volcano plot illustrates 360 proteins identified in our whole-proteome analysis related to mRNA translation based on the Mouse Genome Informatics (MGI) database (Additional file 3: Figure S6a). Among them, 40 out of 47 are significantly down-regulated in SMA MNs compared to WT (Additional file 3: Figure S6a). mRNA translation is tightly regulated in eukaryotic cells by two major processes: initiation and elongation. As it has already

(See figure on next page.)

Fig. 5 NAC and pyruvate modify the proteome of SMA MNs. **a**, **e** Volcano plot of whole proteome analysis in SMA MNs after (**a**) pyruvate or (**e**) NAC treatment; plotted *p* value (-$\log_{10}$) against fold change ($\log_2$) (N = 3). *p* values were determined by unpaired two-sided t-test. Significantly changed proteins with $p < 0.05$ are highlighted in blue (down-regulated) or red (up-regulated). **b, f** GO analysis of significantly changed proteins by (**b**) pyruvate or (**f**) NAC-treated SMA MNs. **c, g** Venn diagram showing the overlap of 'significantly altered proteins in SMA compared to WT' and 'significantly changed proteins by (**c**) pyruvate or (**g**) NAC' treatment in WT MNs or SMA MNs. **d** Levels of proteins altered in SMA compared to WT and by (**d**) pyruvate or (**h**) NAC treatment in SMA; plotted fold change ($\log_2$) comparing with and without pyruvate treatment

Thelen et al. acta neuropathol commun (2020) 8:223

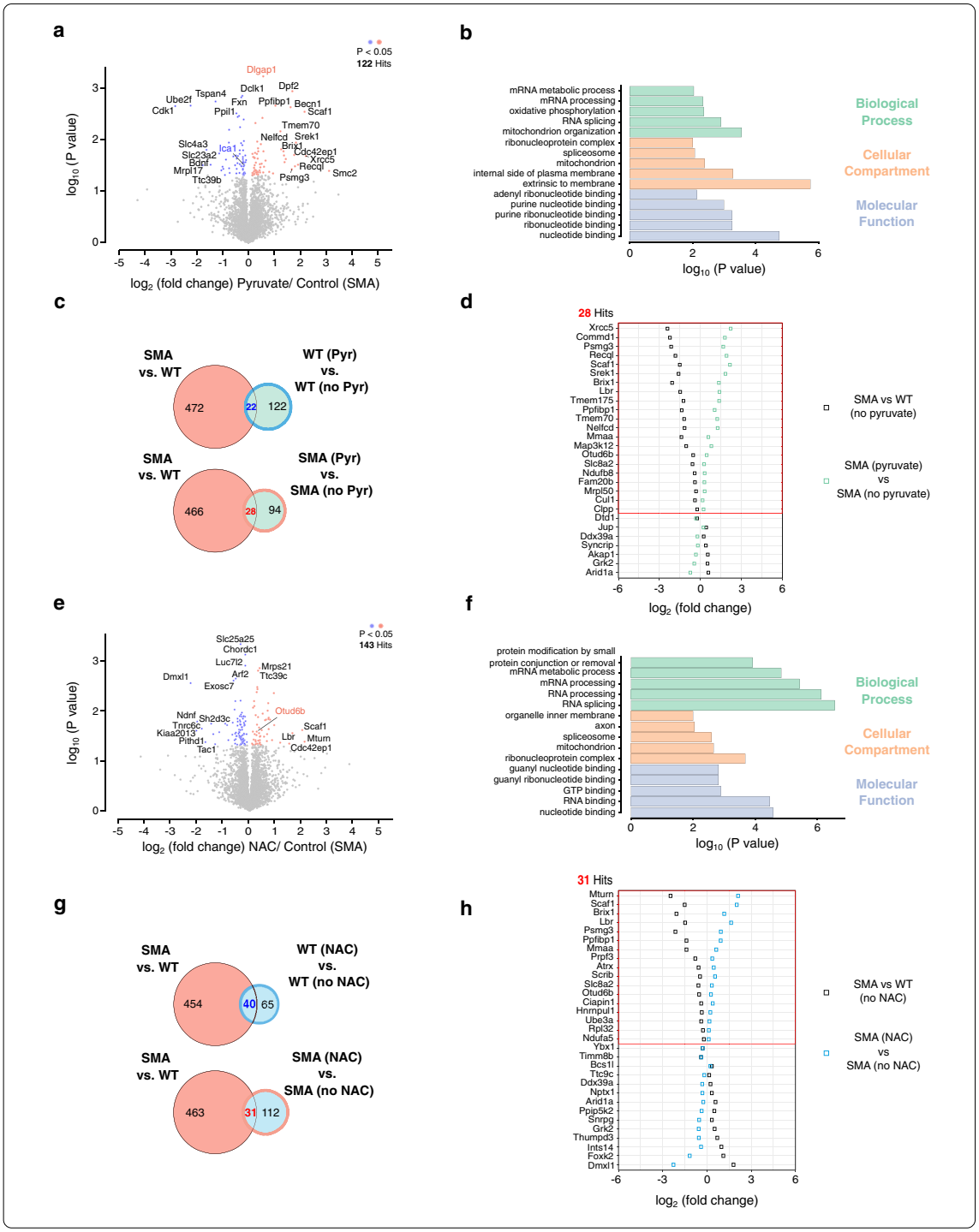

been reported that protein synthesis is impaired in SMA MNs [7, 8, 16], we aimed to seek further which step is disrupted by SMN loss. To distinguish the initiation and elongation of translation, we measured both processes in MNs. First, to assess the rate of protein elongation, we used the SunRiSE assay. In brief, translation initiation was blocked by 2 µg/ml harringtonine at different time intervals, then newly synthesized peptides were labeled with 10 µg/ml puromycin and detected by anti-puromycin antibody (Fig. 6a). The elongation speed was not altered by either NAC or pyruvate treatment in WT and SMA MNs (Fig. 6b, c). Furthermore, the elongation speed between WT and SMA MNs did not show any significant difference (Additional file 3: Figure S6b).

As translational elongation is unaltered in SMA or by ROS modification, we focused on translational initiation next. As one of the well-described translational initiation mechanisms is the cap-dependent translation initiation by 4E-BP1 (eukaryotic translation initiation factor 4E-binding protein 1), we measured the phosphorylation status of 4E-BP1 in WT and SMA MNs. A reduced phosphorylation status of 4E-BP1 indicates that initiation of mRNA translation is impaired in SMA MNs (Fig. 6d). Next, we measured the phosphorylation status in MNs after pharmacological modulation of ROS levels. While a significant difference was not observed by pyruvate or NAC treatment in WT cells, menadione impaired phosphorylation of 4E-BP1. This data suggests that excessive ROS can inhibit mRNA translation at the initiation step (Fig. 6e). Notably, pyruvate and NAC treatment increased the phosphorylation of 4E-BP1 in SMA MNs (Fig. 6f). Taken together, this unprecedented data reveals that mRNA translation is impaired at the initiation step in SMA MNs, while elongation is unaltered. Moreover, the initiation of mRNA translation can be regulated by ROS via 4E-BP1.

SMN protein levels are regulated by pyruvate and ROS via mTOR

Most interestingly, pyruvate increased SMN levels in WT and SMA MNs as well as NSC-34 cells (Fig. 7a, b, and Additional file 3: Figure S7a). To identify the molecular mechanism underlying increased SMN levels, we measured *Smn* mRNA levels in WT MNs and NSC-34 cells after pyruvate treatment and found no significant increase of *Smn* mRNA levels (Additional file 3: Figure S7b). This data suggests a post-transcriptional regulation of SMN levels. Next, we found that the protein synthesis inhibitor anisomycin could prevent pyruvate-induced elevation of SMN levels (Additional file 3: Figure S7c). This data confirms that protein synthesis of SMN is regulated by pyruvate post-transcriptionally. In addition, NAC increased SMN levels in MNs (Fig. 7c, d). As mTOR, especially mTORC1, is a central regulator of protein synthesis [51], we tested whether the increase of SMN levels is mTOR-dependent. We treated MNs with the water-soluble mTOR inhibitor WYE-687 dihydrochloride and subsequently with pyruvate. Indeed, pyruvate failed to increase SMN levels when mTOR activity was inhibited (Fig. 7e). In addition, pyruvate increased mTORC1 activity in WT MNs (Fig. 7f, g and Additional file 3: Figure S7d). Furthermore, a reduction of ROS by NAC treatment in SMA MNs increased the mTORC1 activity (Fig. 7h). Taken together, our data showed that cellular ROS and ATP levels regulate SMN protein synthesis via regulating mTORC1. Furthermore, re-balancing ROS levels with an antioxidant in SMA MNs can increase SMN protein synthesis.

Discussion

Through whole proteome analysis, we identified that SMA MNs exhibit mitochondrial dysfunction. Prior studies have noted mitochondrial defects in SMA, including decreased respiration, increased oxidative stress, and impaired mitochondrial mobility [18, 20]. Here, we further investigated the molecular mechanisms underlying mitochondrial defects and reported that the function of complex I of the electron transport chain in mitochondria is impaired in SMA MNs. Furthermore, due to the dysfunctional complex I, intracellular ATP concentration is lower, and ROS levels

(See figure on next page.)

Fig. 6 ROS regulates initiation of protein translation without altering elongation speed. **a** Scheme of SunRiSE assay. Translation initiation of 10DIV WT or SMA MNs was blocked with 2 µg/ml harringtonine at different time points before adding 10 µg/ml puromycin treatment for 10 min. **b, c** Neither NAC nor pyruvate changes elongation speed in (**b**) WT or (**c**) SMA MNs. Each dot and line represent the average of four independent biological replicates (N = 4). Regression analysis comparing the least square means does not show any significant difference between treatments. **d** Western blot analysis of p-4EBP1 and 4EBP1 levels in WT (blue circles) and SMA MNs (red squares) (N = 5). ATCB was used as loading control. Each dot represents the data from biological replicates. Two-tailed unpaired t-test was used to determine statistical significance $*p < 0.05$, $**p < 0.01$, $***p < 0.001$. **e, f** Western blot analysis of p-4EBP1 and 4EBP1 levels after pharmacological modifications of ROS levels in (**e**) WT MNs (N = 6) and (**f**) SMA MNs (N = 6). Each dot represents the data from biological replicates. One-way ANOVA with Tukey HSD post hoc analysis was used to determine statistical significance for multiple comparisons. Bar graphs depict the mean ± S.D. n.s. $p > 0.05$, $*p < 0.05$, $**p < 0.01$, $***p < 0.001$

Thelen et al. acta neuropathol commun (2020) 8:223

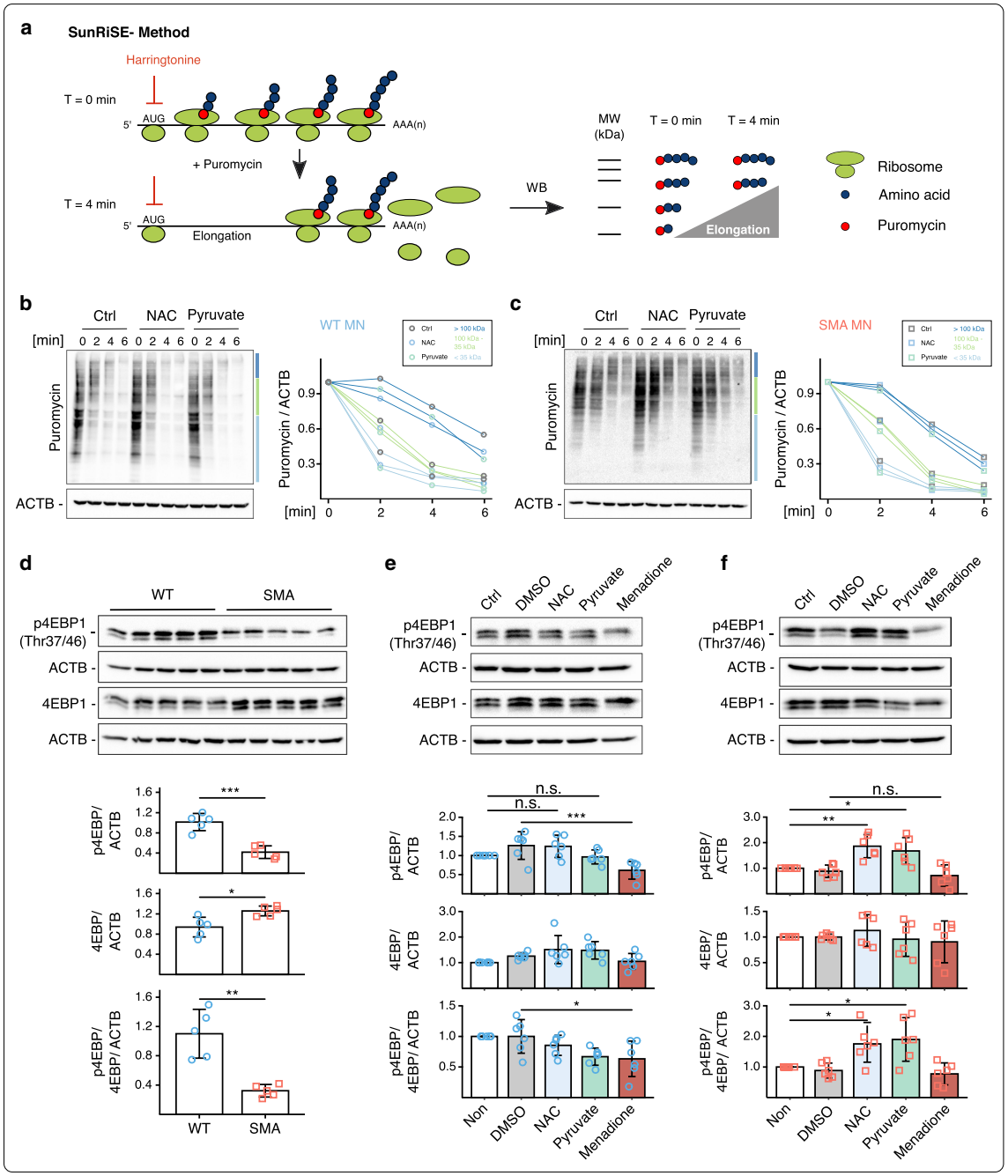

(See figure on next page.)

Fig. 7 SMN levels are regulated by pyruvate and ROS modifying drugs. **a–d** Representative western blot images and quantification of SMN levels after pyruvate treatment for 1 h in (**a**) WT MNs and (**b**) SMA MNs or after ROS modification in (**c**) WT MNs and (**d**) SMA MNs. **e** 100 nM WYE-687 dihydrochloride blocks elevation of SMN levels after pyruvate treatment in WT MNs. **f–h** Representative western blot images and quantification of phosphorylated S6 and total S6 protein levels after pyruvate treatment in (**f**) WT MNs (N = 7) and (**g**) SMA MNs (N = 7) or after (**h**) NAC and menadione treatment in SMA MNs (N = 4). One-way ANOVA with Dunnett post hoc analysis was used to compare each time point with the control (**a**, **b**). One-way ANOVA with Tukey HSD post hoc analysis was used to determine statistical significance for multiple comparisons (**c**-**h**). Each dot represents the quantification of individual biological replicates. Bar graphs depict the mean ± S.D., n.s. $p > 0.05$, *$p < 0.05$, **$p < 0.01$, ***$p < 0.001$

are higher in SMA MNs. Regarding ROS generation, complex I and complex III are the known critical components. However, as the physiological or pathological relevance of complex III in ROS generation seems controversial, we focused on complex I function [22]. Moreover, complex I activity was not altered in the heart, another energy-demanding tissue. This finding indicates that complex I dysfunction can be a neuron-specific phenotype in SMA.

While a previous report did not show changes in the number of axonal mitochondria [20], we found that the number of axonal mitochondria is reduced. This controversy might be explained by methodological differences. In the previous study, mitochondria were labeled by aberrantly expressed mitochondrial proteins, while we used MitoTracker, a membrane potential dependent dye, which does not stain non-functional mitochondria or antibodies against the mitochondrial protein TOM20. This implicates that the proportion of dysfunctional mitochondria in SMA axons is higher compared to WT ones.

It has widely been accepted that neurons use mitochondria as their primary source of energy. However, a recent study suggested that neurons can obtain energy from glycolysis in energy-demanding conditions and locations [52]. Based on our results, glucose uptake is impaired in SMA MNs. Therefore, reduced energy production due to defective mitochondria might not be compensated by glycolysis. Taken together, we could conclude that SMA MNs are in a status of energy deprivation caused by mitochondrial defects as well as impaired glucose uptake. Glycolysis is also impaired in other neurodegenerative diseases such as AD and amyotrophic lateral sclerosis (ALS) [53, 54]. Furthermore, it has been proposed that enhancing glycolysis is neuroprotective in ALS [55]. However, it is unclear whether glycolysis is also impaired in SMA MNs. This needs to be investigated further.

As excessive cellular ROS are harmful to the cellular system, production and scavenging mechanisms are tightly regulated in all living organisms. Imbalanced ROS has been reported in numerous pathological conditions [56, 57]. ROS can be produced by mitochondria and cleared up by enzymes and chelating agents [58]. With our current data, we can speculate that ROS production can be increased by defective mitochondrial complex I, yet it is not clear whether ROS scavenging mechanisms are also altered in SMA MNs. Importantly, we revealed that ROS regulates mRNA translation at the initiation step and this mechanism is dysregulated in SMA. Counteracting this molecular pathway by supplementing pyruvate or the antioxidant NAC restores impaired translational initiation in SMA MNs. Nevertheless, in WT MNs, reducing ROS did not affect protein synthesis as WT MNs do not suffer from oxidative stress. This data intensifies our conclusion that healthy cells tightly regulate the balance of ROS levels, but SMA cells lost their ability to regulate ROS homeostasis due to defective mitochondrial complex I. Furthermore, our data revealed that ROS regulates mRNA translation at the initiation step, contributing to impaired protein synthesis, a known SMA pathology [16, 17]. Additionally, we found that the number and functionality of axonal mitochondria are reduced in SMA MNs. Therefore, to test whether impaired axonal mitochondria also influence protein synthesis in axons, we measured mRNA translation in the axonal compartment of the neurons. In a compartment-specific analysis, we revealed reduced protein synthesis in SMA MNs within the soma and along the axon. In 10 days cultured MNs, active protein synthesis was not observed at the distal part of the axons, while active protein synthesis could be observed and quantified in the proximal part of the axons.

Interestingly, reduction of ROS via pyruvate or NAC led to an increase of SMN protein levels in an mTOR-dependent manner. An increase of SMN levels by pyruvate or NAC was also observed in WT MNs, even though it did not change the overall protein synthesis rate. While the underlying molecular mechanism is unclear, our data suggests that pyruvate and NAC specifically increase SMN protein levels via the mTOR pathway without altering the whole proteome, independent of oxidative stress. It has previously been reported that SMN is involved in ribosome biology, and mTOR activity is reduced in SMA neurons [16, 17]. These findings suggest an SMN-specific feedback mechanism of gene expression.

Thelen et al. acta neuropathol commun (2020) 8:223

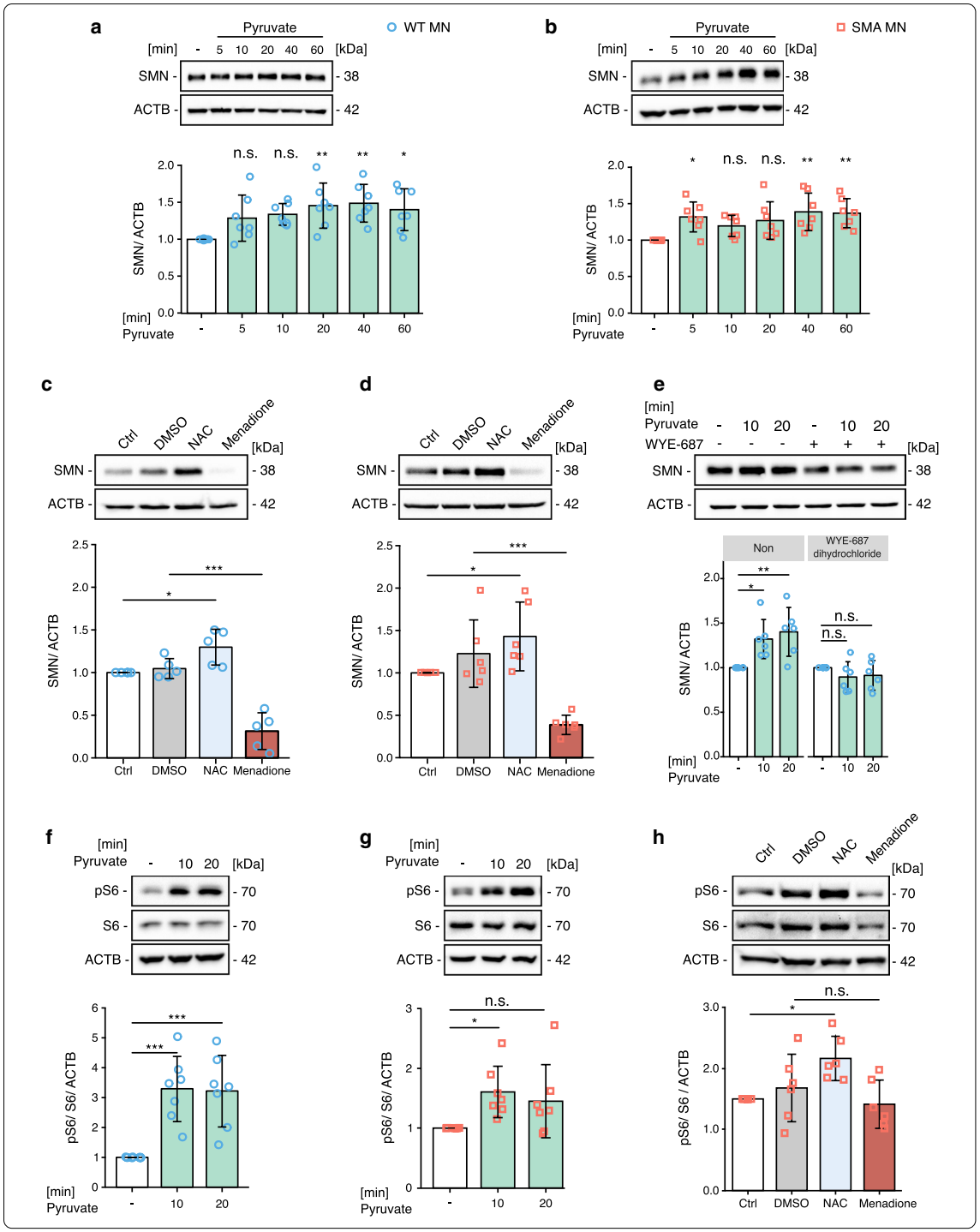

However, the mechanism underlying mTOR-dependent SMN protein synthesis needs to be investigated.

Overall, we unraveled the previously unknown molecular connections between mitochondria and protein synthesis by impairing translation initiation in neurons. This dysfunction contributes to the pathology of SMA via decreased ATP and increased ROS levels.

Conclusion

This study describes the previously unknown mechanism that defective mitochondria influence SMA pathology, especially impaired protein synthesis. With a proteomics approach using an SMA mouse model, we identified that mitochondrial respiratory complex I is dysfunctional in SMA MNs. Due to this, ATP levels are decreased and ROS levels are increased in SMA MNs. Furthermore, we could restore the homeostasis of cellular energy and the redox system in SMA MNs by supplementation of pyruvate. Modifying ROS levels influences protein synthesis at the translation initiation step, which is impaired in SMA MNs. In addition, pyruvate enhances SMN protein synthesis in an mTOR-dependent manner. As mitochondrial defects have been reported in other neurological disorders, our study reveals the basic cellular mechanism of how mitochondria can influence protein synthesis in MNs. This study will lead to new insights into pharmacologically targetable pathways for neurological disorders, including SMA.

Supplementary Information

Supplementary information accompanies this paper at https://doi.org/10.1186/s40478-020-01101-6.

Additional file 1: Supplementary Table S1. Primer sequences. S2. Antibodies and conditions for Western blot (WB) and immunofluorescence (IF). S3. Fluorescence dyes. S4. Drugs and supplements for in vitro assays.

Additional file 2: Mass spectromertry source data. This file contains results of the mass spectrometry including pathway analyses.

Additional file 3: Supplementary Figure S1. Complex I deficiency leads to dysfunctional and fragmented mitochondria. S2. Mitochondrial complex I is impaired in SMA MNs. S3. Optimization of SUnSET assay. S4. Reduction of ROS improves protein synthesis in SMA MNs, but not in WT MNs. S5 Whole cell proteome after modifying ROS levels. S6 Proteins related to translation are significantly changed in SMA MNs without affecting elongation speed. S7. Pyruvate regulates SMN levels.

Abbreviations

4E-BP1: eukaryotic initiation factor 4E (eIF4E)- binding protein 1; ACTB: actin beta; AD: Alzheimer's disease; ALS: amyotrophic lateral sclerosis; ANOVA: analysis of variance; ATP: adenosine triphosphate; Complex I: NADH:ubiquinone oxidoreductase; DIV: days in vitro; DLGAP1: DLG-associated protein 1; DMEM: Dulbecco's Modified Eagle's Medium; eIF4E: eukaryotic translation initiation factor 4E; GO: gene ontology; ICA1: islet cell autoantigen 1; MGI: Mouse Genome Informatics; MN: motor neuron; MS: mass spectrometry; mRNA: messenger ribonucleic acid; miRNA: micro ribonucleic acid; mTORC1: mammalian target of rapamycin complex 1; NAC: N-acetylcysteine; OXPHOS: oxidative phosphorylation; RNA: ribonucleic acid; ROS: reactive oxygen species; S6: ribosomal protein S6; S6K: S6 kinase; SDB-RPS: styrenedivinylbenzene-reverse phase sulfonate; SMA: spinal muscular atrophy; SMN: survival of motor neuron; SunRiSE: SUnSET-based Ribosome Speed of Elongation; SUnSET: surface sensing of translation; TCA: tricarboxylic acid; TSC: tuberous sclerosis complex; WT: wildtype.

Acknowledgements

We are grateful for the support of the proteomics and animal facility at the CECAD and CMMC of the University of Cologne. We also thank Talita França Dück and Marlen C. Lauffer for critically reading our manuscript.

Authors' contributions

MJK and MPT seeded the idea of the project. MPT performed the experiments and data analysis with help of MJK. The manuscript was written by MPT with help of BW and MJK. All authors read and approved the final manuscript.

Funding

Open Access funding enabled and organized by Projekt DEAL. This work is funded by SMA Europe Research Grant to MK and Deutsche Forschungsgemeinschaft (DFG) KY96/1-2 to MK, and DFG Wi945/17-1 to BW, CRC1451 A01 to BW, Research Training Group (RTG) 1960 to BW and Center for Molecular Medicine Cologne (CMMC) C18 to BW.

Availability of data and materials

The mass spectrometry proteomics data have been deposited to the ProteomeXchange Consortium via the PRIDE [59] partner repository with the dataset identifier PXD020403. The results of the mass spectrometry dataset, supporting the conclusions of this article is included within the article as Additional file 2: Mass Spectrometry source data.

Ethics approval and consent to participate

All animal breedings and procedures were performed in accordance with the institutional animal care guidelines and the German animal welfare laws. They are approved under the reference numbers 84-02.04.2015.A378, UniKoeln_Anziege§4.16.020 and UniKoeln_Anziege§4.17.025 of the LANUV (Landesamt für Natur, Umwelt und Verbraucherschutz NRW) state agency of North-Rhine-Westphalia. FVB/N wild type mice were used as controls (Jackson).

Consent for publication

Not applicable.

Competing interests

The authors declare that they have no conflict of interest.

Author details

[1] Institute of Human Genetics, University of Cologne, Kerpener Str. 34, 50931 Cologne, Germany. [2] Center for Molecular Medicine, Cologne, University of Cologne, 50931 Cologne, Germany. [3] Center for Rare Diseases Cologne, University Hospital Cologne, University of Cologne, 50931 Cologne, Germany.

Received: 27 November 2020 Accepted: 8 December 2020
Published online: 22 December 2020

References

1. Lefebvre S, Bürglen L, Reboullet S et al (1995) Identification and characterization of a spinal muscular atrophy-determining gene. Cell 80:155–165. https://doi.org/10.1016/0092-8674(95)90460-3
2. Wirth B, Karakaya M, Kye MJ, Mendoza-Ferreira N (2020) Twenty-five years of spinal muscular atrophy research: from phenotype to genotype to therapy, and what comes next. Annu Rev Genom Hum Genet 21:102319–103602. https://doi.org/10.1146/annurev-genom-102319-103602
3. Lorson CL, Hahnen E, Androphy EJ, Wirth B (1999) A single nucleotide in the SMN gene regulates splicing and is responsible for spinal muscular atrophy. Proc Natl Acad Sci 96:6307–6311. https://doi.org/10.1073/pnas.96.11.6307
4. Feldkötter M, Schwarzer V, Wirth R et al (2002) Quantitative analyses of SMN1 and SMN2 based on real-time lightcycler PCR: fast and highly reliable carrier testing and prediction of severity of spinal muscular atrophy. Am J Hum Genet 70:358–368. https://doi.org/10.1086/338627

5. Gubitz A (2004) The SMN complex. Exp Cell Res 296:51–56. https://doi.org/10.1016/j.yexcr.2004.03.022
6. Pellizzoni L (2002) Essential role for the SMN complex in the specificity of snRNP assembly. Science 298:1775–1779. https://doi.org/10.1126/science.1074962
7. Akten B, Kye MJ, Hao LT et al (2011) Interaction of survival of motor neuron (SMN) and HuD proteins with mRNA cpg15 rescues motor neuron axonal deficits. Proc Natl Acad Sci USA 108:10337–10342. https://doi.org/10.1073/pnas.1104928108
8. Fallini C, Zhang H, Su Y et al (2011) The survival of motor neuron (SMN) protein interacts with the mRNA-binding protein HuD and regulates localization of Poly(A) mRNA in primary motor neuron axons. J Neurosci 31:3914–3925. https://doi.org/10.1523/JNEUROSCI.3631-10.2011
9. Rossoll W, Jablonka S, Andreassi C et al (2003) Smn, the spinal muscular atrophy-determining gene product, modulates axon growth and localization of β-actin mRNA in growth cones of motoneurons. J Cell Biol 163:801–812. https://doi.org/10.1083/jcb.200304128
10. Thelen MP, Kye MJ (2020) The role of RNA binding proteins for local mRNA translation: implications in neurological disorders. Frontiers Mol Biosci 6:161. https://doi.org/10.3389/fmolb.2019.00161
11. Custer SK, Gilson TD, Li H et al (2016) Altered mRNA splicing in SMN-depleted motor neuron-like cells. PLoS ONE 11:e0163954. https://doi.org/10.1371/journal.pone.0163954
12. Gonçalves IDCG, Brecht J, Thelen MP et al (2018) Neuronal activity regulates DROSHA via autophagy in spinal muscular atrophy. Sci Rep. https://doi.org/10.1038/s41598-018-26347-y
13. Jablonka S, Beck M, Lechner BD et al (2007) Defective Ca2+ channel clustering in axon terminals disturbs excitability in motoneurons in spinal muscular atrophy. J Cell Biol 179:139–149. https://doi.org/10.1083/jcb.200703187
14. Liu H, Lu J, Chen H et al (2015) Spinal muscular atrophy patient-derived motor neurons exhibit hyperexcitability. Sci Rep 5:12189. https://doi.org/10.1038/srep12189
15. Mentis GZ, Blivis D, Liu W et al (2011) Early functional impairment of sensory-motor connectivity in a mouse model of spinal muscular atrophy. Neuron 69:453–467. https://doi.org/10.1016/j.neuron.2010.12.032
16. Kye MJ, Niederst ED, Wertz MH et al (2014) SMN regulates axonal local translation via miR-183/mTOR pathway. Hum Mol Genet 23:6318–6331. https://doi.org/10.1093/hmg/ddu350
17. Bernabò P, Tebaldi T, Groen EJN et al (2017) In vivo translatome profiling in spinal muscular atrophy reveals a role for SMN protein in ribosome biology. Cell Rep 21:953–965. https://doi.org/10.1016/j.celrep.2017.10.010
18. Acsadi G, Lee I, Li X et al (2009) Mitochondrial dysfunction in a neural cell model of spinal muscular atrophy. J Neurosci Res 87:2748–2756. https://doi.org/10.1002/jnr.22106
19. Boyd PJ, Tu W-Y, Shorrock HK et al (2017) Bioenergetic status modulates motor neuron vulnerability and pathogenesis in a zebrafish model of spinal muscular atrophy. PLoS Genet 13:e1006744. https://doi.org/10.1371/journal.pgen.1006744
20. Miller N, Shi H, Zelikovich AS, Ma Y-C (2016) Motor neuron mitochondrial dysfunction in spinal muscular atrophy. Hum Mol Genet 25:3395–3406. https://doi.org/10.1093/hmg/ddw262
21. Sharma L, Lu J, Bai Y (2009) Mitochondrial respiratory complex I: structure, function and implication in human diseases. Curr Med Chem 16:1266–1277. https://doi.org/10.2174/092986709787846578
22. Liu Y, Fiskum G, Schubert D (2002) Generation of reactive oxygen species by the mitochondrial electron transport chain. J Neurochem 80:780–787. https://doi.org/10.1046/j.0022-3042.2002.00744.x
23. Stadtman ER (1990) Metal ion-catalyzed oxidation of proteins: biochemical mechanism and biological consequences. Free Radic Biol Med 9:315–325. https://doi.org/10.1016/0891-5849(90)90006-5
24. Topf U, Suppanz I, Samluk L et al (2018) Quantitative proteomics identifies redox switches for global translation modulation by mitochondrially produced reactive oxygen species. Nat Commun 9:324. https://doi.org/10.1038/s41467-017-02694-8
25. Wan L, Ottinger E, Cho S, Dreyfuss G (2008) Inactivation of the SMN complex by oxidative stress. Mol Cell 31:244–254. https://doi.org/10.1016/j.molcel.2008.06.004
26. Kelleher RJ, Bear MF (2008) The autistic neuron: troubled translation? Cell 135:401–406. https://doi.org/10.1016/j.cell.2008.10.017
27. Hara T, Mizushima N (2009) Role of ULK-FIP200 complex in mammalian autophagy: FIP200, a counterpart of yeast Atg17? Autophagy 5:85–87. https://doi.org/10.4161/auto.5.1.7180
28. Noda T, Ohsumi Y (1998) Tor, a phosphatidylinositol kinase homologue, controls autophagy in yeast. J Biol Chem 273:3963–3966. https://doi.org/10.1074/jbc.273.7.3963
29. Scott RC, Schuldiner O, Neufeld TP (2004) Role and regulation of starvation-induced autophagy in the Drosophila fat body. Dev Cell 7:167–178. https://doi.org/10.1016/j.devcel.2004.07.009
30. Cunningham JT, Rodgers JT, Arlow DH et al (2007) mTOR controls mitochondrial oxidative function through a YY1-PGC-1α transcriptional complex. Nature 450:736–740. https://doi.org/10.1038/nature06322
31. Gingras AC, Raught B, Sonenberg N (2001) Regulation of translation initiation by FRAP/mTOR. Genes Dev 15:807–826. https://doi.org/10.1101/gad.887201
32. Yanagiya A, Suyama E, Adachi H et al (2012) Translational homeostasis via the mRNA cap-binding protein, eIF4E. Mol Cell 46:847–858. https://doi.org/10.1016/j.molcel.2012.04.004
33. Pause A, Belsham GJ, Gingras A-C et al (1994) Insulin-dependent stimulation of protein synthesis by phosphorylation of a regulator of 5′-cap function. Nature 371:762–767. https://doi.org/10.1038/371762a0
34. Gingras A-C, Gygi SP, Raught B et al (1999) Regulation of 4E-BP1 phosphorylation: a novel two-step mechanism. Genes Dev 13:1422–1437. https://doi.org/10.1101/gad.13.11.1422
35. Hsieh-Li HM, Chang JG, Jong YJ et al (2000) A mouse model for spinal muscular atrophy. Nat Genet 24:66–70. https://doi.org/10.1038/71709
36. Riessland M, Ackermann B, Förster A et al (2010) SAHA ameliorates the SMA phenotype in two mouse models for spinal muscular atrophy. Hum Mol Genet 19:1492–1506. https://doi.org/10.1093/hmg/ddq023
37. Eggett CJ, Crosier S, Manning P et al (2008) Development and characterisation of a glutamate-sensitive motor neurone cell line. J Neurochem 74:1895–1902. https://doi.org/10.1046/j.1471-4159.2000.0741895.x
38. Morita M, Gravel S-P, Chénard V et al (2013) mTORC1 controls mitochondrial activity and biogenesis through 4E-BP-dependent translational regulation. Cell Metab 18:698–711. https://doi.org/10.1016/j.cmet.2013.10.001
39. Schmidt EK, Clavarino G, Ceppi M, Pierre P (2009) SUnSET, a nonradioactive method to monitor protein synthesis. Nat Methods 6:275–277. https://doi.org/10.1038/nmeth.1314
40. Argüello RJ, Reverendo M, Mendes A et al (2018) SunRiSE—measuring translation elongation at single-cell resolution by means of flow cytometry. J Cell Sci 131:jcs214346. https://doi.org/10.1242/jcs.214346
41. RStudio Team (2019) RStudio: integrated development environment for R. http://www.rstudio.com/
42. Hornburg D, Drepper C, Butter F et al (2014) Deep proteomic evaluation of primary and cell line motoneuron disease models delineates major differences in neuronal characteristics. Mol Cell Proteom 13:3410–3420. https://doi.org/10.1074/mcp.M113.037291
43. Suzuki YJ, Carini M, Butterfield DA (2010) Protein carbonylation. Antioxid Redox Signal 12:323–325. https://doi.org/10.1089/ars.2009.2887
44. Díaz-García CM, Mongeon R, Lahmann C et al (2017) Neuronal stimulation triggers neuronal glycolysis and not lactate uptake. Cell Metab 26:361.e4–374.e4. https://doi.org/10.1016/j.cmet.2017.06.021
45. Desagher S, Glowinski J, Prémont J (1997) Pyruvate protects neurons against hydrogen peroxide-induced toxicity. J Neurosci 17:9060–9067. https://doi.org/10.1523/jneurosci.17-23-09060.1997
46. Adams MJ, Buehner M, Chandrasekhar K et al (1973) Structure-function relationships in lactate dehydrogenase. Proc Natl Acad Sci 70:1968–1972. https://doi.org/10.1073/pnas.70.7.1968
47. Kładna A, Marchlewicz M, Piechowska T et al (2015) Reactivity of pyruvic acid and its derivatives towards reactive oxygen species. Luminescence 30:1153–1158. https://doi.org/10.1002/bio.2879
48. Nyström T (2005) Role of oxidative carbonylation in protein quality control and senescence. EMBO J 24:1311–1317. https://doi.org/10.1038/sj.emboj.7600599
49. Fallini C, Donlin-Asp PG, Rouanet JP et al (2016) Deficiency of the survival of motor neuron protein impairs mRNA localization and local translation in the growth cone of motor neurons. J Neurosci 36:3811–3820. https://doi.org/10.1523/JNEUROSCI.2396-15.2016
50. Jung H, Holt CE (2011) Local translation of mRNAs in neural development. Wiley Interdiscip Rev RNA 2:153–165. https://doi.org/10.1002/wrna.53

51. Sarbassov DD, Sabatini DM (2005) Redox regulation of the nutrient-sensitive raptor-mTOR pathway and complex. J Biol Chem 280:39505–39509. https://doi.org/10.1074/jbc.M506096200
52. Ashrafi G, Wu Z, Farrell RJ, Ryan TA (2017) GLUT4 mobilization supports energetic demands of active synapses. Neuron 93:606.e3–615.e3. https://doi.org/10.1016/j.neuron.2016.12.020
53. An Y, Varma VR, Varma S et al (2018) Evidence for brain glucose dysregulation in Alzheimer's disease. Alzheimer's Dement 14:318–329. https://doi.org/10.1016/j.jalz.2017.09.011
54. Ludolph AC, Langen KJ, Regard M et al (1992) Frontal lobe function in amyotrophic lateral sclerosis: a neuropsychologic and positron emission tomography study. Acta Neurol Scand 85:81–89. https://doi.org/10.1111/j.1600-0404.1992.tb04003.x
55. Manzo E, Lorenzini I, Barrameda D et al (2019) Glycolysis upregulation is neuroprotective as a compensatory mechanism in ALS. bioRxiv. https://doi.org/10.1101/517649
56. Wang H, Guo W, Mitra J et al (2018) Mutant FUS causes DNA ligation defects to inhibit oxidative damage repair in Amyotrophic Lateral Sclerosis. Nat Commun 9:3683. https://doi.org/10.1038/s41467-018-06111-6
57. Hung CH-L, Cheng SS-Y, Cheung Y-T et al (2018) A reciprocal relationship between reactive oxygen species and mitochondrial dynamics in neurodegeneration. Redox Biol 14:7–19. https://doi.org/10.1016/j.redox.2017.08.010
58. He L, He T, Farrar S et al (2017) Antioxidants maintain cellular redox homeostasis by elimination of reactive oxygen species. Cell Physiol Biochem 44:532–553. https://doi.org/10.1159/000485089
59. Perez-Riverol Y, Csordas A, Bai J et al (2019) The PRIDE database and related tools and resources in 2019: improving support for quantification data. Nucleic Acids Res 47:D442–D450. https://doi.org/10.1093/nar/gky1106

Publisher's Note

Supplementary Table 1: Primer sequences

Applications	Name	Sequence	Expected size
qRT-PCR	*Actb*-fw	AGCCATGTACGTAGCCATCC	201
	Actb-rev	CTCTCAGCTGTGGTGGTGAA	
	Smn-fw	ACTCCTCCAGATCGCTCAGA	227
	Smn-rev	AGGGGGTGGCGGGATTATTG	

Supplementary Table 2: Antibodies and conditions for Western blot (WB) and immunofluorescence (IF)

Primary Antibodies	Host species/dilution	Manufacturer/ #catalog	RRID
anti-4E-BP1	rabbit; WB 1:1000	Cell Signaling; #9644	AB_2097841
anti-p4E-BP1 (Thr37/46)	rabbit; WB 1:1000	Cell Signaling; #2855	AB_560835
anti-ACTB, HRP-conjugated	mouse; WB 1:10,000	Santa Cruz; sc-47778 HRP	AB_2714189
anti-ChAT	rabbit; IF 1:100	Thermo Scientific; PA5-26597	AB_2544097
anti-Puromycin	mouse; WB 1:1500 IF 1:150	Merck; MABE343	AB_2566826
anti-S6	mouse; WB 1:1000	Cell Signaling; #2317	AB_2238583
anti-pS6	rabbit; WB 1:1000	Cell Signaling; #2211	AB_331679
anti-S6K	rabbit; WB 1:2000	Cell Signaling; #2708	AB_390722
anti-pS6K	rabbit; WB 1:750	Cell Signaling; #9234	AB_2269803
anti-SMN	mouse; WB 1:3000	BD Biosciences; 610646	AB_397973
anti-Tau	mouse; IF 1:800	Santa Cruz; sc-390476	
anti-Tau	chicken; IF 1:100	Abcam; ab75714	AB_1310734
anti-TOM20	rabbit; IF 1:500	Santa Cruz; sc-11415	AB_2207533

Secondary antibodies	Host species/dilution	Manufacturer/ #catalog	RRID
anti-mouse IgG, HRP-conjugated	goat; WB 1:3000	Dianova; 115-035-146	AB_2307392
anti-rabbit IgG, HRP-conjugated	goat; WB 1:2000	Cell Signaling; #7074	AB_2099233
anti-chicken IgG, AlexaFluor647-conjugated	goat; IF 1:350	Thermo Scientific; A21449	AB_1500594
anti-mouse IgG, AlexaFluor488-conjugated	goat; IF 1:350	Thermo Scientific; A11001	AB_2534069

anti-rabbit IgG, AlexaFluor488-conjugated	donkey; IF 1:350	Thermo Scientific; A21206	AB_2535792
anti-rabbit IgG, AlexaFluor568-conjugated	donkey; IF 1:350	Thermo Scientific; A10042	AB_2534017

Supplementary Table 3: Fluorescence dyes

Fluorescence dye	**Manufacturer/ #catalog**
Alexa Fluor™ 568 Phalloidin	Thermo Scientific; A12380
CellROX™ Green reagent	Thermo Scientific; C10444
DAPI	Thermo Scientific; R37606
MitoTracker® Red CMXRos	Thermo Scientific; M7512

Supplementary Table 4: Drugs and supplements for *in vitro* assays

Drugs/ supplements	**Concentration**	**Solvent**	**Manufacturer/ #catalog**
Anisomycin	40 µM/ 50 µM	Water	Sigma; A9789
Harringtonine	2 mg/ml	DMSO	Abcam; ab141941
Menadione	0.1 µM-100 µM	DMSO	Sigma; M5625
N-Acetyl-L-cysteine (NAC)	1 µM-1000 µM	Water	Sigma; A9165
Puromycin Dihydrochloride	1 µM/ 10 µg/ml	Water	Gibco; A1113803
Sodium pyruvate	1 mM – 50 mM	Water	Sigma; P5280
Sodium lactate	1 mM – 50 mM	Water	Sigma; L7022
WYE-687 dihydrochloride	100 nM	Water	Tocris; #4282

Figure S1

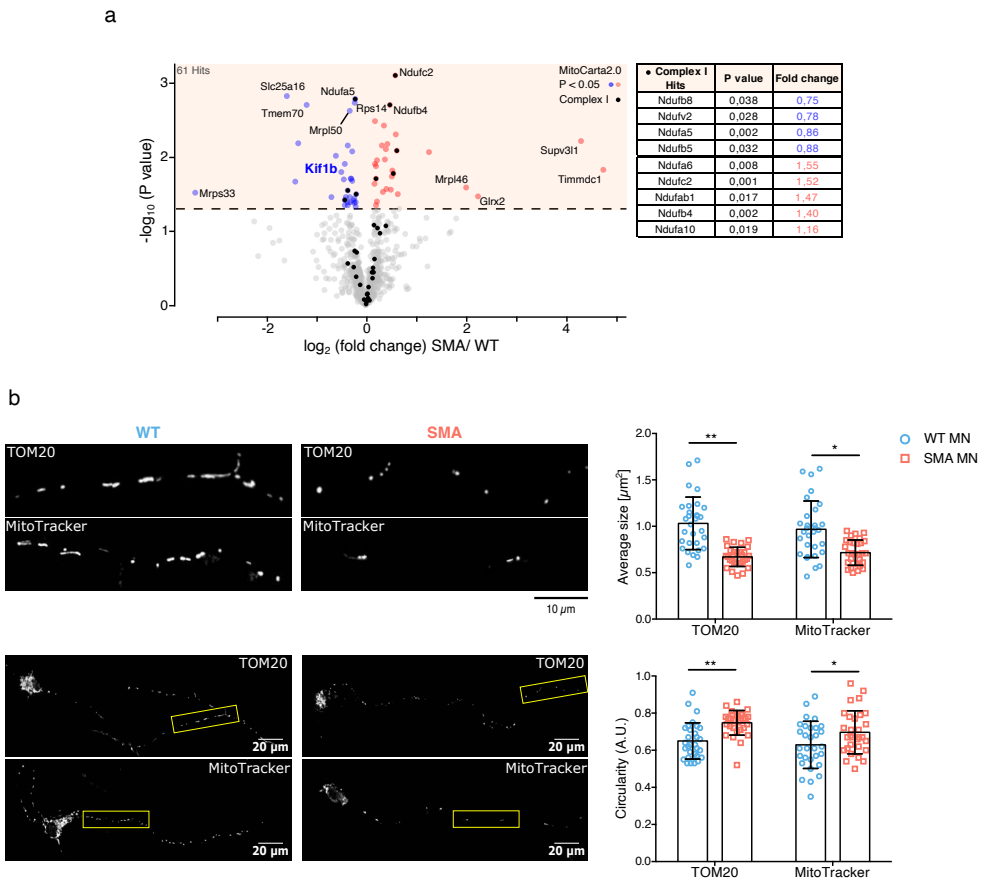

Complex I Hits	P value	Fold change
Ndufb8	0,038	0,75
Ndufv2	0,028	0,78
Ndufa5	0,002	0,86
Ndufb5	0,032	0,88
Ndufa6	0,008	1,55
Ndufc2	0,001	1,52
Ndufab1	0,017	1,47
Ndufb4	0,002	1,40
Ndufa10	0,019	1,16

Fig.S1 Complex I deficiency leads to dysfunctional and fragmented mitochondria.

a Volcano plot of proteins identified in whole proteome analysis and reported in the MitoCarta2.0 database; plotted p-values ($-\log_{10}$) against fold changes ($\log_2$, SMA/ WT). Four independent samples of WT MNs and three independent samples of SMA MNs were used for analysis. P-values were determined using unpaired two-sided t-test. Proteins with $p < 0.05$ are highlighted in blue (32 down-regulated) or red (29 up-regulated).

b Representative images and quantification of mitochondrial size and circularity of 10DIV WT and SMA MNs labelled with anti-TOM20 antibody or MitoTracker®. Enlarged areas are highlighted with yellow boxes in the corresponding image of the whole neuron. Scale bar in enlarged images: 10μm; Scale bar in whole neuron images: 20μm. Each dot represents the quantification of individual neurons (n=30). To compare WT (blue circles) and SMA (red squares), two-way ANOVA with Tukey HSD post hoc analysis was used on independent biological replicates (N=3) to determine statistical significance. Bar graphs depict the mean ± s.d. *p <0.05, **p <0.01.

Figure S2

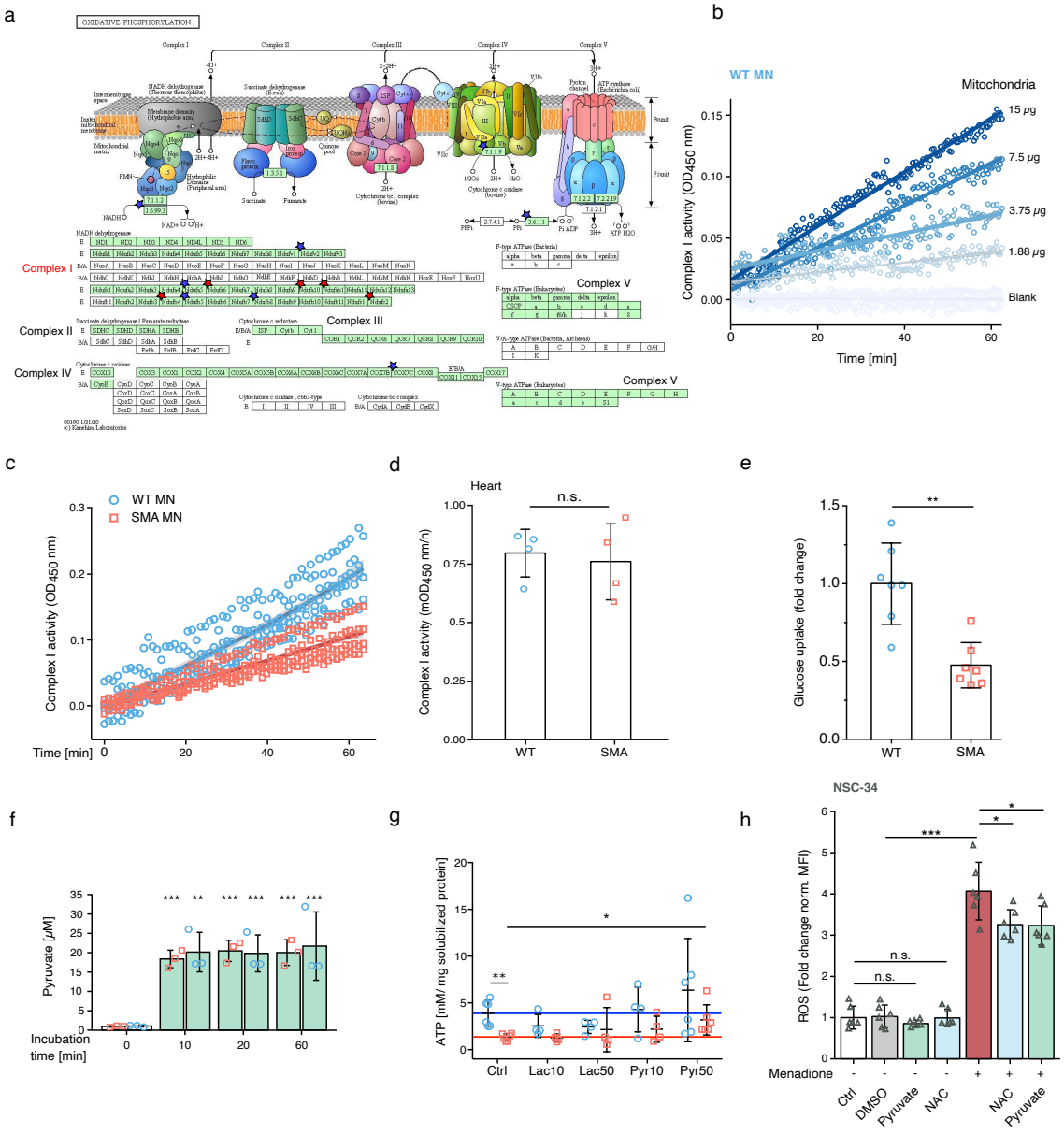
a
OXIDATIVE PHOSPHORYLATION
Complex I
Complex II
Complex III
Complex IV
Complex V
b
WT MN
Mitochondria
15 µg
7.5 µg
3.75 µg
1.88 µg
Blank
Complex I activity (OD450 nm)
Time [min]
c
WT MN
SMA MN
Complex I activity (OD450 nm)
Time [min]
d
Heart
n.s.
Complex I activity (mOD450 nm/h)
WT
SMA
e
**
Glucose uptake (fold change)
WT
SMA
f
Pyruvate [µM]
Incubation time [min]
g
ATP [mM/ mg solubilized protein]
Ctrl
Lac10
Lac50
Pyr10
Pyr50
h
NSC-34
ROS (Fold change norm. MFI)
n.s.
Menadione
Ctrl
DMSO
Pyruvate
NAC
NAC
Pyruvate

Fig.S2 Mitochondrial complex I is impaired in SMA MNs.

a Representation of oxidative phosphorylation KEGG Pathway (mmu00190) [1]. Green boxes highlight organism-specific complexes (Mus musculus). Stars mark significantly up-regulated (red) and down-regulated (blue) proteins in SMA MNs (10DIV).

b Optimization of Complex I activity using different amounts of mitochondria extract isolated from 10DIV WT MNs. Linear regression shows that complex I activity and reaction time is proportional over 1 h.

c Complex I activity using 20 μg mitochondria extract isolated from 10DIV WT and SMA MNs. Linear regression shows that complex I activitiy from WT and SMA MNs is proportional over 1 h, with a reduced slope for SMA MNs.

d Complex I activity rate using 300 μg protein extracts of heart from P7 WT and SMA mice (N=4). Quantification represents the increase of mean OD_{450} nm/ h. Two-way ANOVA with Tukey HSD post hoc analysis was used on independent biological replicates (N=4) to determine statistical significance. n.s. $p > 0.05$.

e Glucose uptake in 10DIV WT and SMA MNs. Each dot represents data from biological replicates (N=7). Two-tailed unpaired t-test was used to determine statistical significance. **p <0.01.

f Pyruvate uptake is increased in WT MNs and SMA after 1 h supplementation (N=3). One-way ANOVA with Dunnett post hoc analysis was used to compare each timepoint with the control. **p <0.01, ***p<0.001.

g Supplementation of WT MNs and SMA MNs with 10 mM/ 50 mM lactate or 10mM/ 50 mM pyruvate for 1 h. 50 mM pyruvate treatment shows a significant increase of ATP levels in SMA MNs (N=6). Two-tailed unpaired t-test was used on independent biological replicates to determine statistical significance. Means of two groups were compared, *p <0.05, **p <0.01.

h Quantification of mean fluorescence intensity of CellROX signal in NSC-34 cells. One hour treatment of 100 μM menadione increases ROS levels, whereas co-treatment of 10 μM NAC or 50 mM reduces menadione-induced ROS (N=6). One-way ANOVA with Tukey HSD post hoc analysis was used on independent biological replicates (N=3) to determine statistical significance. n.s. $p > 0.05$, *p <0.05, ***p <0.001.

Bar graphs scatterplots depict the mean ± s.d.

1. Kanehisa M (2000) KEGG: Kyoto Encyclopedia of Genes and Genomes. Nucleic Acids Research 28:27–30. doi: 10.1093/nar/28.1.27

Figure S3

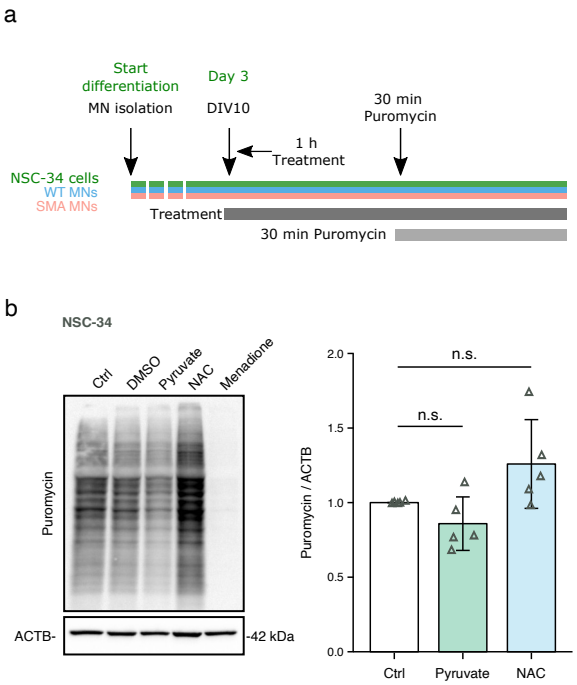

Fig.S3 Optimization of SUnSET assay

a Schematic representation of SUnSET assay in NSC-34 cells, WT MNs and SMA MNs. NSC-34 cells are differentiated for 3 days and MNs are cultured for 10 days before treatment with 50 mM pyruvate, 10 μM NAC or 100 μM menadione for 1 h. Puromycin was added in addition after 30 min of treatment.

b Representative western blot images and quantification of SUnSET assay in NSC-34 cells. Neither 50 mM pyruvate nor 10 μM NAC increased protein synthesis significantly. Each dot represents the quantification of individual biological replicates (N=5). Bar graphs depict the mean ± s.d. Two-tailed unpaired t-test with Holm-Bonferroni correction for multiple comparisons was used to determine statistical significance. n.s. $p > 0.05$.

Figure S4

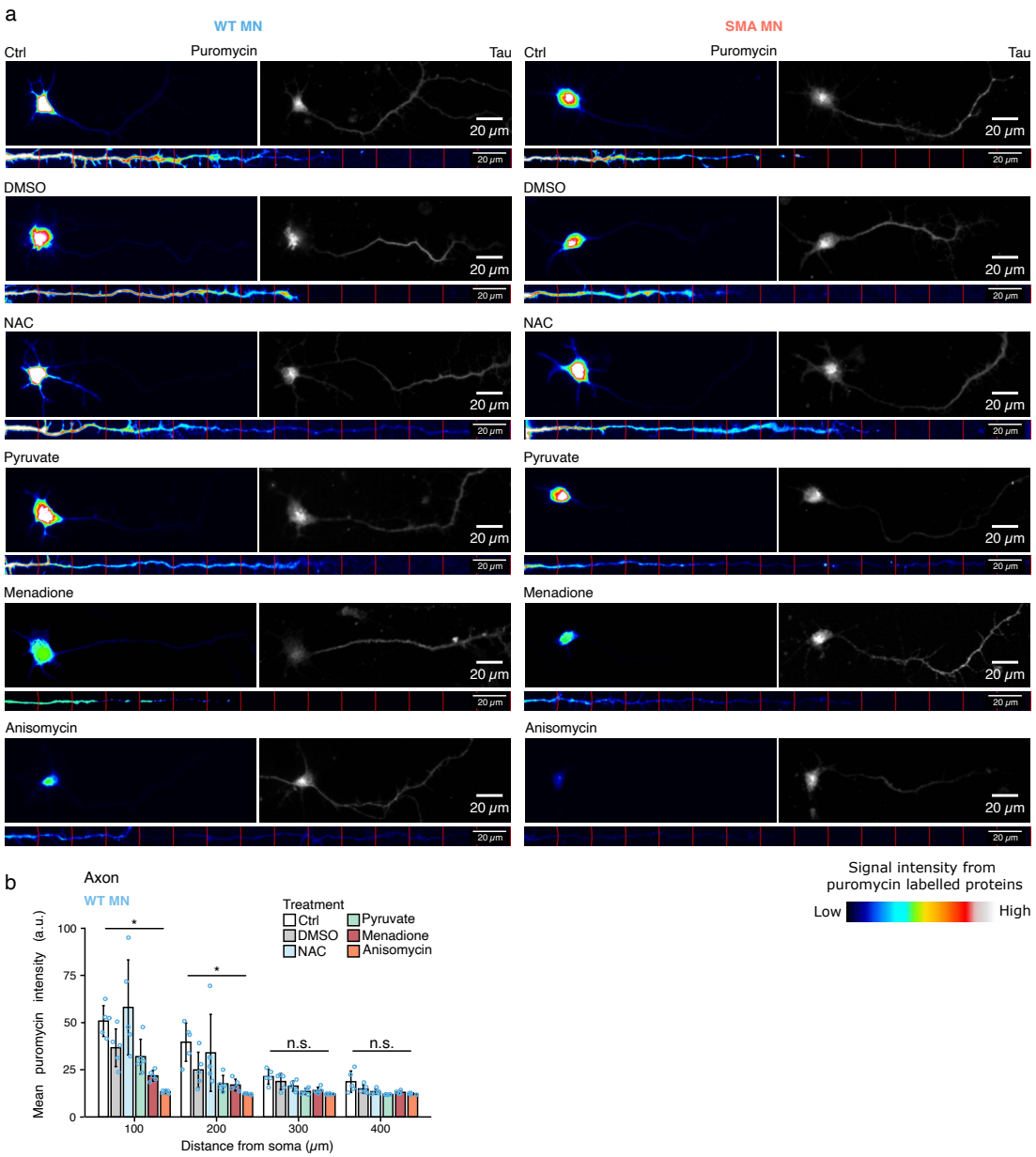

Fig.S4 Reduction of ROS improves protein synthesis in SMA MNs, but not in WT MNs.

a Representative images of WT and SMA MNs after SUnSET assay. Anti-puromycin (rainbow color) and anti-Tau (white) antibodies are used. Tau positive neurites (axons) were selected with a segmented line, straightened and divided into 20 μm bins using the concentric circles plugin. MNs were treated with 10 μM NAC or 50 mM pyruvate or 100 μM menadione or 50 μM anisomycin for 1 h. Images confirm that protein synthesis is blocked by anisomycin or menadione and increased in SMA MNs by 10 μM NAC. Scale bar: 20 μm.

b Quantification of mean puromycin intensity profiles, corresponding to protein levels, against distance in discrete categories. Each dot represents the average quantification of 10 neurons. Data are obtained from 5 individual biological replicates (N=5). Bar graph depict the mean ± s.d. Two-tailed unpaired t-test with Holm-Bonferroni correction for multiple comparisons was used to determine statistical significance. n.s. p >0.05, *p <0.05.

Figure S5

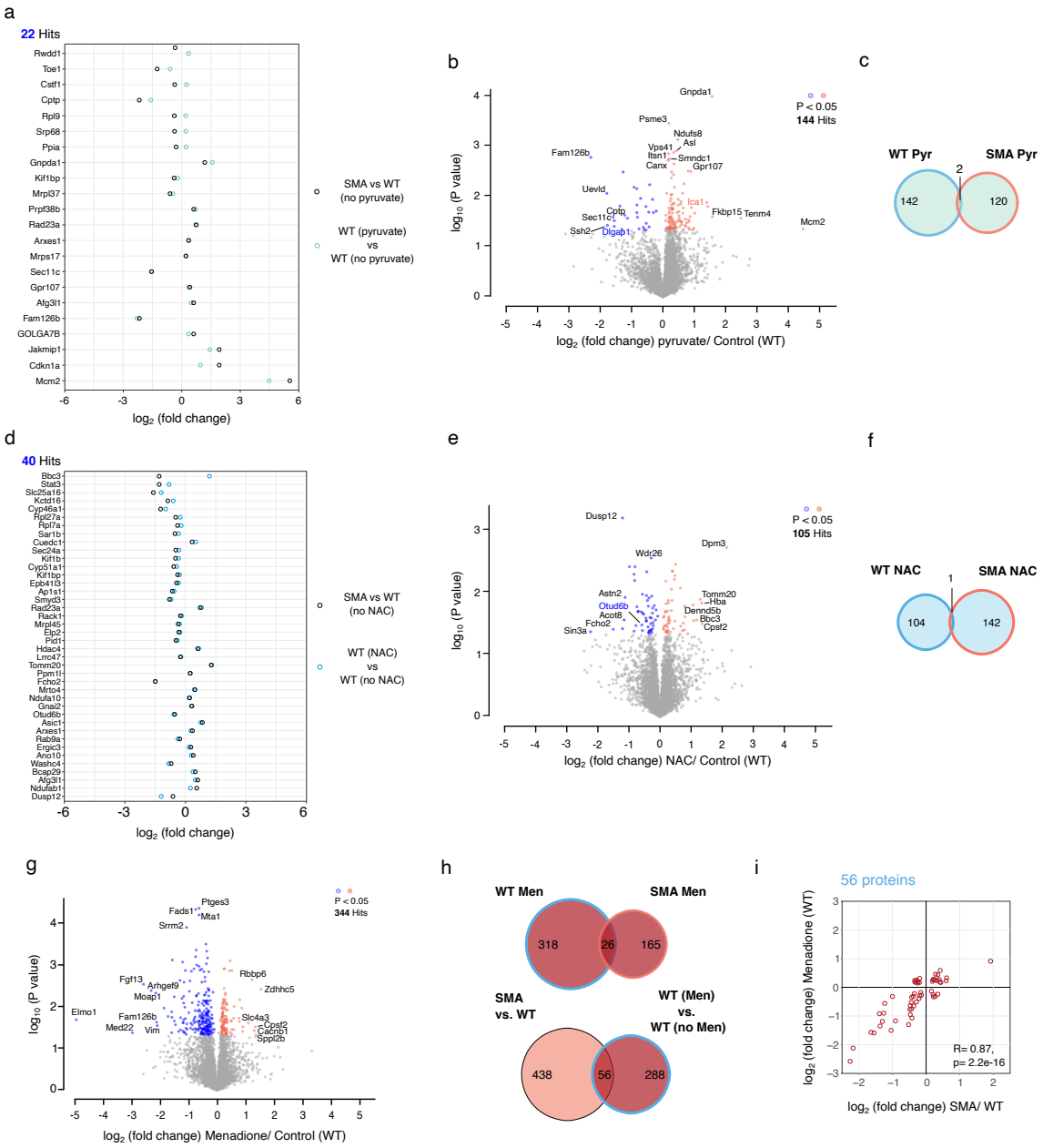
a
22 Hits
SMA vs WT (no pyruvate)
WT (pyruvate) vs WT (no pyruvate)
log2 (fold change)
b
P < 0.05
144 Hits
log10 (P value)
log2 (fold change) pyruvate/ Control (WT)
c
WT Pyr
SMA Pyr
142
2
120
d
40 Hits
SMA vs WT (no NAC)
WT (NAC) vs WT (no NAC)
log2 (fold change)
e
P < 0.05
105 Hits
log10 (P value)
log2 (fold change) NAC/ Control (WT)
f
WT NAC
SMA NAC
104
1
142
g
P < 0.05
344 Hits
log10 (P value)
log2 (fold change) Menadione/ Control (WT)
h
WT Men
SMA Men
318
26
165
SMA vs. WT
WT (Men) vs. WT (no Men)
438
56
288
i
56 proteins
log2 (fold change) Menadione (WT)
R= 0.87,
p= 2.2e-16
log2 (fold change) SMA/ WT

Fig.S5 Whole cell proteome after modifying ROS levels.

a Graph representing 22 proteins changed in SMA MNs compared to WT MNs, and pyruvate treated WT MNs compared to non-treated WT MNs; plotted fold change (log_2) comparing with and without pyruvate treatment.

b Volcano plot of whole proteome analysis after 50 mM pyruvate treatment to WT MNs for 1 h; plotted p-value ($-log_{10}$) against fold change (log_2). Four independent samples were used for analysis. P-values were determined using an unpaired two-sided t-test. Proteins with $p < 0.05$ are highlighted in blue (down-regulated) and red (up-regulated).

c Venn diagram showing quantity of proteins in WT MNs compared to SMA MNs treated with 50 mM pyruvate for 1 h.

d Graph representing 40 proteins changed in SMA MNs compared to WT MNs, and NAC treated WT MNs compared to non-treated WT MNs; plotted fold change (log_2) comparing with and without NAC treatment.

e Volcano plot of whole proteome analysis after 10 μM NAC treatment to WT MNs for 1 h; plotted p-value ($-log_{10}$) against fold change (log_2). Four independent samples were used for analysis. P-values were determined using an unpaired two-sided t-test. Proteins with $p < 0.05$ are highlighted in blue (down-regulated) and red (up-regulated).

f Venn diagram showing quantity of proteins in WT MNs compared to SMA MNs treated with 10 μM NAC for 1 h.

g Volcano plot of whole proteome analysis after 100 μM menadione to WT MNs for 1 h; plotted p-value ($-log_{10}$) against fold change (log_2). Four independent samples were used for analysis. P-values were determined using an unpaired two-sided t-test. Proteins with $p < 0.05$ are highlighted in blue (down-regulated) and red (up-regulated).

h Upper Venn diagram showing quantity of proteins in WT MNs compared to SMA MNs treated with 100 μM menadione for 1 h. Lower Venn diagram representing 56 proteins commonly altered in SMA and after menadione treatment.

i Scatterplot showing the fold changes (log_2) of significantly changed proteins in SMA against WT MNs after menadione treatment.

Figure S6

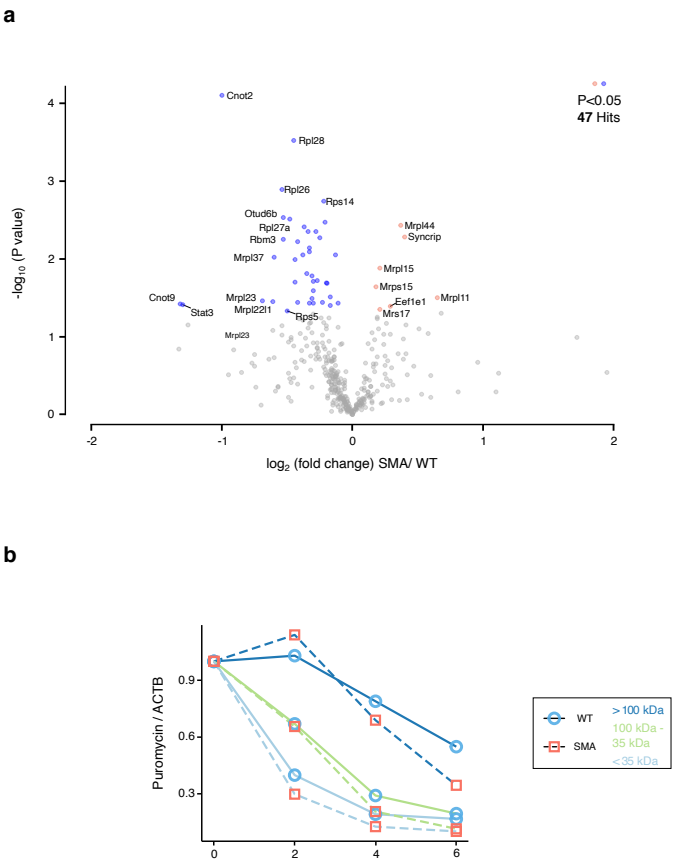

Fig.S6 Proteins related to translation are significantly changed in SMA MNs without affecting elongation speed.

a Volcano plot of translation related proteins comparing WT and SMA MNs; plotted p-value ($-\log_{10}$) against fold change ($\log_2$, SMA/ WT). Four independent samples of WT MNs and three independent samples for SMA MNs were used for analysis. P-values were determined using an unpaired two-sided t-test. Proteins with $p < 0.05$ are highlighted in blue (down-regulated) and red (up-regulated).

b Elongation speed is not altered in SMA MN compared to WT MNs. Each dot and each line represent the average of four independent biological replicates (N=4). Regression analysis comparing the least square means does not show any significant difference between WT MNs and SMA MNs.

Figure S7

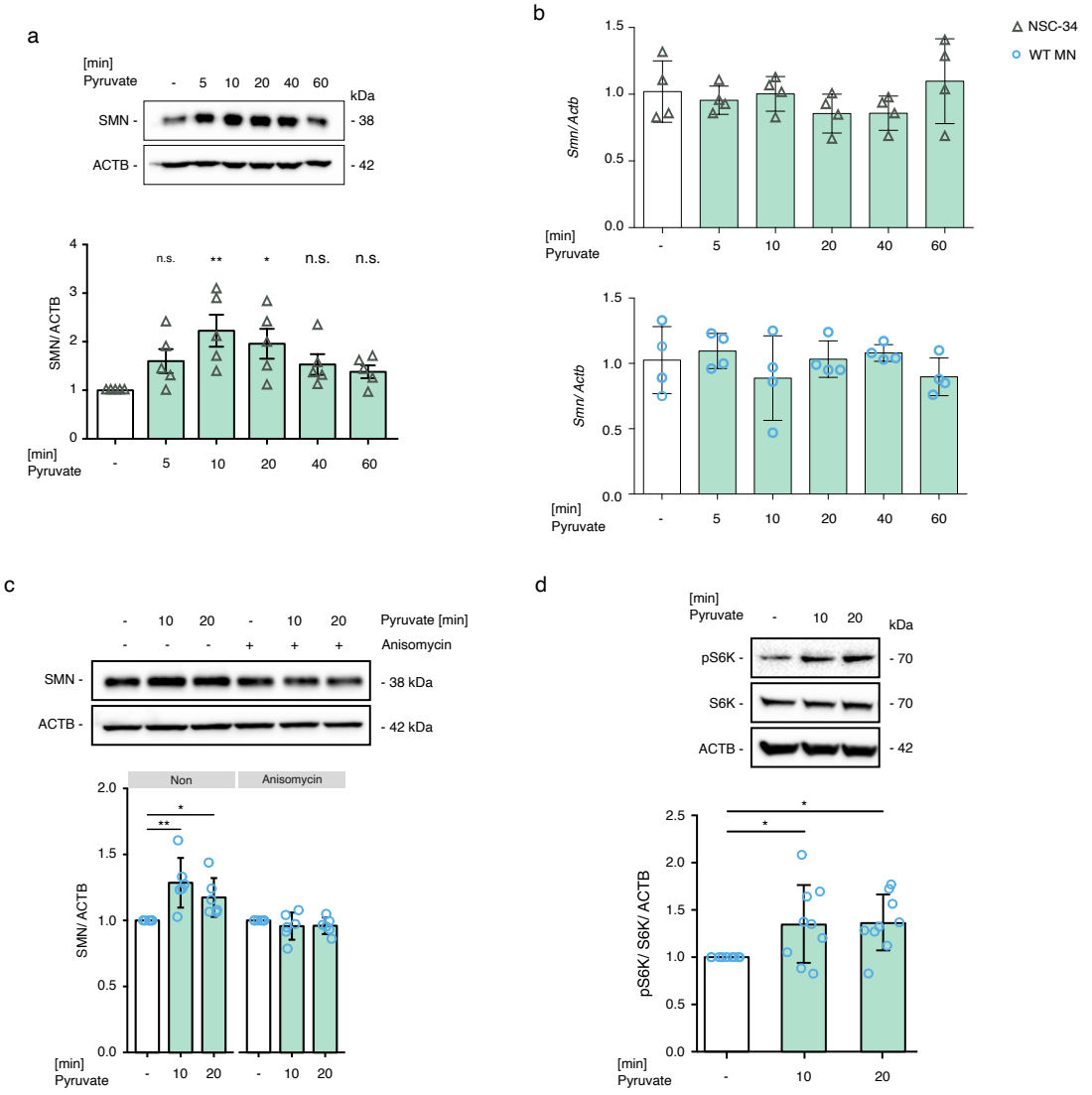

Fig.S7 Pyruvate regulates SMN levels.

a Representative western blot and quantification shows that 50 mM pyruvate increases SMN protein levels in NSC-34 cells after 1 h treatment (N=5). One-way ANOVA with Dunnett post hoc analysis was used to compare each timepoint with the control. n.s. $p>0.05$, *$p<0.05$, **$p<0.01$.

b Quantitative real-time PCR using gene specific Smn primers confirms that pyruvate supplementation did not change Smn transcript levels in NSC-34 cells and WT MNs (N=4). Actb was used as a loading control.

c 50 μM anisomycin prevents pyruvate-induced elevation of SMN protein levels (N=6). 50 mM pyruvate was treated for 10 or 20 min. One-way ANOVA with Tukey HSD post hoc analysis was used to determine statistical significance. *$p<0.05$, **$p<0.01$.

d Representative western blot and quantification show that pyruvate treatment increases phosphorylation status of p70S6 kinase. One-way ANOVA with Tukey HSD post hoc analysis was used to determine statistical significance. *$p<0.05$.
Each dot represents the quantification of individual biological replicates. Bar graph depict the mean ± s.d.

Appendix B Supplementary material

Table S1: Differentially expressed proteins in SMA compared to WT MNs.
List of significantly changed proteins in SMA compared to WT MNs ($p < 0.05$). Gene names, protein names, p-values, and fold change (FC) are listed. Proteins above the red line are down-regulated and below the red line are up-regulated in SMA compared to WT MNs. Gene names in red mark proteins found in the MitoCarta2.0 database. Gene names in blue are related to translation and gene names in purple are both, related to translation and annotated in the MitoCarta2.0 database.

Gene name	Protein name	-$\log_{10}$ p value	$\log_2$ FC SMA/ WT
Cuedc2	CUE domain-containing protein 2	4,17	-1,75
Srek1	Splicing regulatory glutamine/lysine-rich protein 1	4,11	-1,6
Cnot2	CCR4-NOT transcription complex subunit 2	4,1	-1
Ankrd17	Ankyrin repeat domain-containing protein 17	3,87	-0,59
Cops7a	COP9 signalosome complex subunit 7a	3,79	-0,52
Nipbl	Nipped-B-like protein	3,71	-4,78
Ctsc	Dipeptidyl peptidase 1	3,67	-2,74
Rpl28	60S ribosomal protein L28	3,52	-0,45
Ppm1g	Protein phosphatase 1G	3,4	-0,31
Brix1	Ribosome biogenesis protein BRX1 homolog	3,33	-2,07
Slc8a2	Sodium/calcium exchanger 2	3,17	-0,58
Ntrk3	NT-3 growth factor receptor	3,14	-1,55
Ssr3	Translocon-associated protein subunit gamma	3,07	-3,27
Sec13	Protein SEC13 homolog	3,06	-0,54
Fbxo22	F-box only protein 22	3,04	-0,42
Ampd3	AMP deaminase 3	3,02	-1,98
Nasp	Nuclear autoantigenic sperm protein	3,01	-0,42
Son	Protein SON	3	-0,52
Rpl26	60S ribosomal protein L26	2,89	-0,54
Kif1bp	KIF1-binding protein	2,88	-0,39
Ppfibp1	Liprin-beta-1	2,87	-1,39
Rps27	40S ribosomal protein S27	2,87	-0,37
Lbr	Delta(14)-sterol reductase LBR	2,86	-1,48
Slc25a16	Graves disease carrier protein homolog	2,83	-1,59
Fabp5	Fatty acid-binding protein 5	2,81	-0,39
Senp7	Sentrin-specific protease 7	2,8	-0,84
Ndufa5	NADH dehydrogenase [ubiquinone] 1 alpha subcomplex subunit 5	2,79	-0,21
Nup43	Nucleoporin Nup43	2,78	-0,43
Cntnap4	Contactin-associated protein-like 4	2,76	-2,01
Sec61a1	Protein transport protein Sec61 subunit alpha isoform 1	2,74	-0,95
Rps14	40S ribosomal protein S14	2,74	-0,22

Gene name	Protein name	-log10 p value	log2 FC SMA/ WT
Snrpf	Small nuclear ribonucleoprotein F	2,72	-0,83
Tmem70	Transmembrane protein 70, mitochondrial	2,71	-1,19
Rnf11	RING finger protein 11	2,7	-0,77
Eftud2	116 kDa U5 small nuclear ribonucleoprotein component	2,7	-0,61
Vta1	Vacuolar protein sorting-associated protein VTA1 homolog	2,7	-0,43
Btf3l4	Transcription factor BTF3 homolog 4	2,67	-0,38
Edf1	Endothelial differentiation-related factor 1	2,66	-0,51
Phpt1	14 kDa phosphohistidine phosphatase	2,66	-0,31
Cstf1	Cleavage stimulation factor subunit 1	2,64	-0,36
Mrpl50	39S ribosomal protein L50, mitochondrial	2,63	-0,32
Srp68	Signal recognition particle subunit SRP68	2,62	-0,37
Ppp4c	Serine/threonine-protein phosphatase 4 catalytic subunit	2,59	-0,39
Hddc3	Guanosine-3',5'-bis(diphosphate) 3'-pyrophosphohydrolase MESH1	2,56	-0,54
Otud6b	Deubiquitinase OTUD6B	2,53	-0,53
Rpl27a	60S ribosomal protein L27a	2,51	-0,48
Sh3bgrl3	SH3 domain-binding glutamic acid-rich-like protein 3	2,51	-0,45
Fam126b	Protein FAM126B	2,48	-2,17
Recql	ATP-dependent DNA helicase Q1	2,47	-1,83
Poldip3	Polymerase delta-interacting protein 3	2,47	-0,21
Maea	E3 ubiquitin-protein transferase MAEA	2,46	-0,44
Rab5c	Ras-related protein Rab-5C	2,45	-0,4
Ptms	Parathymosin	2,42	-0,56
Rpl13	60S ribosomal protein L13	2,41	-0,37
Dnaja2	DnaJ homolog subfamily A member 2	2,41	-0,24
Cyp46a1	Cholesterol 24-hydroxylase	2,4	-1,23
Psmc1	26S proteasome regulatory subunit 4	2,38	-0,31
Mmaa	Methylmalonic aciduria type A homolog, mitochondrial	2,37	-1,39
Ahcyl1	S-adenosylhomocysteine hydrolase-like protein 1	2,37	-0,41
Rwdd1	RWD domain-containing protein 1	2,35	-0,34
Rps3	40S ribosomal protein S3	2,35	-0,28
Slc35b1	Solute carrier family 35 member B1	2,34	-1,51
Tcea1	Transcription elongation factor A protein 1	2,33	-0,42
Fkbp3	Peptidyl-prolyl cis-trans isomerase FKBP3	2,32	-0,38
Xrcc5	X-ray repair cross-complementing protein 5	2,31	-2,41

Gene name	Protein name	-log$_{10}$ p value	log$_2$ FC SMA/ WT
Mien1	Migration and invasion enhancer 1	2,28	-0,34
Trappc12	Trafficking protein particle complex subunit 12	2,28	-0,34
Rbm15	RNA-binding protein 15	2,28	-0,29
Cggbp1	CGG triplet repeat-binding protein 1	2,27	-3,42
Prpf3	U4/U6 small nuclear ribonucleoprotein Prp3	2,27	-0,79
Rack1	Receptor of activated protein C kinase 1	2,27	-0,25
Dtx3	Probable E3 ubiquitin-protein ligase DTX3	2,26	-0,44
Rbm3	RNA-binding protein 3	2,25	-0,53
Nudt10	Diphosphoinositol polyphosphate phosphohydrolase 3-alpha	2,24	-0,56
Washc4	WASH complex subunit 4	2,23	-0,71
Rpl8	60S ribosomal protein L8	2,22	-0,42
Bub3	Mitotic checkpoint protein BUB3	2,21	-0,42
Iqcb1	IQ calmodulin-binding motif-containing protein 1	2,2	-0,75
Sec61a2	Protein transport protein Sec61 subunit alpha isoform 2	2,2	-0,75
Fam20b	Glycosaminoglycan xylosylkinase	2,2	-0,4
Cox7c	Cytochrome c oxidase subunit 7C, mitochondrial	2,19	-1,36
Tmem175	Endosomal/lysosomal potassium channel TMEM175	2,19	-1,24
Seh1l	Nucleoporin SEH1	2,19	-0,16
Fundc1	FUN14 domain-containing protein 1	2,16	-0,36
Hnrnpul1	Heterogeneous nuclear ribonucleoprotein U-like protein 1	2,16	-0,35
Syvn1	E3 ubiquitin-protein ligase synoviolin	2,15	-0,92
Rplp2	60S acidic ribosomal protein P2	2,14	-0,33
Cc2d1a	Coiled-coil and C2 domain-containing protein 1A	2,14	-0,29
Hddc2	HD domain-containing protein 2	2,13	-0,44
Srpk1	SRSF protein kinase 1	2,12	-0,35
Fcho2	F-BAR domain only protein 2	2,1	-1,49
Apeh	Acylamino-acid-releasing enzyme	2,1	-0,3
Nelfcd	Negative elongation factor D	2,09	-1,16
Rpl31	60S ribosomal protein L31	2,09	-0,33
Ddah2	N(G),N(G)-dimethylarginine dimethylaminohydrolase 2	2,08	-0,33
Ppa2	Inorganic pyrophosphatase 2, mitochondrial	2,08	-0,27
Uba3	NEDD8-activating enzyme E1 catalytic subunit	2,06	-0,96
Tbc1d5	TBC1 domain family member 5	2,06	-0,94
Ints9	Integrator complex subunit 9	2,06	-0,64
Cyp51a1	Lanosterol 14-alpha demethylase	2,05	-0,58
Fads1	Acyl-CoA (8-3)-desaturase	2,05	-0,43

Gene name	Protein name	-log10 p value	log2 FC SMA/ WT
Rpl9	60S ribosomal protein L9	2,05	-0,38
Eif3i	Eukaryotic translation initiation factor 3 subunit I	2,05	-0,13
Ehmt1	Histone-lysine N-methyltransferase EHMT1	2,04	-1,64
Elovl5	Elongation of very long chain fatty acids protein 5	2,03	-0,62
Mrpl37	39S ribosomal protein L37, mitochondrial	2,02	-0,6
Srp54	Signal recognition particle 54 kDa protein	2,01	-0,43
Psmb6	Proteasome subunit beta type-6	2,01	-0,35
Arfgap2	ADP-ribosylation factor GTPase-activating protein 2	2	-0,44
Psmd4	26S proteasome non-ATPase regulatory subunit 4	2	-0,43
Eif3g	Eukaryotic translation initiation factor 3 subunit G	1,99	-0,44
Ddx6	Probable ATP-dependent RNA helicase DDX6	1,99	-0,24
Sar1b	GTP-binding protein SAR1b	1,98	-0,52
Eef1b	Elongation factor 1-beta	1,97	-0,34
Sptbn1	Spectrin beta chain, non-erythrocytic 1	1,97	-0,08
Pih1d1	PIH1 domain-containing protein 1	1,95	-0,93
Dync1li2	Cytoplasmic dynein 1 light intermediate chain 2	1,95	-0,54
Sfpq	Splicing factor, proline- and glutamine-rich	1,94	-0,29
Noc2l	Nucleolar complex protein 2 homolog	1,93	-0,95
Dusp12	Dual specificity protein phosphatase 12	1,93	-0,62
Znf326	DBIRD complex subunit ZNF326	1,93	-0,36
Map3k12	Mitogen-activated protein kinase kinase kinase 12	1,92	-1,04
Scaf1	Splicing factor, arginine/serine-rich 19	1,91	-1,51
Cfdp1	Craniofacial development protein 1	1,91	-0,48
Me1	NADP-dependent malic enzyme	1,91	-0,42
Tram1	Translocating chain-associated membrane protein 1	1,9	-1,66
Smyd3	Histone-lysine N-methyltransferase SMYD3	1,9	-0,79
Slc39a7	Zinc transporter SLC39A7	1,88	-1,22
Itpk1	Inositol-tetrakisphosphate 1-kinase	1,88	-0,78
Sec24a	Protein transport protein Sec24A	1,88	-0,48
Huwe1	E3 ubiquitin-protein ligase HUWE1	1,88	-0,39
Tapt1	Transmembrane anterior posterior transformation protein 1	1,87	-0,55
Urm1	Ubiquitin-related modifier 1	1,87	-0,49
Pde6d	Retinal rod rhodopsin-sensitive cGMP 3',5'-cyclic phosphodiesterase subunit delta	1,87	-0,45
Cul1	Cullin-1	1,87	-0,4
Nsfl1c	NSFL1 cofactor p47	1,87	-0,18
Sptlc1	Serine palmitoyltransferase 1	1,86	-0,49
Ap1s1	AP-1 complex subunit sigma-1A	1,85	-0,65

Gene name	Protein name	-log$_{10}$ p value	log$_2$ FC SMA/ WT
Rab5b	Ras-related protein Rab-5B	1,83	-0,27
Impa1	Inositol monophosphatase 1	1,83	-0,24
Ddx17	Probable ATP-dependent RNA helicase DDX17	1,83	-0,24
Scly	Selenocysteine lyase	1,82	-1,23
Arf4	ADP-ribosylation factor 4	1,81	-0,88
Rpl7	60S ribosomal protein L7	1,81	-0,35
Smap1	Stromal membrane-associated protein 1	1,8	-0,56
Kif1b	Kinesin-like protein KIF1B	1,8	-0,49
Fn3krp	Ketosamine-3-kinase	1,8	-0,36
Hspa2	Heat shock-related 70 kDa protein 2	1,8	-0,29
Capn1	Calpain-1 catalytic subunit	1,79	-1,04
Pcnp	PEST proteolytic signal-containing nuclear protein	1,78	-0,45
Gps1	COP9 signalosome complex subunit 1	1,78	-0,44
Rps11	40S ribosomal protein S11	1,78	-0,31
Ythdc1	YTH domain-containing protein 1	1,77	-0,83
Zranb2	Zinc finger Ran-binding domain-containing protein 2	1,76	-0,43
Lrsam1	E3 ubiquitin-protein ligase LRSAM1	1,75	-0,91
Ube3a	Ubiquitin-protein ligase E3A	1,75	-0,39
Rnf114	E3 ubiquitin-protein ligase RNF114	1,74	-0,37
Fgf13	Fibroblast growth factor 13	1,73	-2,26
Vps25	Vacuolar protein-sorting-associated protein 25	1,73	-0,5
Sf1	Splicing factor 1	1,73	-0,18
Scrib	Protein scribble homolog	1,72	-0,47
Ldha	L-lactate dehydrogenase A chain	1,72	-0,46
Puf60	Poly(U)-binding-splicing factor PUF60	1,72	-0,39
Rpl32	60S ribosomal protein L32	1,72	-0,27
Mrpl43	39S ribosomal protein L43, mitochondrial	1,71	-0,3
Ndufaf2	NADH dehydrogenase [ubiquinone] 1 alpha subcomplex assembly factor 2	1,71	-0,29
Mrps11	28S ribosomal protein S11, mitochondrial	1,7	-0,44
Cpsf7	Cleavage and polyadenylation specificity factor subunit 7	1,7	-0,39
Supt16h	FACT complex subunit SPT16	1,7	-0,34
Mturn	Maturin	1,69	-2,47
Nup188	Nucleoporin NUP188 homolog	1,69	-0,85
Rab27b	Ras-related protein Rab-27B	1,69	-0,64
Gria1	Glutamate receptor 1	1,69	-0,27
Itpa	Inosine triphosphate pyrophosphatase	1,69	-0,21
Eprs	Bifunctional glutamate/proline–tRNA ligase	1,69	-0,2

Gene name	Protein name	-log10 p value	log2 FC SMA/ WT
Eif2s1	Eukaryotic translation initiation factor 2 subunit 1	1,69	-0,2
Sod1	Superoxide dismutase [Cu-Zn]	1,68	-0,27
Tomm5	Mitochondrial import receptor subunit TOM5 homolog	1,67	-1,42
Pcyt1a	Choline-phosphate cytidylyltransferase A	1,67	-0,39
Ppp6c	Serine/threonine-protein phosphatase 6 catalytic subunit	1,67	-0,14
Psmg3	Proteasome assembly chaperone 3	1,66	-2,14
Tbcc	Tubulin-specific chaperone C	1,66	-0,6
Pid1	PTB-containing, cubilin and LRP1-interacting protein	1,66	-0,47
Ubfd1	Ubiquitin domain-containing protein UBFD1	1,65	-0,54
Eml1	Echinoderm microtubule-associated protein-like 1	1,65	-0,48
Cdc37	Hsp90 co-chaperone Cdc37	1,65	-0,22
Fip1l1	Pre-mRNA 3'-end-processing factor FIP1	1,65	-0,19
Mlec	Malectin	1,64	-0,39
Dbnl	Drebrin-like protein	1,63	-0,21
Aup1	Ancient ubiquitous protein 1	1,62	-2
Fkbp1a	Peptidyl-prolyl cis-trans isomerase FKBP1A	1,62	-0,45
Pfdn2	Prefoldin subunit 2	1,62	-0,24
Coro1a	Coronin-1A	1,61	-0,76
Als2	Alsin	1,61	-0,47
Sec61b	Protein transport protein Sec61 subunit beta	1,6	-0,98
Kdm1a	Lysine-specific histone demethylase 1A	1,6	-0,74
Wbp2	WW domain-binding protein 2	1,6	-0,47
Hdac6	Histone deacetylase 6	1,59	-0,46
Plrg1	Pleiotropic regulator 1	1,59	-0,33
Rpl14	60S ribosomal protein L14	1,59	-0,3
Swi5	DNA repair protein SWI5 homolog	1,58	-0,54
Wdr5	WD repeat-containing protein 5	1,58	-0,42
Elp2	Elongator complex protein 2	1,58	-0,33
Toe1	Target of EGR1 protein 1	1,57	-1,26
Commd2	COMM domain-containing protein 2	1,57	-1,07
Cep170b	Centrosomal protein of 170 kDa protein B	1,57	-0,37
Mlf2	Myeloid leukemia factor 2	1,56	-0,47
Erh	Enhancer of rudimentary homolog	1,55	-0,59
Rad23b	UV excision repair protein RAD23 homolog B	1,55	-0,53
Dnal1	Dynein light chain 1, axonemal	1,55	-0,5
Ndufv2	NADH dehydrogenase [ubiquinone] flavoprotein 2, mitochondrial	1,55	-0,36

Gene name	Protein name	-log10 p value	log2 FC SMA/ WT
Lancl1	Glutathione S-transferase LANCL1	1,55	-0,31
Cnpy2	Protein canopy homolog 2	1,55	-0,29
Commd1	COMM domain-containing protein 1	1,54	-2,23
Slc6a11	Sodium- and chloride-dependent GABA transporter 3	1,54	-0,87
Rufy2	RUN and FYVE domain-containing protein 2	1,54	-0,54
Pfn2	Profilin-2	1,54	-0,3
Hdgfl2	Hepatoma-derived growth factor-related protein 2	1,53	-2,03
Dnajc8	DnaJ homolog subfamily C member 8	1,53	-0,33
Pik3r4	Phosphoinositide 3-kinase regulatory subunit 4	1,53	-0,24
Mrps33	28S ribosomal protein S33, mitochondrial	1,52	-3,44
Rrp12	RRP12-like protein	1,52	-0,74
Ccdc91	Coiled-coil domain-containing protein 91	1,52	-0,53
Gatd1	Glutamine amidotransferase-like class 1 domain-containing protein 1	1,52	-0,48
Srrm2	Serine/arginine repetitive matrix protein 2	1,52	-0,42
Bbc3	Bcl-2-binding component 3	1,51	-1,3
Dhcr7	7-dehydrocholesterol reductase	1,51	-0,4
Ybx1	Nuclease-sensitive element-binding protein 1	1,51	-0,34
Pum1	Pumilio homolog 1	1,51	-0,17
Cptp	Ceramide-1-phosphate transfer protein	1,5	-2,18
Srp19	Signal recognition particle 19 kDa protein	1,5	-0,79
Rpl7a	60S ribosomal protein L7a	1,5	-0,39
Elp3	Elongator complex protein 3	1,5	-0,34
Ndufb5	NADH dehydrogenase [ubiquinone] 1 beta subcomplex subunit 5, mitochondrial	1,5	-0,19
Sec11c	Signal peptidase complex catalytic subunit SEC11C	1,49	-1,55
Gla	Alpha-galactosidase A	1,49	-0,54
Ythdf2	YTH domain-containing family protein 2	1,49	-0,31
Gtf2e1	General transcription factor IIE subunit 1	1,48	-1,13
Mdp1	Magnesium-dependent phosphatase 1	1,48	-0,51
Sacm1l	Phosphatidylinositide phosphatase SAC1	1,47	-0,28
Med1	Mediator of RNA polymerase II transcription subunit 1	1,46	-2,53
Mrpl23	39S ribosomal protein L23, mitochondrial	1,46	-0,69
Rpe	Ribulose-phosphate 3-epimerase	1,46	-0,52
Timm8b	Mitochondrial import inner membrane translocase subunit Tim8 B	1,46	-0,4
Ciapin1	Anamorsin	1,46	-0,39
Stx17	Syntaxin-17	1,46	-0,32

Gene name	Protein name	-log$_{10}$ p value	log$_2$ FC SMA/ WT
Ipo7	Importin-7	1,46	-0,21
Yipf5	Protein YIPF5	1,45	-0,8
Asrgl1	Isoaspartyl peptidase/L-asparaginase	1,45	-0,73
Nr2f1	COUP transcription factor 1	1,45	-0,72
Rpl22l1	60S ribosomal protein L22-like 1	1,45	-0,61
Capns1	Calpain small subunit 1	1,45	-0,34
Ermp1	Endoplasmic reticulum metallopeptidase 1	1,45	-0,3
Clptm1l	Cleft lip and palate transmembrane protein 1-like protein	1,45	-0,25
Atrx	Transcriptional regulator ATRX	1,44	-0,57
Mia3	Transport and Golgi organization protein 1 homolog	1,44	-0,48
Rpl19	60S ribosomal protein L19	1,44	-0,42
Ubl4a	Ubiquitin-like protein 4A	1,44	-0,24
Rpl10a	60S ribosomal protein L10a	1,44	-0,23
Retreg2	Reticulophagy regulator 2	1,43	-1,08
Rbsn	Rabenosyn-5	1,43	-0,66
Rpl13a	60S ribosomal protein L13a	1,43	-0,33
Rpl12	60S ribosomal protein L12	1,43	-0,3
Ppia	Peptidyl-prolyl cis-trans isomerase A	1,43	-0,29
Upf1	Regulator of nonsense transcripts 1	1,43	-0,11
Hist1h1a	Histone H1,1	1,42	-2,82
Cnot9	CCR4-NOT transcription complex subunit 9	1,42	-1,32
Rcc1	Regulator of chromosome condensation	1,42	-0,68
Trappc4	Trafficking protein particle complex subunit 4	1,42	-0,52
Ndufb8	NADH dehydrogenase [ubiquinone] 1 beta subcomplex subunit 8, mitochondrial	1,42	-0,42
Htt	Huntingtin	1,42	-0,29
Stat3	Signal transducer and activator of transcription 3	1,41	-1,3
Ublcp1	Ubiquitin-like domain-containing CTD phosphatase 1	1,41	-0,96
Kctd16	BTB/POZ domain-containing protein KCTD16	1,41	-0,87
Cpsf3	Cleavage and polyadenylation specificity factor subunit 3	1,41	-0,57
Naa20	N-alpha-acetyltransferase 20	1,41	-0,5
Clpp	ATP-dependent Clp protease proteolytic subunit, mitochondrial	1,41	-0,24
Cers2	Ceramide synthase 2	1,4	-2,95
Myo16	Unconventional myosin-XVI	1,4	-1,72
Smc4	Structural maintenance of chromosomes protein 4	1,4	-1,11
Czib	CXXC motif containing zinc binding protein	1,4	-0,47

Gene name	Protein name	-log$_{10}$ p value	log$_2$ FC SMA/ WT
Mif	Macrophage migration inhibitory factor	1,4	-0,4
Gstp1	Glutathione S-transferase P 1	1,4	-0,31
Rac3	Ras-related C3 botulinum toxin substrate 3	1,4	-0,29
Hnrnpa0	Heterogeneous nuclear ribonucleoprotein A0	1,4	-0,29
Rab9a	Ras-related protein Rab-9A	1,4	-0,28
Chtop	Chromatin target of PRMT1 protein	1,4	-0,27
Lrrc47	Leucine-rich repeat-containing protein 47	1,4	-0,25
Qars	Glutamine–tRNA ligase	1,4	-0,17
Rnf40	E3 ubiquitin-protein ligase BRE1B	1,39	-1,03
Epb41l3	Band 4,1-like protein 3	1,39	-0,44
Fndc3a	Fibronectin type-III domain-containing protein 3A	1,39	-0,38
Pdhx	Pyruvate dehydrogenase protein X component, mitochondrial	1,39	-0,36
Snrpd2	Small nuclear ribonucleoprotein Sm D2	1,39	-0,32
Rcn2	Reticulocalbin-2	1,39	-0,31
Hmgb3	High mobility group protein B3	1,39	-0,26
Rps15a	40S ribosomal protein S15a	1,39	-0,2
Wbp11	WW domain-binding protein 11	1,38	-0,55
Prmt8	Protein arginine N-methyltransferase 8	1,38	-0,36
Ppif	Peptidyl-prolyl cis-trans isomerase F, mitochondrial	1,38	-0,23
Hmgn2	Non-histone chromosomal protein HMG-17	1,37	-3,35
Ddx20	Probable ATP-dependent RNA helicase DDX20	1,37	-1,37
Usp22	Ubiquitin carboxyl-terminal hydrolase 22	1,37	-0,91
Dad1	Dolichyl-diphosphooligosaccharide–protein glycosyltransferase subunit DAD1	1,37	-0,69
Cluh	Clustered mitochondria protein homolog	1,37	-0,65
Tm9sf4	Transmembrane 9 superfamily member 4	1,37	-0,46
Pds5b	Sister chromatid cohesion protein PDS5 homolog B	1,37	-0,44
Xkr4	XK-related protein 4	1,36	-2,29
Stat5b	Signal transducer and activator of transcription 5B	1,36	-0,7
Iws1	Protein IWS1 homolog	1,36	-0,63
Aaas	Aladin	1,36	-0,38
Nup210	Nuclear pore membrane glycoprotein 210	1,36	-0,31
Blvra	Biliverdin reductase A	1,36	-0,29
Tcerg1	Transcription elongation regulator 1	1,36	-0,27
Ppp1r21	Protein phosphatase 1 regulatory subunit 21	1,36	-0,17
Csnk1e	Casein kinase I isoform epsilon	1,35	-0,81
Cmc1	COX assembly mitochondrial protein homolog	1,35	-0,42
Ttl	Tubulin–tyrosine ligase	1,35	-0,4
Mrpl45	39S ribosomal protein L45, mitochondrial	1,35	-0,36

Gene name	Protein name	-log$_{10}$ p value	log$_2$ FC SMA/ WT
Bclaf1	Bcl-2-associated transcription factor 1	1,35	-0,28
Lta4h	Leukotriene A-4 hydrolase	1,35	-0,26
Trappc3	Trafficking protein particle complex subunit 3	1,35	-0,24
Phactr1	Phosphatase and actin regulator 1	1,34	-0,69
Zw10	Centromere/kinetochore protein zw10 homolog	1,34	-0,63
Mtmr3	Myotubularin-related protein 3	1,34	-0,61
Nans	Sialic acid synthase	1,34	-0,25
Rcor3	REST corepressor 3	1,33	-1,86
Penk	Proenkephalin-A	1,33	-1,03
Camk4	Calcium/calmodulin-dependent protein kinase type IV	1,33	-0,6
Atxn7l3b	Ataxin-7-like protein 3B	1,33	-0,51
Rps5	40S ribosomal protein S5	1,33	-0,5
Hdac1	Histone deacetylase 1	1,33	-0,29
Dtd1	D-aminoacyl-tRNA deacylase 1	1,33	-0,24
Timm50	Mitochondrial import inner membrane translocase subunit TIM50	1,33	-0,2
Snx27	Sorting nexin-27	1,33	-0,19
Psma5	Proteasome subunit alpha type-5	1,33	-0,18
Zdhhc17	Palmitoyltransferase ZDHHC17	1,33	-0,16
Chmp2b	Charged multivesicular body protein 2b	1,32	-0,83
Pds5a	Sister chromatid cohesion protein PDS5 homolog A	1,32	-0,6
Tbl2	Transducin beta-like protein 2	1,32	-0,27
Cab39	Calcium-binding protein 39	1,32	-0,24
Porcn	Protein-serine O-palmitoleoyltransferase porcupine	1,31	-0,95
Atp5md	ATP synthase membrane subunit DAPIT, mitochondrial	1,31	-0,76
Ndrg1	Protein NDRG1	1,31	-0,37
Fam160b1	Protein FAM160B1	1,31	-0,17
Haghl	Hydroxyacylglutathione hydrolase-like protein	3,53	0,95
Cfap36	Cilia- and flagella-associated protein 36	3,45	0,79
Ndufc2	NADH dehydrogenase [ubiquinone] 1 subunit C2	3,11	0,6
Strn	Striatin	2,95	0,18
Pten	Phosphatidylinositol 3,4,5-trisphosphate 3-phosphatase and dual-specificity protein phosphatase PTEN	2,89	0,59
Gnpda1	Glucosamine-6-phosphate isomerase 1	2,81	1,18
Ndufb4	NADH dehydrogenase [ubiquinone] 1 beta subcomplex subunit 4	2,71	0,49

Gene name	Protein name	-log$_{10}$ p value	log$_2$ FC SMA/ WT
Ddi2	Protein DDI1 homolog 2	2,68	0,75
Ubr1	E3 ubiquitin-protein ligase UBR1	2,5	1,18
Dhodh	Dihydroorotate dehydrogenase (quinone), mitochondrial	2,49	0,19
Mrpl44	39S ribosomal protein L44, mitochondrial	2,43	0,37
Cdkn1a	Cyclin-dependent kinase inhibitor 1	2,41	1,92
Dmac2l	ATP synthase subunit s, mitochondrial	2,38	0,21
Pik3ca	Phosphatidylinositol 4,5-bisphosphate 3-kinase catalytic subunit alpha isoform	2,35	0,76
Ergic3	Endoplasmic reticulum-Golgi intermediate compartment protein 3	2,31	0,27
Afg3l1	AFG3-like protein 1	2,31	0,61
Syncrip	Heterogeneous nuclear ribonucleoprotein Q	2,28	0,4
Prmt2	Protein arginine N-methyltransferase 2	2,28	1,04
Gnai2	Guanine nucleotide-binding protein G(i) subunit alpha-2	2,23	0,32
Pelp1	Proline-, glutamic acid- and leucine-rich protein 1	2,22	0,27
Supv3l1	ATP-dependent RNA helicase SUPV3L1, mitochondrial	2,22	4,35
Tbl1xr1	F-box-like/WD repeat-containing protein TBL1XR1	2,19	0,84
Jup	Junction plakoglobin	2,18	0,42
Pgs1	CDP-diacylglycerol–glycerol-3-phosphate 3-phosphatidyltransferase, mitochondrial	2,18	0,44
Ptprj	Receptor-type tyrosine-protein phosphatase eta	2,17	0,57
Bcs1l	Mitochondrial chaperone BCS1	2,16	0,33
Pik3r1	Phosphatidylinositol 3-kinase regulatory subunit alpha	2,16	1,59
Foxk2	Forkhead box protein K2	2,12	1,11
Vdac1	Voltage-dependent anion-selective channel protein 1	2,11	0,41
Ano10	Anoctamin-10	2,1	0,39
GOLGA7B	Golgin subfamily A member 7B	2,09	0,61
Ndufa6	NADH dehydrogenase [ubiquinone] 1 alpha subcomplex subunit 6	2,09	0,63
Cuedc1	CUE domain-containing protein 1	2,08	0,33
Hbb-b1	Hemoglobin subunit beta-1	2,08	3,94
Ttc9c	Tetratricopeptide repeat protein 9C	2,07	0,15
Txndc15	Thioredoxin domain-containing protein 15	2,07	0,58
Tomm20	Mitochondrial import receptor subunit TOM20 homolog	2,07	1,28

Gene name	Protein name	-log$_{10}$ p value	log$_2$ FC SMA/ WT
U2surp	U2 snRNP-associated SURP motif-containing protein	2,07	1,29
Tmed3	Transmembrane emp24 domain-containing protein 3	2,01	1,08
Syn3	Synapsin-3	1,99	0,52
Sdcbp	Syntenin-1	1,99	0,72
Prkaa2	5'-AMP-activated protein kinase catalytic subunit alpha-2	1,97	0,16
Coro1c	Coronin-1C	1,97	0,34
Prkar1a	cAMP-dependent protein kinase type I-alpha regulatory subunit	1,97	0,35
Dhrs7b	Dehydrogenase/reductase SDR family member 7B	1,97	0,39
Asic1	Acid-sensing ion channel 1	1,97	0,84
Immt	MICOS complex subunit Mic60	1,96	0,23
Grk2	Beta-adrenergic receptor kinase 1	1,96	0,52
Brcc3	Lys-63-specific deubiquitinase BRCC36	1,95	0,26
Rab3gap1	Rab3 GTPase-activating protein catalytic subunit	1,95	0,3
Dmxl1	DmX-like protein 1	1,92	1,8
Nln	Neurolysin, mitochondrial	1,91	0,19
Bcap29	B-cell receptor-associated protein 29	1,91	0,49
Ophn1	Oligophrenin-1	1,9	0,69
Hdac4	Histone deacetylase 4	1,89	0,61
Mrpl15	39S ribosomal protein L15, mitochondrial	1,88	0,21
Gtdc1	Glycosyltransferase-like domain-containing protein 1	1,87	1,18
Ddx39a	ATP-dependent RNA helicase DDX39A	1,86	0,24
Sema3c	Semaphorin-3C	1,86	1,1
Arxes1	Adipocyte-related X-chromosome expressed sequence 1	1,84	0,35
Timmdc1	Complex I assembly factor TIMMDC1, mitochondrial	1,83	4,8
Akap1	A-kinase anchor protein 1, mitochondrial	1,82	0,54
Mcm2	DNA replication licensing factor MCM2	1,82	5,54
Vps11	Vacuolar protein sorting-associated protein 11 homolog	1,79	0,25
Ndufab1	Acyl carrier protein, mitochondrial	1,78	0,56
Hprt1	Hypoxanthine-guanine phosphoribosyltransferase	1,77	0,63
Kirrel3	Kin of IRRE-like protein 3	1,77	0,84
Jakmip1	Janus kinase and microtubule-interacting protein 1	1,76	1,92
Agk	Acylglycerol kinase, mitochondrial	1,74	0,53
Rapgef2	Rap guanine nucleotide exchange factor 2	1,74	0,53
Ctnnb1	Catenin beta-1	1,73	0,27

Gene name	Protein name	-log$_{10}$ p value	log$_2$ FC SMA/ WT
Arid1a	AT-rich interactive domain-containing protein 1A	1,73	0,58
Dynll2	Dynein light chain 2, cytoplasmic	1,72	0,27
Hspg2	Basement membrane-specific heparan sulfate proteoglycan core protein	1,72	0,99
Ndufa10	NADH dehydrogenase [ubiquinone] 1 alpha subcomplex subunit 10, mitochondrial	1,71	0,21
Pcdhb8	Protocadherin beta-8	1,71	1,02
Actb	Actin, cytoplasmic 1	1,7	0,32
Exoc5	Exocyst complex component 5	1,69	0,37
Osbpl6	Oxysterol-binding protein-related protein 6	1,67	0,42
Ppm1l	Protein phosphatase 1L	1,66	0,23
Dyrk1a	Dual specificity tyrosine-phosphorylation-regulated kinase 1A	1,65	2,3
Mrps15	28S ribosomal protein S15, mitochondrial	1,64	0,18
Fam114a2	Protein FAM114A2	1,63	0,48
Timp3	Metalloproteinase inhibitor 3	1,62	0,99
Ankib1	Ankyrin repeat and IBR domain-containing protein 1	1,6	2,65
Dgkz	Diacylglycerol kinase zeta	1,59	0,61
Rad23a	UV excision repair protein RAD23 homolog A	1,59	0,73
Mrpl46	39S ribosomal protein L46, mitochondrial	1,59	2,03
Ccdc88a	Girdin	1,58	0,17
Gpr107	Protein GPR107	1,58	0,42
Hspd1	60 kDa heat shock protein, mitochondrial	1,57	0,42
Vdac2	Voltage-dependent anion-selective channel protein 2	1,56	0,51
Txn	Thioredoxin	1,56	0,53
Nup160	Nuclear pore complex protein Nup160	1,56	0,74
Raf1	RAF proto-oncogene serine/threonine-protein kinase	1,55	0,22
Sptan1	Spectrin alpha chain, non-erythrocytic 1	1,55	0,23
Braf	Serine/threonine-protein kinase B-raf	1,54	0,55
Sema7a	Semaphorin-7A	1,54	1,65
Mecr	Enoyl-[acyl-carrier-protein] reductase, mitochondrial	1,53	0,35
Ptp4a2	Protein tyrosine phosphatase type IVA 2	1,53	0,39
Lrrc8d	Volume-regulated anion channel subunit LRRC8D	1,53	0,41
Tmtc3	Protein O-mannosyl-transferase TMTC3	1,53	0,74
B3gat3	Galactosylgalactosylxylosylprotein 3-beta-glucuronosyltransferase 3	1,52	0,49
Prcp	Lysosomal Pro-X carboxypeptidase	1,51	0,19
Snrnp27	U4/U6,U5 small nuclear ribonucleoprotein 27 kDa protein	1,5	0,54

Gene name	Protein name	-log10 p value	log2 FC SMA/ WT
Mrpl11	39S ribosomal protein L11, mitochondrial	1,5	0,65
Ints14	Integrator complex subunit 14	1,5	0,98
Hras	GTPase HRas	1,49	0,36
Thumpd3	THUMP domain-containing protein 3	1,49	0,7
Fkbp2	Peptidyl-prolyl cis-trans isomerase FKBP2	1,49	1,15
Herc4	Probable E3 ubiquitin-protein ligase HERC4	1,48	0,32
Kct2	Keratinocyte-associated transmembrane protein 2	1,48	1,63
Spry4	Protein sprouty homolog 4	1,47	0,92
Glrx2	Glutaredoxin-2, mitochondrial	1,47	2,27
Anapc7	Anaphase-promoting complex subunit 7	1,47	2,89
Extl3	Exostosin-like 3	1,43	0,97
Ptprm	Receptor-type tyrosine-protein phosphatase mu	1,42	0,73
Dnajc11	DnaJ homolog subfamily C member 11	1,4	0,23
Nptx1	Neuronal pentraxin-1	1,4	0,33
Ppip5k2	Inositol hexakisphosphate and diphosphoinositol-pentakisphosphate kinase 2	1,4	0,5
Ktn1	Kinectin	1,4	1,21
R3hdm2	R3H domain-containing protein 2	1,4	4,86
Eef1e1	Eukaryotic translation elongation factor 1 epsilon-1	1,39	0,29
Wdr48	WD repeat-containing protein 48	1,39	0,33
Drap1	Dr1-associated corepressor	1,39	0,35
Nup50	Nuclear pore complex protein Nup50	1,39	1,52
Slc44a3	Choline transporter-like protein 3	1,39	2,51
Gdpd5	Glycerophosphodiester phosphodiesterase domain-containing protein 5	1,38	0,22
Gbe1	1,4-alpha-glucan-branching enzyme	1,38	0,95
Tgfbrap1	Transforming growth factor-beta receptor-associated protein 1	1,37	0,28
Uba5	Ubiquitin-like modifier-activating enzyme 5	1,37	0,28
Lrp8	Low-density lipoprotein receptor-related protein 8	1,37	0,68
Adgrl2	Adhesion G protein-coupled receptor L2	1,36	0,18
Mrps17	28S ribosomal protein S17, mitochondrial	1,35	0,21
Prpf38b	Pre-mRNA-splicing factor 38B	1,35	0,61
Smpdl3b	Acid sphingomyelinase-like phosphodiesterase 3b	1,35	0,78
Rundc3b	RUN domain-containing protein 3B	1,35	0,83
Abhd12	Lysophosphatidylserine lipase ABHD12	1,34	0,24
Actr1b	Beta-centractin	1,34	0,28
Tmed8	Protein TMED8	1,34	0,36
Marcksl1	MARCKS-related protein	1,34	0,47
Vps13a	Vacuolar protein sorting-associated protein 13A	1,34	0,48

Gene name	Protein name	-log$_{10}$ p value	log$_2$ FC SMA/ WT
Myo9b	Unconventional myosin-IXb	1,34	1,15
Snrpg	Small nuclear ribonucleoprotein G	1,33	0,33
Csnk2b	Casein kinase II subunit beta	1,33	0,38
Ndst1	Bifunctional heparan sulfate N-deacetylase/N-sulfotransferase 1	1,33	0,8
Mrto4	mRNA turnover protein 4 homolog	1,32	0,47
Smg1	Serine/threonine-protein kinase SMG1	1,32	2,85
Panx1	Pannexin-1	1,31	0,4

Table S2: Differentially expressed proteins in WT MNs after pyruvate treatment.
List of significantly changed proteins in WT MNs after pyruvate treatment ($p < 0.05$). Gene names, protein names, p-values, and fold changes (FC) are listed. Proteins above the red line are down-regulated and below the red line are up-regulated in pyruvate treated WT compared to untreated WT MNs.

Gene name	Protein name	-log$_{10}$ p value	log$_2$ FC Pyruvate/ WT
Fam126b	Protein FAM126B	2.74	-2.30
Astn2	Astrotactin-2	2.45	-1.27
Got2	Aspartate aminotransferase, mitochondrial	2.20	-0.42
Dnmt1	DNA (cytosine-5)-methyltransferase 1	2.15	-0.92
Vhl	von Hippel-Lindau disease tumor suppressor	2.12	-0.83
Uevld	Ubiquitin-conjugating enzyme E2 variant 3	2.03	-1.79
Esyt1	Extended synaptotagmin-1	1.93	-0.71
Gdap2	Ganglioside-induced differentiation-associated protein 2	1.91	-0.33
Acvr2a	Activin receptor type-2A	1.80	-0.83
Ano8	Anoctamin-8	1.78	-1.37
Rb1cc1	RB1-inducible coiled-coil protein 1	1.77	-0.54
Kif1bp	KIF1-binding protein	1.68	-0.21
Mrpl37	39S ribosomal protein L37, mitochondrial	1.66	-0.45
Gk	Glycerol kinase	1.65	-0.30
Efnb3	Ephrin-B3	1.65	-0.83
Trpc3	Short transient receptor potential channel 3	1.60	-1.22
Enpp4	Bis(5'-adenosyl)-triphosphatase enpp4	1.56	-0.81
Cptp	Ceramide-1-phosphate transfer protein	1.56	-1.59
Micu3	Calcium uptake protein 3, mitochondrial	1.54	-1.13
Sec11c	Signal peptidase complex catalytic subunit SEC11C	1.49	-1.55
Slk	STE20-like serine/threonine-protein kinase	1.44	-0.53
Ssh2	Protein phosphatase Slingshot homolog 2	1.40	-1.77
Dlgap1	Disks large-associated protein 1	1.38	-1.55

Gene name	Protein name	-log$_{10}$ p value	log$_2$ FC Pyruvate/ WT
Apc	Adenomatous polyposis coli protein	1.37	-0.44
Cpsf1	Cleavage and polyadenylation specificity factor subunit 1	1.36	-0.62
Pptc7	Protein phosphatase PTC7 homolog	1.33	-0.76
Borcs6	BLOC-1-related complex subunit 6	1.32	-1.31
Toe1	Target of EGR1 protein 1	1.31	-0.60
Pcsk2	Neuroendocrine convertase 2	1.31	-0.54
Gnpda1	Glucosamine-6-phosphate isomerase 1	3.94	1.57
Psme3	Proteasome activator complex subunit 3	3.41	0.19
Ndufs8	NADH dehydrogenase [ubiquinone] iron-sulfur protein 8, mitochondrial	3.09	0.48
Asl	Argininosuccinate lyase	2.87	0.44
Vps41	Vacuolar protein sorting-associated protein 41 homolog	2.84	0.35
Itsn1	Intersectin-1	2.81	0.18
Smndc1	Survival of motor neuron-related-splicing factor 30	2.71	0.20
Canx	Calnexin	2.68	0.17
Gpr107	Protein GPR107	2.61	0.35
Ctif	CBP80/20-dependent translation initiation factor	2.47	0.81
Sdr39u1	Epimerase family protein SDR39U1	2.46	0.90
Epn1	Epsin-1	2.45	0.28
Cdh13	Cadherin-13	2.40	0.34
Hspe1	10 kDa heat shock protein, mitochondrial	2.33	0.27
Alpl	Alkaline phosphatase, tissue-nonspecific isozyme	2.22	0.68
Atp5pf	ATP synthase-coupling factor 6, mitochondrial	2.15	0.37
Skp1	S-phase kinase-associated protein 1	2.03	0.12
Zwint	ZW10 interactor	2.03	0.63
Ndufs5	NADH dehydrogenase [ubiquinone] iron-sulfur protein 5	2.01	0.29
Txnrd1	Thioredoxin reductase 1, cytoplasmic	2.00	0.26
Farsb	Phenylalanine–tRNA ligase beta subunit	1.93	0.26
Ccnt1	Cyclin-T1	1.91	0.49
Cstf1	Cleavage stimulation factor subunit 1	1.88	0.24
Spryd4	SPRY domain-containing protein 4	1.87	0.58
Ston1	Stonin-1	1.85	1.40
Rwdd1	RWD domain-containing protein 1	1.84	0.35
Rbm12	RNA-binding protein 12	1.82	0.57
Ccdc50	Coiled-coil domain-containing protein 50	1.82	0.34

Gene name	Protein name	-log$_{10}$ p value	log$_2$ FC Pyruvate/ WT
Naa35	N-alpha-acetyltransferase 35, NatC auxiliary subunit	1.81	0.28
Afg3l1	AFG3-like protein 1	1.80	0.49
Jakmip1	Janus kinase and microtubule-interacting protein 1	1.77	1.44
Ica1	Islet cell autoantigen 1	1.75	0.91
Chp1	Calcineurin B homologous protein 1	1.75	0.27
Fat3	Protocadherin Fat 3	1.74	0.65
Capza2	F-actin-capping protein subunit alpha-2	1.74	0.19
Tmed4	Transmembrane emp24 domain-containing protein 4	1.73	0.31
Mrps7	28S ribosomal protein S7, mitochondrial	1.73	0.33
Ube2r2	Ubiquitin-conjugating enzyme E2 R2	1.72	0.29
Pdap1	28 kDa heat- and acid-stable phosphoprotein	1.71	0.30
Picalm	Phosphatidylinositol-binding clathrin assembly protein	1.68	0.21
Rprd1b	Regulation of nuclear pre-mRNA domain-containing protein 1B	1.67	0.51
Ppih	Peptidyl-prolyl cis-trans isomerase H	1.65	0.45
Mrpl12	39S ribosomal protein L12, mitochondrial	1.64	0.20
Mrrf	Ribosome-recycling factor, mitochondrial	1.64	0.64
Ociad1	OCIA domain-containing protein 1	1.64	0.30
Skt	Sickle tail protein	1.64	1.02
Sae1	SUMO-activating enzyme subunit 1	1.60	0.10
Selenof	Selenoprotein F	1.59	0.52
Fundc2	FUN14 domain-containing protein 2	1.57	0.87
Ccny	Cyclin-Y	1.57	0.28
Fkbp15	FK506-binding protein 15	1.57	1.58
Actr2	Actin-related protein 2	1.57	0.23
Srp68	Signal recognition particle subunit SRP68	1.56	0.21
Rap2c	Ras-related protein Rap-2c	1.54	0.52
Tenm4	Teneurin-4	1.54	2.49
Naa10	N-alpha-acetyltransferase 10	1.53	0.25
Naa50	N-alpha-acetyltransferase 50	1.53	0.18
Dnajc2	DnaJ homolog subfamily C member 2	1.53	0.27
Robo1	Roundabout homolog 1	1.52	0.72
Lyar	Cell growth-regulating nucleolar protein	1.51	0.33
Crebbp	CREB-binding protein	1.51	0.82
Psmc4	26S proteasome regulatory subunit 6B	1.49	0.09
Cox6a1	Cytochrome c oxidase subunit 6A1, mitochondrial	1.49	0.55
C1qbp	Complement component 1 Q subcomponent-binding protein, mitochondrial	1.49	0.49

Gene name	Protein name	-log$_{10}$ p value	log$_2$ FC Pyruvate/ WT
Stub1	STIP1 homology and U box-containing protein 1	1.48	0.29
Trap1	Heat shock protein 75 kDa, mitochondrial	1.48	0.22
Ccdc22	Coiled-coil domain-containing protein 22	1.47	0.84
Ubl7	Ubiquitin-like protein 7	1.47	0.30
Mars	Methionine–tRNA ligase, cytoplasmic	1.47	0.19
Col11a1	Collagen alpha-1(XI) chain	1.47	0.57
Vamp7	Vesicle-associated membrane protein 7	1.47	0.60
Mrps9	28S ribosomal protein S9, mitochondrial	1.46	0.43
Ubr4	E3 ubiquitin-protein ligase UBR4	1.46	0.36
Rad23a	UV excision repair protein RAD23 homolog A	1.45	0.76
Gga3	ADP-ribosylation factor-binding protein GGA3	1.44	0.31
Lrpprc	Leucine-rich PPR motif-containing protein, mitochondrial	1.44	0.21
Arxes1	Adipocyte-related X-chromosome expressed sequence 1	1.42	0.37
Cacna1e	Voltage-dependent R-type calcium channel subunit alpha-1E	1.42	0.60
Ubac1	Ubiquitin-associated domain-containing protein 1	1.41	0.38
Tfam	Transcription factor A, mitochondrial	1.41	0.28
Prpf38b	Pre-mRNA-splicing factor 38B	1.40	0.71
Slc33a1	Acetyl-coenzyme A transporter 1	1.38	0.55
Cnot1	CCR4-NOT transcription complex subunit 1	1.38	0.21
Plpp1	Phospholipid phosphatase 1	1.38	0.73
Mpdu1	Mannose-P-dolichol utilization defect 1 protein	1.37	0.41
Casc4	Protein CASC4	1.37	0.29
Sez6l	Seizure 6-like protein	1.37	0.38
Mrps17	28S ribosomal protein S17, mitochondrial	1.37	0.22
Dnaja3	DnaJ homolog subfamily A member 3, mitochondrial	1.36	0.19
Sucla2	Succinate–CoA ligase [ADP-forming] subunit beta, mitochondrial	1.35	0.18
Lamtor2	Ragulator complex protein LAMTOR2	1.35	0.35
Enpp5	Ectonucleotide pyrophosphatase/phosphodiesterase family member 5	1.35	0.23
Pcyox1	Prenylcysteine oxidase	1.35	0.11
Rtn4ip1	Reticulon-4-interacting protein 1, mitochondrial	1.35	0.82
Grsf1	G-rich sequence factor 1	1.35	0.24
Xpnpep1	Xaa-Pro aminopeptidase 1	1.35	0.25

Gene name	Protein name	-log$_{10}$ p value	log$_2$ FC Pyruvate/ WT
Ndufb11	NADH dehydrogenase [ubiquinone] 1 beta subcomplex subunit 11, mitochondrial	1.35	0.45
GOLGA7B	Golgin subfamily A member 7B	1.34	0.35
Htatsf1	HIV Tat-specific factor 1 homolog	1.34	0.37
Rap2a	Ras-related protein Rap-2a	1.34	0.27
Vac14	Protein VAC14 homolog	1.34	0.22
Nap1l4	Nucleosome assembly protein 1-like 4	1.34	0.14
Tpd52l1	Tumor protein D53	1.34	0.99
Csde1	Cold shock domain-containing protein E1	1.33	0.21
Mcm2	DNA replication licensing factor MCM2	1.33	4.48
Usp47	Ubiquitin carboxyl-terminal hydrolase 47	1.33	0.12
Eif5	Eukaryotic translation initiation factor 5	1.33	0.24
Ndufs6	NADH dehydrogenase [ubiquinone] iron-sulfur protein 6, mitochondrial	1.33	0.29
Calr	Calreticulin	1.33	0.23
Hebp2	Heme-binding protein 2	1.32	0.85
Wdr91	WD repeat-containing protein 91	1.32	0.66
Nup62	Nuclear pore glycoprotein p62	1.32	0.36
Cdkn1a	Cyclin-dependent kinase inhibitor 1	1.31	0.95
Rpl9	60S ribosomal protein L9	1.31	0.20
Ppia	Peptidyl-prolyl cis-trans isomerase A	1.31	0.22

Table S3: Differentially expressed proteins in SMA MNs after pyruvate treatment.
List of significantly changed proteins in SMA MNs after pyruvate treatment ($p < 0.05$). Gene names, protein names, p-values, and fold changes (FC) are listed. Proteins above the red line are down-regulated and below the red line are up-regulated in pyruvate treated SMA compared to untreated SMA MNs.

Gene name	Protein name	-log$_{10}$ p value	log$_2$ FC Pyruvate/ SMA
Dclk1	Serine/threonine-protein kinase DCLK1	2.85	-0.23
Fxn	Frataxin, mitochondrial	2.82	-0.27
Tspan4	Tetraspanin-4	2.74	-1.26
Ube2f	NEDD8-conjugating enzyme UBE2F	2.66	-2.22
Cdk1	Cyclin-dependent kinase 1	2.65	-2.81
Ppil1	Peptidyl-prolyl cis-trans isomerase-like 1	2.51	-0.46
Trim67	Tripartite motif-containing protein 67	2.46	-0.36
Prxl2b	Prostamide/prostaglandin F synthase	2.44	-0.41
Fry	Protein furry homolog	2.39	-0.18
Cdr2l	Cerebellar degeneration-related protein 2-like	2.24	-0.32

Gene name	Protein name	-log$_{10}$ p value	log$_2$ FC Pyruvate/ SMA
Sh2d3c	SH2 domain-containing protein 3C	2.19	-0.74
Ppp2r5c	Serine/threonine-protein phosphatase 2A 56 kDa regulatory subunit gamma isoform	1.97	-0.17
Pitpnm2	Membrane-associated phosphatidylinositol transfer protein 2	1.94	-0.75
Snx16	Sorting nexin-16	1.93	-0.28
Rab39b	Ras-related protein Rab-39B	1.89	-0.23
Slc4a3	Anion exchange protein 3	1.80	-1.61
Akap1	A-kinase anchor protein 1, mitochondrial	1.79	-0.33
Rpl35a	60S ribosomal protein L35a	1.79	-0.20
Slc23a2	Solute carrier family 23 member 2	1.73	-1.12
Dtd1	D-aminoacyl-tRNA deacylase 1	1.72	-0.33
Hpf1	Histone PARylation factor 1	1.69	-0.48
Srrt	Serrate RNA effector molecule homolog	1.69	-0.12
Chga	Chromogranin-A	1.68	-0.40
Myo5b	Unconventional myosin-Vb	1.67	-0.58
Crmp1	Dihydropyrimidinase-related protein 1	1.66	-0.21
Grk2	Beta-adrenergic receptor kinase 1	1.63	-0.45
Bag5	BAG family molecular chaperone regulator 5	1.62	-0.21
Abhd5	1-acylglycerol-3-phosphate O-acyltransferase ABHD5	1.61	-0.86
Acp1	Low molecular weight phosphotyrosine protein phosphatase	1.60	-0.09
Snap91	Clathrin coat assembly protein AP180	1.58	-0.20
Pabpc1	Polyadenylate-binding protein 1	1.56	-0.11
Gphn	Gephyrin	1.56	-0.20
Wdr18	WD repeat-containing protein 18	1.55	-0.17
Gpsm1	G-protein-signaling modulator 1	1.55	-0.17
Ddx39a	ATP-dependent RNA helicase DDX39A	1.54	-0.22
Rabif	Guanine nucleotide exchange factor MSS4	1.54	-0.42
Epm2aip1	EPM2A-interacting protein 1	1.52	-0.33
Bdnf	Brain-derived neurotrophic factor	1.51	-1.45
Ankle2	Ankyrin repeat and LEM domain-containing protein 2	1.50	-0.51
Ica1	Islet cell autoantigen 1	1.50	-0.16
Mrpl17	39S ribosomal protein L17, mitochondrial	1.50	-1.75
Hcn3	Potassium/sodium hyperpolarization-activated cyclic nucleotide-gated channel 3	1.49	-0.28
Atp6v1h	V-type proton ATPase subunit H	1.48	-0.18

Gene name	Protein name	-log$_{10}$ p value	log$_2$ FC Pyruvate/ SMA
Pcyt2	Ethanolamine-phosphate cytidylyltransferase	1.48	-0.26
Arhgap26	Rho GTPase-activating protein 26	1.47	-0.99
Arid1a	AT-rich interactive domain-containing protein 1A	1.44	-0.74
Tmem11	Transmembrane protein 11, mitochondrial	1.43	-0.45
Dpysl4	Dihydropyrimidinase-related protein 4	1.43	-0.21
Pithd1	PITH domain-containing protein 1	1.43	-0.96
Snrpb	Small nuclear ribonucleoprotein-associated protein B	1.41	-0.21
Ttc39b	Tetratricopeptide repeat protein 39B	1.40	-1.04
Stambp	STAM-binding protein	1.36	-0.15
Amacr	Alpha-methylacyl-CoA racemase	1.35	-0.34
Atf2	Cyclic AMP-dependent transcription factor ATF-2	1.35	-0.72
Atp6v0a1	V-type proton ATPase 116 kDa subunit a isoform 1	1.35	-0.17
Kif5c	Kinesin heavy chain isoform 5C	1.34	-0.13
Rimklb	Beta-citrylglutamate synthase B	1.34	-0.46
Dnm1l	Dynamin-1-like protein	1.33	-0.21
Slc8a1	Sodium/calcium exchanger 1	1.33	-0.18
Naa25	N-alpha-acetyltransferase 25, NatB auxiliary subunit	1.32	-0.17
Gnl1	Guanine nucleotide-binding protein-like 1	1.32	-0.17
Syncrip	Heterogeneous nuclear ribonucleoprotein Q	1.31	-0.19
Specc1	Cytospin-B	1.31	-0.90
Dlgap1	Disks large-associated protein 1	3.23	0.57
Dpf2	Zinc finger protein ubi-d4	2.94	1.69
Ppfibp1	Liprin-beta-1	2.66	1.04
Becn1	Beclin-1	2.63	1.62
Scaf1	Splicing factor, arginine/serine-rich 19	2.54	2.16
Rhog	Rho-related GTP-binding protein RhoG	2.42	0.54
Slc8a2	Sodium/calcium exchanger 2	2.32	0.27
Tmem70	Transmembrane protein 70, mitochondrial	2.16	1.23
Acyp1	Acylphosphatase-1	1.96	0.34
Srek1	Splicing regulatory glutamine/lysine-rich protein 1	1.94	1.83
Plcd4	1-phosphatidylinositol 4,5-bisphosphate phosphodiesterase delta-4	1.91	0.48
Lypla1	Acyl-protein thioesterase 1	1.83	0.37
Nelfcd	Negative elongation factor D	1.81	1.26
Spats2l	SPATS2-like protein	1.77	0.38
Mmaa	Methylmalonic aciduria type A homolog, mitochondrial	1.77	0.58

Gene name	Protein name	-log$_{10}$ p value	log$_2$ FC Pyruvate/ SMA
Brix1	Ribosome biogenesis protein BRX1 homolog	1.77	1.35
Dock7	Dedicator of cytokinesis protein 7	1.74	0.26
Septin7	Septin-7	1.72	0.16
Ttc39c	Tetratricopeptide repeat protein 39C	1.72	0.33
Cdc42ep1	Cdc42 effector protein 1	1.7	1.76
Tmem175	Endosomal/lysosomal potassium channel TMEM175	1.69	1.37
Xrcc5	X-ray repair cross-complementing protein 5	1.68	2.21
Stk24	Serine/threonine-protein kinase 24	1.66	0.19
Clpp	ATP-dependent Clp protease proteolytic subunit, mitochondrial	1.65	0.23
Comt	Catechol O-methyltransferase	1.64	0.24
Adi1	1,2-dihydroxy-3-keto-5-methylthiopentene dioxygenase	1.63	0.36
Stim2	Stromal interaction molecule 2	1.62	1.44
Tpm4	Tropomyosin alpha-4 chain	1.59	0.66
Lbr	Delta(14)-sterol reductase LBR	1.56	1.39
Fam20b	Glycosaminoglycan xylosylkinase	1.55	0.29
Map4k3	Mitogen-activated protein kinase kinase kinase kinase 3	1.53	0.51
Tst	Thiosulfate sulfurtransferase	1.52	0.44
Recql	ATP-dependent DNA helicase Q1	1.51	1.91
Dhfr	Dihydrofolate reductase	1.5	0.24
Commd1	COMM domain-containing protein 1	1.48	1.79
Gng4	Guanine nucleotide-binding protein G(I)/G(S)/G(O) subunit gamma-4	1.47	0.6
Otud6b	Deubiquitinase OTUD6B	1.46	0.46
Jup	Junction plakoglobin	1.45	0.22
Psmg3	Proteasome assembly chaperone 3	1.42	1.67
Fnbp1	Formin-binding protein 1	1.41	0.25
Rcn1	Reticulocalbin-1	1.4	0.29
Stk38	Serine/threonine-protein kinase 38	1.4	0.43
Mrpl50	39S ribosomal protein L50, mitochondrial	1.39	0.31
Smc2	Structural maintenance of chromosomes protein 2	1.39	3.1
Timm13	Mitochondrial import inner membrane translocase subunit Tim13	1.38	0.22
Ndufb8	NADH dehydrogenase [ubiquinone] 1 beta subcomplex subunit 8, mitochondrial	1.38	0.31
Bet1l	BET1-like protein	1.37	0.37
Map3k12	Mitogen-activated protein kinase kinase kinase 12	1.37	0.8

Gene name	Protein name	-log$_{10}$ p value	log$_2$ FC Pyruvate/ SMA
Micu1	Calcium uptake protein 1, mitochondrial	1.36	0.3
Gltp	Glycolipid transfer protein	1.36	0.36
Plekha2	Pleckstrin homology domain-containing family A member 2	1.36	0.45
Spg7	Paraplegin	1.36	0.57
Cul1	Cullin-1	1.35	0.16
Rbm26	RNA-binding protein 26	1.34	0.22
Cpeb3	Cytoplasmic polyadenylation element-binding protein 3	1.34	0.95
Limch1	LIM and calponin homology domains-containing protein 1	1.33	0.32
Tppp3	Tubulin polymerization-promoting protein family member 3	1.32	0.22
Sorbs1	Sorbin and SH3 domain-containing protein 1	1.32	0.37
Strn3	Striatin-3	1.31	0.16

Table S4: Differentially expressed proteins in WT MNs after NAC treatment.
List of significantly changed proteins in WT MNs after NAC treatment ($p < 0.05$). Gene names, protein names, p-values, and fold changes (FC) are listed. Proteins above the red line are down-regulated and below the red line are up-regulated in NAC treated WT compared to untreated WT MNs.

Gene name	Protein name	-log$_{10}$ p value	log$_2$ FC NAC/ WT
Dusp12	Dual specificity protein phosphatase 12	3.17	-1.2
Wdr26	WD repeat-containing protein 26	2.53	-0.28
Dipk1b	Divergent protein kinase domain 1B	2.39	-0.8
Cyp46a1	Cholesterol 24-hydroxylase	2.39	-0.98
Atg5	Autophagy protein 5	2.31	-0.42
Washc4	WASH complex subunit 4	2.27	-0.83
Stat3	Signal transducer and activator of transcription 3	2.17	-0.81
Ap1s1	AP-1 complex subunit sigma-1A	1.95	-0.56
Clcn3	H(+)/Cl(-) exchange transporter 3	1.93	-0.43
Elp2	Elongator complex protein 2	1.92	-0.26
Astn2	Astrotactin-2	1.9	-1.12
Rabl6	Rab-like protein 6	1.89	-0.35
Pid1	PTB-containing, cubilin and LRP1-interacting protein	1.85	-0.4
Rack1	Receptor of activated protein C kinase 1	1.77	-0.18
Rab9a	Ras-related protein Rab-9A	1.76	-0.37
Slk	STE20-like serine/threonine-protein kinase	1.75	-0.74

Gene name	Protein name	-log$_{10}$ p value	log$_2$ FC NAC/ WT
Smarcb1	SWI/SNF-related matrix-associated actin-dependent regulator of chromatin subfamily B member 1	1.73	-0.23
Ddx3x	ATP-dependent RNA helicase DDX3X	1.7	-0.12
Pum2	Pumilio homolog 2	1.68	-0.69
Kctd16	BTB/POZ domain-containing protein KCTD16	1.67	-0.6
Smyd3	Histone-lysine N-methyltransferase SMYD3	1.67	-0.71
Fyttd1	UAP56-interacting factor	1.65	-0.24
Dhx36	ATP-dependent DNA/RNA helicase DHX36	1.65	-0.55
Ppp2r5b	Serine/threonine-protein phosphatase 2A 56 kDa regulatory subunit beta isoform	1.63	-0.52
Eif4a1	Eukaryotic initiation factor 4A-I	1.6	-0.07
Sec24a	Protein transport protein Sec24A	1.58	-0.32
Ctnnd2	Catenin delta-2	1.57	-0.27
Pygl	Glycogen phosphorylase, liver form	1.57	-0.45
Cdc16	Cell division cycle protein 16 homolog	1.54	-0.14
Acot8	Acyl-coenzyme A thioesterase 8	1.54	-1.15
Cyp51a1	Lanosterol 14-alpha demethylase	1.53	-0.43
Snrpb2	U2 small nuclear ribonucleoprotein B"	1.52	-0.44
Lrrc47	Leucine-rich repeat-containing protein 47	1.5	-0.22
Mrpl45	39S ribosomal protein L45, mitochondrial	1.48	-0.29
Otud6b	Deubiquitinase OTUD6B	1.46	-0.58
Rpl7a	60S ribosomal protein L7a	1.45	-0.21
Icam5	Intercellular adhesion molecule 5	1.45	-0.77
Grip1	Glutamate receptor-interacting protein 1	1.43	-0.38
Usp9x	Probable ubiquitin carboxyl-terminal hydrolase FAF-X	1.4	-0.23
Slc25a16	Graves disease carrier protein homolog	1.4	-1.2
Fcho2	F-BAR domain only protein 2	1.39	-1.5
Kif1bp	KIF1-binding protein	1.38	-0.29
Emc7	ER membrane protein complex subunit 7	1.37	-0.28
Sar1b	GTP-binding protein SAR1b	1.37	-0.34
Golga7	Golgin subfamily A member 7	1.37	-0.56
Gkap1	G kinase-anchoring protein 1	1.36	-0.83
Kif1b	Kinesin-like protein KIF1B	1.35	-0.34
Sin3a	Paired amphipathic helix protein Sin3a	1.35	-2.23
Rpl27a	60S ribosomal protein L27a	1.34	-0.26
Eif4a3	Eukaryotic initiation factor 4A-III	1.34	-0.37
Epb41l3	Band 4.1-like protein 3	1.32	-0.34
Dpm3	Dolichol-phosphate mannosyltransferase subunit 3	2.7	2.15

Gene name	Protein name	-log$_{10}$ p value	log$_2$ FC NAC/ WT
Cuedc1	CUE domain-containing protein 1	2.43	0.51
Smndc1	Survival of motor neuron-related-splicing factor 30	2.32	0.4
Commd8	COMM domain-containing protein 8	2.32	0.41
Afg3l1	AFG3-like protein 1	2.25	0.49
Cyth2	Cytohesin-2	2.19	0.47
Rnpep	Aminopeptidase B	2.16	0.19
Hdac4	Histone deacetylase 4	2.05	0.66
Bcap29	B-cell receptor-associated protein 29	2.03	0.37
Tomm20	Mitochondrial import receptor subunit TOM20 homolog	1.87	1.3
Adnp	Activity-dependent neuroprotector homeobox protein	1.85	0.27
Cdkn1b	Cyclin-dependent kinase inhibitor 1B	1.85	0.39
Arxes1	Adipocyte-related X-chromosome expressed sequence 1	1.81	0.27
Hba	Hemoglobin subunit alpha	1.81	1.35
Usp47	Ubiquitin carboxyl-terminal hydrolase 47	1.8	0.2
Dennd5b	DENN domain-containing protein 5B	1.78	1.07
Rad23a	UV excision repair protein RAD23 homolog A	1.76	0.8
Ccdc50	Coiled-coil domain-containing protein 50	1.69	0.37
Rpn1	Dolichyl-diphosphooligosaccharide–protein glycosyltransferase subunit 1	1.68	0.19
Ppm1l	Protein phosphatase 1L	1.68	0.25
Gga3	ADP-ribosylation factor-binding protein GGA3	1.66	0.17
Hnrnpu	Heterogeneous nuclear ribonucleoprotein U	1.6	0.14
Gnai2	Guanine nucleotide-binding protein G(i) subunit alpha-2	1.59	0.29
Gpalpp1	GPALPP motifs-containing protein 1	1.59	0.81
Itsn1	Intersectin-1	1.58	0.12
Ano10	Anoctamin-10	1.56	0.29
Bbc3	Bcl-2-binding component 3	1.54	1.19
Mrps7	28S ribosomal protein S7, mitochondrial	1.53	0.27
Hist1h1d	Histone H1.3	1.53	0.32
Hopx	Homeodomain-only protein	1.53	1.09
Mtss1	Protein MTSS 1	1.52	0.48
Ndufs8	NADH dehydrogenase [ubiquinone] iron-sulfur protein 8, mitochondrial	1.49	0.3
Asic1	Acid-sensing ion channel 1	1.49	0.76
Ndufab1	Acyl carrier protein, mitochondrial	1.48	0.25

Gene name	Protein name	-log$_{10}$ p value	log$_2$ FC NAC/ WT
Cpsf2	Cleavage and polyadenylation specificity factor subunit 2	1.48	1.36
Ndufa10	NADH dehydrogenase [ubiquinone] 1 alpha subcomplex subunit 10, mitochondrial	1.45	0.18
Cog2	Conserved oligomeric Golgi complex subunit 2	1.45	0.19
Xpnpep1	Xaa-Pro aminopeptidase 1	1.44	0.13
Rictor	Rapamycin-insensitive companion of mTOR	1.44	0.67
Ubac1	Ubiquitin-associated domain-containing protein 1	1.43	0.24
Lamtor3	Ragulator complex protein LAMTOR3	1.4	0.11
Mrto4	mRNA turnover protein 4 homolog	1.4	0.44
Fam98b	Protein FAM98B	1.39	0.13
Snap29	Synaptosomal-associated protein 29	1.38	0.26
Cacna1b	Voltage-dependent N-type calcium channel subunit alpha-1B	1.38	0.79
Clcc1	Chloride channel CLIC-like protein 1	1.37	0.73
Kpna6	Importin subunit alpha-7	1.36	0.22
Ergic3	Endoplasmic reticulum-Golgi intermediate compartment protein 3	1.35	0.18
Hccs	Cytochrome c-type heme lyase	1.35	0.22
Mtrex	Exosome RNA helicase MTR4	1.35	0.24
Stk24	Serine/threonine-protein kinase 24	1.35	0.33
Ptpn11	Tyrosine-protein phosphatase non-receptor type 11	1.32	0.26
Gas1	Growth arrest-specific protein 1	1.32	0.9
Lyplal1	Lysophospholipase-like protein 1	1.31	0.65

Table S5: Differentially expressed proteins in SMA MNs after NAC treatment.
List of significantly changed proteins in SMA MNs after NAC treatment ($p < 0.05$). Gene names, protein names, p-values, and fold changes (FC) are listed. Proteins above the red line are down-regulated and below the red line are up-regulated in NAC treated SMA compared to untreated SMA MNs.

Gene name	Protein name	-log$_{10}$ p value	log$_2$ FC NAC/ SMA
Slc25a25	Calcium-binding mitochondrial carrier protein SCaMC-2	3.32	-0.35
Chordc1	Cysteine and histidine-rich domain-containing protein 1	3.11	-0.17
Luc7l2	Putative RNA-binding protein Luc7-like 2	2.89	-0.17
Arf2	ADP-ribosylation factor 2	2.63	-0.54
Exosc7	Exosome complex exonuclease RRP42	2.59	-0.62
Dmxl1	DmX-like protein 1	2.54	-2.27
Vmp1	Vacuole membrane protein 1	2.19	-0.35

Gene name	Protein name	-log$_{10}$ p value	log$_2$ FC NAC/ SMA
Thumpd3	THUMP domain-containing protein 3	2.18	-0.55
Lsm6	U6 snRNA-associated Sm-like protein LSm6	2.01	-0.58
Mob4	MOB-like protein phocein	1.95	-0.3
Eef1akmt1	EEF1A lysine methyltransferase 1	1.91	-0.34
Cops6	COP9 signalosome complex subunit 6	1.88	-0.23
Nop2	Probable 28S rRNA (cytosine-C(5))-methyltransferase	1.88	-0.38
Ttc9c	Tetratricopeptide repeat protein 9C	1.87	-0.18
Ankle2	Ankyrin repeat and LEM domain-containing protein 2	1.87	-0.23
Csnk1a1	Casein kinase I isoform alpha	1.87	-0.31
Nono	Non-POU domain-containing octamer-binding protein	1.83	-0.26
Hcn3	Potassium/sodium hyperpolarization-activated cyclic nucleotide-gated channel 3	1.83	-0.47
Timm8b	Mitochondrial import inner membrane translocase subunit Tim8 B	1.8	-0.38
Gspt1	Eukaryotic peptide chain release factor GTP-binding subunit ERF3A	1.78	-0.16
Mrpl14	39S ribosomal protein L14, mitochondrial	1.77	-0.36
Sart1	U4/U6.U5 tri-snRNP-associated protein 1	1.77	-0.46
Ndnf	Protein NDNF	1.77	-2.02
Tmem65	Transmembrane protein 65	1.75	-0.22
Manba	Beta-mannosidase	1.75	-0.65
Cog8	Conserved oligomeric Golgi complex subunit 8	1.73	-0.94
Sh2d3c	SH2 domain-containing protein 3C	1.73	-1.48
Fut8	Alpha-(1,6)-fucosyltransferase	1.72	-0.21
Hip1	Huntingtin-interacting protein 1	1.72	-0.37
Clcn6	Chloride transport protein 6	1.71	-0.34
Scn2a	Sodium channel protein type 2 subunit alpha	1.71	-0.36
Rab39b	Ras-related protein Rab-39B	1.7	-0.19
Nlgn1	Neuroligin-1	1.7	-0.87
Pde12	2',5'-phosphodiesterase 12	1.69	-0.21
Ube2r2	Ubiquitin-conjugating enzyme E2 R2	1.69	-0.47
Qrich1	Glutamine-rich protein 1	1.66	-0.29
Nptx1	Neuronal pentraxin-1	1.66	-0.31
Tnrc6c	Trinucleotide repeat-containing gene 6C protein	1.63	-1.84
Fyn	Tyrosine-protein kinase Fyn	1.61	-0.29
Mink1	Misshapen-like kinase 1	1.61	-0.41
G3bp2	Ras GTPase-activating protein-binding protein 2	1.6	-0.36

Gene name	Protein name	-log$_{10}$ p value	log$_2$ FC NAC/ SMA
Kiaa2013	Uncharacterized protein KIAA2013	1.59	-2.05
Ints14	Integrator complex subunit 14	1.56	-0.4
Atl1	Atlastin-1	1.56	-0.41
Foxk2	Forkhead box protein K2	1.56	-1.17
Map1lc3a	Microtubule-associated proteins 1A/1B light chain 3A	1.55	-0.4
Snrpg	Small nuclear ribonucleoprotein G	1.55	-0.53
Snrpb	Small nuclear ribonucleoprotein-associated protein B	1.53	-0.22
Snx12	Sorting nexin-12	1.53	-0.43
Grk2	Beta-adrenergic receptor kinase 1	1.53	-0.56
Ahsa1	Activator of 90 kDa heat shock protein ATPase homolog 1	1.52	-0.12
Armc10	Armadillo repeat-containing protein 10	1.52	-0.21
Pax2	Paired box protein Pax-2	1.52	-1.4
Isyna1	Inositol-3-phosphate synthase 1	1.51	-0.67
Arl5a	ADP-ribosylation factor-like protein 5A	1.5	-0.27
Mllt11	Protein AF1q	1.49	-0.4
Gphn	Gephyrin	1.48	-0.32
Trmt10c	tRNA methyltransferase 10 homolog C	1.48	-0.5
Oscp1	Protein OSCP1	1.48	-0.52
NA	Protein C8orf37 homolog	1.47	-0.35
Scn3b	Sodium channel subunit beta-3	1.46	-0.39
Rabif	Guanine nucleotide exchange factor MSS4	1.45	-0.33
Ppip5k2	Inositol hexakisphosphate and diphosphoinositol-pentakisphosphate kinase 2	1.44	-0.36
Ybx1	Nuclease-sensitive element-binding protein 1	1.43	-0.25
Rab6a	Ras-related protein Rab-6A	1.42	-0.33
Mtg1	Mitochondrial ribosome-associated GTPase 1	1.42	-0.54
Psmd1	26S proteasome non-ATPase regulatory subunit 1	1.41	-0.26
Cpne1	Copine-1	1.41	-0.29
Nedd4	E3 ubiquitin-protein ligase NEDD4	1.41	-0.33
Ubqln1	Ubiquilin-1	1.4	-0.2
Gar1	H/ACA ribonucleoprotein complex subunit 1	1.4	-0.58
Ano8	Anoctamin-8	1.4	-0.82
Rab10	Ras-related protein Rab-10	1.39	-0.22
Ddx5	Probable ATP-dependent RNA helicase DDX5	1.39	-0.25
Trim32	E3 ubiquitin-protein ligase TRIM32	1.39	-0.31
Cdv3	Protein CDV3	1.38	-0.24
Arid1a	AT-rich interactive domain-containing protein 1A	1.38	-0.25

Gene name	Protein name	-log$_{10}$ p value	log$_2$ FC NAC/ SMA
Pabpc1	Polyadenylate-binding protein 1	1.36	-0.11
L1cam	Neural cell adhesion molecule L1	1.36	-0.26
Pithd1	PITH domain-containing protein 1	1.36	-1.7
Trim67	Tripartite motif-containing protein 67	1.35	-0.3
Idh3a	Isocitrate dehydrogenase [NAD] subunit alpha, mitochondrial	1.34	-0.26
Pacs2	Phosphofurin acidic cluster sorting protein 2	1.34	-0.28
Dclk1	Serine/threonine-protein kinase DCLK1	1.33	-0.2
Ggps1	Geranylgeranyl pyrophosphate synthase	1.33	-0.56
Ddx39a	ATP-dependent RNA helicase DDX39A	1.32	-0.32
Pcyt2	Ethanolamine-phosphate cytidylyltransferase	1.32	-0.34
Tac1	Protachykinin-1	1.32	-1.33
Tbcb	Tubulin-folding cofactor B	1.31	-0.18
Erc1	ELKS/Rab6-interacting/CAST family member 1	1.31	-0.36
Slc39a6	Zinc transporter ZIP6	1.31	-0.48
Mrps21	28S ribosomal protein S21, mitochondrial	2.84	0.38
Ttc39c	Tetratricopeptide repeat protein 39C	2.79	0.32
Dhfr	Dihydrofolate reductase	2.46	0.29
Gatd3a	Glutamine amidotransferase-like class 1 domain-containing protein 3A, mitochondrial	2.42	0.3
Fbxo2	F-box only protein 2	2.36	0.27
Ppfibp1	Liprin-beta-1	2.34	0.93
Ube3a	Ubiquitin-protein ligase E3A	2.18	0.17
Sumo3	Small ubiquitin-related modifier 3	2.14	0.71
Pbdc1	Protein PBDC1	2.08	0.18
Rpl32	60S ribosomal protein L32	2.05	0.13
Tm7sf3	Transmembrane 7 superfamily member 3	1.99	0.69
Tle5	TLE family member 5	1.93	0.5
Hnrnpul1	Heterogeneous nuclear ribonucleoprotein U-like protein 1	1.9	0.23
Rexo2	Oligoribonuclease, mitochondrial	1.86	0.32
Plekha2	Pleckstrin homology domain-containing family A member 2	1.85	0.73
Skt	Sickle tail protein	1.82	0.72
Mmaa	Methylmalonic aciduria type A homolog, mitochondrial	1.81	0.63
Wdr33	pre-mRNA 3' end processing protein WDR33	1.81	0.78
Rab1b	Ras-related protein Rab-1B	1.8	0.59
Mrps5	28S ribosomal protein S5, mitochondrial	1.71	0.28

Gene name	Protein name	-log$_{10}$ p value	log$_2$ FC NAC/ SMA
Psmg3	Proteasome assembly chaperone 3	1.7	0.94
Ntmt1	N-terminal Xaa-Pro-Lys N-methyltransferase 1	1.65	0.36
Tmsb10	Thymosin beta-10	1.62	0.73
Atrx	Transcriptional regulator ATRX	1.6	0.46
Scaf1	Splicing factor, arginine/serine-rich 19	1.6	2.02
Adck1	Uncharacterized aarF domain-containing protein kinase 1	1.57	0.12
Otud6b	Deubiquitinase OTUD6B	1.57	0.27
Prpf3	U4/U6 small nuclear ribonucleoprotein Prp3	1.54	0.36
Lbr	Delta(14)-sterol reductase LBR	1.54	1.64
Uchl1	Ubiquitin carboxyl-terminal hydrolase isozyme L1	1.52	0.19
Cdc73	Parafibromin	1.52	0.67
Adgrg1	Adhesion G-protein coupled receptor G1	1.5	0.26
Ndufaf4	NADH dehydrogenase [ubiquinone] 1 alpha subcomplex assembly factor 4	1.48	0.41
Bet1l	BET1-like protein	1.47	0.39
Scrib	Protein scribble homolog	1.47	0.55
Fam91a1	Protein FAM91A1	1.41	0.15
Adpgk	ADP-dependent glucokinase	1.4	0.22
Rnf2	E3 ubiquitin-protein ligase RING2	1.4	0.39
Dmd	Dystrophin	1.4	0.86
Slc8a2	Sodium/calcium exchanger 2	1.39	0.33
Lztfl1	Leucine zipper transcription factor-like protein 1	1.38	0.66
Ctsl	Cathepsin L1	1.37	0.23
Mturn	Maturin	1.37	2.11
Ciapin1	Anamorsin	1.35	0.39
Brix1	Ribosome biogenesis protein BRX1 homolog	1.35	1.17
Dock7	Dedicator of cytokinesis protein 7	1.33	0.09
Usp39	U4/U6.U5 tri-snRNP-associated protein 2	1.33	0.28
Lemd3	Inner nuclear membrane protein Man1	1.33	0.36
Cdc42ep1	Cdc42 effector protein 1	1.33	1.52
Bcs1l	Mitochondrial chaperone BCS1	1.32	0.23
Ndufa5	NADH dehydrogenase [ubiquinone] 1 alpha subcomplex subunit 5	1.31	0.12
Tst	Thiosulfate sulfurtransferase	1.31	0.42

Table S6: Differentially expressed proteins in WT MNs after menadione treatment.
List of significantly changed proteins in WT MNs after menadione treatment ($p < 0.05$). Gene names, protein names, p-values, and fold changes (FC) are listed. Proteins above the red line are down-regulated and below the red line are up-regulated in menadione treated WT compared to untreated WT MNs.

Gene name	Protein name	-log$_{10}$ p value	log$_2$ FC Men/ WT
Ptges3	Prostaglandin E synthase 3	4.35	-0.63
Fads1	Acyl-CoA (8-3)-desaturase	4.32	-0.75
Mta1	Metastasis-associated protein MTA1	4.19	-0.63
Srrm2	Serine/arginine repetitive matrix protein 2	3.89	-1.07
Poldip3	Polymerase delta-interacting protein 3	3.49	-0.39
Adnp	Activity-dependent neuroprotector homeobox protein	3.35	-0.73
Kpna1	Importin subunit alpha-5	3.32	-0.36
Psd	PH and SEC7 domain-containing protein 1	3.19	-0.75
Raf1	RAF proto-oncogene serine/threonine-protein kinase	3.16	-0.33
Ehmt1	Histone-lysine N-methyltransferase EHMT1	3.11	-1.57
Phf6	PHD finger protein 6	3.06	-1.21
Ecpas	Proteasome adapter and scaffold protein ECM29	3.02	-0.37
Mpst	3-mercaptopyruvate sulfurtransferase	2.99	-0.71
Pelo	Protein pelota homolog	2.96	-0.63
Gatad2b	Transcriptional repressor p66-beta	2.9	-0.81
Smad1	Mothers against decapentaplegic homolog 1	2.89	-0.54
Atg12	Ubiquitin-like protein ATG12	2.87	-0.6
Mllt11	Protein AF1q	2.86	-1.11
Toe1	Target of EGR1 protein 1	2.84	-0.9
Dhx30	ATP-dependent RNA helicase DHX30	2.83	-0.29
Klhl22	Kelch-like protein 22	2.83	-0.46
Pcbp2	Poly(rC)-binding protein 2	2.7	-0.42
Son	Protein SON	2.62	-1.3
Scrib	Protein scribble homolog	2.61	-0.95
Usp9x	Probable ubiquitin carboxyl-terminal hydrolase FAF-X	2.6	-0.42
Dtx3	Probable E3 ubiquitin-protein ligase DTX3	2.58	-0.53
Nifk	MKI67 FHA domain-interacting nucleolar phosphoprotein	2.58	-1.16
Fgf13	Fibroblast growth factor 13	2.53	-2.58
Cnot2	CCR4-NOT transcription complex subunit 2	2.43	-0.32
Csde1	Cold shock domain-containing protein E1	2.4	-0.28
Eif5a	Eukaryotic translation initiation factor 5A-1	2.38	-0.29
Arhgef9	Rho guanine nucleotide exchange factor 9	2.38	-2.31
Adar	Double-stranded RNA-specific adenosine deaminase	2.36	-0.97

Gene name	Protein name	-log$_{10}$ p value	log$_2$ FC Men/ WT
Cnot3	CCR4-NOT transcription complex subunit 3	2.34	-0.14
Rnf14	E3 ubiquitin-protein ligase RNF14	2.34	-0.38
Moap1	Modulator of apoptosis 1	2.32	-2.15
Nsun2	tRNA (cytosine(34)-C(5))-methyltransferase	2.31	-0.65
Tnpo3	Transportin-3	2.28	-0.41
Arhgap21	Rho GTPase-activating protein 21	2.27	-0.45
Fkbp5	Peptidyl-prolyl cis-trans isomerase FKBP5	2.26	-0.72
Fip1l1	Pre-mRNA 3'-end-processing factor FIP1	2.25	-0.29
Hoxb6	Homeobox protein Hox-B6	2.25	-0.72
Usp22	Ubiquitin carboxyl-terminal hydrolase 22	2.24	-1.17
Lyar	Cell growth-regulating nucleolar protein	2.23	-1.5
Specc1	Cytospin-B	2.19	-1.23
Wdr11	WD repeat-containing protein 11	2.14	-0.23
Dstn	Destrin	2.14	-0.35
Srgap1	SLIT-ROBO Rho GTPase-activating protein 1	2.14	-0.48
Trappc9	Trafficking protein particle complex subunit 9	2.13	-0.31
Vps41	Vacuolar protein sorting-associated protein 41 homolog	2.13	-0.39
Cdc23	Cell division cycle protein 23 homolog	2.13	-0.43
Nelfb	Negative elongation factor B	2.11	-0.41
Mlf2	Myeloid leukemia factor 2	2.11	-0.64
Gdap2	Ganglioside-induced differentiation-associated protein 2	2.09	-0.37
Tpgs1	Tubulin polyglutamylase complex subunit 1	2.09	-0.87
Bsn	Protein bassoon	2.08	-1.17
Cdk9	Cyclin-dependent kinase 9	2.07	-0.37
Glyr1	Putative oxidoreductase GLYR1	2.07	-0.52
Elavl1	ELAV-like protein 1	2.05	-0.31
Edc4	Enhancer of mRNA-decapping protein 4	2.03	-0.66
Pcbp1	Poly(rC)-binding protein 1	2.02	-0.46
Nup133	Nuclear pore complex protein Nup133	1.98	-0.2
Prickle2	Prickle-like protein 2	1.98	-1.13
Gnl3l	Guanine nucleotide-binding protein-like 3-like protein	1.96	-1.86
Grip1	Glutamate receptor-interacting protein 1	1.95	-0.37
Hnrnpm	Heterogeneous nuclear ribonucleoprotein M	1.92	-0.62
Pelp1	Proline-, glutamic acid- and leucine-rich protein 1	1.91	-0.32
Irf2bp1	Interferon regulatory factor 2-binding protein 1	1.9	-0.77
Macf1	Microtubule-actin cross-linking factor 1	1.89	-0.45
Zmym3	Zinc finger MYM-type protein 3	1.89	-0.68

Gene name	Protein name	-log$_{10}$ p value	log$_2$ FC Men/ WT
Ppp6c	Serine/threonine-protein phosphatase 6 catalytic subunit	1.88	-0.27
Mon2	Protein MON2 homolog	1.88	-0.3
Srrt	Serrate RNA effector molecule homolog	1.88	-0.6
Ntrk3	NT-3 growth factor receptor	1.87	-1.59
Prpf40a	Pre-mRNA-processing factor 40 homolog A	1.86	-0.33
Ncbp1	Nuclear cap-binding protein subunit 1	1.85	-0.39
Pogz	Pogo transposable element with ZNF domain	1.85	-0.99
Smarcc2	SWI/SNF complex subunit SMARCC2	1.84	-0.36
U2af1	Splicing factor U2AF 35 kDa subunit	1.84	-0.52
Smarca2	Probable global transcription activator SNF2L2	1.82	-0.32
Nup43	Nucleoporin Nup43	1.82	-0.35
Hcfc1	Host cell factor 1	1.81	-0.38
Hnrnpa0	Heterogeneous nuclear ribonucleoprotein A0	1.81	-0.51
Zdhhc17	Palmitoyltransferase ZDHHC17	1.8	-0.18
Rmc1	Regulator of MON1-CCZ1 complex	1.79	-0.42
Ptprs	Receptor-type tyrosine-protein phosphatase S	1.79	-0.6
Gprasp1	G-protein coupled receptor-associated sorting protein 1	1.78	-0.33
Scyl1	N-terminal kinase-like protein	1.78	-0.34
Aida	Axin interactor, dorsalization-associated protein	1.77	-0.54
Afdn	Afadin	1.76	-0.47
Crppa	D-ribitol-5-phosphate cytidylyltransferase	1.76	-1.72
Oga	Protein O-GlcNAcase	1.75	-0.27
Dnmt3a	DNA (cytosine-5)-methyltransferase 3A	1.75	-0.61
Eml1	Echinoderm microtubule-associated protein-like 1	1.75	-0.77
Polr2a	DNA-directed RNA polymerase II subunit RPB1	1.74	-1.58
Heatr5b	HEAT repeat-containing protein 5B	1.73	-0.51
Tsc1	Hamartin	1.73	-0.54
Zmat3	Zinc finger matrin-type protein 3	1.73	-1.28
Hook3	Protein Hook homolog 3	1.72	-0.19
Pde4dip	Myomegalin	1.72	-0.38
Sugt1	Protein SGT1 homolog	1.71	-0.17
Xpo5	Exportin-5	1.71	-0.49
Smad4	Mothers against decapentaplegic homolog 4	1.71	-0.53
Celf4	CUGBP Elav-like family member 4	1.71	-0.8
Fbxl20	F-box/LRR-repeat protein 20	1.71	-1.11
Camk2b	Calcium/calmodulin-dependent protein kinase type II subunit beta	1.7	-0.48
Glrx3	Glutaredoxin-3	1.69	-0.3

Gene name	Protein name	-log$_{10}$ p value	log$_2$ FC Men/ WT
Arl3	ADP-ribosylation factor-like protein 3	1.68	-0.27
Eif3m	Eukaryotic translation initiation factor 3 subunit M	1.68	-0.36
Las1l	Ribosomal biogenesis protein LAS1L	1.68	-1.17
Elmo1	Engulfment and cell motility protein 1	1.68	-4.94
Uros	Uroporphyrinogen-III synthase	1.66	-0.35
Ntm	Neurotrimin	1.66	-0.82
Vps33a	Vacuolar protein sorting-associated protein 33A	1.65	-0.39
Dlg3	Disks large homolog 3	1.65	-0.61
Hnrnph2	Heterogeneous nuclear ribonucleoprotein H2	1.65	-0.62
Pcm1	Pericentriolar material 1 protein	1.65	-0.65
Map3k12	Mitogen-activated protein kinase kinase kinase 12	1.65	-1.5
Sart3	Squamous cell carcinoma antigen recognized by T-cells 3	1.64	-0.51
Wdr13	WD repeat-containing protein 13	1.63	-0.24
Fads2	Acyl-CoA 6-desaturase	1.63	-0.43
Syt11	Synaptotagmin-11	1.63	-0.48
NA	UPF0600 protein C5orf51 homolog	1.63	-0.51
Znf512	Zinc finger protein 512	1.63	-0.74
Rdh11	Retinol dehydrogenase 11	1.62	-0.26
Fam126b	Protein FAM126B	1.62	-2.12
Smyd5	SET and MYND domain-containing protein 5	1.61	-0.38
Gtf2i	General transcription factor II-I	1.61	-0.8
Eif4enif1	Eukaryotic translation initiation factor 4E transporter	1.61	-1.19
Stat3	Signal transducer and activator of transcription 3	1.61	-1.19
Anp32e	Acidic leucine-rich nuclear phosphoprotein 32 family member E	1.6	-0.42
Pcbp4	Poly(rC)-binding protein 4	1.6	-0.64
Mmaa	Methylmalonic aciduria type A homolog, mitochondrial	1.6	-0.92
Prkaa2	5'-AMP-activated protein kinase catalytic subunit alpha-2	1.59	-0.13
Cbx3	Chromobox protein homolog 3	1.59	-0.19
Gapdh	Glyceraldehyde-3-phosphate dehydrogenase	1.59	-0.34
Tardbp	TAR DNA-binding protein 43	1.58	-0.51
Vcpip1	Deubiquitinating protein VCIP135	1.58	-0.55
Golga4	Golgin subfamily A member 4	1.58	-1.06
Prmt1	Protein arginine N-methyltransferase 1	1.56	-0.23
Dmac2l	ATP synthase subunit s, mitochondrial	1.56	-0.25
Ctnnd2	Catenin delta-2	1.56	-0.29

Gene name	Protein name	-log$_{10}$ p value	log$_2$ FC Men/ WT
Mbd3	Methyl-CpG-binding domain protein 3	1.56	-0.87
Mcoln1	Mucolipin-1	1.56	-1.46
Dhx57	Putative ATP-dependent RNA helicase DHX57	1.55	-0.27
Stk39	STE20/SPS1-related proline-alanine-rich protein kinase	1.55	-0.62
Txndc17	Thioredoxin domain-containing protein 17	1.54	-0.32
Mark2	Serine/threonine-protein kinase MARK2	1.54	-0.61
Vim	Vimentin	1.54	-2.1
Vps28	Vacuolar protein sorting-associated protein 28 homolog	1.53	-0.36
Metap1	Methionine aminopeptidase 1	1.52	-0.2
Fndc3a	Fibronectin type-III domain-containing protein 3A	1.52	-0.31
Camk2g	Calcium/calmodulin-dependent protein kinase type II subunit gamma	1.52	-0.37
Bcr	Breakpoint cluster region protein	1.52	-0.45
Diaph1	Protein diaphanous homolog 1	1.51	-0.37
Prkar1a	cAMP-dependent protein kinase type I-alpha regulatory subunit	1.5	-0.24
Park7	Protein/nucleic acid deglycase DJ-1	1.5	-0.27
Aarsd1	Alanyl-tRNA editing protein Aarsd1	1.49	-0.35
Sst	Somatostatin	1.49	-0.35
Sh2b1	SH2B adapter protein 1	1.48	-0.56
Afap1	Actin filament-associated protein 1	1.48	-0.57
Syngap1	Ras/Rap GTPase-activating protein SynGAP	1.48	-0.64
Lrrc58	Leucine-rich repeat-containing protein 58	1.48	-0.93
Pclo	Protein piccolo	1.48	-1.09
Fry	Protein furry homolog	1.47	-0.39
Ltn1	E3 ubiquitin-protein ligase listerin	1.47	-0.43
Hnrnpll	Heterogeneous nuclear ribonucleoprotein L-like	1.47	-0.48
Rims1	Regulating synaptic membrane exocytosis protein 1	1.47	-0.76
Vps18	Vacuolar protein sorting-associated protein 18 homolog	1.46	-0.44
Snu13	NHP2-like protein 1	1.46	-0.51
Ppp1cc	Serine/threonine-protein phosphatase PP1-gamma catalytic subunit	1.45	-0.09
Tex10	Testis-expressed protein 10	1.45	-0.15
Agfg2	Arf-GAP domain and FG repeat-containing protein 2	1.45	-0.29
Camsap1	Calmodulin-regulated spectrin-associated protein 1	1.45	-0.48
Cep170b	Centrosomal protein of 170 kDa protein B	1.45	-0.65

Gene name	Protein name	-log$_{10}$ p value	log$_2$ FC Men/ WT
Limk1	LIM domain kinase 1	1.45	-0.74
Sbf2	Myotubularin-related protein 13	1.45	-0.85
Tox4	TOX high mobility group box family member 4	1.45	-1.05
Mycbp2	E3 ubiquitin-protein ligase MYCBP2	1.44	-0.31
Apc	Adenomatous polyposis coli protein	1.44	-0.42
Rasgrp2	RAS guanyl-releasing protein 2	1.44	-0.5
Spire1	Protein spire homolog 1	1.44	-1.28
Sae1	SUMO-activating enzyme subunit 1	1.43	-0.21
Camk2a	Calcium/calmodulin-dependent protein kinase type II subunit alpha	1.43	-0.32
Bcas3	Breast carcinoma-amplified sequence 3 homolog	1.43	-0.36
Fbll1	rRNA/tRNA 2'-O-methyltransferase fibrillarin-like protein 1	1.43	-0.67
Arih1	E3 ubiquitin-protein ligase ARIH1	1.42	-0.32
Ethe1	Persulfide dioxygenase ETHE1, mitochondrial	1.42	-0.42
Eif2s3x	Eukaryotic translation initiation factor 2 subunit 3, X-linked	1.41	-0.27
Rell2	RELT-like protein 2	1.41	-1.19
Fbxw11	F-box/WD repeat-containing protein 11	1.4	-0.25
Reps1	RalBP1-associated Eps domain-containing protein 1	1.4	-0.29
Fahd1	Acylpyruvase FAHD1, mitochondrial	1.4	-0.35
Trim28	Transcription intermediary factor 1-beta	1.4	-0.39
Hnrnph1	Heterogeneous nuclear ribonucleoprotein H	1.4	-0.53
Ddx20	Probable ATP-dependent RNA helicase DDX20	1.4	-1.35
Cyp46a1	Cholesterol 24-hydroxylase	1.39	-0.56
Rtcb	tRNA-splicing ligase RtcB homolog	1.38	-0.13
Srpk1	SRSF protein kinase 1	1.38	-0.22
Ahi1	Jouberin	1.38	-0.36
Abhd5	1-acylglycerol-3-phosphate O-acyltransferase ABHD5	1.38	-0.77
Mtg1	Mitochondrial ribosome-associated GTPase 1	1.38	-1.16
Hnrnpu	Heterogeneous nuclear ribonucleoprotein U	1.37	-0.2
Pdlim7	PDZ and LIM domain protein 7	1.37	-1.13
Ablim3	Actin-binding LIM protein 3	1.37	-1.59
Med22	Mediator of RNA polymerase II transcription subunit 22	1.37	-2.97
Ctnnd1	Catenin delta-1	1.36	-0.48
Ppp2r5b	Serine/threonine-protein phosphatase 2A 56 kDa regulatory subunit beta isoform	1.36	-0.51

Gene name	Protein name	-log$_{10}$ p value	log$_2$ FC Men/ WT
Ankmy2	Ankyrin repeat and MYND domain-containing protein 2	1.36	-0.53
Slc30a1	Zinc transporter 1	1.35	-0.31
Sh3pxd2b	SH3 and PX domain-containing protein 2B	1.35	-0.42
Zfand5	AN1-type zinc finger protein 5	1.35	-0.54
Dynlt3	Dynein light chain Tctex-type 3	1.34	-0.34
Dus3l	tRNA-dihydrouridine(47) synthase [NAD(P)(+)]-like	1.34	-0.47
Iqsec1	IQ motif and SEC7 domain-containing protein 1	1.34	-0.48
Anp32b	Acidic leucine-rich nuclear phosphoprotein 32 family member B	1.34	-0.58
Trmt6	tRNA (adenine(58)-N(1))-methyltransferase non-catalytic subunit TRM6	1.33	-0.2
Tra2a	Transformer-2 protein homolog alpha	1.33	-0.28
Yy1	Transcriptional repressor protein YY1	1.33	-0.49
Ostf1	Osteoclast-stimulating factor 1	1.33	-0.53
Wasl	Neural Wiskott-Aldrich syndrome protein	1.33	-1.08
Polr2c	DNA-directed RNA polymerase II subunit RPB3	1.32	-0.3
Uba6	Ubiquitin-like modifier-activating enzyme 6	1.31	-0.29
Tbce	Tubulin-specific chaperone E	1.31	-0.3
Aip	AH receptor-interacting protein	1.31	-0.4
Actr1b	Beta-centractin	3.09	0.46
Cox6b1	Cytochrome c oxidase subunit 6B1	2.9	0.24
Mrpl15	39S ribosomal protein L15, mitochondrial	2.9	0.27
Spcs2	Signal peptidase complex subunit 2	2.86	0.52
Arxes1	Adipocyte-related X-chromosome expressed sequence 1	2.85	0.44
Rbbp6	E3 ubiquitin-protein ligase RBBP6	2.64	1.23
Mrpl12	39S ribosomal protein L12, mitochondrial	2.43	0.25
Zdhhc5	Palmitoyltransferase ZDHHC5	2.41	1.54
Ckap4	Cytoskeleton-associated protein 4	2.32	0.3
Mtch2	Mitochondrial carrier homolog 2	2.28	0.29
Tmed10	Transmembrane emp24 domain-containing protein 10	2.17	0.23
Dnajc11	DnaJ homolog subfamily C member 11	2.16	0.28
Adgrb1	Adhesion G protein-coupled receptor B1	2.16	0.8
Ganab	Neutral alpha-glucosidase AB	2.15	0.23
Cuedc1	CUE domain-containing protein 1	2.11	0.24
Rpn2	Dolichyl-diphosphooligosaccharide–protein glycosyltransferase subunit 2	2.1	0.29

Gene name	Protein name	-log$_{10}$ p value	log$_2$ FC Men/ WT
Slc25a20	Mitochondrial carnitine/acylcarnitine carrier protein	2.09	0.22
Vti1a	Vesicle transport through interaction with t-SNAREs homolog 1A	2.08	0.33
Hspe1	10 kDa heat shock protein, mitochondrial	2.07	0.19
Ndufs8	NADH dehydrogenase [ubiquinone] iron-sulfur protein 8, mitochondrial	2.05	0.36
Cttn	Src substrate cortactin	2.04	0.3
Canx	Calnexin	2.02	0.2
Thtpa	Thiamine-triphosphatase	2.0	0.6
Tfam	Transcription factor A, mitochondrial	1.97	0.25
Lrp1	Prolow-density lipoprotein receptor-related protein 1	1.96	0.16
Ddah2	N(G),N(G)-dimethylarginine dimethylaminohydrolase 2	1.96	0.18
Fh	Fumarate hydratase, mitochondrial	1.96	0.27
Arg2	Arginase-2, mitochondrial	1.96	0.87
Cpd	Carboxypeptidase D	1.92	0.33
Nufip2	Nuclear fragile X mental retardation-interacting protein 2	1.91	0.22
Tmed4	Transmembrane emp24 domain-containing protein 4	1.91	0.36
Dhodh	Dihydroorotate dehydrogenase (quinone), mitochondrial	1.86	0.21
Rps7	40S ribosomal protein S7	1.84	0.19
Kpnb1	Importin subunit beta-1	1.83	0.19
Spcs3	Signal peptidase complex subunit 3	1.83	0.2
Grpel1	GrpE protein homolog 1, mitochondrial	1.79	0.19
Rps19	40S ribosomal protein S19	1.78	0.21
Emc7	ER membrane protein complex subunit 7	1.77	0.28
Mars	Methionine–tRNA ligase, cytoplasmic	1.76	0.18
Lzic	Protein LZIC	1.76	0.32
Impa1	Inositol monophosphatase 1	1.75	0.2
Snrpd3	Small nuclear ribonucleoprotein Sm D3	1.74	0.16
Gpr107	Protein GPR107	1.72	0.59
Svop	Synaptic vesicle 2-related protein	1.72	0.77
Eif2s1	Eukaryotic translation initiation factor 2 subunit 1	1.71	0.17
Rwdd1	RWD domain-containing protein 1	1.7	0.24
Sec11a	Signal peptidase complex catalytic subunit SEC11A	1.7	0.34
Uqcrb	Cytochrome b-c1 complex subunit 7	1.69	0.28
Pcyox1	Prenylcysteine oxidase	1.69	0.31
Afg3l1	AFG3-like protein 1	1.69	0.33
Afg3l2	AFG3-like protein 2	1.67	0.1

Gene name	Protein name	-log$_{10}$ p value	log$_2$ FC Men/ WT
Vdac1	Voltage-dependent anion-selective channel protein 1	1.66	0.18
Ppm1f	Protein phosphatase 1F	1.66	0.51
Chmp2a	Charged multivesicular body protein 2a	1.65	0.27
Atp5mg	ATP synthase subunit g, mitochondrial	1.65	0.35
Entpd5	Ectonucleoside triphosphate diphosphohydrolase 5	1.65	0.49
Fgd5	FYVE, RhoGEF and PH domain-containing protein 5	1.64	0.79
Lrrc59	Leucine-rich repeat-containing protein 59	1.63	0.17
Ndufc2	NADH dehydrogenase [ubiquinone] 1 subunit C2	1.63	0.23
Usp39	U4/U6.U5 tri-snRNP-associated protein 2	1.63	0.33
Glg1	Golgi apparatus protein 1	1.61	0.26
Crkl	Crk-like protein	1.61	0.29
M6pr	Cation-dependent mannose-6-phosphate receptor	1.61	0.36
Ergic3	Endoplasmic reticulum-Golgi intermediate compartment protein 3	1.6	0.25
Slc4a3	Anion exchange protein 3	1.6	1.1
Pdia3	Protein disulfide-isomerase A3	1.58	0.2
Ndufs6	NADH dehydrogenase [ubiquinone] iron-sulfur protein 6, mitochondrial	1.57	0.23
Ndufb10	NADH dehydrogenase [ubiquinone] 1 beta subcomplex subunit 10	1.55	0.23
Kif5b	Kinesin-1 heavy chain	1.54	0.17
Nap1l4	Nucleosome assembly protein 1-like 4	1.51	0.16
Pdia6	Protein disulfide-isomerase A6	1.51	0.17
Pgm1	Phosphoglucomutase-1	1.51	0.2
Cdkn1a	Cyclin-dependent kinase inhibitor 1	1.51	0.91
Cpsf2	Cleavage and polyadenylation specificity factor subunit 2	1.51	1.35
Wdr1	WD repeat-containing protein 1	1.5	0.18
Sel1l	Protein sel-1 homolog 1	1.5	0.2
Rpn1	Dolichyl-diphosphooligosaccharide–protein glycosyltransferase subunit 1	1.49	0.18
Rpl12	60S ribosomal protein L12	1.49	0.18
Snap29	Synaptosomal-associated protein 29	1.49	0.25
Sod2	Superoxide dismutase [Mn], mitochondrial	1.48	0.24
Ano10	Anoctamin-10	1.48	0.27
Mrpl22	39S ribosomal protein L22, mitochondrial	1.48	0.34
Timm44	Mitochondrial import inner membrane translocase subunit TIM44	1.47	0.19
Arpc5	Actin-related protein 2/3 complex subunit 5	1.47	0.26

Gene name	Protein name	-log$_{10}$ p value	log$_2$ FC Men/ WT
Atp5f1c	ATP synthase subunit gamma, mitochondrial	1.46	0.24
Prpsap2	Phosphoribosyl pyrophosphate synthase-associated protein 2	1.46	0.24
Mpc1	Mitochondrial pyruvate carrier 1	1.45	0.52
Atp1a1	Sodium/potassium-transporting ATPase subunit alpha-1	1.44	0.24
Sidt2	SID1 transmembrane family member 2	1.44	0.59
Pgs1	CDP-diacylglycerol–glycerol-3-phosphate 3-phosphatidyltransferase, mitochondrial	1.43	0.17
Lemd2	LEM domain-containing protein 2	1.43	0.32
Micos10	MICOS complex subunit Mic10	1.43	0.36
Timm13	Mitochondrial import inner membrane translocase subunit Tim13	1.42	0.22
Bclaf1	Bcl-2-associated transcription factor 1	1.42	0.25
Alg9	Alpha-1,2-mannosyltransferase ALG9	1.42	0.33
Cacnb1	Voltage-dependent L-type calcium channel subunit beta-1	1.42	1.31
Cops4	COP9 signalosome complex subunit 4	1.41	0.16
Ppm1l	Protein phosphatase 1L	1.4	0.27
Abcb10	ATP-binding cassette sub-family B member 10, mitochondrial	1.4	0.9
Gpaa1	Glycosylphosphatidylinositol anchor attachment 1 protein	1.38	0.47
Rack1	Receptor of activated protein C kinase 1	1.37	0.15
Rpl5	60S ribosomal protein L5	1.37	0.18
Reep5	Receptor expression-enhancing protein 5	1.37	0.3
Ociad1	OCIA domain-containing protein 1	1.37	0.32
Zpr1	Zinc finger protein ZPR1	1.36	0.06
Rap1a	Ras-related protein Rap-1A	1.35	0.18
Os9	Protein OS-9	1.35	0.34
Adpgk	ADP-dependent glucokinase	1.35	0.36
Ndufb5	NADH dehydrogenase [ubiquinone] 1 beta subcomplex subunit 5, mitochondrial	1.34	0.31
Prpsap1	Phosphoribosyl pyrophosphate synthase-associated protein 1	1.34	0.52
Ddost	Dolichyl-diphosphooligosaccharide–protein glycosyltransferase 48 kDa subunit	1.33	0.32
Srsf1	Serine/arginine-rich splicing factor 1	1.33	0.33
Prkcsh	Glucosidase 2 subunit beta	1.32	0.18
Phb2	Prohibitin-2	1.32	0.22

Gene name	Protein name	-$\log_{10}$ p value	$\log_2$ FC Men/ WT
Sppl2b	Signal peptide peptidase-like 2B	1.32	1.37
Pa2g4	Proliferation-associated protein 2G4	1.31	0.13
Por	NADPH–cytochrome P450 reductase	1.31	0.24
Atp5f1d	ATP synthase subunit delta, mitochondrial	1.31	0.28
Tomm40	Mitochondrial import receptor subunit TOM40 homolog	1.31	0.29

ACKNOWLEDGEMENTS

First and foremost, I would like to express my sincere gratitude to my supervisor, Dr. Min Jeong Kye, for giving me the opportunity to work in her group. I am deeply grateful for her support, scientific advice, encouragement, and optimism. Thank you for the fascinating project and for giving me the freedom to develop throughout the project. I am thankful for the generous support to attend so many international conferences and further training.

I would like to offer my special thanks to Prof. Brunhilde Wirth for agreeing to review my thesis and guiding my project. I am thankful for the excellent mentoring. Moreover, I am grateful to Bruni for welcoming me into her group.

I would like to extend my sincere thanks to Prof. Dr. Elena Rugarli for kindly agreeing to review my thesis and beyond this for supporting my project with her scientific advice. I am thankful to Prof. Dr. Niels Gehring for taking the chair in my thesis defense.

A huge thanks to all past and present members of the AG Kye, AG Wirth, AG Zempel, AG Beck, and the diagnostics team of the Institute. I would also like to thank Dr. Uwe Becker, the Institute's secretary, for all administrative issues and possible concerns. Thanks to Natalia for all her advice, scientifically and beyond. I especially thank my colleagues Wiebke, Inês, and Johanna. But also Franca, Hanna, and Talita for their technical support.

I thank Wiebke and Inês for the countless hours we spend on motor neuron preparation side by side. But most importantly, for the cheerful companionship.

My gratitude goes to the animal caretakers of the CMMC Animal Facility for supporting my work. Moreover, a special thanks to the people of the proteomics facility at the CECAD who supported the project.

Most importantly, I would like to express my great gratitude to my family. To my parents Georg and Gabriele, to my brother Martin and to my sister Christine. For the constant support and motivation on my journey. Further, I like to thank Martin for all the scientific discussions and appreciated feedback.

Finally, my deepest gratitude goes to Annika for all the support and motivation. For all the joy you bring to my life. Ich liebe dich!

EIDESSTATTLICHE ERKLÄRUNG

Hiermit versichere ich an Eides statt, dass ich die vorliegende Dissertation selbstständig und ohne die Benutzung anderer als der angegebenen Hilfsmittel und Literatur angefertigt habe. Alle Stellen, die wörtlich oder sinngemäß aus veröffentlichten und nicht veröffentlichten Werken dem Wortlaut oder dem Sinn nach entnommen wurden, sind als solche kenntlich gemacht. Ich versichere an Eides statt, dass diese Dissertation noch keiner anderen Fakultät oder Universität zur Prüfung vorgelegen hat; dass sie - abgesehen von unten angegebenen Teilpublikationen und eingebundenen Artikeln und Manuskripten - noch nicht veröffentlicht worden ist sowie, dass ich eine Veröffentlichung der Dissertation vor Abschluss der Promotion nicht ohne Genehmigung des Promotionsausschusses vornehmen werde. Die Bestimmungen dieser Ordnung sind mir bekannt. Darüber hinaus erkläre ich hiermit, dass ich die Ordnung zur Sicherung guter wissenschaftlicher Praxis und zum Umgang mit wissenschaftlichem Fehlverhalten der Universität zu Köln gelesen und sie bei der Durchführung der Dissertation zugrundeliegenden Arbeiten und der schriftlich verfassten Dissertation beachtet habe und verpflichte mich hiermit, die dort genannten Vorgaben bei allen wissenschaftlichen Tätigkeiten zu beachten und umzusetzen. Ich versichere, dass die eingereichte elektronische Fassung der eingereichten Druckfassung vollständig entspricht.

Teilpublikationen:
Teilpublikationen sind in Kapitel 8 angegeben. Die in dieser Dissertation eingebundenen Ergebnisse wurden in einem Wissenschaftsartikel der Fachzeitschrift *Acta Neuropathologica Communications* mit dem Titel "Mitochondrial defects in the respiratory complex I contribute to impaired translational initiation via ROS and energy homeostasis in SMA motor neurons" veröffentlicht. Der Autorenbeitrag ist in der Originalpublikation im Anhang enthalten.

Köln, 23.05.2021 — Max Thelen

. . . . — . . . .

Ort, Datum — **Maximilian Paul Thelen**